

**CABLE SUSPENDED PARALLEL ROBOTS:
DESIGN, WORKSPACE, AND CONTROL**

By

Jason L. Pusey

A thesis submitted to the Faculty of the University of Delaware in partial fulfillment of the requirements for the degree of Master of Science in Mechanical Engineering

Spring 2006

Copyright 2006 Jason L. Pusey
All Rights Reserved

UMI Number: 1435861

Copyright 2006 by
Pusey, Jason L.

All rights reserved.

UMI[®]

UMI Microform 1435861

Copyright 2006 by ProQuest Information and Learning Company.
All rights reserved. This microform edition is protected against
unauthorized copying under Title 17, United States Code.

ProQuest Information and Learning Company
300 North Zeeb Road
P.O. Box 1346
Ann Arbor, MI 48106-1346

**CABLE SUSPENDED PARALLEL ROBOTS:
DESIGN, WORKSPACE, AND CONTROL**

By

Jason L. Pusey

Approved: _____

Thomas S. Buchanan, Ph.D.
Chair of the Department of Mechanical Engineering

Approved: _____

Eric W. Kaler, Ph.D.
Dean of the College of Engineering

Approved: _____

Conrado M. Gempeaw II, Ph.D.
Vice Provost for Academic and International Programs

I certify that I have read this thesis and that in my opinion it meets the academic and professional standard required by the University of Delaware as a thesis for the degree of Master of Science in Mechanical Engineering.

Approved: _____

Sunil K. Agrawal, Ph.D.
Professor in charge of thesis on behalf of the Advisory Committee

I certify that I have read this thesis and that in my opinion it meets the academic and professional standard required by the University of Delaware as a thesis for the degree of Master of Science in Mechanical Engineering.

Approved: _____

Michael D. Greenberg, Ph.D.
Member of thesis committee

I certify that I have read this thesis and that in my opinion it meets the academic and professional standard required by the University of Delaware as a thesis for the degree of Master of Science in Mechanical Engineering.

Approved: _____

Michael Keefe, Ph.D.
Member of thesis committee

ACKNOWLEDGMENTS

I would like to thank Dr. Sunil Kumar Agrawal for all his advice and guidance in the areas of this research. His support and energetic interest in robotics research has been an enormous inspiration. I am grateful for the experiences and knowledge opportunities he has presented me and it has been my privilege to work with him. I would also like to thank Dr. Abbas Fattah for his advice and guidance on parallel manipulators was of great assistance to the project.

In addition, I would like to thank all my colleagues in the Robotics and Control Laboratory at the University of Delaware for any help they gave me over the past years and the friendship they have gave me. I would especially like to acknowledge Abdullah Basar Alp, Gregory Pease and Steven Pledgie for their assistance in this study.

Finally, I would like to express my deepest gratitude to my parents and to my family, for their never-ending encouragement and support.

DEDICATION

To my parents – Philip and BethAnn Pusey

TABLE OF CONTENTS

LIST OF TABLES	ix
LIST OF FIGURES	x
ABSTRACT	xx
Chapter	
1 INTRODUCTION	1
1.1 History	3
1.2 Literature Survey	15
1.3 Scope of Present Work	28
2 KINEMATICS AND DYNAMICS.....	30
2.1 Introduction	30
2.2 Kinematics	32
2.2.1 Forward or Direct Kinematics	32
2.2.2 Inverse Kinematics	33
2.2.3 Kinematic and Geometric Model	34
2.2.4 Geometric Jacobian	38
2.2.5 Analytic Jacobian	43
2.2.6 Acceleration.....	46
2.3 Dynamics	48
2.3.1 Dynamic Equations of Motion	49
2.3.2 Calculation of Inertia.....	55
2.4 Conclusion	55
3 WORKSPACE AND ANALYTICAL DESIGN.....	57
3.1 Introduction	57
3.2 Workspace Model.....	59
3.3 Workspace Definition.....	62

3.4	Performance Indices	64
3.5	Simulation Studies and Analysis	67
	3.5.1 Workspace Volume	73
	3.5.2 Global Conditioning Index	95
3.6	Conclusion	110
4	PRACTICAL DESIGN APPLICATIONS	113
	4.1 Introduction	113
	4.2 Problem Statement	114
	4.3 Design Model	115
	4.4 Case Study Results	117
	4.4.1 Surface 1 and 2: Cylinder	118
	4.4.2 Surface 3: Simple Plane	125
	4.5 Conclusion	135
5	FORCE CONTROL	137
	5.1 Introduction	137
	5.2 Control Law Partitioning	141
	5.3 Selection of a Force Control Law	146
	5.4 Hybrid Force/Position Controller	157
	5.5 Simulation Studies	165
	5.5.1 Case 1	168
	5.5.2 Case 2	177
	5.5.3 Case 3	184
	5.5.4 Case 4	192
	5.5.5 Case 5	199
	5.6 Discussion and Analysis of Results	206
	5.7 Additional Comments	210
	5.8 Conclusion	212
6	CONCLUSION	213
	6.1 Summary	213
	6.2 Future Work	214

Appendix

Appendix A: Plots of Workspace Volume	217
Appendix B: Plots of GCI	249
Appendix C: Geometries	281
REFERENCES	283

LIST OF TABLES

Table 3.1 Cable Suspended Parallel Robots Studied	72
Table 3.2 Set of Orientations.....	73
Table 3.3 Examples of the Symmetry within the Data.....	80
Table 3.4 Orientation Range can travel when ($\psi = 0^\circ$, $\theta = 0^\circ$), (r_{end}/r_{base}) = 100%.....	87
Table 3.5 Cable Forces and Conditioning Index Values for (x_o, y_o, z_o) = (1, 1, 10) and (ψ, θ, ϕ) = (30°, 60°, 0°).....	90
Table 4.1 Design Surfaces.....	115
Table 4.2 Cable Suspended Parallel Robots Considered for Surfaces 1 & 2.....	119
Table 4.3 Cable Suspended Parallel Robots Considered for Surfaces 3	126
Table 4.4 Set of Orientations Used for Robots Encountering Surface 3.....	126
Table 5.1 Values used in Simulation.....	166
Table 5.2 Natural and Artificial Constraints for Case 1	169
Table 5.3 Natural and Artificial Constraints for Case 2.....	177
Table 5.4 Natural and Artificial Constraints for Case 3.....	184
Table 5.5 Natural and Artificial Constraints for Case 4.....	192
Table 5.6 Natural and Artificial Constraints for Case 5.....	200

LIST OF FIGURES

Fig. 1.1 Original Gough Platform Tire Testing Machine Constructed in 1955	3
Fig. 1.2 Upgraded Gough Platform Tire Testing Machine used today	4
Fig. 1.3 Stewart Platform and the flight simulator	5
Fig. 1.4 NIST RoboCrane in a lifting application	13
Fig. 1.5 NIST RoboCrane Lunar Rover Prototype Model	13
Fig. 1.6 University of Delaware Cable Suspended Parallel Robot	14
Fig. 2.1 General 6-6 cable suspended parallel manipulator	35
Fig. 2.2 Modeling of the i^{th} cable vector loop	37
Fig. 2.3 Free Body Diagram of MP	50
Fig. 3.1 A schematic of a 6-6 cable suspended parallel robot.....	60
Fig. 3.2a (Left) Schematic of BP, 3.2b (Right) Schematic of MP	61
Fig. 3.3a Schematic of BP and MP for $\gamma = 45^\circ$	69
Fig. 3.3b Schematic of BP and MP for $\gamma = 0^\circ$	70
Fig. 3.4 Workspace Volume for $\gamma = 0^\circ$, $(r_{end}/r_{base}) = 100\%$, 50%, 1%, and for $\phi = 0^\circ$	76
Fig. 3.5 Workspace Volume for $\gamma = 15^\circ$, $(r_{end}/r_{base}) = 100\%$, 50%, 1%, and for $\phi = 0^\circ$	77
Fig. 3.6 Workspace Volume for $\gamma = 30^\circ$, $(r_{end}/r_{base}) = 100\%$, 50%, 1%, and for $\phi = 0^\circ$	78

Fig. 3.7 Workspace Volume for $\gamma = 45^\circ$, $(r_{end}/r_{base}) = 100\%$, 50% , 1% , and for $\phi = 0^\circ$	79
Fig. 3.8 Graph of Average Workspace Volume vs. ϕ for geometry $\gamma = 0^\circ$	82
Fig. 3.9 Graph of Average Workspace Volume vs. ϕ for geometry $\gamma = 15^\circ$	83
Fig. 3.10 Graph of Average Workspace Volume vs. ϕ for geometry $\gamma = 30^\circ$	84
Fig. 3.11 Graph of Average Workspace Volume vs. ϕ for geometry $\gamma = 45^\circ$	85
Fig. 3.12 Limits of MP ϕ Orientation for $(\psi = 0^\circ, \theta = 0^\circ)$, $(r_{end}/r_{base}) = 100\%$, where (top left) is for $\gamma = 0^\circ$, (top right) is for $\gamma = 15^\circ$, (bottom left) is for $\gamma = 30^\circ$, (bottom right) is for $\gamma = 45^\circ$	86
Fig. 3.13 Workspace Volume vs. $(r_{end}/r_{base})\%$ for $(\psi, \theta, \phi) = (0^\circ, 0^\circ, 0^\circ)$, with reduced step size to 0.1 along all three (x_O, y_O, z_O) axes	89
Fig. 3.14 Cable Suspended Parallel Robot for $\gamma = 0^\circ$, $(r_{end}/r_{base}) = 100\%$, at $(x_O, y_O, z_O) = (1, 1, 10)$ and $(\psi, \theta, \phi) = (30^\circ, 60^\circ, 0^\circ)$	91
Fig. 3.15 Cable Suspended Parallel Robot for $\gamma = 0^\circ$, $(r_{end}/r_{base}) = 55.319\%$, at $(x_O, y_O, z_O) = (1, 1, 10)$ and $(\psi, \theta, \phi) = (30^\circ, 60^\circ, 0^\circ)$	92
Fig. 3.16 Cable Suspended Parallel Robot for $\gamma = 0^\circ$, $(r_{end}/r_{base}) = 55.318\%$, at $(x_O, y_O, z_O) = (1, 1, 10)$ and $(\psi, \theta, \phi) = (30^\circ, 60^\circ, 0^\circ)$	93
Fig 3.17 Cable Suspended Parallel Robot for $\gamma = 0^\circ$, $(r_{end}/r_{base}) = 10\%$, at $(x_O, y_O, z_O) = (1, 1, 10)$ and $(\psi, \theta, \phi) = (30^\circ, 60^\circ, 0^\circ)$	94
Fig. 3.18 GCI distribution for $\gamma = 0^\circ$, $(r_{end}/r_{base}) = 100\%$, 50% , 1% , and for $\phi = 0^\circ$	96
Fig. 3.19 GCI distribution for $\gamma = 15^\circ$, $(r_{end}/r_{base}) = 100\%$, 50% , 1% , and for $\phi = 0^\circ$	97
Fig. 3.20 GCI distribution for $\gamma = 30^\circ$, $(r_{end}/r_{base}) = 100\%$, 50% , 1% , and for $\phi = 0^\circ$	98

Fig. 3.21 GCI distribution for $\gamma = 45^\circ$, $(r_{end}/r_{base}) = 100\%$, 50% , 1% , and for $\phi = 0^\circ$	99
Fig. 3.22 Graph of Average GCI vs. ϕ for geometry $\gamma = 0^\circ$	100
Fig. 3.23 Graph of Average GCI vs. ϕ for geometry $\gamma = 15^\circ$	101
Fig. 3.24 Graph of Average GCI vs. ϕ for geometry $\gamma = 30^\circ$	102
Fig. 3.25 Graph of Average GCI vs. ϕ for geometry $\gamma = 45^\circ$	103
Fig. 3.26 Simple sketch of cable tensions and their normal tangential components.....	105
Fig. 3.27 Workspace of Cable Suspended Parallel Robot Displaying Conditioning Index Distribution for $\gamma = 0^\circ$, $(r_{end}/r_{base}) = 100\%$, and $(\psi, \theta, \phi) = (0^\circ, 0^\circ, 0^\circ)$	107
Fig. 3.28 Workspace of Cable Suspended Parallel Robot Displaying Conditioning Index Distribution for $\gamma = 0^\circ$, $(r_{end}/r_{base}) = 100\%$, and $(\psi, \theta, \phi) = (30^\circ, 350^\circ, 0^\circ)$	108
Fig. 3.29 Workspace of Cable Suspended Parallel Robot Displaying Conditioning Index Distribution for $\gamma = 0^\circ$, $(r_{end}/r_{base}) = 100\%$, and $(\psi, \theta, \phi) = (30^\circ, 330^\circ, 0^\circ)$	109
Fig. 3.30 Workspace of Cable Suspended Parallel Robot Displaying Conditioning Index Distribution with a large value of z_O for $\gamma = 0^\circ$, $(r_{end}/r_{base}) = 100\%$, and $(\psi, \theta, \phi) = (0^\circ, 0^\circ, 0^\circ)$	110
Fig. 4.1 Three Dimensional view of all four γ geometries	117
Fig. 4.2 Workspace Volume vs. $(r_{end}/r_{base})\%$ for Surface 1	120
Fig. 4.3 GCI vs. $(r_{end}/r_{base})\%$ for Surface 1	121
Fig. 4.4 Workspace Volume vs. $(r_{end}/r_{base})\%$ for Surface 2	122
Fig. 4.5 GCI vs. $(r_{end}/r_{base})\%$ for Surface 2	123

Fig. 4.6 Workspace Volume displaying the conditioning index distribution for Surface 1.....	124
Fig. 4.7 Workspace Volume displaying the conditioning index distribution for Surface 2.....	125
Fig. 4.8 Workspace vs. ϕ for $\gamma = 0^\circ$, Surface 3.....	127
Fig. 4.9 Workspace vs. ϕ for $\gamma = 15^\circ$, Surface 3.....	128
Fig. 4.10 Workspace vs. ϕ for $\gamma = 30^\circ$, Surface 3.....	129
Fig. 4.11 Workspace vs. ϕ for $\gamma = 45^\circ$, Surface 3.....	130
Fig. 4.12 GCI vs. ϕ for $\gamma = 0^\circ$, Surface 3.....	131
Fig. 4.13 GCI vs. ϕ for $\gamma = 15^\circ$, Surface 3.....	132
Fig. 4.14 GCI vs. ϕ for $\gamma = 30^\circ$, Surface 3.....	133
Fig. 4.15 GCI vs. ϕ for $\gamma = 45^\circ$, Surface 3.....	134
Fig. 4.16 Workspace Conditioning Index Distribution for $(\psi, \theta, \phi) = (0^\circ, 0^\circ, 0^\circ)$, $\gamma = 0^\circ$, $(r_{end}/r_{base}) = 100\%$, Surface 3.....	135
Fig. 5.1 Spring Mass System exposed to friction damping.....	143
Fig. 5.2 Parallel robot assembling a peg into a hole.....	148
Fig. 5.3 Subtasks of a parallel robot assembling a peg into a hole	160
Fig. 5.4 Hybrid Force/Position Controller.....	163
Fig. 5.5 Hybrid Force/Position Controller with Decision Making Block	164
Fig. 5.6 Plot of the position and orientation of the MP as the Case 1 task is executed for the traditional parallel manipulator	170
Fig. 5.7 Plots of the forces and moments acting on the MP as the Case 1 task is executed for the traditional parallel manipulator	171
Fig. 5.8 Plots of the input force experienced by each actuator as the Case 1 task is executed for the traditional parallel manipulator.....	172

Fig. 5.9 Plot of the position and orientation of the MP as the Case 1 task is executed for the cable suspended parallel manipulator.....	173
Fig. 5.10 Plots of the forces and moments acting on the MP as the Case 1 task is executed for the cable suspended parallel manipulator.....	174
Fig. 5.11 Plots of the tensions experienced by each cable as the Case 1 task is executed for the cable suspended parallel manipulator.....	175
Fig. 5.12 Plot of the position and orientation of the MP as the Case 2 task is executed for the traditional parallel manipulator	178
Fig. 5.13 Plots of the forces and moments acting on the MP as the Case 2 task is executed for the traditional parallel manipulator	179
Fig. 5.14 Plots of the input force experienced by each actuator as the Case 2 task is executed for the traditional parallel manipulator	180
Fig. 5.15 Plot of the position and orientation of the MP as the Case 2 task is executed for the cable suspended parallel manipulator.....	181
Fig. 5.16 Plots of the forces and moments acting on the MP as the Case 2 task is executed for the cable suspended parallel manipulator.....	182
Fig. 5.17 Plots of the tensions experienced by each cable as the Case 2 task is executed for the cable suspended parallel manipulator.....	183
Fig. 5.18 Desired trajectory of the MP for Case 3 task	185
Fig. 5.19 Plot of the position and orientation of the MP as the Case 3 task is executed for the traditional parallel manipulator	186
Fig. 5.20 Plots of the forces and moments acting on the MP as the Case 3 task is executed for the traditional parallel manipulator	187
Fig. 5.21 Plots of the input force experienced by each actuator as the Case 3 task is executed for the traditional parallel manipulator	188
Fig. 5.22 Plot of the position and orientation of the MP as the Case 3 task is executed for the cable suspended parallel manipulator.....	189
Fig. 5.23 Plots of the forces and moments acting on the MP as the Case 3 task is executed for the cable suspended parallel manipulator.....	190

Fig. 5.24 Plots of the tensions experienced by each cable as the Case 3 task is executed for the cable suspended parallel manipulator.....	191
Fig. 5.25 Plot of the position and orientation of the MP as the Case 4 task is executed for the traditional parallel manipulator	193
Fig. 5.26 Plots of the forces and moments acting on the MP as the Case 4 task is executed for the traditional parallel manipulator	194
Fig. 5.27 Plots of the input force experienced by each actuator as the Case 4 task is executed for the traditional parallel manipulator	195
Fig. 5.28 Plot of the position and orientation of the MP as the Case 4 task is executed for the cable suspended parallel manipulator.....	196
Fig. 5.29 Plots of the forces and moments acting on the MP as the Case 4 task is executed for the cable suspended parallel manipulator.....	197
Fig. 5.30 Plots of the tensions experienced by each cable as the Case 4 task is executed for the cable suspended parallel manipulator.....	198
Fig. 5.31 Plot of the position and orientation of the MP as the Case 5 task is executed for the traditional parallel manipulator	200
Fig. 5.32 Plots of the forces and moments acting on the MP as the Case 5 task is executed for the traditional parallel manipulator	201
Fig. 5.33 Plots of the input force experienced by each actuator as the Case 5 task is executed for the traditional parallel manipulator	202
Fig. 5.34 Plot of the position and orientation of the MP as the Case 5 task is executed for the cable suspended parallel manipulator.....	203
Fig. 5.35 Plots of the forces and moments acting on the MP as the Case 5 task is executed for the cable suspended parallel manipulator.....	204
Fig. 5.36 Plots of the tensions experienced by each cable as the Case 5 task is executed for the cable suspended parallel manipulator.....	205
Fig. 3.4a Workspace Volume for $\gamma = 0^\circ$, $(r_{end}/r_{base}) = 100\%$, 50% , 1% and $\phi = 10^\circ$	217
Fig. 3.4b Workspace Volume for $\gamma = 0^\circ$, $(r_{end}/r_{base}) = 100\%$, 50% , 1% and $\phi = 350^\circ$	218

Fig. 3.4c Workspace Volume for $\gamma = 0^\circ$, $(r_{end}/r_{base}) = 100\%$, 50% , 1% and $\phi = 20^\circ$	219
Fig. 3.4d Workspace Volume for $\gamma = 0^\circ$, $(r_{end}/r_{base}) = 100\%$, 50% , 1% and $\phi = 340^\circ$	220
Fig. 3.4e Workspace Volume for $\gamma = 0^\circ$, $(r_{end}/r_{base}) = 100\%$, 50% , 1% and $\phi = 30^\circ$	221
Fig. 3.4f Workspace Volume for $\gamma = 0^\circ$, $(r_{end}/r_{base}) = 100\%$, 50% , 1% and $\phi = 330^\circ$	222
Fig. 3.4g Workspace Volume for $\gamma = 0^\circ$, $(r_{end}/r_{base}) = 100\%$, 50% , 1% and $\phi = 40^\circ$	223
Fig. 3.4h Workspace Volume for $\gamma = 0^\circ$, $(r_{end}/r_{base}) = 100\%$, 50% , 1% and $\phi = 320^\circ$	224
Fig. 3.4i Workspace Volume for $\gamma = 0^\circ$, $(r_{end}/r_{base}) = 100\%$, 50% , 1% and $\phi = 50^\circ$	225
Fig. 3.4j Workspace Volume for $\gamma = 0^\circ$, $(r_{end}/r_{base}) = 100\%$, 50% , 1% and $\phi = 310^\circ$	226
Fig. 3.4k Workspace Volume for $\gamma = 0^\circ$, $(r_{end}/r_{base}) = 100\%$, 50% , 1% and $\phi = 60^\circ$	227
Fig. 3.4l Workspace Volume for $\gamma = 0^\circ$, $(r_{end}/r_{base}) = 100\%$, 50% , 1% and $\phi = 300^\circ$	228
Fig. 3.5a Workspace Volume for $\gamma = 15^\circ$, $(r_{end}/r_{base}) = 100\%$, 50% , 1% and $\phi = 10^\circ$	229
Fig. 3.5b Workspace Volume for $\gamma = 15^\circ$, $(r_{end}/r_{base}) = 100\%$, 50% , 1% and $\phi = 350^\circ$	230
Fig. 3.5c Workspace Volume for $\gamma = 15^\circ$, $(r_{end}/r_{base}) = 100\%$, 50% , 1% and $\phi = 20^\circ$	231
Fig. 3.5d Workspace Volume for $\gamma = 15^\circ$, $(r_{end}/r_{base}) = 100\%$, 50% , 1% and $\phi = 340^\circ$	232

Fig. 3.5e Workspace Volume for $\gamma = 15^\circ$, $(r_{end}/r_{base}) = 100\%$, 50% , 1% and $\phi = 30^\circ$	233
Fig. 3.5f Workspace Volume for $\gamma = 15^\circ$, $(r_{end}/r_{base}) = 100\%$, 50% , 1% and $\phi = 330^\circ$	234
Fig. 3.5g Workspace Volume for $\gamma = 15^\circ$, $(r_{end}/r_{base}) = 100\%$, 50% , 1% and $\phi = 40^\circ$	235
Fig. 3.5h Workspace Volume for $\gamma = 15^\circ$, $(r_{end}/r_{base}) = 100\%$, 50% , 1% and $\phi = 320^\circ$	236
Fig. 3.5i Workspace Volume for $\gamma = 15^\circ$, $(r_{end}/r_{base}) = 100\%$, 50% , 1% and $\phi = 50^\circ$	237
Fig. 3.5j Workspace Volume for $\gamma = 15^\circ$, $(r_{end}/r_{base}) = 100\%$, 50% , 1% and $\phi = 310^\circ$	238
Fig. 3.6a Workspace Volume for $\gamma = 30^\circ$, $(r_{end}/r_{base}) = 100\%$, 50% , 1% and $\phi = 10^\circ$	239
Fig. 3.6b Workspace Volume for $\gamma = 30^\circ$, $(r_{end}/r_{base}) = 100\%$, 50% , 1% and $\phi = 350^\circ$	240
Fig. 3.6c Workspace Volume for $\gamma = 30^\circ$, $(r_{end}/r_{base}) = 100\%$, 50% , 1% and $\phi = 20^\circ$	241
Fig. 3.6d Workspace Volume for $\gamma = 30^\circ$, $(r_{end}/r_{base}) = 100\%$, 50% , 1% and $\phi = 340^\circ$	242
Fig. 3.6e Workspace Volume for $\gamma = 30^\circ$, $(r_{end}/r_{base}) = 100\%$, 50% , 1% and $\phi = 30^\circ$	243
Fig. 3.6f Workspace Volume for $\gamma = 30^\circ$, $(r_{end}/r_{base}) = 100\%$, 50% , 1% and $\phi = 330^\circ$	244
Fig. 3.7a Workspace Volume for $\gamma = 45^\circ$, $(r_{end}/r_{base}) = 100\%$, 50% , 1% and $\phi = 10^\circ$	245
Fig. 3.7b Workspace Volume for $\gamma = 45^\circ$, $(r_{end}/r_{base}) = 100\%$, 50% , 1% and $\phi = 350^\circ$	246

Fig. 3.7c Workspace Volume for $\gamma = 45^\circ$, $(r_{end}/r_{base}) = 100\%$, 50% , 1% and $\phi = 20^\circ$	247
Fig. 3.7d Workspace Volume for $\gamma = 45^\circ$, $(r_{end}/r_{base}) = 100\%$, 50% , 1% and $\phi = 340^\circ$	248
Fig. 3.18a GCI for $\gamma = 0^\circ$, $(r_{end}/r_{base}) = 100\%$, 50% , 1% , and $\phi = 10^\circ$	249
Fig. 3.18b GCI for $\gamma = 0^\circ$, $(r_{end}/r_{base}) = 100\%$, 50% , 1% , and $\phi = 350^\circ$	250
Fig. 3.18c GCI for $\gamma = 0^\circ$, $(r_{end}/r_{base}) = 100\%$, 50% , 1% , and $\phi = 20^\circ$	251
Fig. 3.18d GCI for $\gamma = 0^\circ$, $(r_{end}/r_{base}) = 100\%$, 50% , 1% , and $\phi = 340^\circ$	252
Fig. 3.18e GCI for $\gamma = 0^\circ$, $(r_{end}/r_{base}) = 100\%$, 50% , 1% , and $\phi = 30^\circ$	253
Fig. 3.18f GCI for $\gamma = 0^\circ$, $(r_{end}/r_{base}) = 100\%$, 50% , 1% , and $\phi = 330^\circ$	254
Fig. 3.18g GCI for $\gamma = 0^\circ$, $(r_{end}/r_{base}) = 100\%$, 50% , 1% , and $\phi = 40^\circ$	255
Fig. 3.18h GCI for $\gamma = 0^\circ$, $(r_{end}/r_{base}) = 100\%$, 50% , 1% , and $\phi = 320^\circ$	256
Fig. 3.18i GCI for $\gamma = 0^\circ$, $(r_{end}/r_{base}) = 100\%$, 50% , 1% , and $\phi = 50^\circ$	257
Fig. 3.18j GCI for $\gamma = 0^\circ$, $(r_{end}/r_{base}) = 100\%$, 50% , 1% , and $\phi = 310^\circ$	258
Fig. 3.18k GCI for $\gamma = 0^\circ$, $(r_{end}/r_{base}) = 100\%$, 50% , 1% , and $\phi = 60^\circ$	259
Fig. 3.18l GCI for $\gamma = 0^\circ$, $(r_{end}/r_{base}) = 100\%$, 50% , 1% , and $\phi = 300^\circ$	260
Fig. 3.19a GCI for $\gamma = 15^\circ$, $(r_{end}/r_{base}) = 100\%$, 50% , 1% , and $\phi = 10^\circ$	261
Fig. 3.19b GCI for $\gamma = 15^\circ$, $(r_{end}/r_{base}) = 100\%$, 50% , 1% , and $\phi = 350^\circ$	262
Fig. 3.19c GCI for $\gamma = 15^\circ$, $(r_{end}/r_{base}) = 100\%$, 50% , 1% , and $\phi = 20^\circ$	263
Fig. 3.19d GCI for $\gamma = 15^\circ$, $(r_{end}/r_{base}) = 100\%$, 50% , 1% , and $\phi = 340^\circ$	264
Fig. 3.19e GCI for $\gamma = 15^\circ$, $(r_{end}/r_{base}) = 100\%$, 50% , 1% , and $\phi = 30^\circ$	265
Fig. 3.19f GCI for $\gamma = 15^\circ$, $(r_{end}/r_{base}) = 100\%$, 50% , 1% , and $\phi = 330^\circ$	266

Fig. 3.19g GCI for $\gamma = 15^\circ$, $(r_{end}/r_{base}) = 100\%$, 50% , 1% , and $\phi = 40^\circ$	267
Fig. 3.19h GCI for $\gamma = 15^\circ$, $(r_{end}/r_{base}) = 100\%$, 50% , 1% , and $\phi = 320^\circ$	268
Fig. 3.19i GCI for $\gamma = 15^\circ$, $(r_{end}/r_{base}) = 100\%$, 50% , 1% , and $\phi = 50^\circ$	269
Fig. 3.19j GCI for $\gamma = 15^\circ$, $(r_{end}/r_{base}) = 100\%$, 50% , 1% , and $\phi = 310^\circ$	270
Fig. 3.20a GCI for $\gamma = 30^\circ$, $(r_{end}/r_{base}) = 100\%$, 50% , 1% , and $\phi = 10^\circ$	271
Fig. 3.20b GCI for $\gamma = 30^\circ$, $(r_{end}/r_{base}) = 100\%$, 50% , 1% , and $\phi = 350^\circ$	272
Fig. 3.20c GCI for $\gamma = 30^\circ$, $(r_{end}/r_{base}) = 100\%$, 50% , 1% , and $\phi = 20^\circ$	273
Fig. 3.20d GCI for $\gamma = 30^\circ$, $(r_{end}/r_{base}) = 100\%$, 50% , 1% , and $\phi = 340^\circ$	274
Fig. 3.20e GCI for $\gamma = 30^\circ$, $(r_{end}/r_{base}) = 100\%$, 50% , 1% , and $\phi = 30^\circ$	275
Fig. 3.20f GCI for $\gamma = 30^\circ$, $(r_{end}/r_{base}) = 100\%$, 50% , 1% , and $\phi = 330^\circ$	276
Fig. 3.21a GCI for $\gamma = 45^\circ$, $(r_{end}/r_{base}) = 100\%$, 50% , 1% , and $\phi = 10^\circ$	277
Fig. 3.21b GCI for $\gamma = 45^\circ$, $(r_{end}/r_{base}) = 100\%$, 50% , 1% , and $\phi = 350^\circ$	278
Fig. 3.21c GCI for $\gamma = 45^\circ$, $(r_{end}/r_{base}) = 100\%$, 50% , 1% , and $\phi = 20^\circ$	279
Fig. 3.21d GCI for $\gamma = 45^\circ$, $(r_{end}/r_{base}) = 100\%$, 50% , 1% , and $\phi = 340^\circ$	280
Fig. 3.3c Schematic of BP and MP for $\gamma = 30^\circ$	281
Fig. 3.3d Schematic of BP and MP for $\gamma = 15^\circ$	282

ABSTRACT

A cable suspended parallel robot is based on the idea of a Gough-Stewart platform parallel link manipulator. The unique feature is that cables are used as the links and winches are the actuators. Traditional parallel manipulators generally use heavy prismatic actuators, which tend to be large and cumbersome. Using cables dramatically decreases the weight of the parallel robot and increases the distance in which it is able to reach. These characteristics make cable suspended parallel robots useful for tasks such as cargo handling, inspection of airplanes, shipbuilding, and camera positioning in large sport stadiums.

Cables are only capable of supplying pulling tension forces but no pushing compressive forces. The attractive features related to the use of cables, as opposed to traditional actuators, are that cables have a large strength to weight ratio, lightweight, and can extend long distances. Since cables can only pull and not push, the existing theory on parallel robots is slightly modified to incorporate the additional characteristic pertaining to the cables. The current work includes some existing theory on cable-actuated robots and parallel manipulators to form additional ideas about the workspace, design, and control of a 6-degree-of-freedom cable suspended parallel robot.

Chapter 1

INTRODUCTION

Parallel robots have recently become a large area of interest in the field of robotics. A parallel robot consists of an end effector, or moving platform (MP), with n degrees of freedom connected by at least two independent kinematic chains to a fixed inertial base, or base platform (BP). The end effector is used to perform an operation or move through the environment with respect to its inertial base. The MP is actuated through n simple actuators and, typically, the number of degrees of freedom is equal to the number of n independent kinematic chains. The actuators are generally, but not limited to, prismatic or revolute actuators. Parallel manipulators are known as closed-loop kinematic chains [1]. The robot that drew a large amount of attention in the past has been the classic serial robot most likely because the analysis of the parallel robots is slightly more complex than that of the serial robot. A serial robot is constructed from a succession of rigid bodies each linked to a previous and following rigid body by one degree of freedom. The first link is fixed to an inertial system such as the ground and the last link, referred to as the end effector, is free standing. Serial robots are known as an open-looped kinematic chain [1].

Parallel robots generally have larger load capacities, faster, more accurate motions, and a larger stiffness throughout their workspace as compared to the serial robots [1]. These attributes make them quite attractive in real world applications. The increased popularity of parallel robots has opened many questions on the analysis and control of new designs as well as their potential applications. Prismatic actuators are

used to drive many of the traditional parallel robots. Some common prismatic actuators include hydraulic and pneumatic pistons and motor driven lead screws. These systems tend to be large, heavy, cumbersome and limited by their length of travel. Cable suspended parallel robots are slightly different from the traditional parallel robots. In a cable suspended parallel robot, the MP is suspended and manipulated by the attached cables that are connected to the BP. The cables act as the prismatic links and motor driven winches actuate the cables. Using cables dramatically decreases the weight of the parallel robot and increases the distance in which it is able to reach.

The National Institute of Standards and Technology (NIST) designed a parallel robot known as RoboCrane, where the traditional actuators are replaced by cable winch systems and the MP is suspended from the cables. A cable suspended parallel robot was also designed and constructed at the University of Delaware by the author to analyze the workspace, design, and control of the robot. The design included an articulated base, which allowed the variation of the cable connection points to be changed to different radii. This thesis will study the design and workspace of cable suspended parallel robots. The work presented in this thesis will also include the preliminary work for a hybrid position/force controller tailored to the dynamics of a cable suspended parallel robot.

This chapter will begin with a brief history on the parallel robot and attempt to expose a view on the evolution of the robotic research in the direction of parallel robot designs. It then will continue with a general literature survey of the subject matter covered throughout the thesis. Finally, the chapter ends discussing the topics that will be addressed in the subsequent chapters of this thesis.

1.1 History

The use of robotics has been recognized as an efficient tool to the industrial world ([2 - 4]). Many of the underlying mechanisms, which form the robotic structures today, have existed long before robotics technology was born and date back many centuries. In 1947, Gough presented the basic principals and design for a six-degree-of-freedom parallel mechanism to test the wear and tear of tires for the Dunlop tire industry. In 1955, Dunlop built a functional prototype of Gough's design as shown in Fig. 1.1.

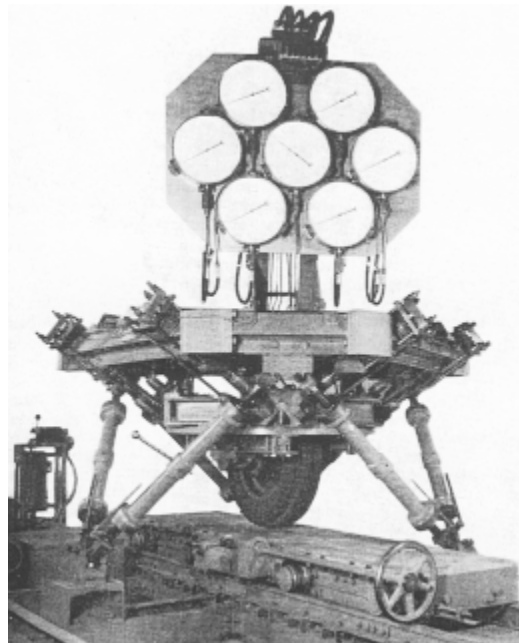


Fig. 1.1 Original Gough Platform Tire Testing Machine Constructed in 1955

The parallel mechanism consisted of a MP and BP connected together by six linear prismatic actuators. The MP is connected to each prismatic link by a ball and socket joint and the BP is connected to each link by a universal joint. The MP is adjusted through manually turning each lead screw to obtain new positions and orientations. The

tire is attached to the MP and rides on a conveyer belt system, which simulates the road surface conditions [5]. In 2000, the Dunlop tire-testing machine was upgraded to a newer modern robotic version where the position and orientation of the MP is automated through a computer interface. A picture of the Dunlop tire-testing machine is given in Fig. 1.2, which is still operational and used today.



Fig. 1.2 Upgraded Gough Platform Tire Testing Machine used today

In 1965, Stewart proposed an idea for a six-degree-of-freedom parallel platform mechanism [6]. Throughout his article, he suggested several parallel robotic designs including flight simulators, ocean oil drilling platforms and multi cable cranes. A conceptual sketch of Stewart's flight simulator design is given in Fig. 1.3.

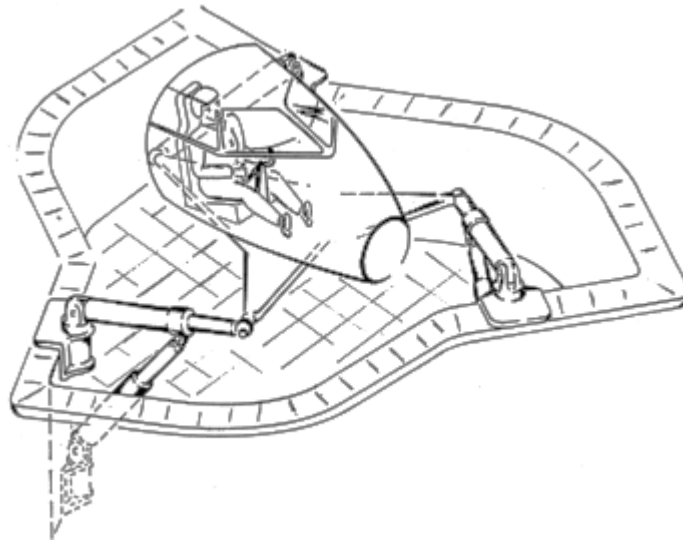


Fig. 1.3 Stewart Platform and the flight simulator

At the end of his article, Stewart suggested a modification of his design, which was the Gough platform created several years before. The actual Stewart platform design found little attention in field of robotics however, the Gough platform has received tremendous interest and various designs, including those suggested by Stewart, are used as parallel robots today based on this model. Ironically, many of the parallel robots are incorrectly acknowledged as the Stewart platform when it is actually Gough's design that is being addressed. For the sake of reference purposes, this paper will refer to the parallel platform as the Stewart-Gough platform.

Despite the early emergence of the parallel mechanism, many of the robotic manipulators currently used in industry incorporate a large number of serial robots. The modeling and control of serial robots tend to be easier than the parallel robots. The computational capacity needed to control a serial robot is less intense than that of the general parallel robot. In addition, serial robots generally have a larger workspace than

parallel robots. However, serial robots tend to possess very small load capacities compared to the actual weights of the robot themselves and are less accurate. This is a result of the open link cantilever structure of the serial robot where each link must support its own weight plus all of the following links and the weight of a possible load at the end effector. The cantilever structure of the serial robot provokes small deflections in each link that adds up to a large positioning error at the end effector. Several methods are used to correct this undesirable feature. One possible solution is to stiffen up each link by adding more material to each link making it stronger and less susceptible to deflection. Increasing the weight of the manipulator's link causes the inertial forces of each link to become more prevalent during the robot's dynamic motion. In order to compensate for the increased inertial forces, larger motors and/or gearing are sought out to preserve the desired velocity and acceleration characteristics. A larger motor increases the mass and inertia of the system and gearing creates problems with backlash, cogging, and friction.

The study of flexible robots is another area of research that tries to compensate for the deflection, backlash, etc through modeling flexible behavior of the robot and using the model in the control law ([7 - 23]). While the subject of flexible robotics generally focuses on increasing the accuracy of the robots, the issue of dramatically increasing the robots strength to weight ratio is not completely addressed. One journal article addressed this specific issue and set up criteria for the design of serial manipulators with a high stiffness to weight ratio [24]. This paper provided useful information relevant to the design of the serial robot links. However, in industry, serial robots are readily available from various companies and to design a robot from scratch may not be reasonable. With this in mind, researchers ventured into areas which focused

on using existing robots in redundant ([19], [21], [25 - 36]) and cooperative ([37 - 44]) tasks. A redundant robotic system is one in which the system has more degrees of freedom than is needed to obtain the desired position and orientation. Examples of redundant parallel manipulators include ARCHI a redundant parallel manipulator ([45 - 46]), ParaDex a 7-DOF redundant parallel manipulator [47], and Eureka a 5-DOF redundant parallel mechanism [48]. A cooperative robotic system is one where two or more independent robotic systems work together to complete a desired task. The types of robotic systems that are of interest here are those where two or more robots hold the same object and work together as they execute the desired task. The combined efforts allow the robots to increase their load carrying capabilities, stiffness and accuracy. For instance, consider two serial robots each possessing six-degree-of-freedom, holding a rigid block. The base of each serial robot is fixed to the ground and each end effector is rigidly connected to the block creating a closed loop system. The weight of the block is distributed among each supporting robot. Since each robot already possesses six-degrees-of-freedom, the combined efforts of both robots generally results in a system that is redundantly actuated. To execute a task both robots must cooperate in such a way that each robot does not fight against the other. Additional related subjects include the study of robotic hand designs ([19], [49 - 53]), robotic hand controllers ([11], [19], [43], [52], [54 - 60]) and walking robots ([61 - 65]). However, these mechanisms are intermittently closed looped mechanisms because as the leg is lifted from the ground or the fingers discontinue contact with an object, the mechanism is no longer a true closed loop manipulator at that instant.

In studying different mechanisms such as the robotic hands, cooperative serial robots and cooperative redundantly actuated robots it is seen that when an object is

manipulated through multiple contact points the stiffness is increased, the system has a larger strength to weight ratio and the deflection is decreased. As these systems became more understood and as computer and electronic technology advanced, the design of parallel robots as an alternative likewise grew. The cooperative redundantly actuated system of robots does increase the agility, stiffness, and accuracy but the redundant actuation is not always needed.

The multiple closed loop kinematic chains that make up the parallel robot provide several advantages over that of the open loop serial robot. The parallel robotic manipulators appeared attractive because they can be designed with the minimum number of actuators. For robotic manipulators it is desirable for the robot to have one actuator for each degree of freedom. Reducing the number of actuators simplifies the control, design, and reduces cost. In addition, as the MP and any additional load attached to the MP, dynamically executes a task, the total weight of the MP and load is distributed throughout the supporting limbs. Since each limb only carries a fraction of the total weight, the stress experienced by each limb and the strain within the limb is reduced thus increasing the stiffness, accuracy and potential load capacity. Therefore, the parallel robots are able to perform faster, more accurate motions throughout their workspace compared to serial robots because of their closed loop structure, and the size and weight of the actuator itself can be reduced.

The concept of the parallel mechanism is not by any means a new idea. Gough designed a functional parallel mechanism in 1947 as previously mentioned. Even before this structure was created, there are documentations of parallel mechanisms that date back much earlier. Many of the preexisting parallel mechanical designs have been utilized and transformed into parallel robotic manipulators that are used today. Some

parallel robots that currently exist today include TRI-SCOTT 6-DOF decoupled parallel manipulator [66], DELTA parallel robot ([67 - 70]), Delta-4 parallel robot [71], CaPaMan Cassino parallel manipulator with 3-DOF [72], modified 6-PSU parallel platform [73], PARA-ARM a 5-Bar parallel manipulator [74], and Agile Eye a 3-DOF spherical parallel camera orienting mechanism [75]. Existing applications where parallel robots are used include milling machines [76], 4-DOF heavy parts handling [77], 5-DOF in-parallel haptic interface [78], underground excavation [79], force reflecting joystick ([80 - 82]), radiation applications [83], active vibration isolation [84], and climbing tubular structures [85], just to name a few. Other designs of parallel robots with 3-DOF include the cylindrical parallel robots [86], spherical parallel robots ([75], [87 - 91]), and translational parallel robots ([92 - 104]). Additional articles on planar parallel robots are presented in references ([90], [105 - 121]). One article analyzed several N-DOF parallel manipulators with a passive constraining leg and prismatic actuators for the possible use in machining applications to increase the accuracy of the end effector [122]. Industrial applications of the parallel robot include NASA's flight simulators, VARIAX milling machine, and Fanuc's 6-DOF positioning parallel robot. Another area where parallel robots began to draw attention was in the field of miniaturized manipulation such as micro and nano manipulators ([123 - 128]). Applications where miniaturized parallel robots may be used include surgery and electronic component assembly. Since the parallel robots are to operate on such a small scale, new actuation techniques must be sought out. Some actuation techniques and designs that are currently being researched include MEMS [125], Nitinol wires [123], flexure hinges ([128 - 129]), and piezoelectric elements ([124], [129 - 131]). Tasks at this scale benefit from the stiffness and accuracy that is provided by the parallel robot structure. Other research has focused on parallel

robots known as minimanipulators ([132 - 135]). Minimanipulators are parallel manipulators, which contain the minimum number of limbs that connect MP to the BP. Minimanipulators are designed with the base mounted revolute actuators and inextensible limbs to reduce the number of limbs. This specific type of design focuses on lowering the inertia, weight, number of parts, and complexity of analysis.

Parallel robots possess many attractive attributes where serial robots lack. However, parallel robots typically have a small useful workspace because of the limitations on the prismatic actuator's range of motion. Some research has focused on combining serial and parallel robots in an attempt to increase the useful workspace ([136 - 141]). Other research has investigated the analysis of hyper-redundant parallel robots ([142 - 143]). Hyper-redundant parallel robots consist of serially connected parallel robotic units in successive stages. Some existing hyper-redundant parallel robots include a hyper-redundant snake [144], planar elephant robotic trunk [145], a backbone cable driven parallel robot [146], TETROBOT highly hyper-redundant parallel robot [147], and a double parallel robot for enlarging workspace [143]. These robotic systems provide an increased workspace although the weight of the system also increases.

Cable driven parallel robots provide means of increasing the useful workspace without significantly increasing the weight of the mechanism. The cables possess a high strength to weight ratio and can easily be actuated through a winch system. Since the cables are small, the inertial properties of the cables are usually considered negligible. The analysis of cable driven mechanisms is not a relatively large area in the study of robotics. However, as the robotics technology matures, the analysis of cable driven mechanisms expands. Cable driven mechanisms are also referred to as wire or tendon driven mechanisms.

Research has designed and proposed cable driven mechanisms for various applications. The wire driven parallel manipulator designs range from an apparatus used to measure a robot's pose [148], to conceptual designs for space applications [149], to haptic interfaces [109], and instrumentation for wind tunnels [150]. Other wire actuated mechanisms include a cable driven backbone [146], FALCON an ultra high speed wire driven parallel robot [151], tendon driven manipulators for force transmission ([152 - 153]), cable parallel manipulator for large radio telescope [154], planar parallel cable driven robots ([116 - 118], [121], [155 - 157]) and tendon driven hands ([50], [55]). Additional references on the design of general tendon driven manipulators are given in references ([158 - 159], [160 - 161]). One parallel mechanism obtains 6-DOF in a design where three cables are attached to a central prismatic link [162]. Analysis of the workspace and design of tendon driven parallel robots are found in references ([156], [163 - 166]).

The cable suspended parallel robot is another area in wire driven mechanisms that has received a great deal of attention especially by the National Institute for Standards and Technology (NIST). A large area where cable suspended mechanisms are used is in the field of industrial cranes. Most crane designs today incorporate the use of only one main cable to manipulate a given load. For these types of cranes, the load must be oriented by a crew of riggers on the ground, who help suppress the sway and adjust the orientation of the load when in motion. This process becomes very time consuming because the load in most cases must be moved very slowly in order to avoid potentially dangerous sway or spin of the load. Some papers on crane concepts used today are found in references ([167 - 168]). Different methods of control have been proposed to help suppress the undesirable motion resulting from crane operation ([169 - 171]). These

articles address that multiple cables provide additional control of the manipulated load. Some research on parallel robotic cranes includes CABLEV a three cable robotic crane attached to an overhead trolley system [172], a cable array robotic crane that uses four cables ([20], [173]), and a three-cable crane [174]. NIST created a 6-DOF cable suspended parallel robotic crane which they called RoboCrane ([175 - 178]). RoboCrane uses six cables to connect the MP to the BP. As its name suggests, RoboCrane is a robotic crane where the MP is suspended from the BP and held in position by not only the cables but also gravity. The actuation of a cable suspended parallel robot is different from other parallel manipulators because cable can only possess tension forces.

NIST proposed numerous applications for RoboCrane [177]. Some of the suggested usages for RoboCrane include waste tank redemption [179], underwater platform [180], a lunar rover [181], double hull ship welder [182], large-scale manufacturing ([183 - 184]), ship repair [185], shipbuilding [186], bridge construction [187], and sculpting assistance [188]. NIST has also developed real time control and virtual environment software that is used to control and study various applications for the NIST RoboCrane ([189 - 193]). The NIST RoboCrane is shown in Fig. 1.4 where it is used in a material handling lifting application and Fig. 1.5 shows RoboCrane as a lunar rover.

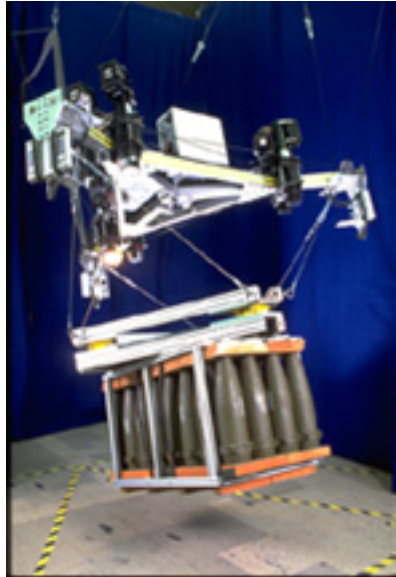


Fig. 1.4 NIST RoboCrane in a lifting application



Fig. 1.5 NIST RoboCrane Lunar Rover Prototype Model

A systematic analysis for the particular geometry selected in the design of the cable suspended parallel robot by NIST is still lacking. The University of Delaware has designed a 6-DOF cable suspended parallel robot to analyze the different aspects of its design, workspace and control. Pictures of the University of Delaware cable suspended parallel robot is shown in Fig 1.6.

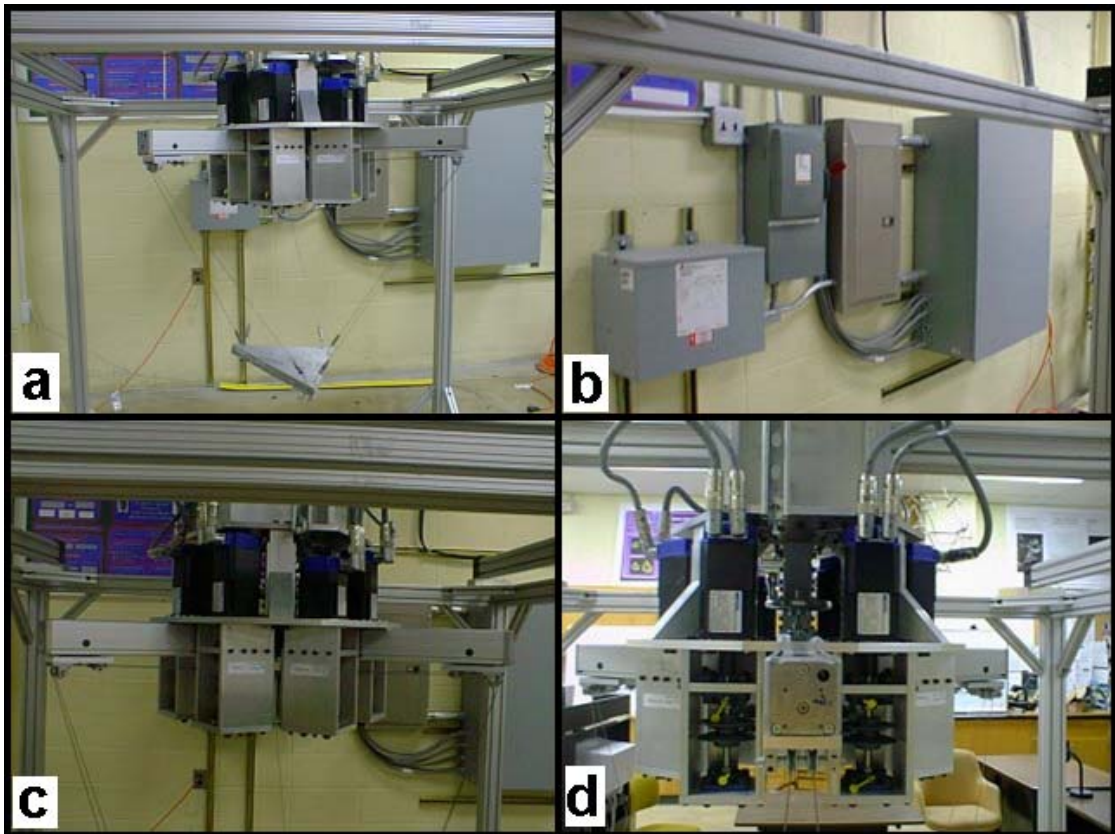


Fig. 1.6 University of Delaware Cable Suspended Parallel Robot

The cable robot is designed with six cables that attach the MP to the BP. The BP is designed so that the cable connection points can be uniformly configured to

different radial positions. The BP is also mounted to a two-dimensional gantry crane system that is used to reposition the BP + MP system to different positions parallel to the ground. The analysis of the workspace, path planning, and position control has already been previously conducted for the University of Delaware cable robot in references ([194 - 197]). Previous work on design and workspace optimization of planar cable suspended parallel robot initiated the design and construction of a prototype, which now exists at the University of Delaware ([106 - 107]). The robot was constructed by Lauren McIllwain with the assistance of the author on the design.

1.2 Literature Survey

This section will present a literary survey of research topics that are used throughout each of the successive chapters. There is a large amount of research in the literature related to parallel robots and mechanisms. A large majority of the literature has been published within the previous decade. The parallel manipulators studied include various designs, techniques of actuation, methods of control, and analysis tools used to identify and compare the performance of each system. The preceding sections mentioned several articles on various designs of parallel robots. Some additional articles found in the literature that discussed the general synthesis and selection of parallel robot designs are given in references ([110], [135], [155], [163], [198 - 212]). The isotropic design of parallel manipulators is considered in references ([213 - 214]) and for tendon driven manipulators [160]. The study of the optimal design of parallel manipulators is found in references ([69 - 70], [93], [100], [103], [106], [108], [215 - 220]). Other techniques and analysis for the design of robotic manipulators are found in references ([221 - 226]). To analyze a particular robotic design, generally the first step is to define the kinematic and dynamic equations for the robot.

Kinematics is the study of the motion of a body or system of bodies without regard to the forces and/or moments that cause it. There are several methods used to determine the kinematic equations for robotic manipulators. Some of these methods include Kirchhoff's circulation law [227], Screw Theory ([19], [228 - 238]), quaternion kinematics ([239 - 240]), quasi-coordinate modeling [241], and instantaneous kinematics ([242 - 243]). Some of the techniques used to reduce the complexity of the kinematic equations include Grobner-Sylvester hybrid method [244], Bernstein polynomials [87], Hansen's algorithm based on numeric interval analysis [245], Natural Orthogonal Complement (NOC) ([246 - 247]), least squares [248], damped least squares [249], polar least squares [250], decoupled polar least squares ([251 - 252]), and other numerical methods ([80], [253 - 259]). Other methods can be found in references ([25], [78], [120], [260 - 262]).

When creating the kinematic equations two different approaches are generally used. The first approach, known as the inverse kinematics, assumes that the location of the end effector is known relative to some inertial frame and the joint displacements of the robot are desired. Therefore, given a desired end effector location, determine the joint displacements that allow the end effector to reach this point. The second approach, referred to as the forward or direct kinematics, is opposite to that of the inverse kinematics. For the forward kinematics, the joint displacements are given and the end effector position is desired.

The forward kinematic problem for serial manipulators is much easier to solve than the inverse kinematic problem. This is opposite to that of the parallel manipulator where the inverse kinematic solution is much easier to solve for than the forward kinematics. For many parallel manipulators the forward kinematics is quite

complex and its solution presents a challenging task because the kinematic equations are highly nonlinear. Many efforts have been put forth in the past towards finding the solution to the kinematic equations for various parallel manipulators. One article addresses the forward kinematic solutions for a large set of 6-DOF parallel manipulator designs [202]. The difficulty with the forward kinematics of parallel manipulators is finding the solution in closed form. The definition of a closed-form solution is defined differently within the robotics community. Generally, the definition of a closed-form solution falls within two different categories. The first category is the analytical closed-form solution where no numerical routines are used to obtain an n th order polynomial in one variable. The other definition of closed-form kinematic solution is sometimes referred to as the real-time closed-form solution. For these solutions, the analytical kinematic equations can be solved within milliseconds on a computer since only linear and/or quadratic equations are to be solved with simple trigonometric functions. There are very few parallel manipulators, which yield real-time analytic closed-form solutions. Very few parallel mechanisms present closed form solutions to their kinematic equations. Some of the designs, which have found closed form solutions, usually are those with reduced degrees-of-freedom or possess a unique configuration [263]. Other designs with a closed form solution include the (3-2-1) parallel mechanism ([263 - 265]), (3-1-1-1) fully parallel manipulator ([253], [263]), (6-6P) parallel mechanism [240] and (3-PSP) parallel mechanism [266]. For the (6-6) parallel manipulator the kinematic equations were reduced to a 20-degree polynomial, which has the potential of up to 40 possible solutions ([244], [255], [267 - 271]). The (6-6) parallel manipulator is defined as one where six prismatic links connect the MP to the BP where the connection points do not intersect one another. The forward kinematic equations for other parallel manipulators

were also derived. It was discovered that the (3-6) parallel manipulator yielded a 16-degree polynomial equation ([258], [272]), and the (3-3) parallel manipulator yielded an 8-degree polynomial equation [273]. It was also found that a 3-DOF translational 3UPU parallel manipulator also yielded an 8-degree polynomial with 16 possible configuration solutions [98]. The multiple possible solutions resulting from the polynomial equations complicate the kinematics. In many cases, numerical methods must be used to find the kinematic solutions. Additional articles that find a closed form solution to the kinematic equations of various parallel manipulator designs are found in references ([111 - 113], [274 - 275]).

Other techniques incorporate additional sensors in the design, which allows the direct kinematic solution to be found in closed form. One article in the literature found a closed form kinematic solution using three extra linear displacement sensors on a nearly general (6-6) parallel manipulator ([276 - 277]). Another design integrated two extra rotary sensors to solve the direct kinematic equations for a general (6-6) parallel manipulator [278]. A different design incorporated a camera into the parallel manipulator to find a linear algebraic solution to the direct kinematics, which was solved using the least-squares numerical method [248]. In another article, a four cable suspended parallel crane used two infrared sensors and one position sensor to obtain a closed form kinematic solution [279]. Other articles where extra sensors were used to solve the kinematic equations of parallel manipulators are found in references ([270], [280 - 282]). The kinematics for cable suspended parallel manipulators is studied in references ([112 - 113], [279]). Additional articles addressing the kinematics of wire driven parallel manipulators are found in references ([117], [148], [153], [168]).

Several articles are written on the kinematics of many specific parallel mechanisms. Many of the parallel mechanism and designs have faced resistance from the industrial community because of their inherent complex features. Directions toward broadening the communication between industry and research and development community have been established through many technical organizations. These organizations have been constructed to focus on organizing and dispersing the research and development efforts. As a result, of these efforts, the analysis of parallel manipulators is becoming a well-developed topic. Additional discussion on the concerns and issues that arise with the general analysis and acceptance of parallel mechanism is found in reference [216].

Dynamics is the study of forces and moments, which act on a body or system of bodies. When the forces and/or moments acting on a body or system of bodies do not cause any motion, then the body or system of bodies is in static equilibrium. Articles discussing the static balancing of parallel manipulators are given in references ([88], [283]). In reference [117], the kinematics and statics of a cable driven planar parallel manipulator is analyzed. There are several different methods used to determine the dynamic equations of robotic manipulators. Some common methods used include Newton-Euler force and moment equations ([57], [67], [118], [143], [284 - 289]), Lagrangian energy method ([14], [20], [71], [172 - 173], [290 - 299]), Hamilton's principle of virtual work ([68], [174], [232], [291], [297], [299 - 305]), and Kane's method [306]. Techniques used to compute the dynamic equations of motion are found in references ([239], [241], [247], [260], [291], [302], [305], [307 - 311]). Another area of study common to robotic manipulators is the analysis of the manipulator's forward and inverse force transmission capabilities. The forward force transmission analysis is to

determine the forces and moments generated at the end effector given the magnitude of the manipulator's actuator forces and moments. Conversely, the inverse force transmission analysis is to determine the forces and moments of the actuators given the forces and moments at the end effector. The force transmission is important for topics relating to manipulator design and force controlled tasks. Some articles found on force transmission analysis are discussed in references ([60], [152 - 153], [237], [312 - 314]). The study of the inertial properties is another important topic of robotic manipulators. References presented on this topic are found in ([141], [298], [315 - 317]). For cable suspended parallel robots, the inertial properties of the cables can be neglected due to the relative size and mass of the cable with respect to the remaining manipulator and load. Considering the mass and inertial properties of the cables significantly complicates the dynamic equations of motion for parallel manipulators. Numerical approximations may be necessary in order to solve the dynamic equations. One reference found discusses the models for slackened and tightened cables [318]. This may be useful for cable robots where the deflection and weight of the cable are significant and must be modeled.

Once the kinematic and dynamic equations for a particular robot are derived, there are several tools and performance measures used to evaluate and further define the robot. The workspace is one common tool used to evaluate the manipulator's motion and orientation abilities. The workspace is generally defined as the set of locations within the surrounding environment that can be reached by a point on the end effector with a desired orientation. When defining the workspace for a manipulator the translational DOF and rotational DOF must both be represented. Consider a 6-DOF serial robot with all revolute joints and a wrist. The first three revolute joints are used to obtain the translational degrees of freedom and the wrist incorporates the remaining three rotational

degrees of freedom. Therefore, if the end effector of a serial robot is able to translate to a point in the workspace the wrist is used to obtain the desired orientations. It is understood that not all the orientations may be possible though a large range is generally possible. The workspace for a serial robot is generally represented by a three dimensional volume of points. The volume of the workspace is a good representation of the translational motion however, the orientations possible at each point within the workspace are not always clear. Despite this, the three dimensional volume is still a good representation of the workspace for a serial robot because in many cases if the end effector is able to reach the point in space the wrist can obtain a large range of orientations. When studying serial robots, two different types of workspaces are generally studied. The first type of workspace is known as the *Dexterous Workspace*, which is defined as the set of locations where the end effector is able to reach with all orientations. The second type of workspace is the *Reachable* or *Maximal Workspace* and is defined as the set of locations that the end effector is able to reach with at least one orientation.

This combination of the translational and rotational degrees of freedom is not easily represented with a parallel robotic manipulator because the translational and rotational components are coupled through the multiple closed loop structure. Therefore, the complete workspace should be represented in a six-dimensional workspace, which is graphically not possible. As a result, the workspace of a parallel manipulator must be divided up into subsets of the workspace. In reference [1], Merlet presented six definitions used to describe the different types of workspace of a parallel manipulator. Two of the definitions have already been mentioned. Another type of workspace is the *Constant Orientation* or *Translation Workspace*, which is defined as the set of locations

of the end effector can reach with a fixed orientation. The *Orientation Workspace* is the set of possible rotations around a fixed reference point in space. The *Inclusive Orientation Workspace* is the set of locations that the end effector may reach with at least one orientation from a selected range of orientations imposed on the orientation parameter. Finally, the *Total Orientation Workspace* is the set of locations that the end effector may reach with all the orientations from a selected range of orientations imposed on the orientation parameter.

Various articles present definitions for the workspace of robotic manipulators. These articles discussed different types of workspace such as the orientation workspace ([256], [319 - 323]), constant orientation or translational workspace ([256], [322], [324 - 325]), inclusive orientation workspace ([303], [326]), total orientation workspace ([256], [322]), reachable or maximal workspace ([19], [256], [327 - 329]), dexterous workspace ([19], [256], [330]), manipulability workspace [331], dynamic workspace [42], controllable workspace [164], and workspace boundaries ([332 - 333]). The definitions of the different workspaces possible are found in reference [1]. Articles presenting methods for calculating the workspace of a robotic manipulator are given in ([91], [325], [334 - 335]). Other articles analyzing the workspace optimization are found in references ([105 - 108], [205], [333], [336 - 338]). Some articles found in the literature discussing the workspace for tendon and wire driven mechanisms are given in references ([106 - 107], [148], [156], [165 - 166], [197], [339]). Additional references related to the workspace analysis for parallel robotic manipulators are discussed in ([340 - 341]).

The singularity analysis of parallel manipulators is a very important step in the design of robotic manipulators. The singularities are the poses where the robotic

manipulator either gains or loses a degree of freedom. Articles written on methods for calculating the singularities are found in references ([137], [342 - 347]). Other articles analyzing the singularities of specific robotic manipulators are given in ([74], [101 - 102], [108], [110], [114], [138], [143], [165], [200], [214], [220], [234], [348 - 352]). Additional references that discuss the singularity analysis of general classes and types of manipulators are found in ([89], [115], [353 - 355]).

When analyzing a robotic manipulator it is useful to not only know the singular configurations but also know when the manipulator is close to the singular configurations. The ideal manipulator is one that is isotropically designed. Various methods are used to determine how close a manipulator is to a singular or isotropic configuration. Many of these methods focus on analyzing the manipulator's Jacobian matrix. The Jacobian is a mathematical mapping between the joint rates in the joint space to the linear and angular velocities in the task space. Some common methods used to analyze the Jacobian matrix of a robotic manipulator include the calculating the manipulability ([19], [32], [37], [145], [246], [331], [338], [356 - 358]), condition number ([19], [215], [246], [359 - 361]), conditioning index [246], and global conditioning index (GCI) ([103], [211], [359], [362]). The mathematical derivation and explanation of the manipulability is given in references ([19], [246], [338], [358]) and the GCI is given in reference [359].

The analysis of the Jacobian matrix is useful when studying the workspace of a robotic manipulator. The manipulability is defined as the square root of the determinant of the product of the manipulator Jacobian by its transpose ([246], [358]). The condition number, conditioning index, and GCI calculations all deal with the eigenvalues of the manipulator's Jacobian matrix. The eigenvalues are all calculated for

a specific orientation and location of the end effector. Therefore, not only does each point in the workspace need to be considered but also each orientation associated with each individual point must be considered. For parallel robots, this analysis becomes extremely cumbersome and overwhelming. The calculation of the GCI provides a larger overview of the behavior of the condition number throughout the workspace. For instance, if the MP of a parallel robot was fixed to a constant orientation and condition number was calculated at all the translational points surrounding the BP at some discrete grid size. Then all these points could be somehow averaged such that a “global” insight is given for that particular workspace, hence the calculation of the GCI. The condition number, conditioning index provide a means to measure the level of how close the manipulator is to an isotropic or singular configuration for a specific location and orientation in space. The GCI provides an overall general idea of the behavior of the condition number throughout the workspace in question. This thesis will use the condition number, conditioning index and GCI for the performance analysis of the cable suspended parallel robot. The derivation and further explanation of the condition number, conditioning index, and GCI will be provided later in Chapter 3.

Another common method of measuring the performance of a robotic manipulator is by analyzing the stiffness of the robot. The stiffness map of a robot provides the designer with an insight to the capabilities of the end effector to apply a force within its workspace. Stiffness mapping is a common method used to portray the level of stiffness of a manipulator within its workspace. Articles written on the stiffness mapping of parallel manipulators is discussed in reference ([205], [363]). The stiffness analysis for specific parallel manipulator platforms is presented in references ([36], [76],

[128], [132], [134], [165], [186], [205], [364 - 366]). In references [186], stiffness of a cable suspended parallel robotic crane (RoboCrane) is analyzed.

For a robotic manipulator the study of topics such as the workspace, singularities, stiffness, performance indices, and the derivation of the kinematic and dynamic equations are all fundamental steps to the analysis of any robotic design. Generally, these areas of study provide aid to the fabrication and formation of control laws and trajectory planning. The control of robotic manipulators is an ever-growing topic in an already enormous field of study. Many articles have been written on the control of robotic manipulators. Small portions of these articles are written specifically for parallel manipulators. The control of parallel manipulators is becoming an increased topic of interest in the field of robotics. Some controllers written for parallel manipulators include inverse dynamics and H_∞ position control [367], stiffness control [368], adaptive control ([369 - 370]), fractional order control [371], integer order control [371], force and acceleration control [18], position control ([45 - 46]), PD feedback Lyapunov control [33], cooperative control ([38 - 39]), instantaneous kinematic control [242], impedance control [372], and feedback position control ([194 - 196]). The area of control that is relevant to the current study includes position and force controllers. The focus of this is with the combined interaction of the position and force controllers specifically, the hybrid force/position controller. There is an increased interest in force control to enhance the functionality of robotic manipulators in assembly operations. A few articles found in the literature investigating assembly tasks using robotic manipulators are given in references ([2], [38], [373 - 383]). Other areas where force controllers have become popular are with haptic interfaces [384], and object detection [385]. Robotic manipulators are not usually driven in force control mode in industry.

The main method of control in industry typically relates to various position control schemes. Industry is always seeking means of expanding the capability of robot manipulators to encompass a greater number of possible tasks. The study of force controllers has recently increased and become more prominent in research due to the technological advances with computers and sensors. The computer process power has dramatically increased allowing the implementation of more sophisticated controllers to be used on robotic manipulators.

Some of the different types of force controller designs include impedance control ([372], [374], [379], [386 - 400]), sliding mode force control ([169], [396], [401 - 404]), switching control [405], active compliant force control ([54], [406 - 410]), and passive compliant force control [7]. Various articles written on the hybrid force/position controller are found in references ([10], [12], [23], [398], [411 - 420]). Some of the hybrid force/position control variants include fractional order hybrid force/position control [421], robust hybrid force/position control [30], robust nonlinear hybrid force/position control [16], dynamic hybrid force/position control [422], hybrid impedance control [423], and quasi-static hybrid force/position control [17]. Other forms of force controllers include parallel force/position control ([52], [398 - 399] [424 - 425]), integral force control with robustness [426], hybrid force/vision control ([427 - 428]), force feedback adaptive control [11], model-based force control for machining [429], adaptive force control for position/velocity controlled robots [430], and dynamic hybrid force/velocity control [431].

The force sensors used to measure the interaction between the environment and the manipulator generally are noisy. Many articles have been written on the stability of the force controller due to this undesirable noise ([409], [417], [419], [432]). Another

area where the notion of stability of force controllers arises is in the flexibility of the links ([10], [433]). In addition, several articles have analyzed the contact transition between the end effector and its environment ([54], [59], [291], [394], [432], [434 - 436]). This transition between the environment and the end effector become very important in routine operations such as assembly tasks. Several articles are written on assembly tasks for robotic manipulators ([2], [38], [373 - 383]). A large source of error and instability that arises in forced controlled tasks results from friction. There are several sources of friction, which provoke instability. One source of friction resides within the manipulator itself, and another source results from the interaction with the environment. If the sources can be identified, measured, and modeled then the performance of the system can be improved. However, this is not an easy task especially when various environmental parameters are changed dynamically. A few articles written on identifying and modeling friction are given in references ([12], [191], [316 - 317], [381], [437 - 445]). Additional references addressing the control of friction are found in ([12], [43], [381], [442 - 443], [445 - 450]).

An area of study related to all robotic manipulators is that of calibration of the manipulator. When a robotic manipulator is created the machining of the individual parts is done within some prescribed tolerance. This tolerance leads to small inaccuracies within the system. Very little calibration analysis has been found for parallel manipulators. Some articles found on the calibration of parallel manipulators are given in references ([82], [261], [451 - 455]).

The general goal of a robotic manipulator is for it to execute some task or set of tasks. The measure of how well a particular robotic manipulator accomplishes a given task is achieved through the performance analysis of the robotic manipulator. These

performance measures can also be used in the creation of a trajectory. For instance, the condition number can be used as a guide to the areas within a workspace that are singular or isotropic. Other techniques are used to specify and create the trajectory for a parallel manipulator. Articles discussing the trajectory planning and sensor processing for manipulators are given in references ([137], [456 - 461]).

A significant volume of work has been done on the analysis of parallel manipulators in the areas of kinematics and design. Fewer studies are found in the areas of dynamics and control for parallel manipulators, although this subject is slowly growing. The topics related to singularities and workspace analysis is also increasing, but many studies surround specific platforms. However, it is very apparent that recently there is a huge increase in areas pertaining to parallel robotic research. The current study intends to support and provide additional insight to the proliferating analysis of robotic research.

1.3 Scope of Present Work

The types of robotic manipulators addressed within this thesis pertain to parallel manipulators, specifically the cable suspended parallel robots. The goal of the present work is to analyze the workspace and design of a cable suspended parallel robot and present preliminary ideas for a hybrid force/position controller. In Chapter 2, the kinematic and dynamic equations of motion are derived for a general, six-degree-of-freedom (DOF) cable suspended parallel robot. Thesis equations will be used in the subsequent chapters as needed. Chapter 3 presents a study on the workspace and design of a refined range of cable suspended parallel robots. In Chapter 4, practical design applications are presented to confirm the trends discovered in the preceding chapter. In that chapter, three surface cases are presented for which the cable suspended parallel

robots are to orient their MP perpendicular to the surface to see how much surface the robot is able to reach. Chapter 5 presents preliminary ideas for a hybrid force/position controller to be used on a cable suspended parallel robot. The derivation for a hybrid force/position controller to be used on a traditional parallel robot is given and a Matlab Simulink program was created to simulate the controller. A discussion on the use of this type of controller for a cable suspended parallel robot is also briefly given. Finally, the conclusions of the thesis are presented in Chapter 6 with a brief interlude to possible future work.

Chapter 2

KINEMATICS AND DYNAMICS

2.1 Introduction

In this chapter, the kinematics and dynamics of a cable suspended parallel robot will be derived. Kinematics and dynamics are the basis for the analysis of any robotic system. Once these equations are obtained, the designer is able to evaluate and/or automate the system. A large portion of research has been devoted towards obtaining the kinematic and dynamic equations, however there exists only a limited set of papers pertaining to cable actuated robots and still a smaller set focuses on cable suspended parallel robots.

Kinematics is the study of the motion of a body or system of bodies without regard to the forces and/or torques that cause it. Kinematics deals with the position, velocity, and acceleration as well as any higher order derivatives of the position vector. The derivatives are taken with respect to time as well as other variables. When studying kinematics the only concern is with the geometrical and time properties of motion. As a designer, there are two separate approaches to the kinematic study of a body or system of bodies. One perspective is the *kinematic synthesis*, which entails designing a manipulator to attain certain desired kinematic properties. For example, given a preferred range of positions and orientations and possibly the time derivatives of an end effector, the designer must determine the geometry and joint motion of the manipulator. The other perspective, termed

kinematic analysis, is opposite to that of the kinematic synthesis. The kinematic analysis involves the study of motion among the various links of a given manipulator. This approach has two additional subsets referred to in robotics as the *forward* or *direct kinematics* and the *inverse kinematics*, which will be defined in the following sections. For parallel robots, the inverse kinematics can be found exactly in closed form as will be seen in the following sections. The study of the kinematics is a key point of interest in the analysis and design of robotic manipulators [326].

Dynamics is the study of the forces and/or torques applied to a system, which causes motion of a body or system of bodies. If the forces and/or torques are applied to a system and do not cause any motion, then the system is in static equilibrium. The dynamics of robotic manipulators is a very complex subject. In general, the manipulator is to perform some prescribed motion in its environment. To execute this motion, input forces and/or torques must be applied to the manipulator's active joints. In the calculation of the needed input force and torque, one must also incorporate all the external forces acting on the manipulator. This calculation can become extremely complex due to possible uncontrollable phenomenon such as friction. In many cases, approximations for friction are made. The validation of these approximations is usually justified through the performance characteristics observed from a model and experimental data.

This chapter will begin with a brief explanation of the forward and inverse kinematics. Next, the position kinematics is presented for a general cable suspended parallel robot. This is followed with the derivation of the velocity kinematics using the geometric Jacobian and the analytic Jacobian through the form of the inverse kinematics. Then the kinematic acceleration equations are derived for the general

parallel robot. After that, the dynamics are presented using the Newton Euler method and the Jacobian given is shown to be the same as the one derived for the kinematics in the geometric Jacobian section. Next, the inertia term is briefly mentioned for completeness and finally a conclusion is given summarizing the chapter.

2.2 Kinematics

When defining a task or trajectory for a robotic manipulator the individual links that make up the manipulator must be carefully coordinated to accomplish the desired task. The task is defined according to either the joint space or the task space. The task space sometimes referred to as the operational space, end effector space, or Cartesian space, is the subset of the vector space that includes all locations of the end effector. If the desired motion is define in task space, then the end effector trajectory is given and the joint motions that product this motion are to be found. The solution to this problem is to solve for the inverse kinematics. The joint space or actuator space is the vector space spanned by the joint variables. If the trajectory is defined according to the joint space then, the individual joint inputs are given and the resulting end effector motion is to be determined. The solution method sought out for this problem is the forward or direct kinematics.

2.2.1 Forward or Direct Kinematics

Forward kinematics is defined as follows: given the joint displacements and their time derivatives determine the trajectory of the end effector. In the case of cable robots, the joint displacements are the lengths of the cables, which attach the MP to the BP. An exact closed form solution for the forward kinematics of a six degree-of-freedom parallel manipulator based on the actuating link displacements has not

been found. The complexity of the solutions resides within the multiple kinematic chains that make up the parallel robot. For the general 6-6 Stewart-Gough Platform, the forward kinematic equations yield up to 40 solutions ([267], [269]). It has been proven that for a 3-3 Stewart-Gough Platform the solutions can be reduced to an 8th degree polynomial, which yields up to 8 solutions. Other solutions are available for specific parallel robots, but no closed form solution exists for the general 6-6 Stewart-Gough Platform based only on the given cable lengths. Many control schemes implemented on robots use the forward kinematics as part of their feedback. For parallel robots, this information is in general found only through the numerical approximations of the forward kinematic equations. This inhibits the controllers' effectiveness because of increased computation time for the forward kinematics and accuracy of numerical approximation procedure. Common methods employed to avoid the cumbersome nonlinear forward kinematic equations include the placement of additional sensors. These sensors are used to speed up computation time and accuracy and in some cases yield a closed form solution. If three additional displacement transducers are placed between the MP and BP, an exact closed form solution can be found.

2.2.2 Inverse Kinematics

Inverse kinematics is defined as follows: given the end effector trajectory determine the corresponding joint displacements, velocities, and accelerations. The solution of the inverse position kinematics can be found in closed form for parallel robots. This is different from that of serial robots where the inverse position kinematics in general yields multiple solutions. The kinematics for the cable

suspended parallel robots will be derived in the inverse kinematic since the equations can be found in closed form.

2.2.3 Kinematic and Geometric Model

In this section, the kinematic equations for a general 6-6 cable suspended parallel robot is derived. The inertial coordinate system \mathcal{F}_O with its base unit vectors $\mathbf{x}_O, \mathbf{y}_O, \mathbf{z}_O$ is attached to the BP, with its origin located at the point O , as shown in Fig. 2.1. The coordinate frame for the MP \mathcal{F}_E with base unit vectors $\mathbf{x}_E, \mathbf{y}_E, \mathbf{z}_E$ is located at the center of mass O_E of the MP. There are six connection points on the BP represented as (b_1, \dots, b_6) and similarly six connection points on the end effector or MP, represented as (a_1, \dots, a_6) . A sketch of a general cable suspended parallel robot is given in Fig. 2.1.

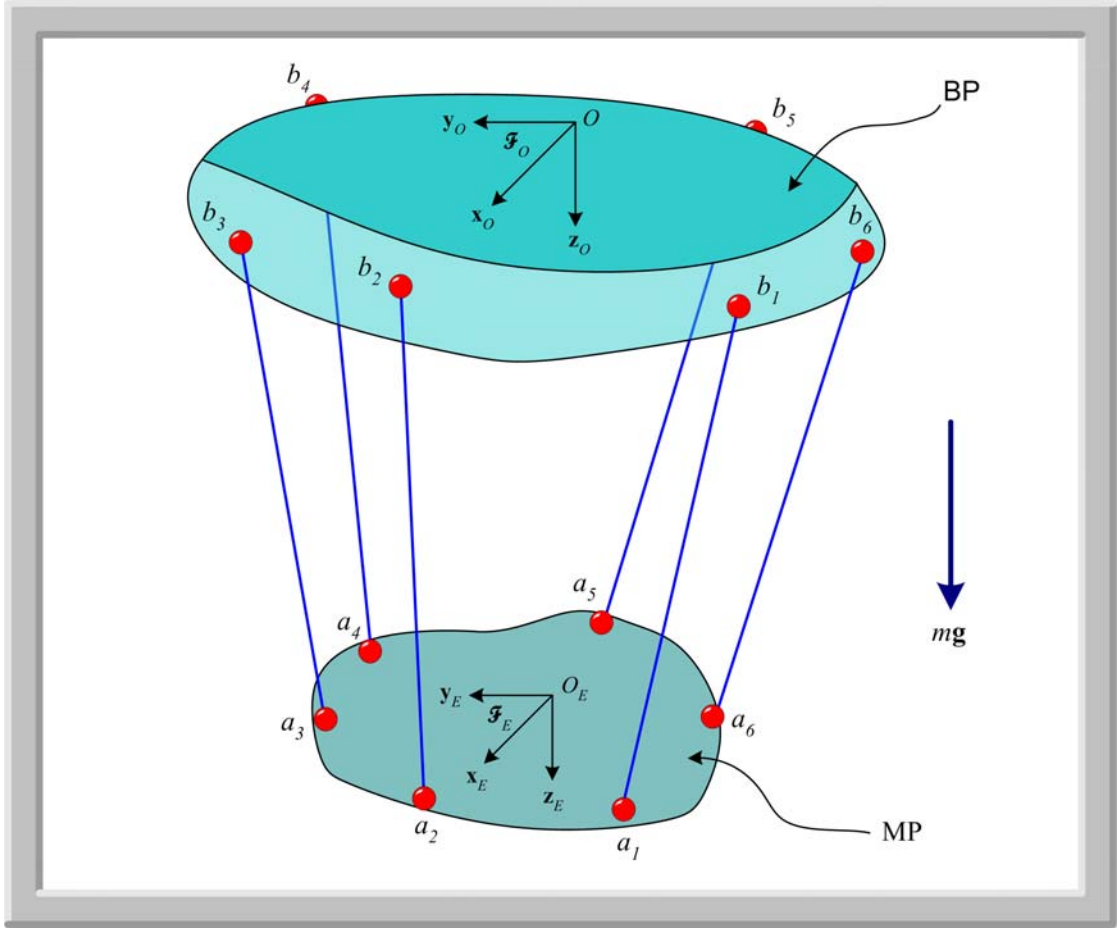


Fig. 2.1 General 6-6 cable suspended parallel manipulator

The position vector from point b_i to point a_i , i.e. the cable vector ${}^O\mathbf{l}_i$ shown in Fig. 2.2, can be expressed with respect to frame \mathcal{F}_O as

$${}^O\mathbf{l}_i = {}^O\mathbf{p} + {}^O\mathbf{R}_E {}^E\mathbf{a}_i - {}^O\mathbf{b}_i, i = 1, \dots, 6 \quad (2.1)$$

where ${}^O\mathbf{p}$ represents the position vector from point O to point O_E expressed in frame \mathcal{F}_O . The vector ${}^O\mathbf{b}_i$ is the position vector from point O to point b_i expressed in frame \mathcal{F}_O . The vector ${}^E\mathbf{a}_i$ is the position vector from point O_E to point a_i expressed with

respect to frame \mathcal{F}_E . The matrix ${}^o\mathbf{R}_E$ is the rotation matrix relating the orientation of the moving frame \mathcal{F}_E with respect to the fixed frame \mathcal{F}_O . The rotation matrix given in Eq. (2.2) is a fixed axis rotation sequence by the roll-pitch-yaw angles of ψ , θ , and ϕ about the \mathbf{x}_O , \mathbf{y}_O , and \mathbf{z}_O axis, respectively.

$$(2.2) \quad {}^o\mathbf{R}_E = \begin{bmatrix} c(\phi)c(\theta) & -s(\phi)c(\psi) + c(\phi)s(\theta)s(\psi) & s(\phi)s(\psi) + c(\phi)s(\theta)c(\psi) \\ s(\phi)c(\theta) & c(\phi)c(\psi) + s(\phi)s(\theta)s(\psi) & -c(\phi)s(\psi) + s(\phi)s(\theta)c(\psi) \\ -s(\theta) & c(\theta)s(\psi) & c(\theta)c(\psi) \end{bmatrix}$$

In Eq. (2.2), $s(\arg)$ and $c(\arg)$ stand for the sine and cosine of the appropriate angle argument (\arg). The magnitude of vector ${}^o\mathbf{l}_i$ is

$$l_i^2 = \|\mathbf{l}_i\|^2 = l_{ix}^2 + l_{iy}^2 + l_{iz}^2, i = 1, \dots, 6. \quad (2.3)$$

This equation is the position constraint equation for the cable suspended parallel manipulator. The constraint equation is an expression relating the behavior of the bodies that make up the system through their bounding interactions and/or connections that restricts their motion.

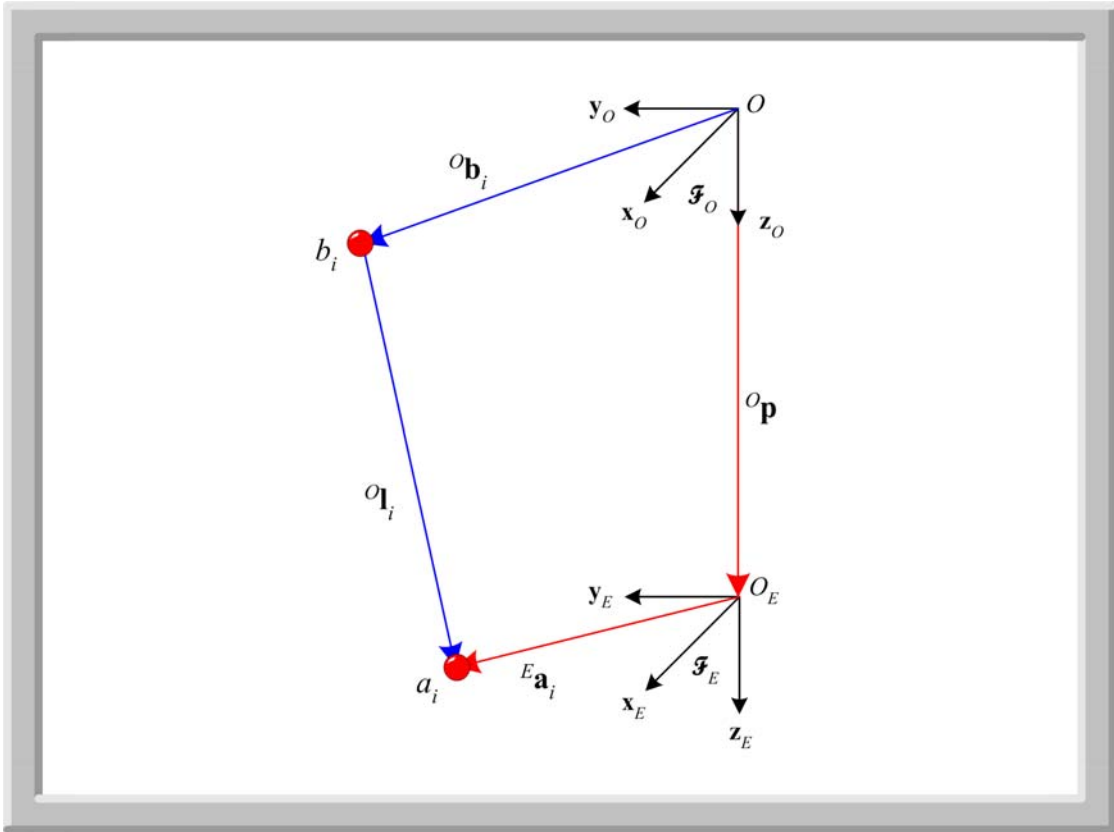


Fig. 2.2 Modeling of the i^{th} cable vector loop

There are several ways of determining the relationship between the joint velocities and the velocity of the MP. This relationship is in terms of a matrix called the Jacobian matrix or simply the Jacobian. The Jacobian is a mapping between the joint rates in the joint space to the linear and angular velocities in the task space. There are two common methods used to determine the Jacobian for a robotic manipulator. One method is referred to as the geometric Jacobian and the other is analytic Jacobian. Both of these methods will be described in the following sections.

2.2.4 Geometric Jacobian

The geometric Jacobian, as its name suggests, uses the geometry of the individual robotic manipulator under study. An equation representing the magnitude of the cable lengths is sought in order to derive the velocity kinematics in the inverse form. This equation referred to as the constraint equation can be derived by taking the dot product of the position vector loop Eq. (2.1). The dot product operator is performed because it yields a convenient expression that eliminates the unactuated joint rates when the velocity relationship is derived. Taking the vector loop equation and rewriting it using the dot product notation the equation becomes,

$$l_i^2 = {}^o\mathbf{l}_i \bullet {}^o\mathbf{l}_i = ({}^o\mathbf{l}_i)^T ({}^o\mathbf{l}_i), \quad (2.4)$$

$$l_i^2 = ({}^o\mathbf{p} + {}^o\mathbf{R}_E {}^E\mathbf{a}_i - {}^o\mathbf{b}_i)^T ({}^o\mathbf{p} + {}^o\mathbf{R}_E {}^E\mathbf{a}_i - {}^o\mathbf{b}_i). \quad (2.5)$$

Taking the derivative of the left and right hand sides of Eq. (2.5) with respect to time, one obtains the velocity relationship given in Eq. (2.6) shown below.

$$2l_i\dot{l}_i = ({}^o\dot{\mathbf{p}} + {}^o\dot{\mathbf{R}}_E {}^E\mathbf{a}_i)^T ({}^o\mathbf{p} + {}^o\mathbf{R}_E {}^E\mathbf{a}_i - {}^o\mathbf{b}_i) + ({}^o\mathbf{p} + {}^o\mathbf{R}_E {}^E\mathbf{a}_i - {}^o\mathbf{b}_i)^T ({}^o\dot{\mathbf{p}} + {}^o\dot{\mathbf{R}}_E {}^E\mathbf{a}_i) \quad (2.6)$$

A dot above each term denotes the derivative with respect to time. The terms ${}^o\dot{\mathbf{b}}_i$ and ${}^E\dot{\mathbf{a}}_i$ are both set equal to zero because they are both constant in the expressed frame.

Now, using the linear algebra identity

$$\mathbf{c}^T\mathbf{d} + \mathbf{d}^T\mathbf{c} = 2\mathbf{c}^T\mathbf{d} = 2\mathbf{d}^T\mathbf{c}, \quad (2.7)$$

where \mathbf{c} and \mathbf{d} are arbitrary column vectors, Eq. (2.6) is simplified to

$$2l_i\dot{l}_i = 2\left({}^o\mathbf{p} + {}^o\mathbf{R}_E {}^E\mathbf{a}_i - {}^o\mathbf{b}_i\right)^T \left({}^o\dot{\mathbf{p}} + {}^o\dot{\mathbf{R}}_E {}^E\mathbf{a}_i\right). \quad (2.8)$$

Substitute Eq. (2.1) into Eq. (2.8) and simplify to obtain,

$$l_i\dot{l}_i = \left({}^o\mathbf{1}_i\right)^T \left({}^o\dot{\mathbf{p}} + {}^o\dot{\mathbf{R}}_E {}^E\mathbf{a}_i\right). \quad (2.9)$$

Now the derivative of the rotation matrix is

$${}^o\dot{\mathbf{R}}_E = {}^o\boldsymbol{\Omega}_E {}^o\mathbf{R}_E, \quad (2.10)$$

where ${}^o\boldsymbol{\Omega}_E$ is defined as the angular velocity cross product matrix of the MP with respect to the BP.

$${}^o\boldsymbol{\Omega}_E = \begin{bmatrix} 0 & -\omega_z & \omega_y \\ \omega_z & 0 & -\omega_x \\ -\omega_y & \omega_x & 0 \end{bmatrix} = {}^o\boldsymbol{\omega}_E \times = {}^o\dot{\mathbf{R}}_E {}^o\mathbf{R}_E^T \quad (2.11)$$

After substituting Eq. (2.10) into Eq. (2.9) it becomes

$$l_i\dot{l}_i = \left({}^o\mathbf{1}_i\right)^T \left({}^o\dot{\mathbf{p}} + {}^o\boldsymbol{\Omega}_E {}^o\mathbf{R}_E {}^E\mathbf{a}_i\right). \quad (2.12)$$

Applying the substitution

$${}^o \mathbf{a}_i = {}^o \mathbf{R}_E {}^E \mathbf{a}_i \quad (2.13)$$

to Eq. (2.12), simplifies the results and yield the following equation,

$$l_i \dot{l}_i = {}^o \mathbf{l}_i^T {}^o \dot{\mathbf{p}} + {}^o \mathbf{l}_i^T ({}^o \boldsymbol{\omega}_E \times {}^o \mathbf{a}_i). \quad (2.14)$$

Now using the linear algebra identity

$$\begin{aligned} \mathbf{u} \bullet \mathbf{v} \times \mathbf{w} &= \mathbf{v} \times \mathbf{w} \bullet \mathbf{u} \\ &= \mathbf{v} \bullet \mathbf{w} \times \mathbf{u} \\ &= \mathbf{w} \times \mathbf{u} \bullet \mathbf{v} \end{aligned} \quad (2.15)$$

where \mathbf{u} , \mathbf{v} and \mathbf{w} are arbitrary column vectors, Eq. (2.14) can be rewritten as

$$l_i \dot{l}_i = {}^o \mathbf{l}_i^T {}^o \dot{\mathbf{p}} + ({}^o \mathbf{a}_i \times {}^o \mathbf{l}_i)^T {}^o \boldsymbol{\omega}_E, \quad i = 1, \dots, 6. \quad (2.16)$$

Eq. (2.16) represents six equations, one for each of the kinematic chains present in the 6-DOF cable suspended parallel manipulator. Now rearrange Eq. (2.16) in the following matrix form,

$$\mathbf{B} \dot{\mathbf{q}} = \mathbf{A} \mathbf{t} \quad (2.17)$$

where matrix and vector variables in Eq. (2.17) are defined in the subsequent equations Eq. (2.18), Eq. (2.19), Eq. (2.20), and Eq. (2.21) given below.

$$\mathbf{t} = \begin{bmatrix} {}^o \dot{\mathbf{p}} \\ {}^o \boldsymbol{\omega}_E \end{bmatrix} \quad (2.18)$$

$$\dot{\mathbf{q}}_i = [\dot{l}_1, \dot{l}_2, \dot{l}_3, \dot{l}_4, \dot{l}_5, \dot{l}_6]^T \quad (2.19)$$

$$\mathbf{B} = \begin{bmatrix} l_1 & 0 & 0 & 0 & 0 & 0 \\ 0 & l_2 & 0 & 0 & 0 & 0 \\ 0 & 0 & l_3 & 0 & 0 & 0 \\ 0 & 0 & 0 & l_4 & 0 & 0 \\ 0 & 0 & 0 & 0 & l_5 & 0 \\ 0 & 0 & 0 & 0 & 0 & l_6 \end{bmatrix} \quad (2.20)$$

$$\mathbf{A} = \begin{bmatrix} {}^o\mathbf{l}_1^T, & ({}^o\mathbf{a}_1 \times {}^o\mathbf{l}_1)^T \\ {}^o\mathbf{l}_2^T, & ({}^o\mathbf{a}_2 \times {}^o\mathbf{l}_2)^T \\ {}^o\mathbf{l}_3^T, & ({}^o\mathbf{a}_3 \times {}^o\mathbf{l}_3)^T \\ {}^o\mathbf{l}_4^T, & ({}^o\mathbf{a}_4 \times {}^o\mathbf{l}_4)^T \\ {}^o\mathbf{l}_5^T, & ({}^o\mathbf{a}_5 \times {}^o\mathbf{l}_5)^T \\ {}^o\mathbf{l}_6^T, & ({}^o\mathbf{a}_6 \times {}^o\mathbf{l}_6)^T \end{bmatrix} \quad (2.21)$$

The vector \mathbf{t} is known as the twist vector of the MP. The twist vector incorporates the linear and angular velocities of the MP with respect to the BP. The matrices \mathbf{B} and \mathbf{A} are the partial geometric Jacobians. Pre-multiplying both sides of Eq. (2.17) by the inverse of \mathbf{B} yields

$$\dot{\mathbf{q}} = \mathbf{J}\mathbf{t} \quad (2.22)$$

where,

$$\mathbf{J} = \mathbf{B}^{-1}\mathbf{A} \quad (2.23)$$

is the Geometric Jacobian matrix of the robot manipulator. Eq. (2.22) presents the relationship between the joint velocities given by $\dot{\mathbf{q}}$ and the twist velocities \mathbf{t} of the MP.

The same result given by Eq. (2.22) could also be obtained if initially both sides of Eq. (2.9) were divided by l_i , the magnitude of the cable lengths and then simplified with the substitutions. To verify this, Eq. (2.24) shows the division by l_i just mentioned.

$$\dot{l}_i = \begin{pmatrix} {}^o\mathbf{1}_i \\ l_i \end{pmatrix}^T ({}^o\dot{\mathbf{p}} + {}^o\mathbf{R}_E {}^E\mathbf{a}_i) \quad (2.24)$$

Now substitute Eq. (2.10), Eq. (2.11), and Eq. (2.13) into Eq. (2.24) and expand the result in matrix form yields Eq. (2.22). The Jacobian is the same as given by Eq. (2.23) multiplied out which is seen from the following equation as

$$\mathbf{J} = \begin{bmatrix} \left(\frac{o\mathbf{l}_1}{l_1} \right)^T, & \left({}^o\mathbf{a}_1 \times \left(\frac{o\mathbf{l}_1}{l_1} \right) \right)^T \\ \left(\frac{o\mathbf{l}_2}{l_2} \right)^T, & \left({}^o\mathbf{a}_2 \times \left(\frac{o\mathbf{l}_2}{l_2} \right) \right)^T \\ \left(\frac{o\mathbf{l}_3}{l_3} \right)^T, & \left({}^o\mathbf{a}_3 \times \left(\frac{o\mathbf{l}_3}{l_3} \right) \right)^T \\ \left(\frac{o\mathbf{l}_4}{l_4} \right)^T, & \left({}^o\mathbf{a}_4 \times \left(\frac{o\mathbf{l}_4}{l_4} \right) \right)^T \\ \left(\frac{o\mathbf{l}_5}{l_5} \right)^T, & \left({}^o\mathbf{a}_5 \times \left(\frac{o\mathbf{l}_5}{l_5} \right) \right)^T \\ \left(\frac{o\mathbf{l}_6}{l_6} \right)^T, & \left({}^o\mathbf{a}_6 \times \left(\frac{o\mathbf{l}_6}{l_6} \right) \right)^T \end{bmatrix}. \quad (2.25)$$

Both Eq. (2.23) and Eq. (2.25) are the Geometric Jacobian form of a general cable suspended parallel robot. The Geometric Jacobian will be used exclusively in this study.

2.2.5 Analytic Jacobian

In this section, the general derivation of the analytic Jacobian will be presented. The analytic Jacobian as opposed to the geometric Jacobian is different in that it directly uses the differentiation of the kinematic functions with respect to the joint variables when deriving the inverse kinematics. Obtaining a closed form solution for the position and orientation variables is not always possible. However, for parallel robots it is easier to derive the direct or forward kinematic equations. The direct kinematic functions are found from the dot product of the vector loop equations given by Eq. (2.5), which is written again below for quick reference.

$$l_i = \sqrt{\left({}^o\mathbf{p} + {}^o\mathbf{R}_E {}^E\mathbf{a}_i - {}^o\mathbf{b}_i \right)^T \left({}^o\mathbf{p} + {}^o\mathbf{R}_E {}^E\mathbf{a}_i - {}^o\mathbf{b}_i \right)} \quad (2.26)$$

It is again noted here that Eq. (2.26) represents six equations, each equation for a given value of i , where $i=1,\dots,6$ and that this equation is the constraint equation. This constraint equation is the equation gives the magnitude of the actuator link lengths. Where \mathbf{q} is defined as the vector of the links lengths as

$$\mathbf{q} = [l_1, l_2, l_3, l_4, l_5, l_6]^T. \quad (2.27)$$

At this point for the geometric Jacobian Eq. (2.26) is differentiated with respect to time and carefully separated to form the geometric Jacobian relating the joint rate of displacements to the linear and angular velocity of the MP. To find the analytic Jacobian Eq. (2.26) is not differentiated with respect to time but with respect to the variables representing the position $({}^o p_x, {}^o p_y, {}^o p_z)$ and orientation (ψ, θ, ϕ) of the MP. For simplicity, these variables will be denoted in the vector

$$\mathbf{X}_A = [{}^o p_x, {}^o p_y, {}^o p_z, \psi, \theta, \phi]^T. \quad (2.28)$$

Eq. (2.26) is written in the form where the joint variables are easily known given \mathbf{X}_A . The form sought out for the analytical Jacobian is one that transforms the MP linear velocities and the time rate changes of orientation of the MP to the joint rates of the actuators which is shown by the following equation

$$\dot{\mathbf{q}} = \mathbf{J}_A \dot{\mathbf{X}}_A. \quad (2.29)$$

The analytic Jacobian \mathbf{J}_A is expressed as

$$\mathbf{J}_A = \frac{\partial \mathbf{q}}{\partial \mathbf{X}_A} = \begin{bmatrix} \frac{\partial l_1}{\partial {}^o p_x} & \frac{\partial l_1}{\partial {}^o p_y} & \frac{\partial l_1}{\partial {}^o p_z} & \frac{\partial l_1}{\partial \psi} & \frac{\partial l_1}{\partial \theta} & \frac{\partial l_1}{\partial \phi} \\ \frac{\partial l_2}{\partial {}^o p_x} & \frac{\partial l_2}{\partial {}^o p_y} & \frac{\partial l_2}{\partial {}^o p_z} & \frac{\partial l_2}{\partial \psi} & \frac{\partial l_2}{\partial \theta} & \frac{\partial l_2}{\partial \phi} \\ \frac{\partial l_3}{\partial {}^o p_x} & \frac{\partial l_3}{\partial {}^o p_y} & \frac{\partial l_3}{\partial {}^o p_z} & \frac{\partial l_3}{\partial \psi} & \frac{\partial l_3}{\partial \theta} & \frac{\partial l_3}{\partial \phi} \\ \frac{\partial l_4}{\partial {}^o p_x} & \frac{\partial l_4}{\partial {}^o p_y} & \frac{\partial l_4}{\partial {}^o p_z} & \frac{\partial l_4}{\partial \psi} & \frac{\partial l_4}{\partial \theta} & \frac{\partial l_4}{\partial \phi} \\ \frac{\partial l_5}{\partial {}^o p_x} & \frac{\partial l_5}{\partial {}^o p_y} & \frac{\partial l_5}{\partial {}^o p_z} & \frac{\partial l_5}{\partial \psi} & \frac{\partial l_5}{\partial \theta} & \frac{\partial l_5}{\partial \phi} \\ \frac{\partial l_6}{\partial {}^o p_x} & \frac{\partial l_6}{\partial {}^o p_y} & \frac{\partial l_6}{\partial {}^o p_z} & \frac{\partial l_6}{\partial \psi} & \frac{\partial l_6}{\partial \theta} & \frac{\partial l_6}{\partial \phi} \end{bmatrix} \quad (2.30)$$

and the vectors

$$\dot{\mathbf{q}} = [\dot{l}_1, \dot{l}_2, \dot{l}_3, \dot{l}_4, \dot{l}_5, \dot{l}_6]^T, \quad (2.31)$$

$$\dot{\mathbf{X}}_A = [{}^o \dot{p}_x, {}^o \dot{p}_y, {}^o \dot{p}_z, \dot{\psi}, \dot{\theta}, \dot{\phi}]^T \quad (2.32)$$

are simply the time derivatives of the MP's position and orientation $\dot{\mathbf{X}}_A$ and joint lengths $\dot{\mathbf{q}}$. The differentiation will be executed with respect to the variables describing the MP's position and orientation, however the angular velocity is not expressed in frame \mathcal{F}_O as given in Eq. (2.32). To express everything in the inertial frame \mathcal{F}_O the analytic Jacobian must be multiplied by an additional transformation matrix.

2.2.6 Acceleration

In this section, the inverse kinematic equations relating the acceleration of the MP to the acceleration of the cables will be derived. Taking Eq. (2.22) and differentiating both sides of it with respect to time yields the expression

$$\ddot{\mathbf{q}} = \dot{\mathbf{J}}\dot{\mathbf{t}} + \mathbf{J}\ddot{\mathbf{t}} \quad (2.33)$$

where the chain rule of differentiation is applied. This equation relates the acceleration of the cables $\ddot{\mathbf{q}}$ to the acceleration of the MP $\ddot{\mathbf{t}}$, which is simply the time derivative of the twist vector. The representation of these vectors is given in the following subsequent equations.

$$\ddot{\mathbf{q}} = [\ddot{l}_1 \quad \ddot{l}_2 \quad \ddot{l}_3 \quad \ddot{l}_4 \quad \ddot{l}_5 \quad \ddot{l}_6]^T \quad (2.34)$$

$$\ddot{\mathbf{t}} = \begin{bmatrix} {}^o\ddot{\mathbf{p}} \\ {}^o\dot{\boldsymbol{\omega}}_E \end{bmatrix} \quad (2.35)$$

The derivative of the robot geometric Jacobian is computed by taking the derivative of the individual matrix terms with respect to time. The expression for these terms which make up the matrix $\dot{\mathbf{J}}$ are given as follows

$$\frac{d}{dt} \left(\frac{{}^o\mathbf{l}_i}{l_i} \right) = {}^o\boldsymbol{\omega}_E \times \left(\frac{{}^o\mathbf{l}_i}{l_i} \right), \quad (2.36)$$

$$\frac{d}{dt} \left({}^o\mathbf{R}_E {}^E\mathbf{a}_i \times \left(\frac{{}^o\mathbf{l}_i}{l_i} \right) \right) = ({}^o\dot{\mathbf{R}}_E {}^E\mathbf{a}_i + {}^o\mathbf{R}_E {}^E\dot{\mathbf{a}}_i) \times \left(\frac{{}^o\mathbf{l}_i}{l_i} \right) + {}^o\mathbf{R}_E {}^E\mathbf{a}_i \times \frac{d}{dt} \left(\frac{{}^o\mathbf{l}_i}{l_i} \right). \quad (2.37)$$

Substituting Eq. (2.36), Eq. (2.10), and Eq. (2.11) into Eq. (2.37) and noting that ${}^E \dot{\mathbf{a}}_i = 0$, the equation becomes

$$\frac{d}{dt} \left({}^o \mathbf{R}_E {}^E \mathbf{a}_i \times \left(\frac{{}^o \mathbf{l}_i}{l_i} \right) \right) = {}^o \dot{\mathbf{R}}_E {}^E \mathbf{a}_i \times \left(\frac{{}^o \mathbf{l}_i}{l_i} \right) + {}^o \mathbf{R}_E {}^E \mathbf{a}_i \times \left({}^o \boldsymbol{\omega}_E \times \left(\frac{{}^o \mathbf{l}_i}{l_i} \right) \right). \quad (2.38)$$

Using Eq. (2.36) and (2.38) the time derivative of the Jacobian matrix, Eq. (2.25) becomes

$$\mathbf{j} = \begin{bmatrix} \left({}^o \boldsymbol{\omega}_E \times \left(\frac{{}^o \mathbf{l}_1}{l_1} \right) \right)^T & \left({}^o \boldsymbol{\omega}_E \times {}^o \mathbf{R}_E {}^E \mathbf{a}_1 \times \left(\frac{{}^o \mathbf{l}_1}{l_1} \right) + {}^o \mathbf{R}_E {}^E \mathbf{a}_1 \times \left({}^o \boldsymbol{\omega}_E \times \left(\frac{{}^o \mathbf{l}_1}{l_1} \right) \right) \right)^T \\ \left({}^o \boldsymbol{\omega}_E \times \left(\frac{{}^o \mathbf{l}_2}{l_2} \right) \right)^T & \left({}^o \boldsymbol{\omega}_E \times {}^o \mathbf{R}_E {}^E \mathbf{a}_2 \times \left(\frac{{}^o \mathbf{l}_2}{l_2} \right) + {}^o \mathbf{R}_E {}^E \mathbf{a}_2 \times \left({}^o \boldsymbol{\omega}_E \times \left(\frac{{}^o \mathbf{l}_2}{l_2} \right) \right) \right)^T \\ \left({}^o \boldsymbol{\omega}_E \times \left(\frac{{}^o \mathbf{l}_3}{l_3} \right) \right)^T & \left({}^o \boldsymbol{\omega}_E \times {}^o \mathbf{R}_E {}^E \mathbf{a}_3 \times \left(\frac{{}^o \mathbf{l}_3}{l_3} \right) + {}^o \mathbf{R}_E {}^E \mathbf{a}_3 \times \left({}^o \boldsymbol{\omega}_E \times \left(\frac{{}^o \mathbf{l}_3}{l_3} \right) \right) \right)^T \\ \left({}^o \boldsymbol{\omega}_E \times \left(\frac{{}^o \mathbf{l}_4}{l_4} \right) \right)^T & \left({}^o \boldsymbol{\omega}_E \times {}^o \mathbf{R}_E {}^E \mathbf{a}_4 \times \left(\frac{{}^o \mathbf{l}_4}{l_4} \right) + {}^o \mathbf{R}_E {}^E \mathbf{a}_4 \times \left({}^o \boldsymbol{\omega}_E \times \left(\frac{{}^o \mathbf{l}_4}{l_4} \right) \right) \right)^T \\ \left({}^o \boldsymbol{\omega}_E \times \left(\frac{{}^o \mathbf{l}_5}{l_5} \right) \right)^T & \left({}^o \boldsymbol{\omega}_E \times {}^o \mathbf{R}_E {}^E \mathbf{a}_5 \times \left(\frac{{}^o \mathbf{l}_5}{l_5} \right) + {}^o \mathbf{R}_E {}^E \mathbf{a}_5 \times \left({}^o \boldsymbol{\omega}_E \times \left(\frac{{}^o \mathbf{l}_5}{l_5} \right) \right) \right)^T \\ \left({}^o \boldsymbol{\omega}_E \times \left(\frac{{}^o \mathbf{l}_6}{l_6} \right) \right)^T & \left({}^o \boldsymbol{\omega}_E \times {}^o \mathbf{R}_E {}^E \mathbf{a}_6 \times \left(\frac{{}^o \mathbf{l}_6}{l_6} \right) + {}^o \mathbf{R}_E {}^E \mathbf{a}_6 \times \left({}^o \boldsymbol{\omega}_E \times \left(\frac{{}^o \mathbf{l}_6}{l_6} \right) \right) \right)^T \end{bmatrix}. \quad (2.39)$$

Substituting the derived terms given by Eq. (2.39), Eq. (2.35), Eq. (2.34) and Eq. (2.25) into Eq. (2.33) gives the kinematic acceleration equation for a parallel robot. This relationship could also have been found by directly differentiating the velocity

equation. However, the details of this specific method are not given here. An article in the literature that discusses the acceleration analysis of parallel manipulators is found in reference [462].

2.3 Dynamics

The dynamic equations of motion are used to describe the forces and moments that are involved as the robotic manipulator executes a desired task. These equations are represented in either forward or inverse dynamic form. The forward dynamic problem determines the response of the end effector given the input forces or torques. This is useful in simulation and real time feedback control schemes. The inverse dynamic problem solves for the input forces or torques needed to perform a desired task. The inverse dynamic equations are useful in deriving control laws for a manipulator using control law partitioning or computed torque methods, which will be discussed later in Chapter 5.

There are several methods used to obtain the dynamic equations of motion for multi-body systems. A few of the more traditional methods commonly used include the Lagrangian energy method ([14], [20], [71], [172 - 173], [290 - 296], [298]), D'Alembert's virtual displacement principle ([290], [460]), Kane's method [306], Hamilton's Principle of virtual work ([68], [174], [232], [291], [297], [299 - 305]), and the Newton-Euler force and moment equations ([57], [67], [118], [143], [284 - 289]). This chapter will apply the Newton-Euler method to derive the equations of motion.

2.3.1 Dynamic Equations of Motion

Dynamics is the study of the forces and torques that cause the body or system of bodies to move. To obtain the dynamic equations of motion for the cable suspended parallel robot, the forces and moments are summed up for the MP. A free body diagram is given in Fig. 2.3 to show all the forces and moments acting on the MP. The cables that attach the MP to the BP are considered massless; therefore under this assumption have no inertial effects on the dynamics of the MP. Neglecting the mass and inertial effects of the cables significantly simplifies the dynamic equations of motion. If the mass and inertia of the cables were considered then the solutions to the dynamic equations would have to be sought out using methods such as the natural orthogonal complement (NOC) method ([246 - 247], [302]). The MP and BP are considered rigid bodies with a uniformly distributed mass. The frame \mathcal{F}_O is fixed to the BP and is considered the inertial frame.

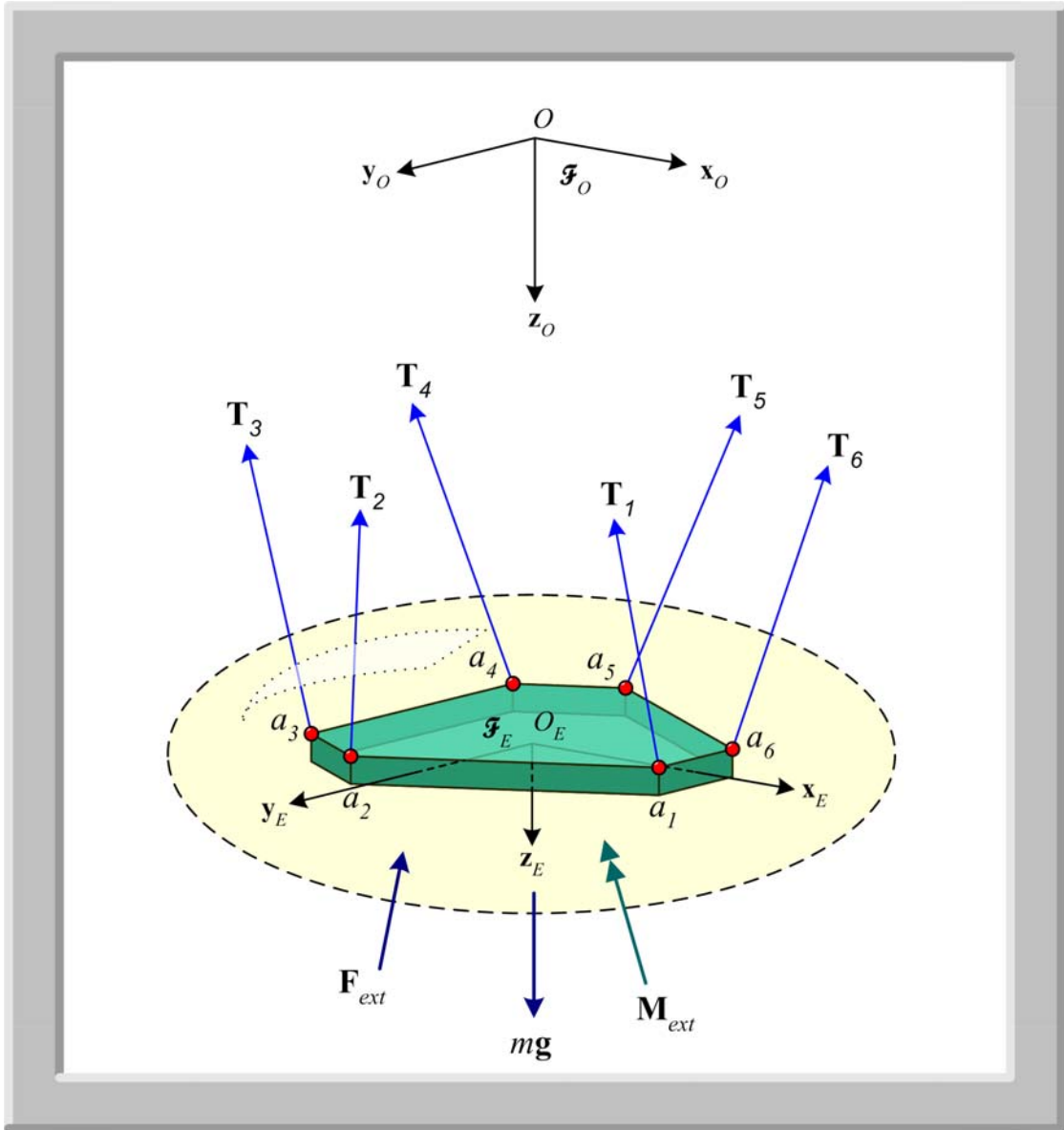


Fig. 2.3 Free Body Diagram of MP

The sum of the forces acting on the MP is expressed in the following equation

$$\sum \mathbf{F} = m\mathbf{g} - \mathbf{F}_{ext} - \sum_{i=1}^6 \mathbf{T}_i = \mathbf{M}(x)\ddot{\mathbf{x}} + \mathbf{0}. \quad (2.40)$$

The first term on the left hand side of Eq. (2.40) is the mass of the MP, m , times the gravity vector, \mathbf{g} , and the next term \mathbf{F}_{ext} is the vector of all the external forces acting from the environment on the MP. \mathbf{T}_i is the vector describing the cable force pertaining to each cable and is summed for all six cables. The matrix $\mathbf{M}(x)$ is the diagonal mass matrix given as

$$\mathbf{M}(x) = \begin{bmatrix} m & 0 & 0 \\ 0 & m & 0 \\ 0 & 0 & m \end{bmatrix}. \quad (2.41)$$

The dependence of (x) is for such cases where the mass is unevenly distributed over the MP. The matrix given by Eq. (2.41) assumes uniform mass distribution for the MP. The vector $\ddot{\mathbf{x}}$ is the translational linear acceleration of the frame \mathcal{F}_E , rigidly attached to the MP center of mass, with respect to the inertial frame \mathcal{F}_O rigidly attached to the BP. According to the kinematic analysis, $\ddot{\mathbf{x}}$ is the vector defined as ${}^O\ddot{\mathbf{p}}$ in the previous sections. The sum of the moments about point O_E with respect to frame \mathcal{F}_O is given by

$$\sum \mathbf{M}_{O_E} = \mathbf{0} - \mathbf{M}_{ext} - \sum_{i=1}^6 ({}^O\mathbf{a}_i \times \mathbf{T}_i) = \mathbf{I}^O \dot{\boldsymbol{\omega}}_E + {}^O\boldsymbol{\omega}_E \times \mathbf{I}^O \boldsymbol{\omega}_E. \quad (2.42)$$

The first zero term after the equal sign is placed there to remind us that gravity causes no moments on the body with respect to the MP coordinate system if the MP coordinate system is placed at the body's center of mass. The term \mathbf{M}_{ext} is the external moments acting on the MP from the environment, including the pure

moments and any moments caused by the external forces \mathbf{F}_{ext} . The third term on the left hand side of Eq. (2.42) is the sum of the moments acting on the MP caused by each of the cables attached at point a_i . The term $\mathbf{I}^o \dot{\boldsymbol{\omega}}_E$ represents the Coriolis forces and the cross product expression ${}^o \boldsymbol{\omega}_E \times \mathbf{I}^o \boldsymbol{\omega}_E$ is the centrifugal forces. The matrix \mathbf{I} is the inertia matrix of the MP defined according to frame \mathcal{F}_E . The vectors ${}^o \dot{\boldsymbol{\omega}}_E$ and ${}^o \boldsymbol{\omega}_E$ are the angular acceleration and angular velocity, respectively, of the MP expressed in the inertial frame \mathcal{F}_O .

For most robotic manipulators it is convenient to combine the force and moment equations into one complete matrix equation just as was done for the kinematic equations. In order to combine the above equations into one matrix equation of motion consider the following substitutions.

Gravity vector:

$$\mathbf{G}(x) = \begin{bmatrix} m\mathbf{g} \\ \mathbf{0}_{3 \times 1} \end{bmatrix} \quad (2.43)$$

where $\mathbf{G}(x)$ is a 6-dimensional vector.

External Forces and Moments:

$$\mathbf{f}_{ext} = \begin{bmatrix} \mathbf{F}_{ext} \\ \mathbf{M}_{ext} \end{bmatrix} = \begin{bmatrix} \mathbf{F}_{x,ext} \\ \mathbf{F}_{y,ext} \\ \mathbf{F}_{z,ext} \\ \mathbf{M}_{x,ext} \\ \mathbf{M}_{y,ext} \\ \mathbf{M}_{z,ext} \end{bmatrix} \quad (2.44)$$

Mass-Inertia Matrix:

$$\mathbf{D}(x) = \begin{bmatrix} \mathbf{M}(x) & \mathbf{0}_{3 \times 3} \\ \mathbf{0}_{3 \times 3} & \mathbf{I}(x) \end{bmatrix} \quad (2.45)$$

Coriolis and Centripetal Matrix:

$$\mathbf{C}(x, \dot{x}) \dot{\mathbf{X}} = \begin{bmatrix} \mathbf{0}_{3 \times 1} \\ \mathbf{I}^o \dot{\boldsymbol{\omega}}_E + {}^o \boldsymbol{\omega}_E \times \mathbf{I}^o \boldsymbol{\omega}_E \end{bmatrix} \quad (2.46)$$

Cable forces and Moments:

$$\sum_{i=1}^6 \boldsymbol{\tau}_i = \begin{bmatrix} \sum_{i=1}^6 \mathbf{T}_i \\ \sum_{i=1}^6 {}^o \mathbf{a}_i \times \mathbf{T}_i \end{bmatrix} = \begin{bmatrix} \mathbf{T}_1 + \mathbf{T}_2 + \mathbf{T}_3 + \mathbf{T}_4 + \mathbf{T}_5 + \mathbf{T}_6 \\ {}^o \mathbf{a}_1 \times \mathbf{T}_1 + {}^o \mathbf{a}_2 \times \mathbf{T}_2 + {}^o \mathbf{a}_3 \times \mathbf{T}_3 + {}^o \mathbf{a}_4 \times \mathbf{T}_4 + {}^o \mathbf{a}_5 \times \mathbf{T}_5 + {}^o \mathbf{a}_6 \times \mathbf{T}_6 \end{bmatrix} \quad (2.47)$$

Now, note that for one cable the following can be written

$$\boldsymbol{\tau}_i = \begin{bmatrix} \mathbf{T}_i \\ {}^o \mathbf{a}_i \times \mathbf{T}_i \end{bmatrix} = \begin{bmatrix} \|\mathbf{T}_i\| \hat{\mathbf{e}}_i \\ {}^o \mathbf{a}_i \times \|\mathbf{T}_i\| \hat{\mathbf{e}}_i \end{bmatrix} = \begin{bmatrix} \hat{\mathbf{e}}_i \\ {}^o \mathbf{a}_i \times \hat{\mathbf{e}}_i \end{bmatrix} \|\mathbf{T}_i\| \quad (2.48)$$

where $\hat{\mathbf{e}}_i$ is the unit vector along the length of the cable and is expressed as

$$\hat{\mathbf{e}}_i = \left(\frac{{}^o \mathbf{1}_i}{\|{}^o \mathbf{1}_i\|} \right) \quad (2.49)$$

with the base of the vector located at the tip of the vector ${}^o\mathbf{b}_i$ and pointing in the direction from the point b_i to the point a_i . Using this in the cable forces and moments term, the following can be written

$$\begin{aligned}
\sum_{i=1}^6 \tau_i &= \left[\begin{array}{c} \hat{\mathbf{e}}_1 \|\mathbf{T}_1\| + \hat{\mathbf{e}}_2 \|\mathbf{T}_2\| + \hat{\mathbf{e}}_3 \|\mathbf{T}_3\| + \hat{\mathbf{e}}_4 \|\mathbf{T}_4\| + \hat{\mathbf{e}}_5 \|\mathbf{T}_5\| + \hat{\mathbf{e}}_6 \|\mathbf{T}_6\| \\ {}^o\mathbf{a}_1 \times \hat{\mathbf{e}}_1 \|\mathbf{T}_1\| + {}^o\mathbf{a}_2 \times \hat{\mathbf{e}}_2 \|\mathbf{T}_2\| + {}^o\mathbf{a}_3 \times \hat{\mathbf{e}}_3 \|\mathbf{T}_3\| + {}^o\mathbf{a}_4 \times \hat{\mathbf{e}}_4 \|\mathbf{T}_4\| + {}^o\mathbf{a}_5 \times \hat{\mathbf{e}}_5 \|\mathbf{T}_5\| + {}^o\mathbf{a}_6 \times \hat{\mathbf{e}}_6 \|\mathbf{T}_6\| \end{array} \right] \\
&= \begin{bmatrix} \hat{\mathbf{e}}_1 & \hat{\mathbf{e}}_2 & \hat{\mathbf{e}}_3 & \hat{\mathbf{e}}_4 & \hat{\mathbf{e}}_5 & \hat{\mathbf{e}}_6 \\ {}^o\mathbf{a}_1 \times \hat{\mathbf{e}}_1 & {}^o\mathbf{a}_2 \times \hat{\mathbf{e}}_2 & {}^o\mathbf{a}_3 \times \hat{\mathbf{e}}_3 & {}^o\mathbf{a}_4 \times \hat{\mathbf{e}}_4 & {}^o\mathbf{a}_5 \times \hat{\mathbf{e}}_5 & {}^o\mathbf{a}_6 \times \hat{\mathbf{e}}_6 \end{bmatrix} \begin{bmatrix} \|\mathbf{T}_1\| \\ \|\mathbf{T}_2\| \\ \|\mathbf{T}_3\| \\ \|\mathbf{T}_4\| \\ \|\mathbf{T}_5\| \\ \|\mathbf{T}_6\| \end{bmatrix} \\
&= \mathbf{J}^T \mathbf{u} \\
(2.50)
\end{aligned}$$

where it can be seen that

$$\mathbf{J}^T = \begin{bmatrix} \hat{\mathbf{e}}_1 & \hat{\mathbf{e}}_2 & \hat{\mathbf{e}}_3 & \hat{\mathbf{e}}_4 & \hat{\mathbf{e}}_5 & \hat{\mathbf{e}}_6 \\ {}^o\mathbf{a}_1 \times \hat{\mathbf{e}}_1 & {}^o\mathbf{a}_2 \times \hat{\mathbf{e}}_2 & {}^o\mathbf{a}_3 \times \hat{\mathbf{e}}_3 & {}^o\mathbf{a}_4 \times \hat{\mathbf{e}}_4 & {}^o\mathbf{a}_5 \times \hat{\mathbf{e}}_5 & {}^o\mathbf{a}_6 \times \hat{\mathbf{e}}_6 \end{bmatrix} \quad (2.51)$$

is the transpose of the geometric Jacobian. And

$$\mathbf{u} = [\|\mathbf{T}_1\| \quad \|\mathbf{T}_2\| \quad \|\mathbf{T}_3\| \quad \|\mathbf{T}_4\| \quad \|\mathbf{T}_5\| \quad \|\mathbf{T}_6\|]^T \quad (2.52)$$

is a vector of the magnitude of the cable forces. Rewriting the equations of motion in matrix form and using the previous substitutions results in:

$$-\mathbf{J}^T \mathbf{u} = \mathbf{D}(x) \ddot{\mathbf{X}} + \mathbf{C}(x, \dot{x}) \dot{\mathbf{X}} - \mathbf{G}(x) + \mathbf{f}_{ext} \quad (2.53)$$

2.3.2 Calculation of Inertia

The inertia matrix \mathbf{I} for the MP used in the previous equations of motion is a matrix represented by the following:

$$\mathbf{I} = \begin{bmatrix} \mathbf{I}_{xx} & \mathbf{I}_{xy} & \mathbf{I}_{xz} \\ \mathbf{I}_{yx} & \mathbf{I}_{yy} & \mathbf{I}_{yz} \\ \mathbf{I}_{zx} & \mathbf{I}_{zy} & \mathbf{I}_{zz} \end{bmatrix} = \begin{bmatrix} \int (y^2 + z^2) dm & \int (-xy) dm & \int (-xz) dm \\ \int (-yx) dm & \int (x^2 + z^2) dm & \int (-yz) dm \\ \int (-zx) dm & \int (-zy) dm & \int (x^2 + y^2) dm \end{bmatrix} \quad (2.54)$$

Most of the MPs considered are constructed of or can be broken up into simpler shapes whose inertia is already known relative to axes specific to each shape. This is possible because the mass moment of inertia is an additive quantity. By using the parallel axis theorem, all the individual shapes can be related to one coordinate frame. The mass moment of the entire body can be calculated as the sum of the moment of inertia of all the individual bodies. The geometries considered in this thesis can all be approximated as thin plates [463].

2.4 Conclusion

In this chapter, the kinematics and dynamics equations for a three-dimensional cable suspended parallel robot are derived which will be used in the following chapters. The kinematics is derived in the inverse form due to the ease of derivation and closed form solution. The inverse kinematics yields the cable lengths for a given position and orientation of the MP. In the derivation for the kinematics, the Jacobian is found and presented using two different methods, the geometric and

analytic method. The Jacobian transforms the velocity of the MP to the joint rates in the actuators. The dynamics are derived using the Newton-Euler method. In the derivation of the dynamics, the inertias of the cables were assumed negligible. Finally, the inertia matrix is presented in general form.

Chapter 3

WORKSPACE AND ANALYTICAL DESIGN

3.1 Introduction

This chapter analyzes the workspace of a cable suspended parallel robot. Workspace is generally defined as the set of locations that a point on the MP is capable of reaching. For a serial robot, this definition usually can be associated with two types of workspaces. The first type referred to as the *Dexterous Workspace* is defined as the set of locations where the end effector is able to reach with all orientations [1]. The second type referred to as the *Reachable* or *Maximal Workspace* is defined as the set of locations that the end effector is able to reach with at least one orientation ([1], [327]). The translational motion of the end effector is most often achieved through the first three joints for a serial robot. The orientation is obtained through a wrist that incorporates the remaining three joints.

A parallel robot has redundant links that connect the end effector or MP to the ground or BP. The translation and orientation of the MP is achieved only through the coupled motion of the redundant links. Due to this coupling between the redundant links, the translation and orientation cannot be simply divided into one set of joints causing translation and another set of joints causing orientation. The increased complexity of the parallel robot led to more refined subsets of workspaces. Several different types of workspaces are defined by Merlet in addition to the ones already mentioned [1]. Another type of workspace is the *Constant Orientation* or

Translational Workspace [1], the set of locations that the end effector, is able to reach when the orientation is fixed. Similarly, the *Orientation Workspace* ([1], [320], [323]) is the range of orientations that the end effector may rotate through at one fixed point. The *Inclusive Orientation Workspace* [1] is the set of locations that the end effector may reach with at least one orientation from a selected range of orientations imposed on the orientation parameter. Finally, the *Total Orientation Workspace* [1] is defined as the set of locations the end effector can reach with all orientations from a selected range of orientation imposed on the orientation parameter [1].

Cable suspended parallel robots are slightly different from the traditional parallel robots. Their difference lies within the actuation used to move the end effector. Common actuators include pneumatic and hydraulic pistons, and motor driven lead screws. These actuators can push and pull on the MP. However, for cable actuation, the MP is suspended from cables under the force of gravity and cables can only pull not push. Therefore, the workspace criteria for cable suspended parallel robots must also incorporate the notion of equilibrium in its definitions. The workspace for cable suspended parallel robots is defined as all points within a given search region that yield tensions for all the cables. The types of workspaces considered in this chapter include the Constant Orientation or Translational Workspace and the Total Orientation Workspace.

The goal of this chapter is to not only determine the workspaces but also observe and compare the changes in the workspace as different geometric parameters are varied. Since the geometric configuration parameters of a cable suspended parallel robot include an endless list of possibilities, the chapter will begin with the description of the range models that are considered in the current analysis. The next section

proceeds to provide the definition for the workspace of cable suspended parallel robot as opposed to traditional parallel robots. Then the chapter presents definitions of performance indices used to evaluate and measure the capabilities of one robotic design against another. The chapter continues with the details of the simulation studies and an explanation of the results found. The results are separated into sections emphasizing particular trends discovered. Due to the large amount of data, not all the figures could be presented on the individual shapes of the constant orientation workspace. Sample graphs are given in some sections with the completed set given in the appendices. Finally, the chapter ends with the conclusion that summarizes the results pointing out useful trends.

3.2 Workspace Model

The model studied is that of a general 6-6 cable suspended parallel robot. Several models are studied to retrieve a fundamental understanding of the effects that the geometric shape, MP size, and MP orientation impose on the workspace. The scope of the specific range of models that were studied is described in this section.

One restriction used to focus the enormous range of models pertained to the cable connection points. The base points of the manipulator (b_1, \dots, b_6) are all contained within the same plane ($\mathbf{z}_O = 0$) as shown in Fig. 3.1. These points are positioned at a radial distance r_{base} from the base coordinate system \mathcal{F}_O that is located at O the center of the BP. The MP similarly has a set of connection points (a_1, \dots, a_6) located at a radial distance r_{end} from the moving coordinate frame \mathcal{F}_E attached to O_E the center of mass of the MP. These points are located on the ($\mathbf{z}_E = 0$) plane relative to frame \mathcal{F}_E . The cables are connected between points b_i on the base to points a_i on the MP as seen in Fig 3.1.

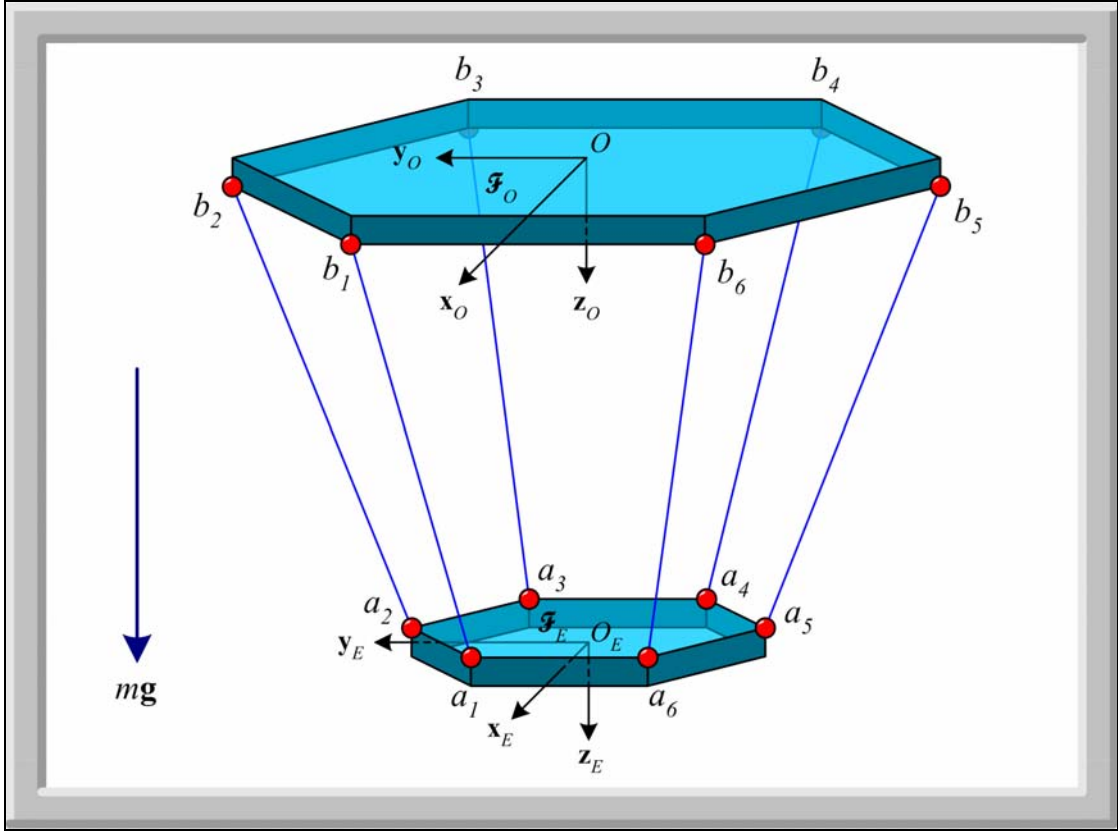


Fig. 3.1 A schematic of a 6-6 cable suspended parallel robot

The position vector of point b_i on the base frame is defined by

$${}^o\mathbf{b}_i = \begin{bmatrix} r_{base} \cos(\beta_i) \\ r_{base} \sin(\beta_i) \\ 0 \end{bmatrix}. \quad (3.1)$$

The variable r_{base} is the radial distance from the base coordinate frame \mathcal{F}_O and β_i denotes the angular location of point b_i on BP with respect to the positive \mathbf{x}_O axis as depicted in Fig. 3.2a. The position vector of the cable connection points on the MP is as follows:

$${}^E \mathbf{a}_i = \begin{bmatrix} r_{end} \cos(\alpha_i) \\ r_{end} \sin(\alpha_i) \\ 0 \end{bmatrix} \quad (3.2)$$

The variable r_{end} is the radial distance from the MP coordinate frame \mathcal{F}_E and α_i denotes the angular location of point a_i on the MP with respect to the positive \mathbf{x}_E axis as shown in Fig. 3.2b. In the analysis r_{base} is fixed to a constant value and r_{end} is varied over a discrete range from r_{end} equal to r_{base} and smaller.

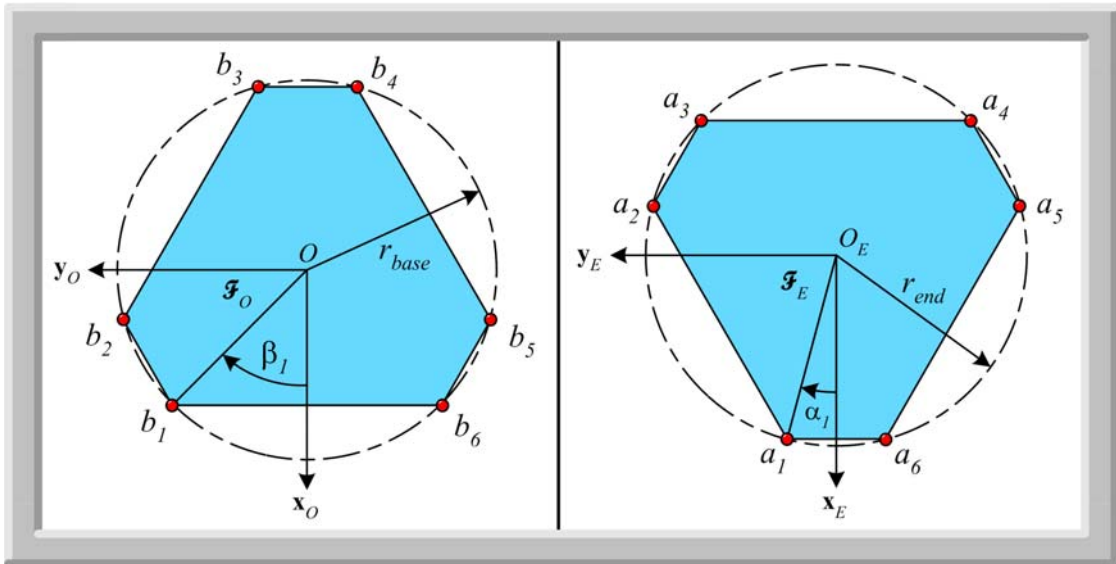


Fig. 3.2a (Left) Schematic of BP, 3.2b (Right) Schematic of MP

Another restriction used to narrow the types of parallel robot geometries considered is the arrangement of the cable connection points a_i and b_i are on the circle r_{end} and r_{base} of the MP and BP respectively. A geometric parameter γ is used to

define the placement of the points a_i and b_i . Using γ , the connection points are symmetrically configured on the radius of the platform in question to form a range of semi hexagonal shapes. The complete definition of γ is given in a later section.

3.3 Workspace Definition

As previously mentioned, the workspace for a cable suspended parallel robot is defined as the set of locations yielding tension in all the cables. For the current analysis, no dynamic effects are considered. The static equilibrium of the cable suspended parallel robot is used to find the force of each cable. The static force and moment balance on the MP are

$$\begin{aligned}\Sigma \mathbf{F} &= m\mathbf{g} - \sum_{i=1}^6 \mathbf{T}_i = \mathbf{0}, \\ \Sigma \mathbf{M}_{O_E} &= -\sum_{i=1}^6 ({}^o \mathbf{a}_i \times \mathbf{T}_i) = \mathbf{0}\end{aligned}\tag{3.3}$$

where it can be seen that there are no external moments applied to MP and the only forces considered are the cable tension forces and the gravitational force. All other external forces and moments are ignored. To relate the external forces represented by Eq. (3.3) to the forces in the cables, the dual relationship between kinematics and statics can be used as follows:

$$\mathbf{f}_{ext} = \mathbf{J}^T \mathbf{T}\tag{3.4}$$

where \mathbf{T} is the vector of cable forces present in each cable, \mathbf{J} is the Geometric Jacobian matrix of the robot defined in Eq. (2.26), and \mathbf{f}_{ext} is a 6 dimensional vector containing the external forces and moments given by

$$\mathbf{f}_{ext} = \begin{bmatrix} m\mathbf{g} \\ \mathbf{0}_{3 \times 1} \end{bmatrix}. \quad (3.5)$$

The first three rows in Eq. (3.5) represent the external forces and similarly the last three rows represent the external moments in the \mathbf{x}_O , \mathbf{y}_O , and \mathbf{z}_O direction, respectively. For this section, the gravitational force is considered as an external force. Now, to obtain the equations for the force of each cable, Eq. (3.4) is rearranged in the following manner

$$\mathbf{T} = \tilde{\mathbf{J}}\mathbf{f}_{ext} \quad (3.6)$$

where

$$\tilde{\mathbf{J}} = (\mathbf{J}^T)^{-1} \quad (3.7)$$

The workspace volume for the cable robot is later on characterized by the set of points where the center of mass of the MP can be positioned while all cables are in tensions. To this end, at each point within the possible workspace, the equation describing the force in each cable is used to see if tension is obtainable ([1], [106 - 107], [246]).

3.4 Performance Indices

Performance indices are qualitative and/or quantitative tools used to measure and compare various aspects of a robot's abilities and characteristics. These attributes of the robot, for example, may relate to the robot's ability to accurately maintain a prescribed motion or force transmission or it may incorporate the volume of space in which the robot is able to perform the task also referred to as the robot's workspace.

The Jacobian for the cable suspended parallel robot is defined in the preceding Chapter 2 entitled Kinematics and Dynamics. The quality of performance of a robot with respect to the force and velocity transmission can be addressed through examining the behavior of the robot's Jacobian matrix (\mathbf{J}). This is determined through checking the condition number of \mathbf{J} or $\tilde{\mathbf{J}}$. The condition number κ is defined as

$$\kappa(\tilde{\mathbf{J}}) \equiv \frac{\sigma_l}{\sigma_s}, \quad (3.8)$$

the ratio of the largest singular value σ_l to the smallest singular value σ_s of the matrix $\tilde{\mathbf{J}}$. The singular value is the square root of the eigenvalues of $\tilde{\mathbf{J}}\tilde{\mathbf{J}}^T$ and $\tilde{\mathbf{J}}^T\tilde{\mathbf{J}}$. The condition number ranges from

$$1 \leq \kappa < \infty. \quad (3.9)$$

When the condition number approaches one the matrix is said to be well conditioned or isotropic, i.e., is far from singularities. Conversely, as the condition number approaches infinity, the matrix is said to be ill conditioned. An ill conditioned

Jacobian matrix will amplify any error present in the kinematic or dynamic motion. Using the condition number directly as presented in Eq. (3.8) is not very convenient due to the presence of the infinite right hand bound. This bound makes it difficult to obtain a useful “scaled” measurement. It is more common in practice to use an inverted form of the condition number referred to as the conditioning index η , defined as

$$\eta = \left(\frac{1}{\kappa} \right), \quad (3.10)$$

where the bound on η is now normalized to the range defined between

$$0 \leq \eta \leq 1. \quad (3.11)$$

When the conditioning index is near zero the Jacobian matrix of the robotic manipulator is ill conditioned and more susceptible to error; when the conditioning index is near one the robot is well conditioned. The range presented by the conditioning index allows different robots to be compared on a closed right and left bounded scale as opposed to the bounds presented by simply using the condition number directly.

So, the condition number or the conditioning index can be used as a performance index to measure force and velocity transmission. However, the condition number is computed at each individual point in the possible workspace region studied, for a specific orientation of the end effector. This is useful information but in order to obtain a general understanding of the behavior of the condition number

over the entire workspace volume for one specific constant orientation the detailed information becomes overwhelming. The Global Conditioning Index (GCI) is used to obtain a comprehensive or “global” perspective of the condition number’s behavior over the entire workspace for the constant orientation chosen [359]. Using the conditioning index, due to its convenient bounds and the size of the workspace volume, the GCI is defined as

$$GCI = \frac{\int (\eta) dW}{\int dW}. \quad (3.12)$$

The denominator of the right hand side of Eq. (3.12) is the workspace volume of the robot manipulator and the numerator is the conditioning index pertaining to a particular point in the workspace. The GCI is bounded by the range

$$0 \leq GCI \leq 1. \quad (3.13)$$

Similarly, when the GCI is near zero the entire workspace tends to be ill conditioned and when the GCI is near one the entire workspace tends to be well conditioned.

The GCI supplies the designer with another performance index tool that can be used. The GCI is a way of comparing the entire workspace volume to Jacobian performance. In general, when designing a robot, you want the largest workspace with the least amount of singularities where the singularities result from a bad or ill conditioned Jacobian. In addition, a good robotic design incorporates one with an agile MP, i.e. one that is able to orient itself over a large range of motion. Other

attractive attributes for a good robotic design is one with a large strength to weight ratio, high accuracy, and quick response or fast motion. Due to the difficulty of obtaining the exact solution to the integral's in Eq. (3.12) a discrete version of GCI definition is sought and expressed as

$$GCI = \frac{\sum_{j=1}^n (\eta_j)}{w} \quad (3.14)$$

where w is the total number of n discrete “good” points that form the workspace and the numerator is the summation of the conditioning index for each point in the grid defining the workspace volume. For cable suspended parallel robots the “good” points refers to those points that yield tension in all the cables. Eq. (3.14) is much easier to compute the GCI. However, the accuracy of the results depends on how small the search region is discretized ([99], [103], [246], [359], [361 - 362], [464]).

3.5 Simulation Studies and Analysis

This section will explain the details of the simulations studied including the complete definition of γ , the specific models considered and the set of constant orientations used for the study. The following subsections will present the analysis of the results found from the simulations with the addition of selected case studies to help support and explain the trends discovered.

As mentioned, several different models are used to attain a better understanding of the effect that the geometric parameters have on the workspace. Four different geometric designs are studied and compared. These designs included a geometric configuration for $\gamma = 45^\circ, 30^\circ, 15^\circ$ and 0° , where γ is the angle between

BP connection points (b_1, b_2) , (b_3, b_4) , (b_5, b_6) and MP connection points (a_1, a_6) , (a_2, a_3) , (a_4, a_5) as shown in Fig. 3.3a. The design for $\gamma = 45^\circ$, 30° and 15° is a symmetric semi-hexagon and the design for $\gamma = 0^\circ$ is where the MP and BP are equilateral triangles, the ideal case of the 3-3 Stewart platform. The configuration of the cable suspended parallel robot for $\gamma = 45^\circ$ is shown in Fig. 3.3a and for $\gamma = 0^\circ$ is shown in Fig. 3.3b. The figures for $\gamma = 15^\circ$ and $\gamma = 30^\circ$ are found in Appendix C. When $\gamma = 0^\circ$ the base points $(b_1$ and $b_2)$, $(b_3$ and $b_4)$, $(b_5$ and $b_6)$ become one ideal connection point. Similarly, the MP connection points $(a_1$ and $a_6)$, $(a_2$ and $a_3)$, $(a_4$ and $a_5)$ become one ideal point. The orientation of the MP to the BP is in such a way that the long side of MP would line up with the short side of the BP when \mathcal{F}_E is aligned with \mathcal{F}_O as seen in Fig. 3.3a. Dissimilar BP to MP geometries is not considered in this current study, in other words mismatching the γ angles for the BP to MP. When $\gamma = 60^\circ$ the platform is a regular hexagon and no solutions exist because the Jacobian matrix is singular and therefore was not considered any further.

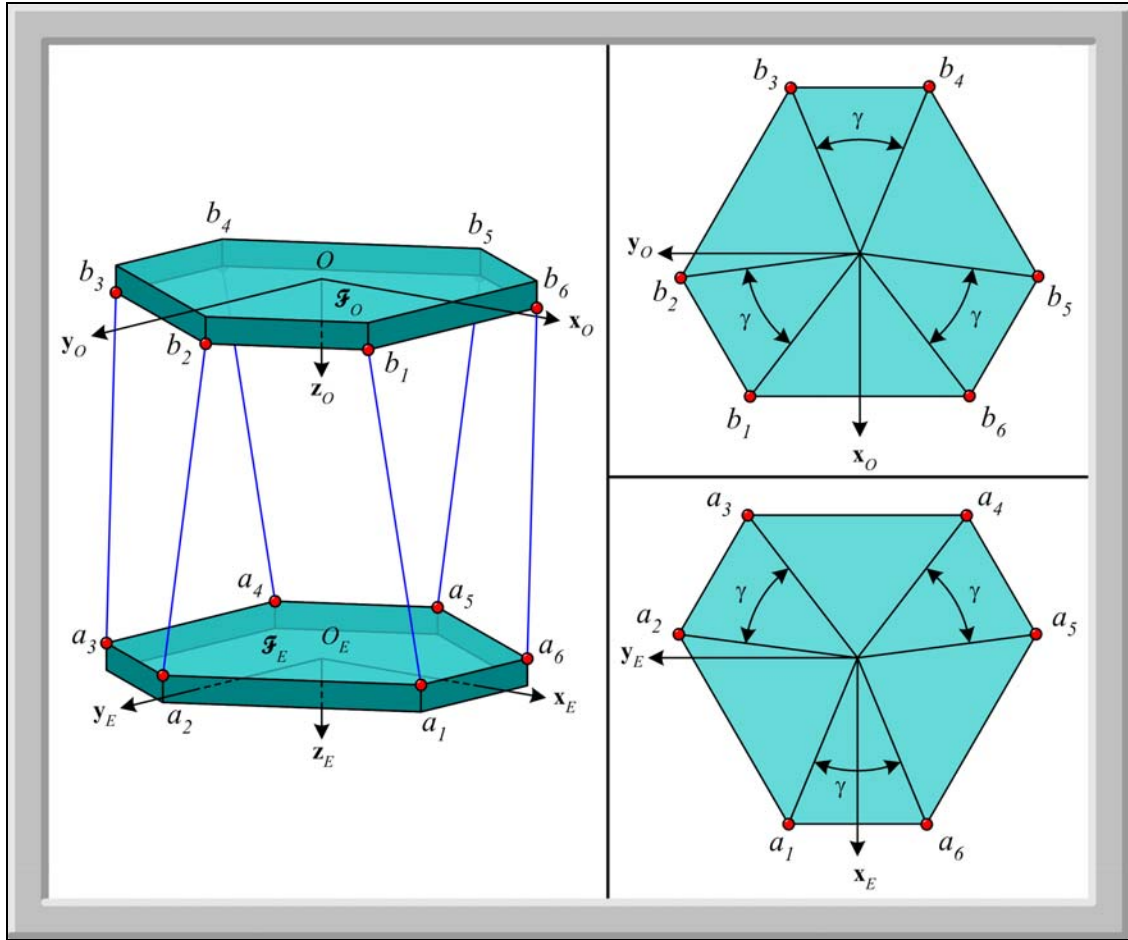


Fig. 3.3a Schematic of BP and MP for $\gamma = 45^\circ$

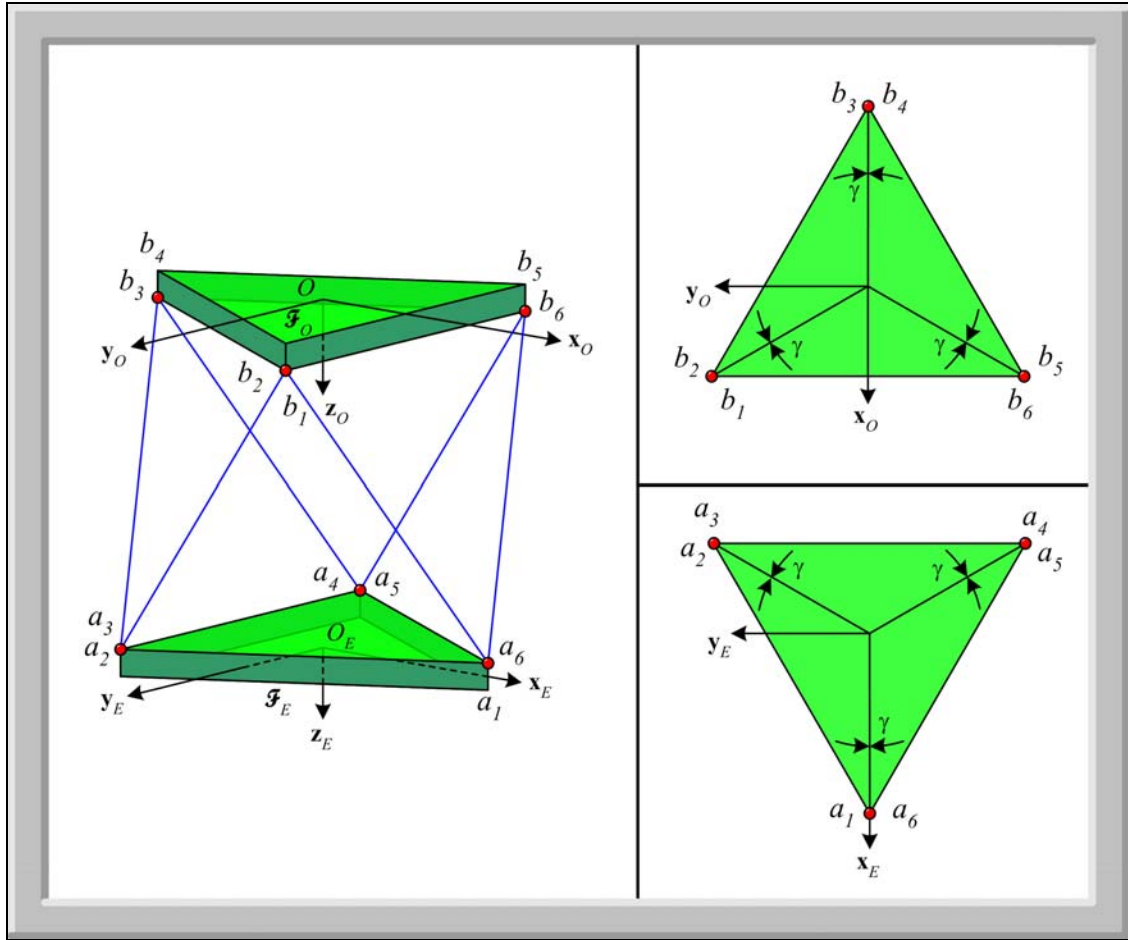


Fig. 3.3b Schematic of BP and MP for $\gamma = 0^\circ$

A program was created in Matlab for workspace analysis of cable suspended parallel robots. The program inputs include the connection points of the BP and MP, the radius of these connection points on both platforms, the given constant orientation of the MP, the desired search volume and incremental step size for the mesh search. Preliminary runs were executed for each geometry using large step sizes and various dimensions, the resulting workspace was analyzed and the constant values were chosen. To keep consistency, the step size was fixed along all

three axes ($\mathbf{x}_O, \mathbf{y}_O, \mathbf{z}_O$) to 0.4, the search for possible workspace volume was fixed to the region of ($-8 \leq \mathbf{x}_O \leq 8, -8 \leq \mathbf{y}_O \leq 8, 0 \leq \mathbf{z}_O \leq 10$), and finally ($r_{base} = 6$) was fixed constant for every model considered. The step size was chosen based on computer computation time. With the fixed r_{base} value selected, the search region was chosen such that all possible locations that the MP could possibly reach were generously included for a given MP radius (r_{end}).

Once a particular geometry, MP size, and MP orientation is selected, the program checks every point in the volume to see if all the cables yield tensions when the MP is positioned at a point of the possible workspace volume. If the point in question does yield tension in all the cables, the condition number of the Jacobian at that point for the constant orientation is computed and the point is included in the set of points that define the workspace volume. After all the points in the search volume are checked, a global condition index is computed over the workspace of good points, where again “good points” refers to points that result in tension in all cables. The weight of the MP, ($mg = 10$), is held constant for every parallel robot considered. The cables holding the MP are only checked to see if all of them contain pulling forces and are not slack.

The Matlab program was run numerous times for a variety of geometries and sizes for an elaborate set of constant orientations. Four different geometries and three different ratios of the MP to the BP are extensively studied. Table 3.1 displays a list of all the parallel robots considered.

Table 3.1: Cable Suspended Parallel Robots Studied		
Parallel Robot	$(r_{end}/r_{base})\%$	Geometry γ (deg)
Robot 1	100%	0°
Robot 2	50%	0°
Robot 3	1%	0°
Robot 4	100%	15°
Robot 5	50%	15°
Robot 6	1%	15°
Robot 7	100%	30°
Robot 8	50%	30°
Robot 9	1%	30°
Robot 10	100%	45°
Robot 11	50%	45°
Robot 12	1%	45°

Table 3.1 Cable Suspended Parallel Robots Studied

The workspace sizes as well as the behavior of the Jacobian matrix are used as the performance indices for each parallel robot at each constant orientation. For parallel robots, the orientation greatly affects the properties of the workspace due to the coupled translation and orientation of the redundant links, as was previously mentioned. Because of this, the workspace analysis for each parallel robot was studied for a large set of orientations. These orientations included all combinations of the following discrete list given in Table 3.2.

Table 3.2: Set of Orientations	
	Degree
ψ	0°, 10°, 20°, 30°, 330°, 340°, 350°
θ	0°, 10°, 20°, 30°, 330°, 340°, 350°
ϕ	0°, 10°, 20°, 30°, 40°, 50°, 60°, 300°, 310°, 320°, 330°, 340°, 350°

Table 3.2 Set of Orientations

Where ψ is the rotation of the MP about the x_o axis, θ is the rotation of the MP about the y_o axis, and ϕ is the rotation of the MP about the z_o axis. The orientation of the MP with respect to the BP is related through rotation matrix defined in Eq. (2.2).

For this analysis, each individual robot given in Table 3.1 is set to every constant orientation combination given in Table 3.2 to determine the Constant Orientation or Translational Workspace for that specific robot at the particular orientation chosen. Once each robot is checked for the complete set of orientations, the orientations are combined to get different perspectives on the Total Orientation Workspace. Additional case studies may be included in certain sections in order to emphasize and further support any trends revealed. The specific conditions pertaining to the study will be mentioned in the corresponding sections in which they are used.

3.5.1 Workspace Volume

One of the performance indices commonly used to evaluate any type of robotic manipulator is the size and shape of the workspace volume. As previously mentioned, the workspace for parallel manipulators is complicated by the fact that the translation and orientation of the manipulator's end effector is couple together. Many serial robots are designed in such a way that this difficulty is almost eliminated. One

example is a 6-DOF serial robot integrated with a concurrent axis wrist. For this specific type of serial robot, the workspace is defined by the translation of the first three joints, for the remaining three joints incorporate the orientation. So it is possible to generally define the workspace as a three dimensional volume. This representation is not possible for a 6-DOF parallel robot. The workspace volume for a parallel robot changes as the orientation of the MP changes. The MP may be able to reach certain points in space but possibly with only a limited set of orientations. A complete representation of the workspace for a parallel robot must be presented by a six dimensional workspace for which a graphical illustration is not possible. The workspace can only be represented as subsets of this workspace. The definitions of these subsets were previously given [1].

The types of workspace that are studied in this chapter include the *Constant Orientation Workspace* and the *Total Orientation Workspace*. The workspace volume is determined for the twelve robots given in Table 3.1 for every constant orientation combination of ψ , θ , and ϕ mentioned in Table 3.2. This inevitably led to an extensive collection of Constant Orientation Workspace data where a graphical representation of the “good” points with their corresponding conditioning index values can be displayed for each of the robot and orientation configuration. Due to the vast amount of information involved the individual workspace volume shapes for each robot at every constant orientation is not presented. However, the trends pertaining to certain aspects of the workspace will be discussed. The data from the Constant Orientation Workspace is combined for the set of discrete orientations to form the Total Orientation Workspace. In order to present the results for the Total Orientation Workspace in a systematic and comprehensive manner the

data is organized into a series of subset plots. The results displayed in Fig. 3.4, Fig. 3.5, Fig. 3.6, Fig. 3.7 and continued in Appendix (A) present the variation in the workspace volume for $\gamma = 0^\circ, 15^\circ, 30^\circ, 45^\circ$ respectively where each surface represents a value for $(r_{end}/r_{base}) = 100\%, 50\%, 1\%$. The three surfaces in each graph correspond to a constant value of ϕ . The top most surface in every plot is the $(r_{end}/r_{base}) = 100\%$ surface followed by the surface for $(r_{end}/r_{base}) = 50\%$, and the bottom surface is for $(r_{end}/r_{base}) = 1\%$. Each surface is constructed from the values associated with the number of good points that make up the workspace volume for a particular range of orientations. If an orientation did not produce any workspace points then the point was set to zero for the surface. The surface gives an idea of the magnitude of the Total Orientation Workspace as a particular MP rotates through a set of orientations pertaining to a constant value of ϕ .

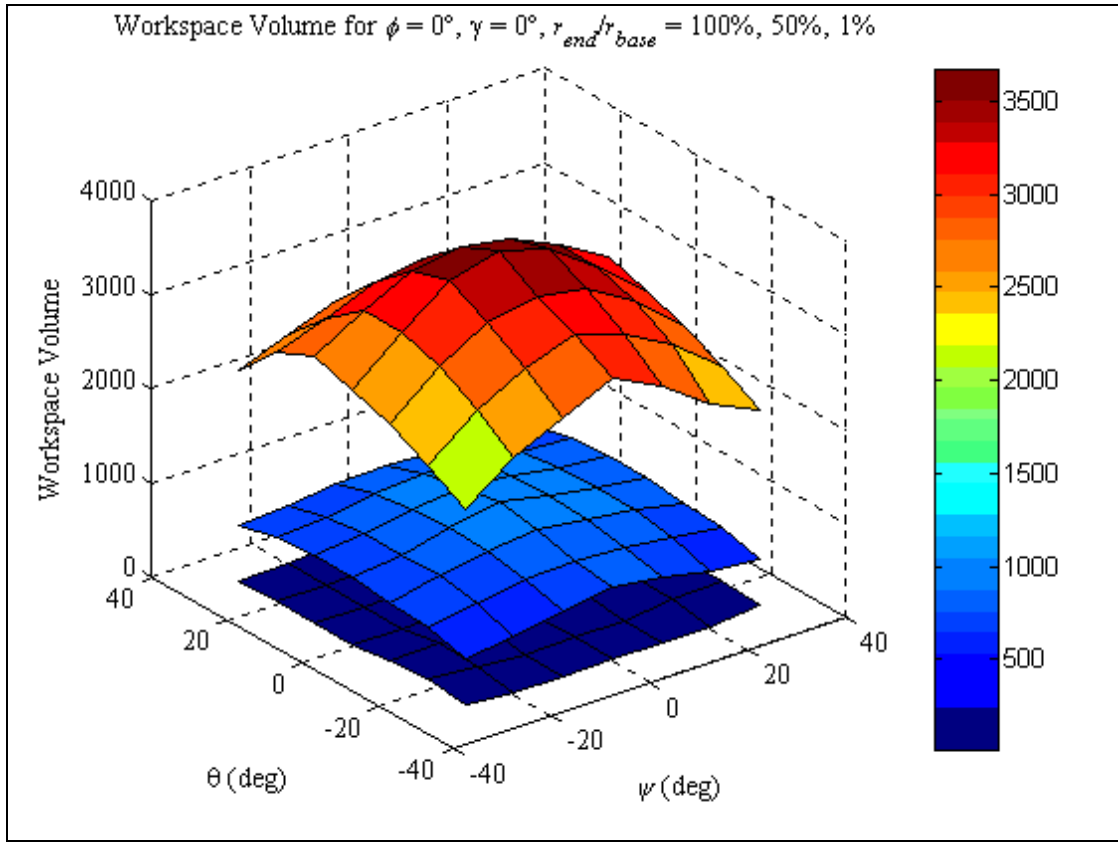


Fig. 3.4 Workspace Volume for $\gamma = 0^\circ$, $(r_{end}/r_{base}) = 100\%$, 50% , 1% , and for $\phi = 0^\circ$

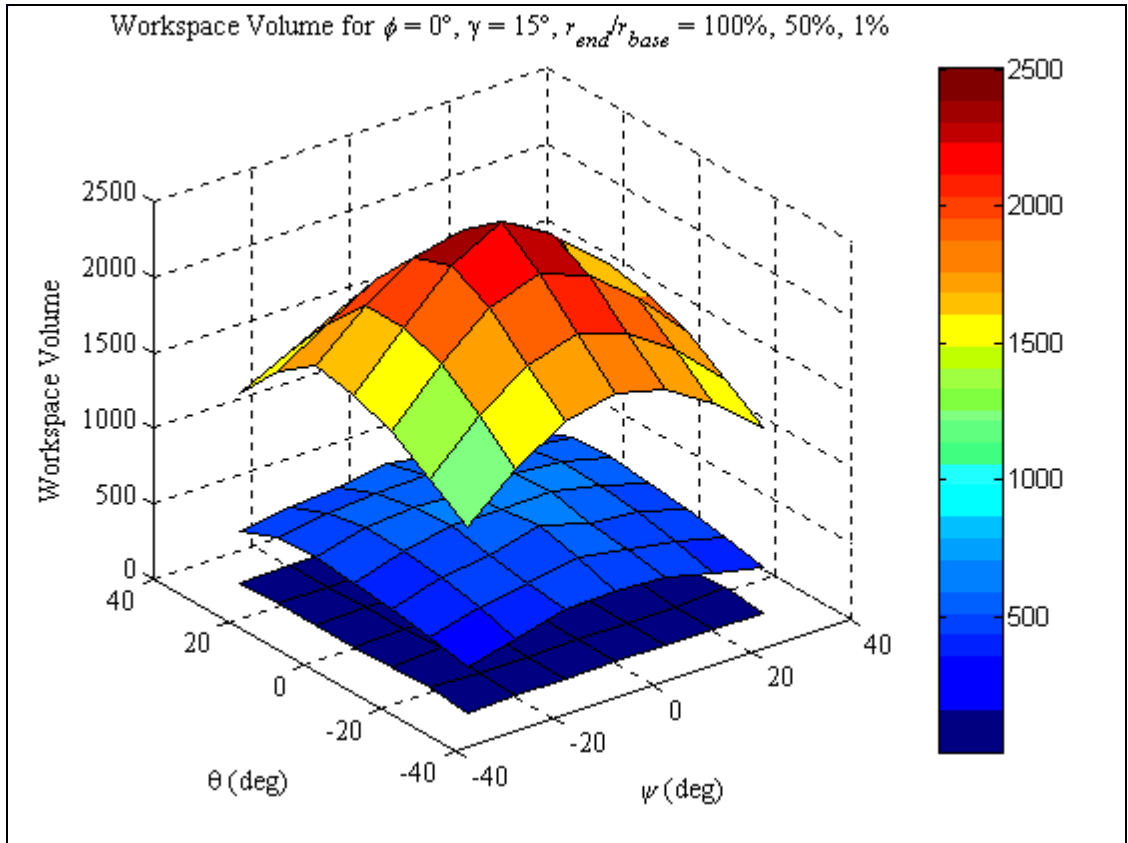


Fig. 3.5 Workspace Volume for $\gamma = 15^\circ$, $(r_{end}/r_{base}) = 100\%$, 50% , 1% , and for $\phi = 0^\circ$

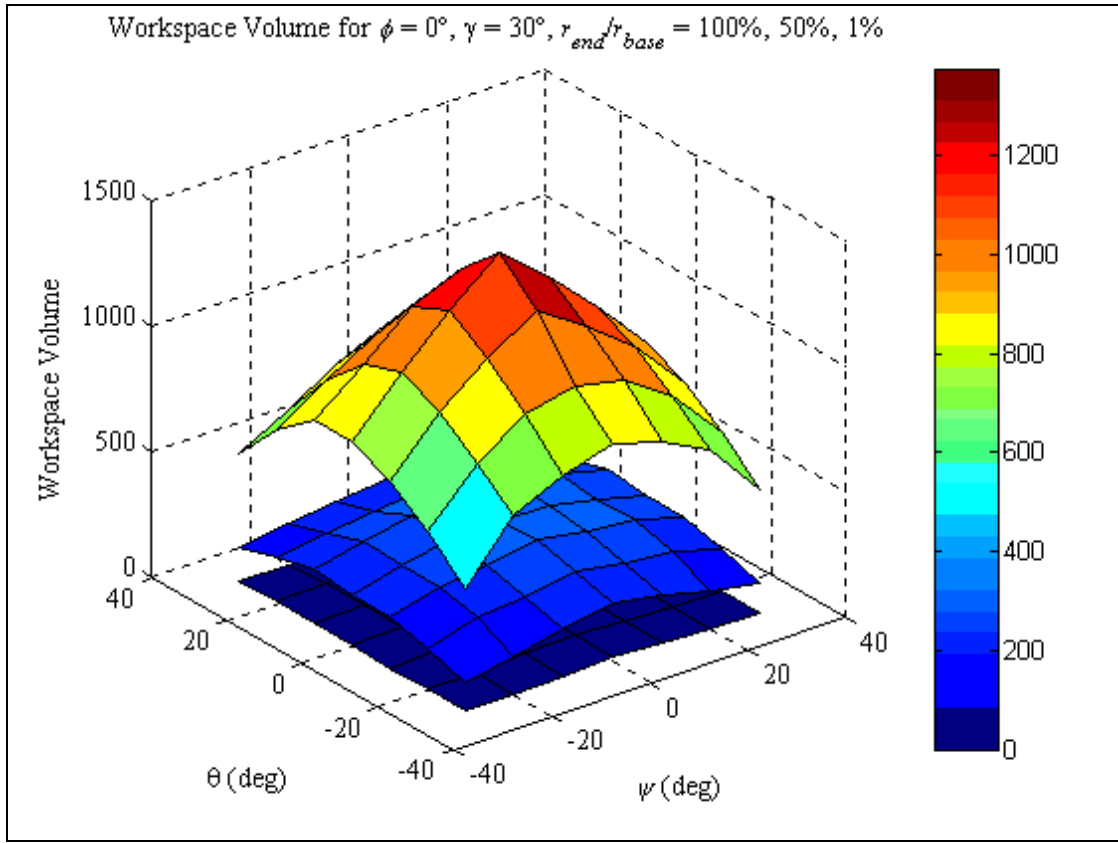


Fig. 3.6 Workspace Volume for $\gamma = 30^\circ$, $(r_{end}/r_{base}) = 100\%$, 50% , 1% , and for $\phi = 0^\circ$

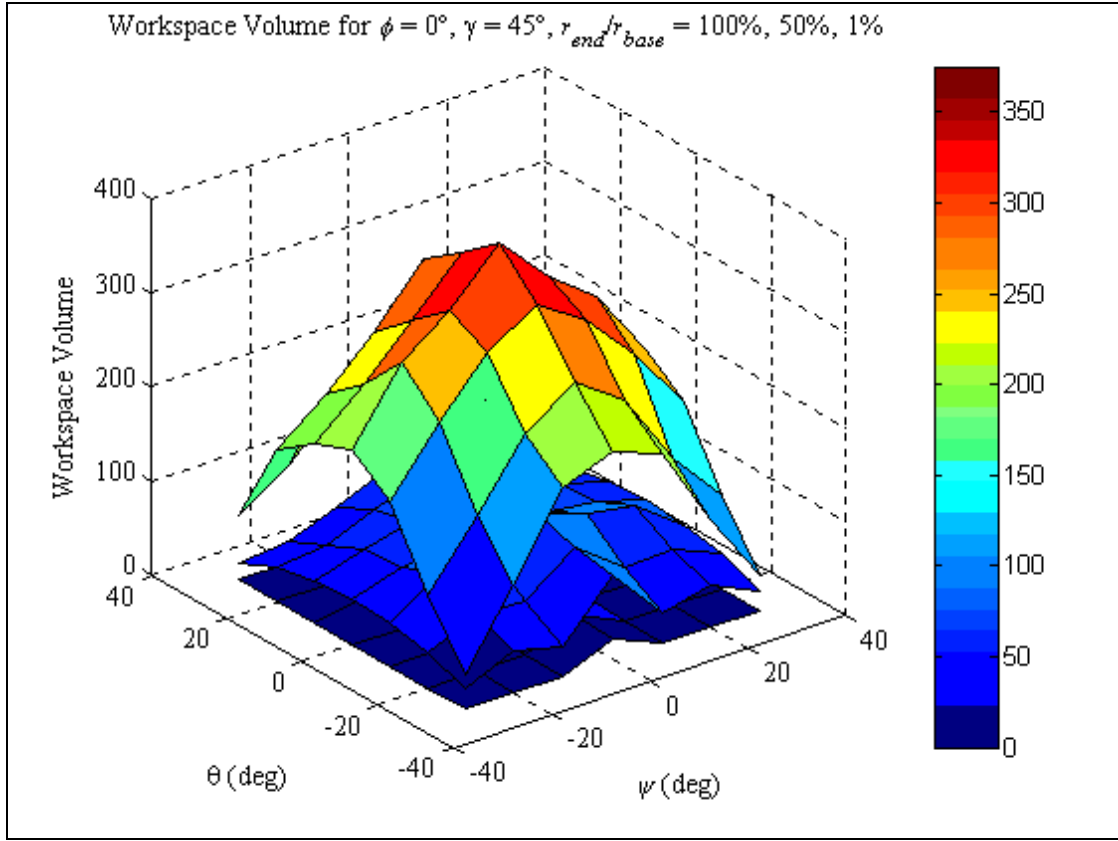


Fig. 3.7 Workspace Volume for $\gamma = 45^\circ$, $(r_{end}/r_{base}) = 100\%, 50\%, 1\%$, and for $\phi = 0^\circ$

The behavior of the workspace given by Fig. 3.4, Fig. 3.5, Fig. 3.6, Fig. 3.7 with the completed set of graphs given in Appendix (A), reveal several useful trends. One trend noticed is that the workspace volume for a positive rotation of the MP is exactly matched by a mirrored negative rotation of the MP in both magnitude as well as a reflected shape. This is directly related to the symmetric geometry chosen for the MP and the BP. Some specific examples of the symmetric rotations are given in Table 3.3 and are easily verified through a quick check of the workspace surfaces given by Fig. 3.4, Fig. 3.5, Fig. 3.6, Fig. 3.7, and Appendix (A).

Table 3.3: Examples of the Symmetry within the Data	
(ψ, θ, ϕ) Rotation 1	(ψ, θ, ϕ) Mirrored Rotation 2
$(30^\circ, 30^\circ, 0^\circ)$	$(-30^\circ, 30^\circ, 0^\circ)$
$(10^\circ, -30^\circ, 20^\circ)$	$(-10^\circ, -30^\circ, -20^\circ)$
$(10^\circ, 30^\circ, 20^\circ)$	$(-10^\circ, 30^\circ, -20^\circ)$
$(10^\circ, 10^\circ, 10^\circ)$	$(-10^\circ, 10^\circ, -10^\circ)$
$(-10^\circ, 10^\circ, 10^\circ)$	$(10^\circ, 10^\circ, -10^\circ)$
$(30^\circ, 20^\circ, 10^\circ)$	$(-30^\circ, 20^\circ, -10^\circ)$
$(30^\circ, 30^\circ, 10^\circ)$	$(-30^\circ, 30^\circ, -10^\circ)$
$(30^\circ, 10^\circ, 10^\circ)$	$(-30^\circ, 10^\circ, -10^\circ)$
$(20^\circ, -20^\circ, 30^\circ)$	$(-20^\circ, -20^\circ, -30^\circ)$
$(\pm\psi, \pm\theta, \pm\phi)$	$(\mp\psi, \pm\theta, \mp\phi)$

Table 3.3 Examples of the Symmetry within the Data

The mirror pattern related to the workspace volume is given by the last row in Table 3.3 if the angular values considered are between $\pm\pi$ radians or $\pm 180^\circ$ degrees. If the angular values considered are between $(0 \leq \text{angle} < 2\pi)$ radians or $(0^\circ \leq \text{angle} < 180^\circ)$ then the mirrored workspace is given by

$$(\psi, \theta, \psi) \leftrightarrow (\text{abs}|2\pi - \psi|, \theta, \text{abs}|2\pi - \psi|) \quad (3.15)$$

or,

$$(\psi, \theta, \psi) \leftrightarrow (\text{abs}|360^\circ - \psi|, \theta, \text{abs}|360^\circ - \psi|). \quad (3.16)$$

In Eq. (3.15) and Eq. (3.16), the left hand side is the current rotation and the right hand side yields the mirrored workspace of this rotation.

To reduce the extensive amount of data pertaining to the multiple orientations observed, averages of the workspace volumes are used. All the workspace volume magnitudes for every set of ψ and θ orientations related to a fixed value of ϕ are averaged for a particular γ geometry and (r_{end}/r_{base}) size. That is, each surface given by Fig. 3.4, Fig. 3.5, Fig. 3.6, Fig. 3.7 and Appendix (A) is averaged forming an Average Workspace Volume for the specific value of ϕ , γ and (r_{end}/r_{base}) that define the surface. If a surface contains constant orientations that do not yield any workspace volume points then these orientations are excluded from the average workspace volume calculation. This data is then graphed over the set of ϕ orientations versus the average workspace volume value, which is presented in Fig. 3.8 for $\gamma = 0^\circ$, Fig. 3.9 for $\gamma = 15^\circ$, Fig. 3.10 for $\gamma = 30^\circ$, and Fig. 3.11 for $\gamma = 45^\circ$.

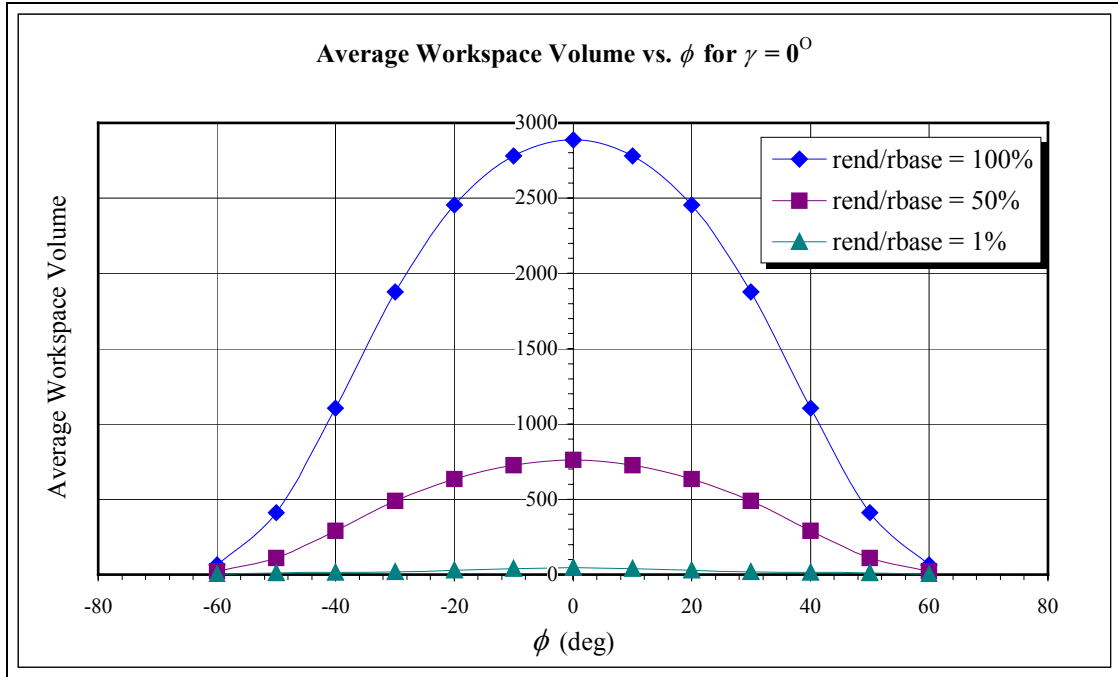


Fig. 3.8 Graph of Average Workspace Volume vs. ϕ for geometry $\gamma = 0^\circ$

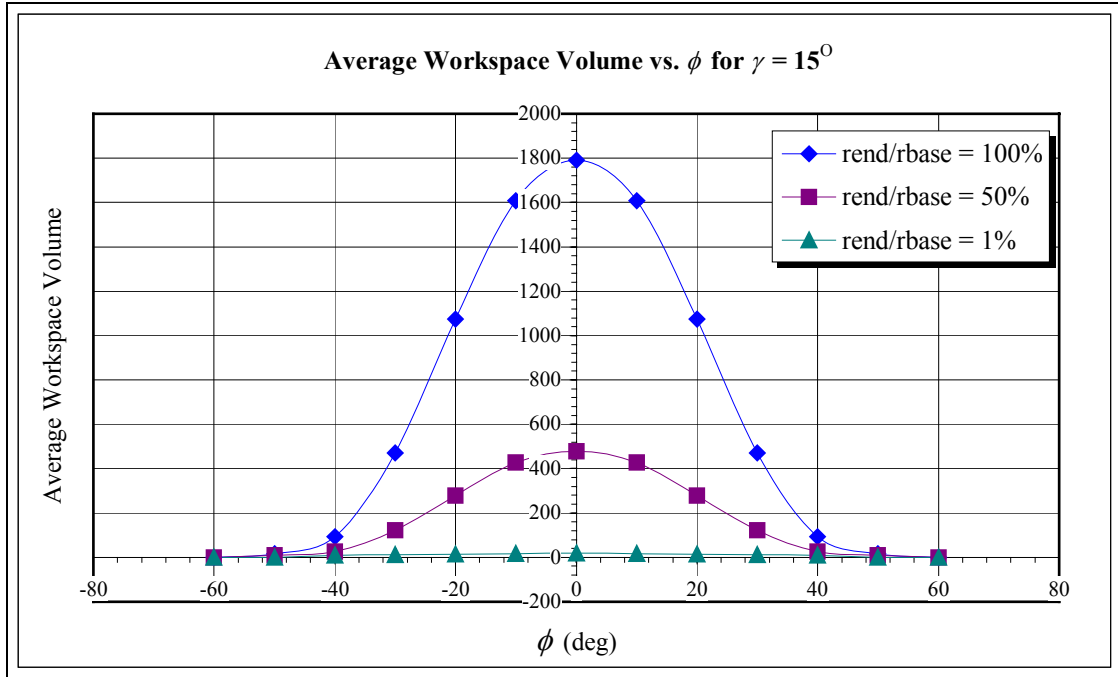


Fig. 3.9 Graph of Average Workspace Volume vs. ϕ for geometry $\gamma = 15^\circ$

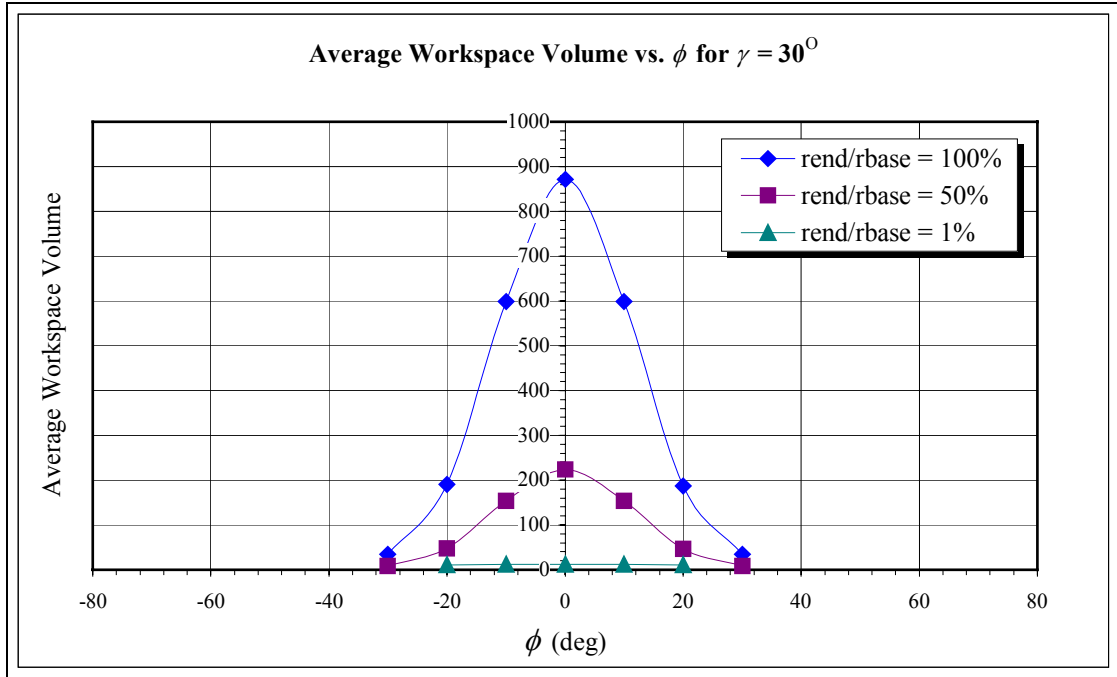


Fig. 3.10 Graph of Average Workspace Volume vs. ϕ for geometry $\gamma = 30^\circ$

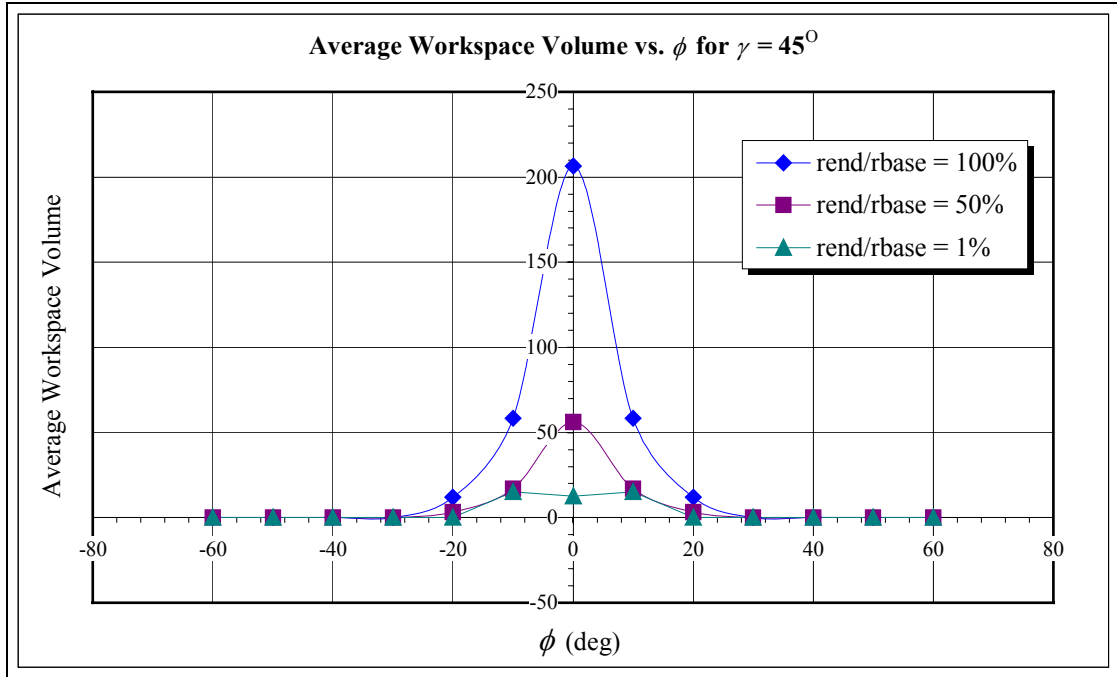


Fig. 3.11 Graph of Average Workspace Volume vs. ϕ for geometry $\gamma = 45^\circ$

From these graphs it is observed that the average workspace volume decreases as the MP rotates itself away from the orientations associated with $\phi = 0^\circ$ and towards orientations related to $\phi = \pm 60^\circ$. In addition, as γ increases and (r_{end}/r_{base}) decreases the range of possible orientations decrease and eventually cease to exist. The limit on the range of orientation of the MP may partially be explained by observing the behavior of the cables as the MP attempts to reach these different orientations. The span of orientations is restricted since cables are only able to pull and not push.

For example, consider the case where the rotation of the MP about the \mathbf{x}_O and \mathbf{y}_O axes is fixed to $\psi = 0^\circ$, $\theta = 0^\circ$ and the MP is rotated by ϕ about the \mathbf{z}_O axis as far as it is able to go. A sketch of the four cable suspended parallel robots with

$(r_{end}/r_{base}) = 100\%$ is given in Fig. 3.12 displaying the configuration of the maximum rotation possible for this example.

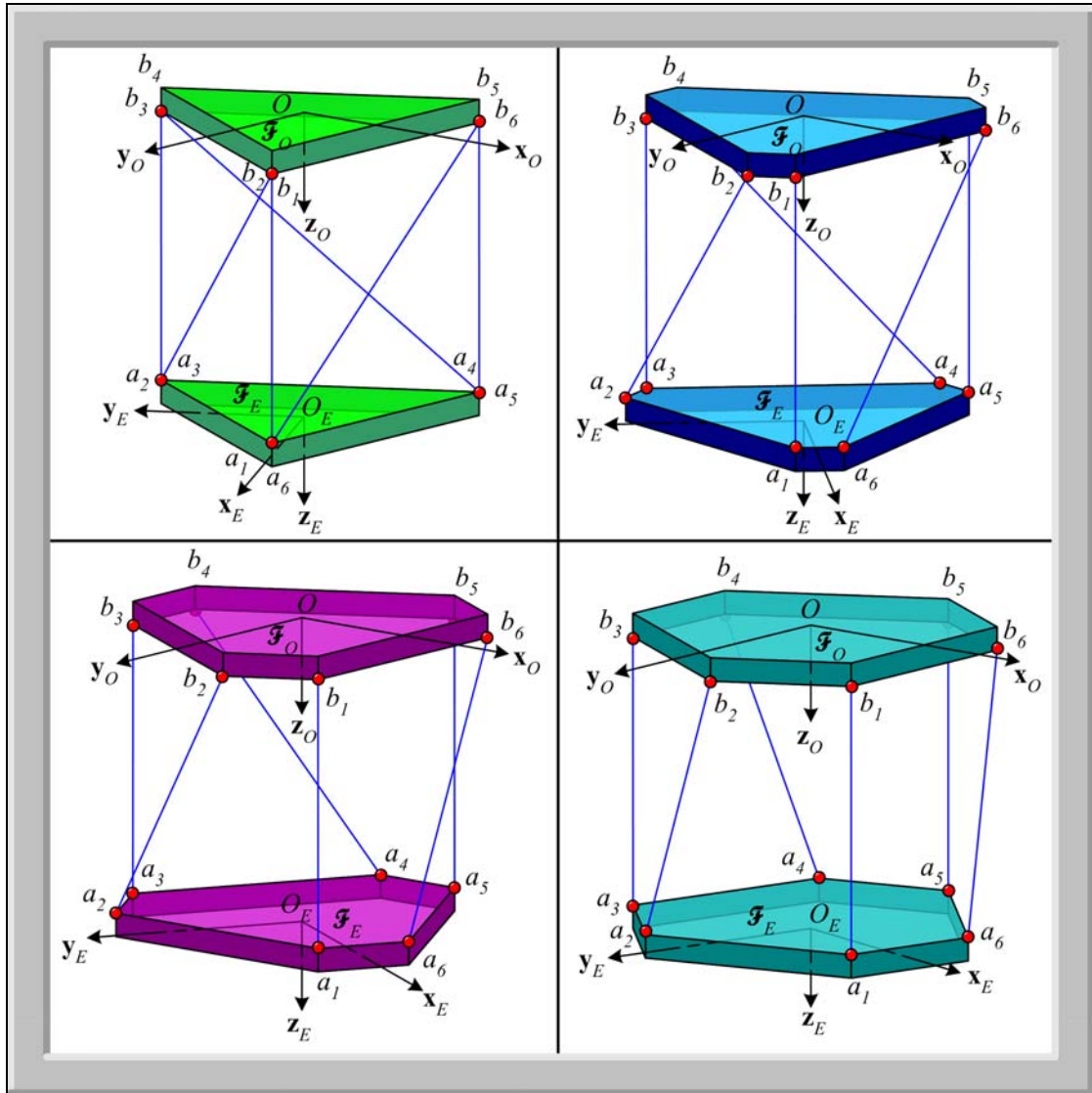


Fig. 3.12 Limits of MP ϕ Orientation for $(\psi = 0^\circ, \theta = 0^\circ)$, $(r_{end}/r_{base}) = 100\%$, where (top left) is for $\gamma = 0^\circ$, (top right) is for $\gamma = 15^\circ$, (bottom left) is for $\gamma = 30^\circ$, (bottom right) is for $\gamma = 45^\circ$

The value of the maximum ϕ angle that the MP is able to rotate through for each γ value with $(r_{end}/r_{base}) = 100\%$ is given in Table 3.4. It is noted that at this maximum orientation, the MP aligns itself with the BP and every other cable is positioned vertically with the direction of gravity and parallel to the \mathbf{z}_O axis. Any additional rotation about the \mathbf{z}_O axis is physically not possible for the cables would have to oppose equilibrium with gravity and the cables are only capable of pulling not pushing.

Table 3.4: Orientation Range MP can travel when $(\psi = 0^\circ, \theta = 0^\circ), (r_{end}/r_{base}) = 100\%$	
Geometry γ	Orientation Range on ϕ
0°	$\pm 60^\circ$
15°	$\pm 45^\circ$
30°	$\pm 30^\circ$
45°	$\pm 15^\circ$

Table 3.4 Orientation Range can travel when $(\psi = 0^\circ, \theta = 0^\circ), (r_{end}/r_{base}) = 100\%$

However, the surfaces given in Fig. 3.4, Fig. 3.5, Fig. 3.6, Fig. 3.7, and Appendix (A) show that rotations past the ϕ limitations given by Table 3.4 are in fact possible, but only when the MP is oriented by a large ψ and θ angles. For these few unique orientations, the workspace is extremely small. It is easily seen now that the geometry pertaining to $\gamma = 60^\circ$ is not able to rotate at all about the \mathbf{z}_O axis when the MP is initially parallel to the BP under static conditions. This configuration, when tested, resulted in a singular Jacobian matrix. The further detailed investigation of this exact singularity is left for future work.

Another trend observed from the workspace surfaces relates to the ratio of the MP to the BP, which is denoted by (r_{end}/r_{base}) . For all γ values, it is found that as the ratio (r_{end}/r_{base}) decreases the workspace volume also decreases. The geometry $\gamma = 0^\circ$ has the largest workspace volume compared to other γ values of the same size and orientation and as γ increases the workspace decreases. The workspace volume is the largest when the ratio of the MP to the BP is $(r_{end}/r_{base}) = 100\%$, i.e. the same size, for any γ value. This trend contradicted the case for a two dimensional planar cable suspended parallel robot, where the workspace increased as the MP size decreased [107].

A case study was conducted to further support the trends regarding the ratio (r_{end}/r_{base}) . In this study the orientation of the MP is fixed to $(\psi, \theta, \phi) = (0^\circ, 0^\circ, 0^\circ)$, for all four γ geometry values and the Constant Orientation Workspace is determined for $(r_{end}/r_{base}) = 100\%, 90\%, 80\%, 70\%, 60\%, 50\%, 40\%, 30\%, 20\%, 10\%$ and 1% . The possible workspace volume is fixed to the region of $(-8 \leq x_O \leq 8, -8 \leq y_O \leq 8, 0 \leq z_O \leq 10)$, and $(r_{base} = 6)$ is fixed constant for every model considered. However, the step size is reduced to 0.1 along all three (x_O, y_O, z_O) axes to increase the accuracy. A plot of the workspace volume versus (r_{end}/r_{base}) is displayed in Fig. 3.13.

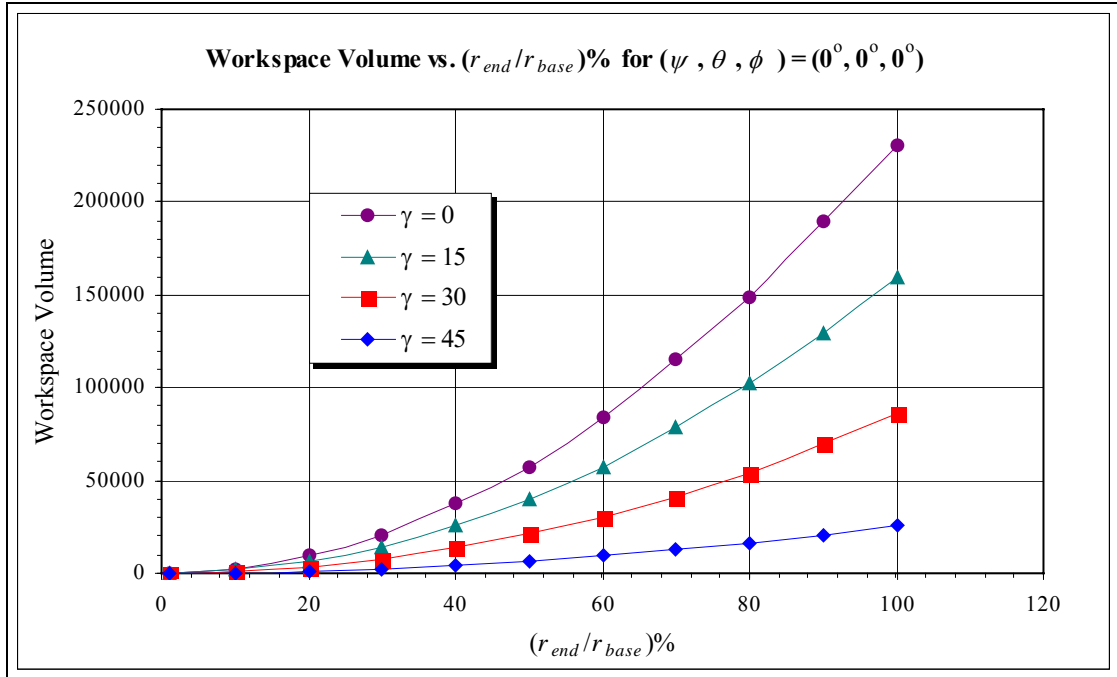


Fig. 3.13 Workspace Volume vs. $(r_{end}/r_{base})\%$ for $(\psi, \theta, \phi) = (0^\circ, 0^\circ, 0^\circ)$, with reduced step size to 0.1 along all three (x_0, y_0, z_0) axes

From the plot, it is observed that as (r_{end}/r_{base}) increases the workspace volume increases with the maximum value reached when $(r_{end}/r_{base}) = 100\%$. The curves appear to be smooth and therefore present no evidence to support any other maximum for this particular case study.

In an attempt to begin to understand, on a local level, why the workspace increases as the ratio of the MP to the BP increases several points are chosen with various orientations. At each point the condition number and the tension values for the cables are computed for several different ratios of (r_{end}/r_{base}) . The tension values of each cable and corresponding conditioning index for that particular point and orientation are the specified ratio is given in Table 3.5. The values of the cable forces

are given in Fig. 3.14, Fig. 3.15, Fig. 3.16, and Fig. 3.17 for the ratio $(r_{end}/r_{base}) = 100\%$, 55.319% , 55.318% and 10% respectively.

Table 3.5 Cable Forces and Conditioning Index Values for $(x_o, y_o, z_o) = (1, 1, 10)$ and $(\psi, \theta, \phi) = (30^\circ, 60^\circ, 0^\circ)$							
(r_{end}/r_{base}) %	T ₁	T ₂	T ₃	T ₄	T ₅	T ₆	Conditionin g Index
100%	1.3209	2.3605	0.68469	3.0053	2.8393	1.3577	0.039942
55.319%	0.98239	2.5328	2.8428e-005	3.6975	3.4091	0.39941	0.017609
55.318%	0.98236	2.5328	-1.5265e-006	3.6976	3.4091	0.39937	0.017608
10%	-7.7891	11.181	-8.1901	12.031	15.779	-12.219	0.0026668

Table 3.5 Cable Forces and Conditioning Index Values for $(x_o, y_o, z_o) = (1, 1, 10)$ and $(\psi, \theta, \phi) = (30^\circ, 60^\circ, 0^\circ)$

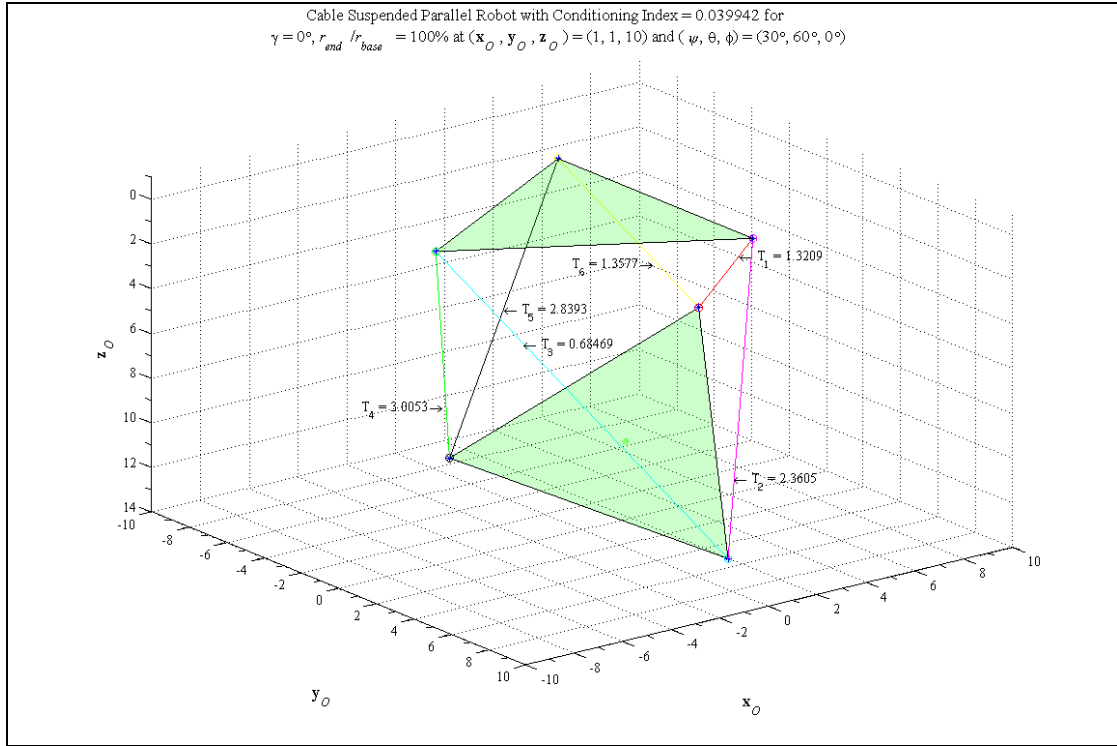


Fig. 3.14 Cable Suspended Parallel Robot for $\gamma = 0^\circ$, $(r_{end}/r_{base}) = 100\%$, at $(x_o, y_o, z_o) = (1, 1, 10)$ and $(\psi, \theta, \phi) = (30^\circ, 60^\circ, 0^\circ)$

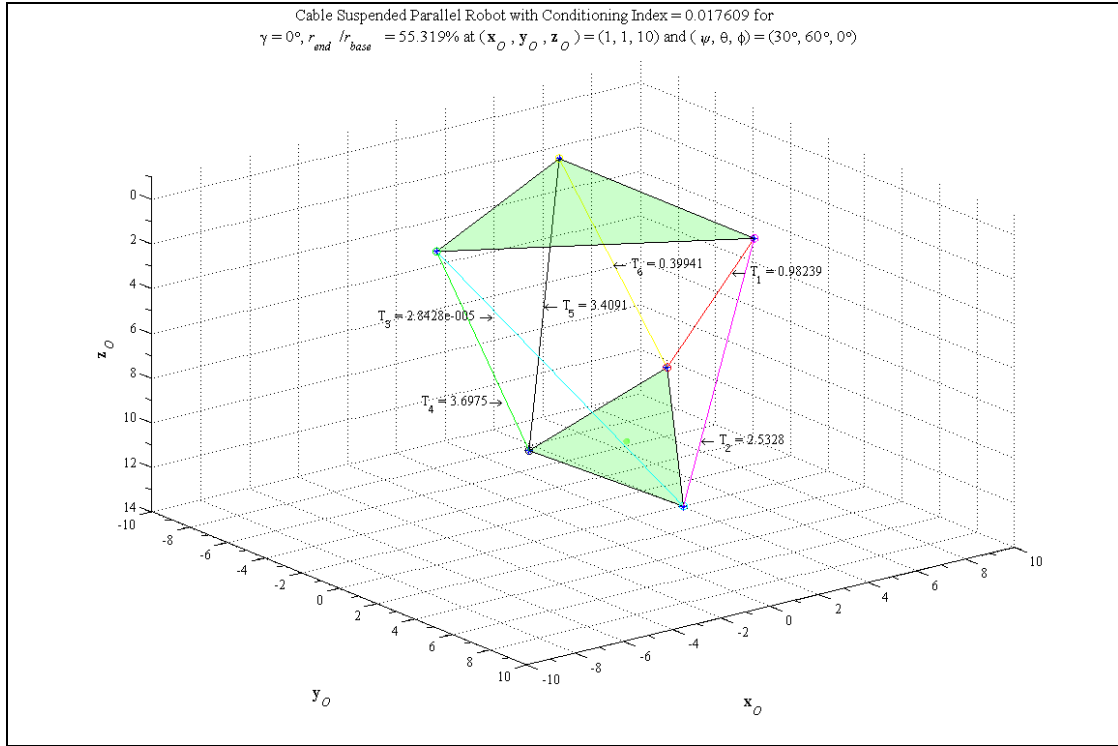


Fig. 3.15 Cable Suspended Parallel Robot for $\gamma = 0^\circ$, $(r_{end}/r_{base}) = 55.319\%$, at $(x_o, y_o, z_o) = (1, 1, 10)$ and $(\psi, \theta, \phi) = (30^\circ, 60^\circ, 0^\circ)$

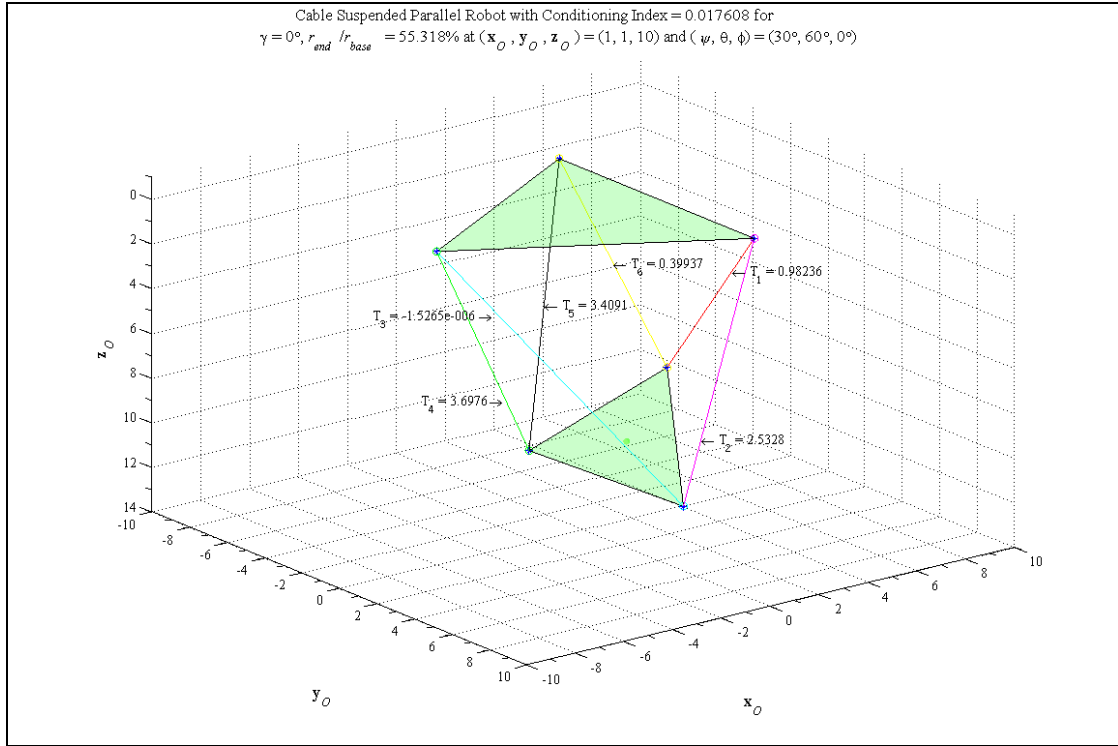


Fig. 3.16 Cable Suspended Parallel Robot for $\gamma = 0^\circ$, $(r_{end}/r_{base}) = 55.318\%$, at $(x_o, y_o, z_o) = (1, 1, 10)$ and $(\psi, \theta, \phi) = (30^\circ, 60^\circ, 0^\circ)$

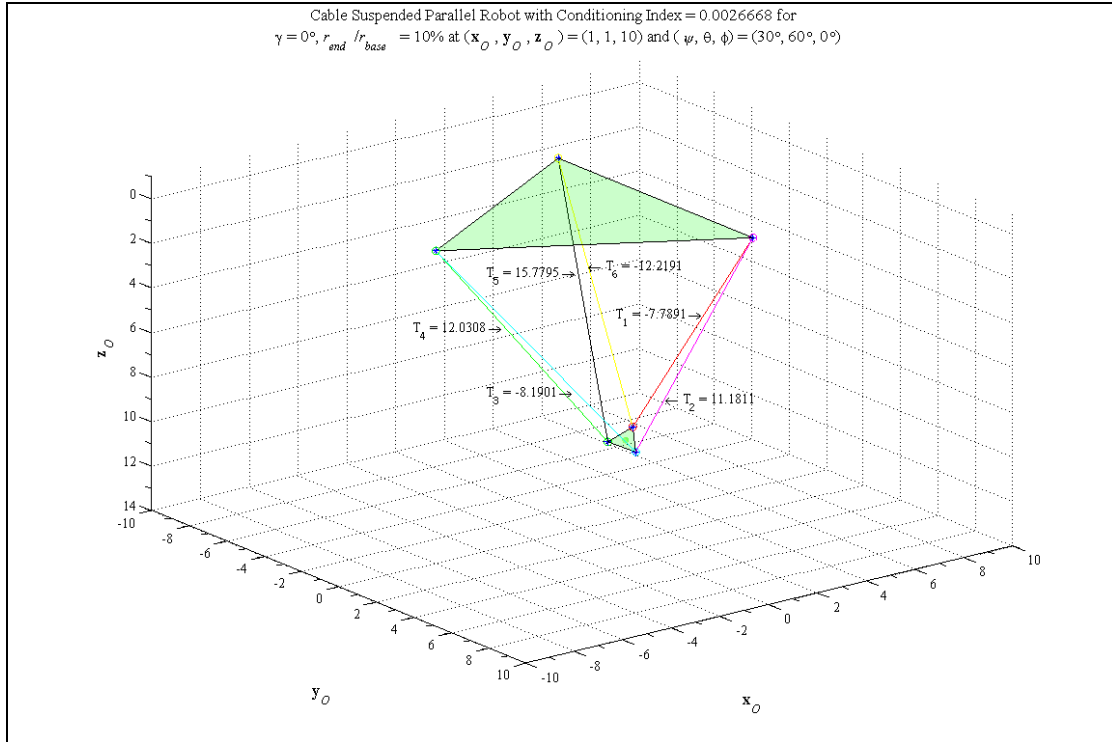


Fig 3.17 Cable Suspended Parallel Robot for $\gamma = 0^\circ$, $(r_{end}/r_{base}) = 10\%$, at $(x_o, y_o, z_o) = (1, 1, 10)$ and $(\psi, \theta, \phi) = (30^\circ, 60^\circ, 0^\circ)$

As the MP decreases in size, relative to the BP, the cables are not able to maintain tension and, at some point, the MP begins to require the cable to push to hold the MP at the desired orientation and position in question. These figures reveal that the cable force in cable 3 becomes negative when $(r_{end}/r_{base}) = 55.318\%$. This means that cable 3 must push on the MP in order to maintain that specific position and orientation. The conditioning index as shown in Table 3.5 is not singular but is tending towards an ill conditioned number as the ratio of the MP to the BP decreases. After comparing several different situations, it is found and verified that the cables do require pushing forces to maintain the desired position and orientation. The condition

number at a majority of the “good” points defining the workspace volume is comparably well behaved for positions and orientations where (r_{end}/r_{base}) is the largest possible.

3.5.2 Global Conditioning Index

The Global Conditioning Index (GCI) is used to encompass a more general perspective of the behavior of the condition number over the entire workspace volume into one value. As mentioned before, when the GCI is near one the robot Jacobian is well conditioned and when it is near zero the Jacobian is ill conditioned. After the MP is checked at each point in the region under study and all the “good” points are obtained with their corresponding condition number, then the GCI is calculated to get a comprehensive understanding of the condition number for the entire workspace. The GCI values are displayed in Fig. 3.18, Fig. 3.19, Fig. 3.20, and Fig. 3.21 and continued in Appendix (B) in a manner similar to that for the workspace volume results. The three surfaces in each plot are created from the individual Constant Orientation Workspace GCI values over the complete set of ψ and θ angles related to a constant value of ϕ for a particular γ geometry. The ratio $(r_{end}/r_{base}) = 100\%$, 50% , and 1% defines the three surfaces in each plot starting from the top surface and proceeding to the bottom surface respectively.

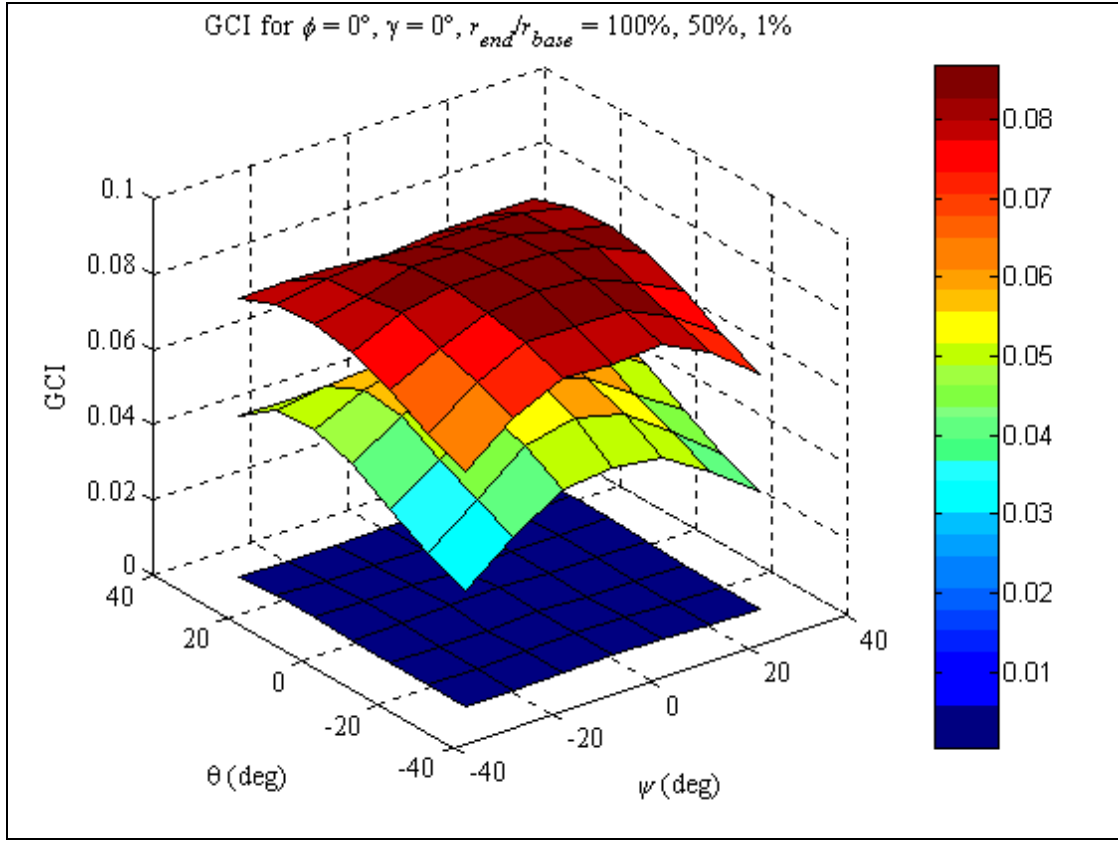


Fig. 3.18 GCI distribution for $\gamma = 0^\circ$, $(r_{end}/r_{base}) = 100\%, 50\%, 1\%$, and for $\phi = 0^\circ$

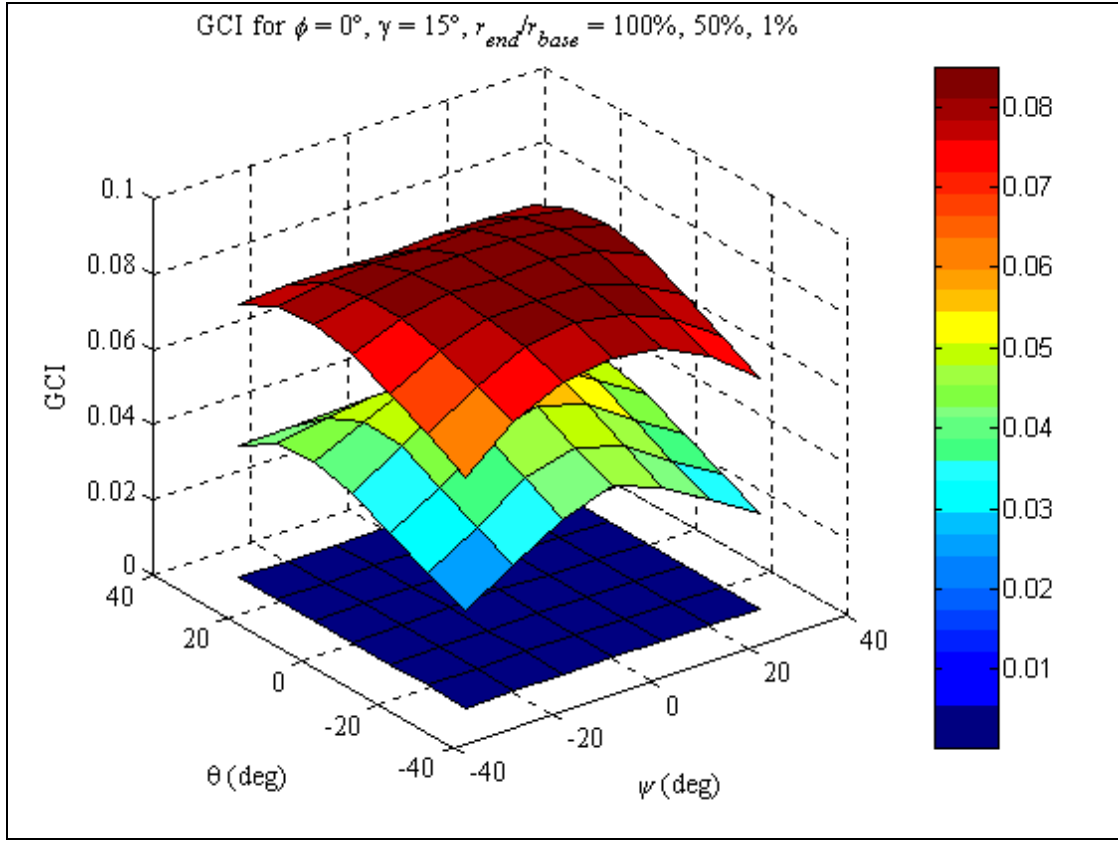


Fig. 3.19 GCI distribution for $\gamma = 15^\circ$, $(r_{end}/r_{base}) = 100\%$, 50% , 1% , and for $\phi = 0^\circ$

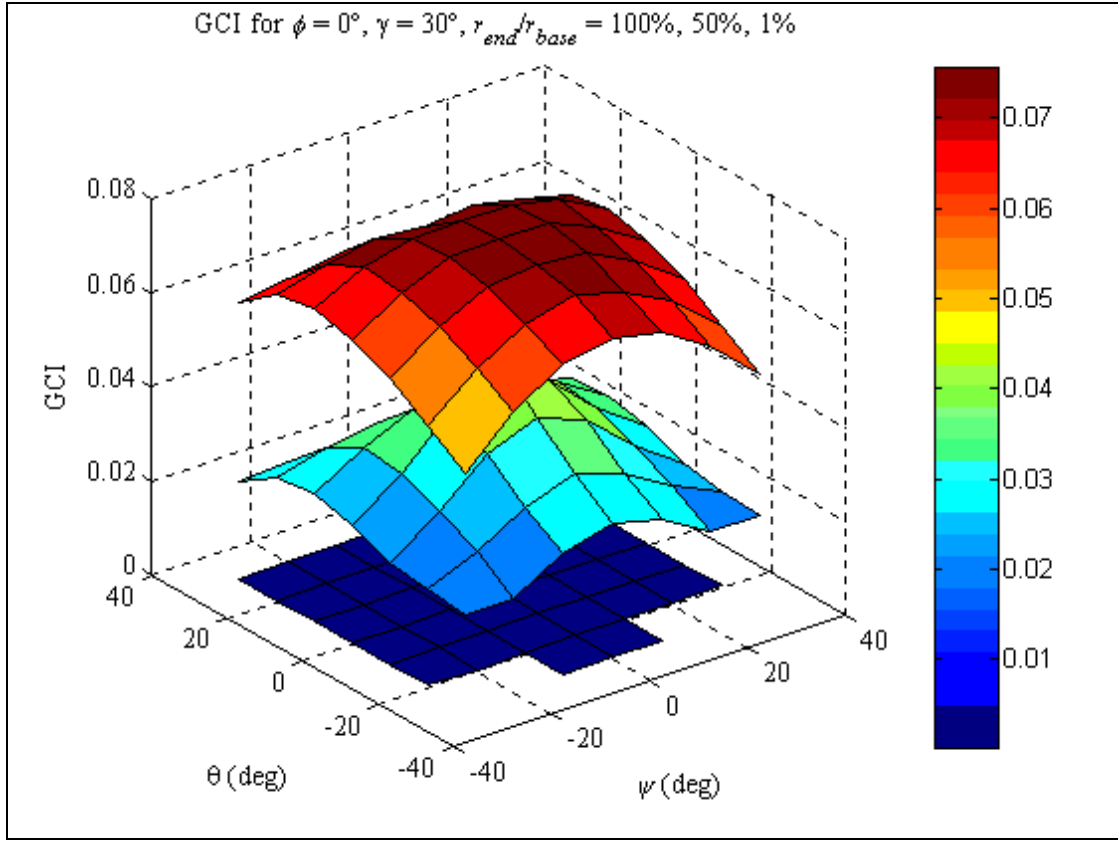


Fig. 3.20 GCI distribution for $\gamma = 30^\circ$, $(r_{end}/r_{base}) = 100\%$, 50% , 1% , and for $\phi = 0^\circ$

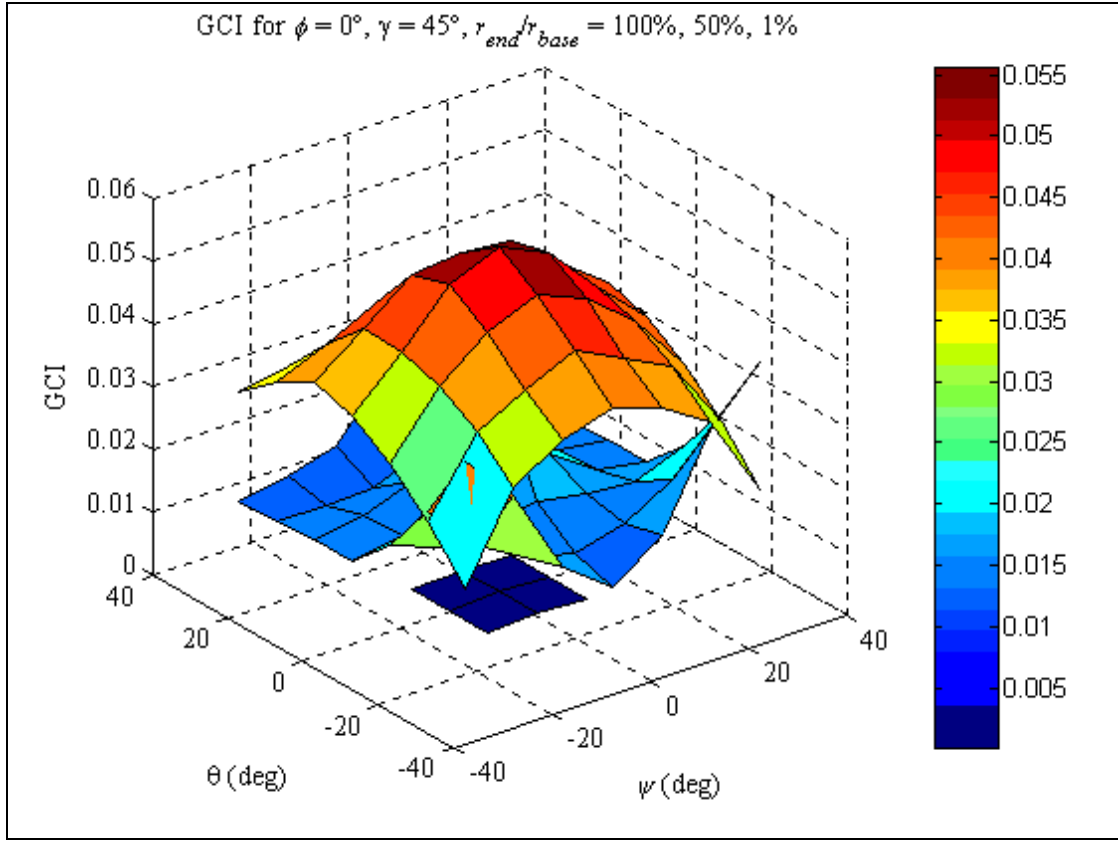


Fig. 3.21 GCI distribution for $\gamma = 45^\circ$, $(r_{end}/r_{base}) = 100\%$, 50% , 1% , and for $\phi = 0^\circ$

The trends discovered for the GCI behavior follow patterns similar to those found for the workspace volume magnitude. One trend found is that as the ratio of the MP to the BP decreases the GCI also decreases. Another pattern displayed from the graphs is that the smaller the γ value the better the GCI. When the MP rotates from the orientation $(\psi, \theta, \phi) = (0^\circ, 0^\circ, 0^\circ)$, the GCI generally tends to decrease. Again, due to symmetry of the parallel robot the GCI, values are mirrored in the same fashion as the workspace volume magnitudes.

The average of the GCI values are used to consolidate the extensive amount of data pertaining to the multiple orientations observed. All the GCI values for every constant orientation related to a fixed value of ϕ (rotation about the \mathbf{z}_O axis) are averaged for each γ geometry angle and (r_{end}/r_{base}) percent ratio. This data is then graphed over the set of orientations related to the constant ϕ versus the average GCI value, which is presented in Fig. 3.22, Fig. 3.23, Fig. 3.24 and Fig. 3.25 for $\gamma = 0^\circ$, 15° , 30° , and 45° respectively.

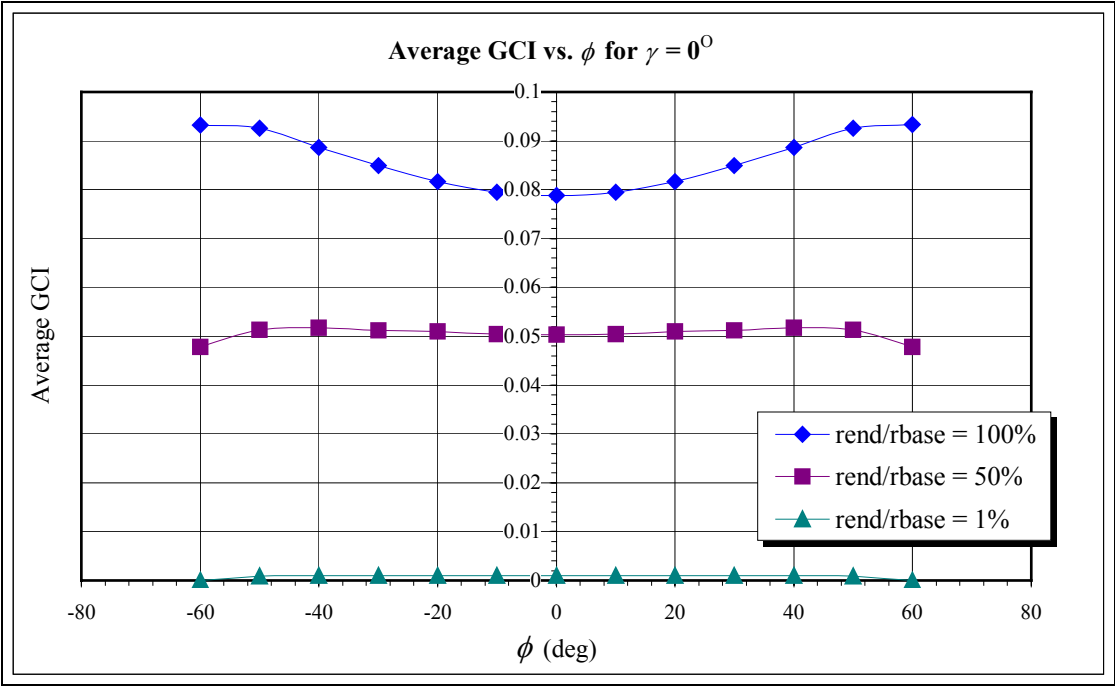


Fig. 3.22 Graph of Average GCI vs. ϕ for geometry $\gamma = 0^\circ$

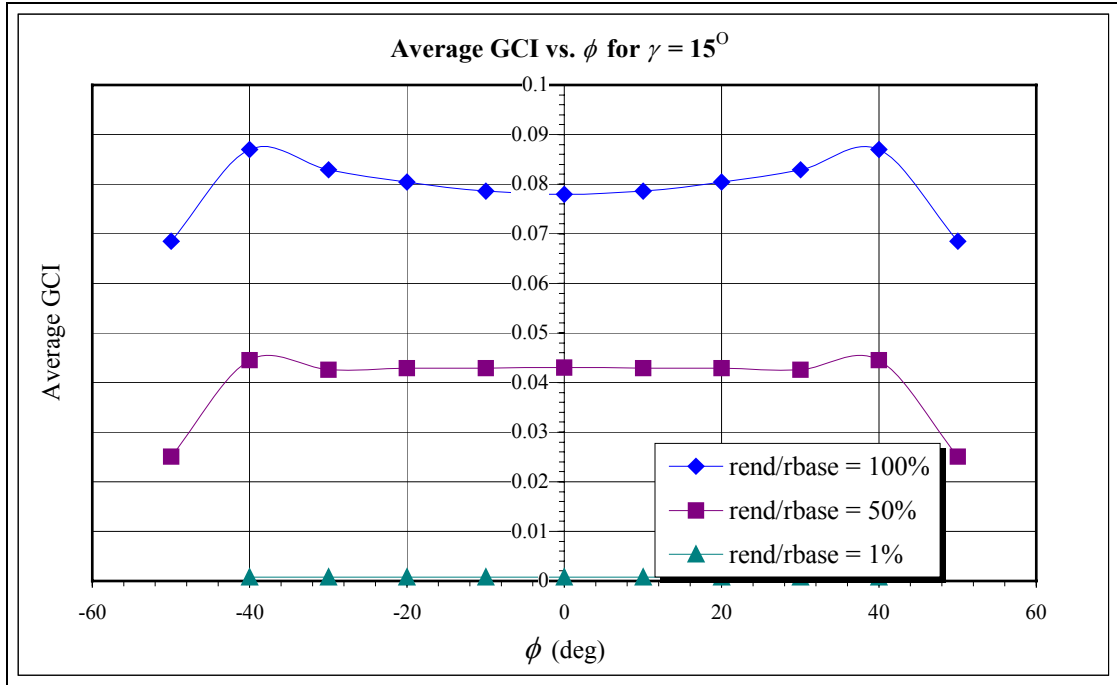


Fig. 3.23 Graph of Average GCI vs. ϕ for geometry $\gamma = 15^\circ$

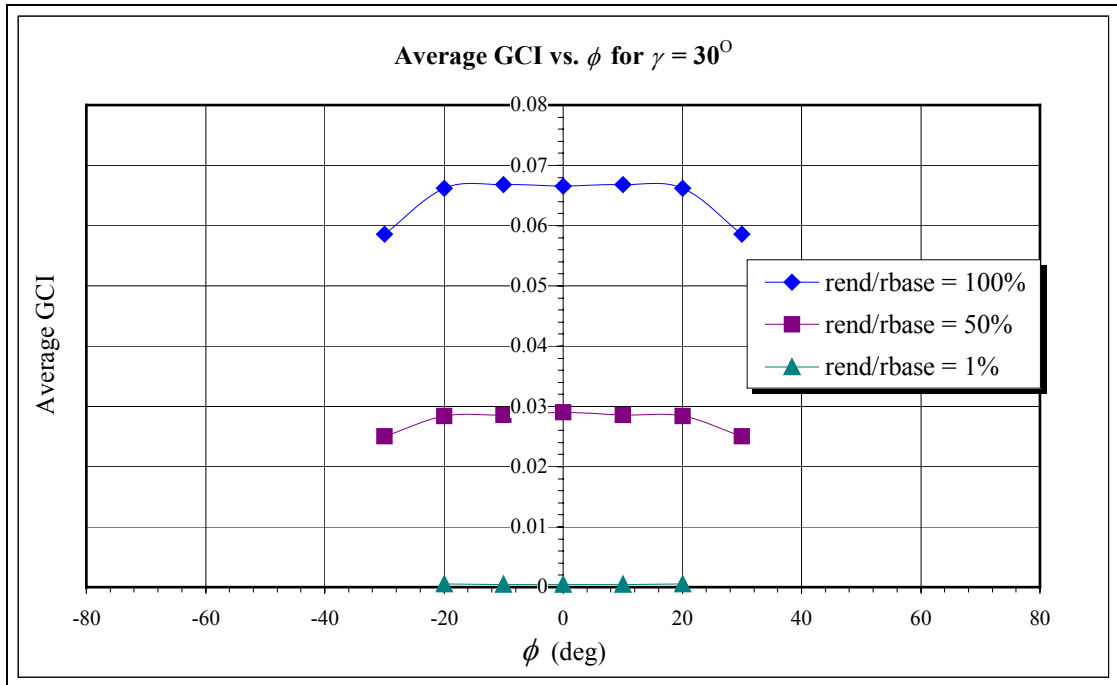


Fig. 3.24 Graph of Average GCI vs. ϕ for geometry $\gamma = 30^\circ$

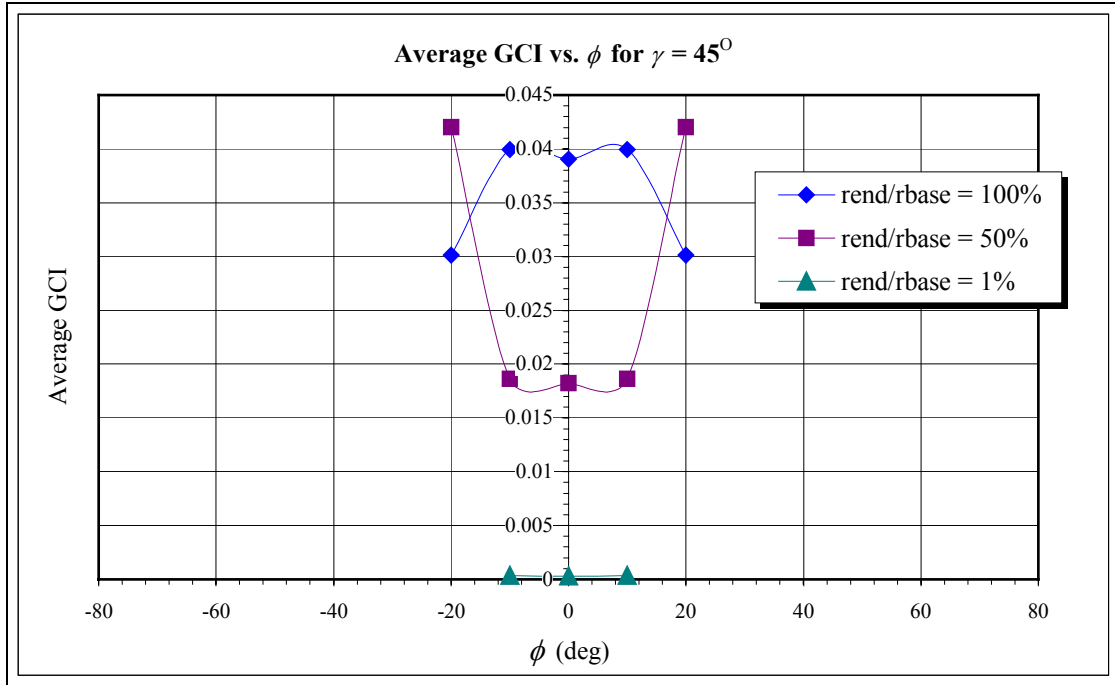


Fig. 3.25 Graph of Average GCI vs. ϕ for geometry $\gamma = 45^\circ$

From the graphs it is observed that the average GCI value increases slightly as the MP rotates itself from the set of orientations associated with $\phi = 0^\circ$, and then decreases as it approaches $\phi = \pm 60^\circ$ from $\phi = 0^\circ$. Taking a closer look at these trends it is noticed that at a certain set of ϕ orientations the average GCI reaches a maximum value then quickly decreases. The orientation where the maximum average GCI is reached appears to be somewhere near the orientations presented in Table 3.4. The data for the parallel robot with $\gamma = 45^\circ$ and $(r_{end}/r_{base}) = 50\%$ presented in Fig. 3.25, tends to not conform to this trend. The number of good points found for the workspace is very small, influencing the accuracy of the GCI

calculation. Choosing a smaller mesh size does produce a more accurate GCI value. For this study, however, the topic was not investigated any further.

The GCI, unfortunately due to its definition, gives only a “global” view of behavior of the condition number. This has the advantage of consolidating an intense amount of data into a format that is easier to analyze however it can be misleading because the exact behavior is generalized. Some specific points will be discussed in an attempt to understand how the condition number is distributed over the workspace.

The condition number is calculated at each point in the workspace that yielded tension in all the cables for a specific orientation, geometry, and size of the MP. The behavior of the condition number depends on the constant orientation selected for the MP and its position in the workspace. However, certain trends of the condition number value are present in the workspace volume. In each workspace volume, the condition number is noticeably larger for points near the ($z_O = 0$), plane. That is, when the MP is close to the BP the condition number increases or the conditioning index decreases. This was expected, for as the MP approaches the BP the cables become increasingly horizontal, which causes the normal force component to decrease and the horizontal force component to increase. The static equilibrium equations require the weight of the MP, ($m\mathbf{g}$), to be balanced by the normal force component in the cables. As the MP approaches the BP, the horizontal force component in each cable increases in order to maintain the vertical force required to balance the force of gravity. In other words, as the cables approach a horizontal orientation the tensions in the cables approach infinite values. A simple two-dimensional diagram is given in Fig. 3.26, to further explain the point visually. The concept further extends to the three-dimensional case for some angle is always present

in at least some of the cables for all the designs considered. The design pertaining to the case of $\gamma = 60^\circ$, did not yield any solutions and as stated previously was not considered any further. Even though the condition number increased as the MP approached the BP, the possible workspace volume was not restricted by this. The limitation on the possible workspace is due to the tension in the cables, i.e. the fact that the cables are only able to pull and not push on the MP.

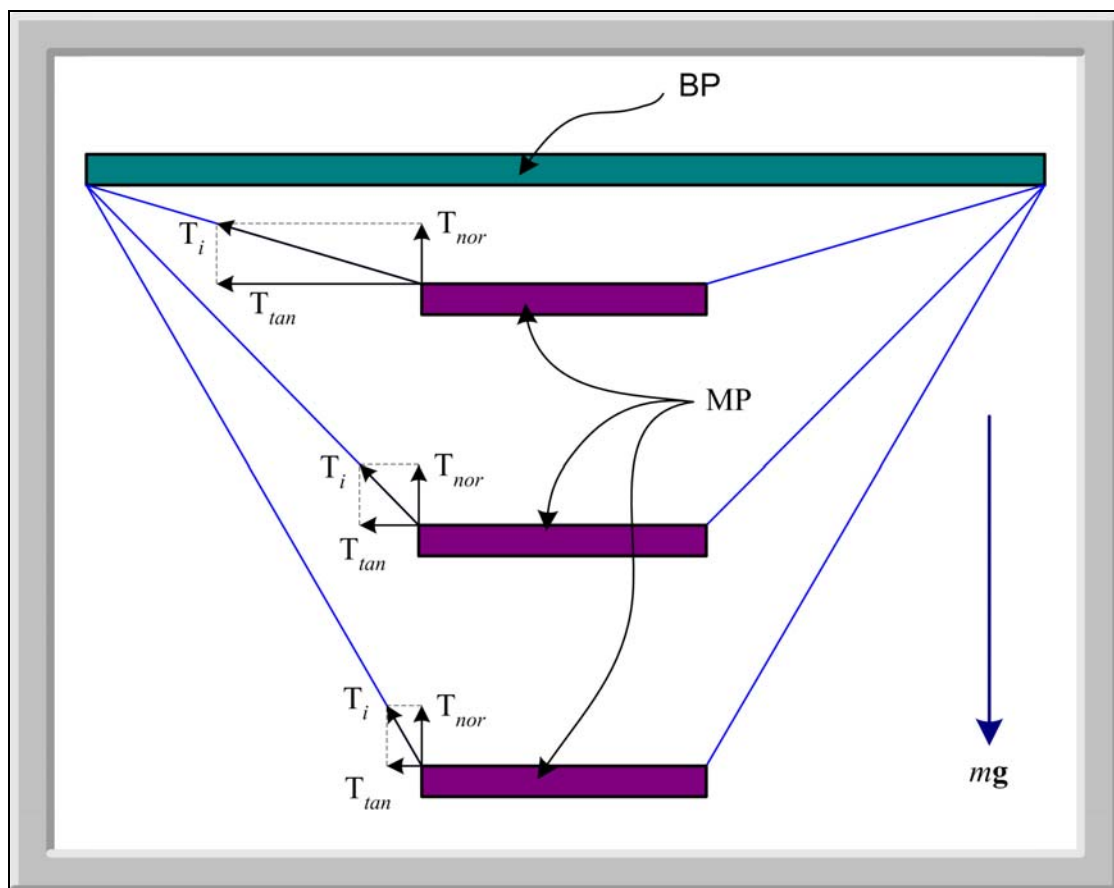


Fig. 3.26 Simple sketch of cable tensions and their normal tangential components

The defining shape of the workspace volume for a specific parallel robot depends on the constant orientation of the MP. As the MP rotated to different orientations, the Constant Orientation Workspace revealed many interesting trends. Only selected graphs that support the trends found will be shown as needed instead of presenting *all* the individual Constant Orientation Workspace plots, for each of the cable suspended parallel robots. The distribution of the conditioning index η is used instead of the condition number κ because the conditioning index gives a normalized value that can be compared easier.

One observation revealed that for the orientation of $(\psi, \theta, \phi) = (0^\circ, 0^\circ, 0^\circ)$ the workspace is maximum for any geometry chosen, an example is shown in Fig. 3.27 where $\gamma = 0^\circ$ and $(r_{end}/r_{base}) = 100\%$. Another common trend that appeared in most of the workspace shapes was the main cluster of workspace volume points for any constant orientation of the MP studied is generally located around the \mathbf{z}_O axis. In addition, it is noticed that the workspace has a concentrated region where the conditioning index is larger than the surrounding area. This region is generally located to one side of the volume if there is a rotation about the \mathbf{x}_O and/or \mathbf{y}_O axes and towards the center if there is no rotation about these axes. In Fig. 3.27 this region is located in the center of the workspace and near the $\mathbf{z}_O = 6$ plane surrounding the \mathbf{z}_O axis. When the MP is rotated, this cluster of workspace points with better conditioning index values shifts from the center towards the side with the connection point closest to the BP. An example of this is shown in Fig. 3.28 for $\gamma = 0^\circ$ and $(\psi, \theta, \phi) = (30^\circ, 350^\circ, 0^\circ)$. This trend still holds when the MP is rotated about only one of the \mathbf{x}_O or \mathbf{y}_O axes at a time while the other is held constant as shown in Fig. 3.29 for $\gamma = 0^\circ$ and $(\psi, \theta, \phi) = (30^\circ, 330^\circ, 0^\circ)$.

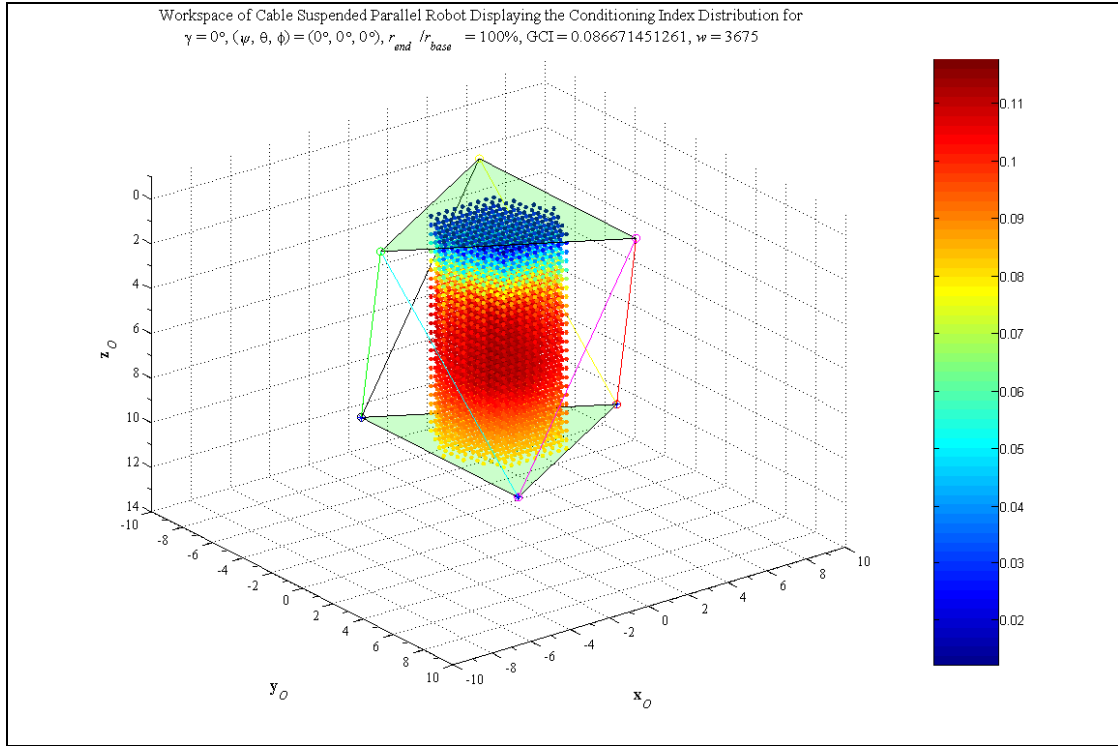


Fig. 3.27 Workspace of Cable Suspended Parallel Robot Displaying Conditioning Index Distribution for $\gamma = 0^\circ$, $(r_{end}/r_{base}) = 100\%$, and $(\psi, \theta, \phi) = (0^\circ, 0^\circ, 0^\circ)$

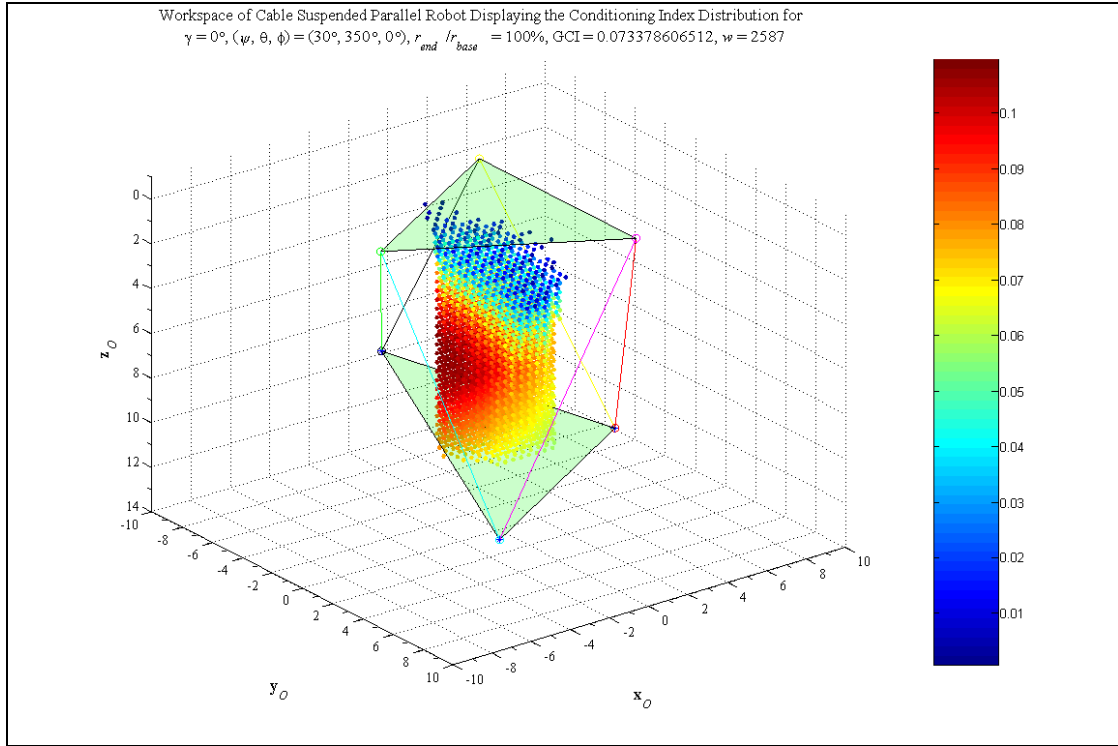


Fig. 3.28 Workspace of Cable Suspended Parallel Robot Displaying Conditioning Index Distribution for $\gamma = 0^\circ, (r_{end}/r_{base}) = 100\%$, and $(\psi, \theta, \phi) = (30^\circ, 350^\circ, 0^\circ)$

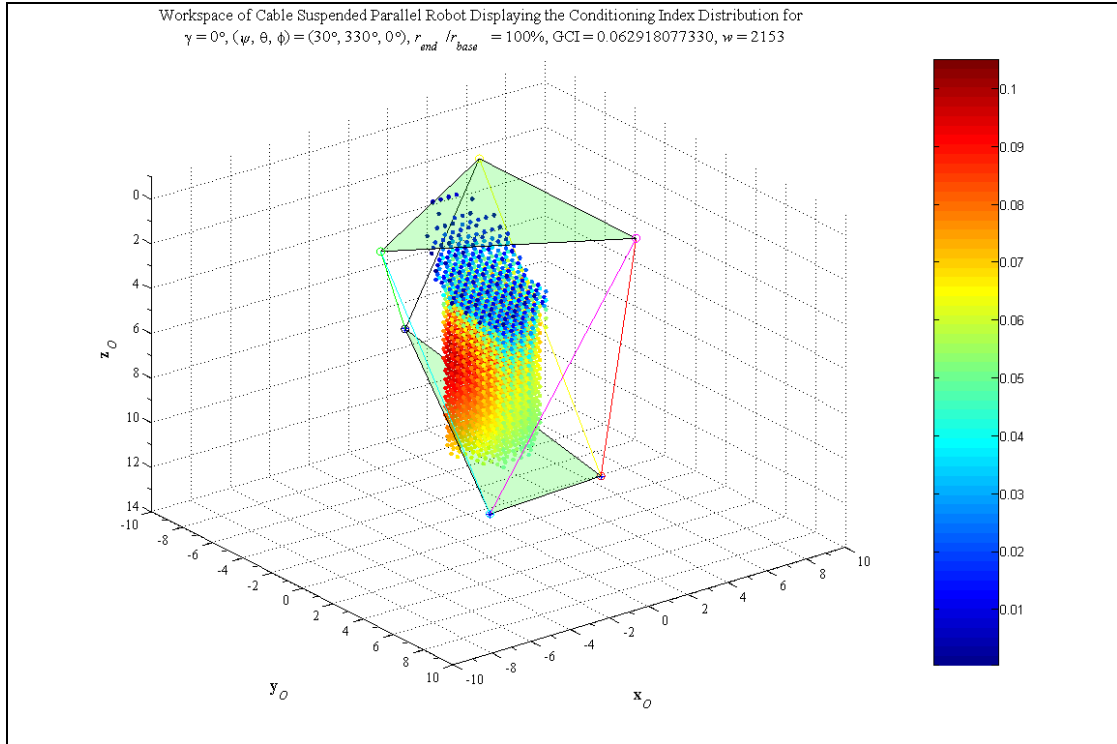


Fig. 3.29 Workspace of Cable Suspended Parallel Robot Displaying Conditioning Index Distribution for $\gamma = 0^\circ$, $(r_{end}/r_{base}) = 100\%$, and $(\psi, \theta, \phi) = (30^\circ, 330^\circ, 0^\circ)$

For each of the Constant Workspace Orientation graphs just mentioned there is some level of general symmetry that is noticed throughout the workspace. One trend that is not completely clear is the variation of the conditioning index value for large distances away from the BP. A separate study revealed that as the MP tends towards infinity along the \mathbf{z}_O axis, the conditioning index for these locations tends towards zero, and the Jacobian becomes ill conditioned as displayed in Fig. 3.30 for $\mathbf{z}_O = 100$, $\gamma = 0^\circ$, $(r_{end}/r_{base}) = 100\%$, and $(\psi, \theta, \phi) = (0^\circ, 0^\circ, 0^\circ)$. The step size along each axis was set to 0.4 and the search region spanned the area $(-8 \leq \mathbf{x}_O \leq 8, -8 \leq \mathbf{y}_O \leq 8)$ to remain consistent with the majority data. The only change was the

extension search region along the z_O axis. A decreasing conditioning index is not a desirable trait for any robotic manipulator. For a cable suspended parallel robot this means that at distances far away from the BP the MP will result in poor transmission of the position and orientation as well as the transmission forces and moments.

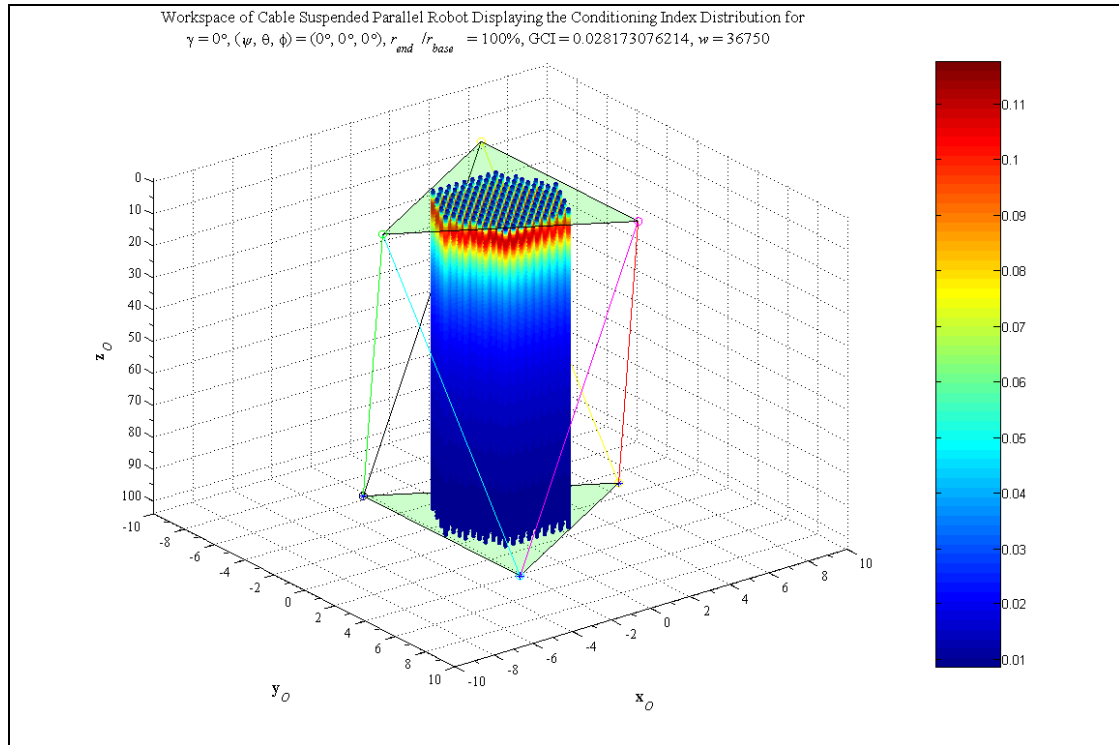


Fig. 3.30 Workspace of Cable Suspended Parallel Robot Displaying Conditioning Index Distribution with a large value of z_O for $\gamma = 0^\circ$, $(r_{end}/r_{base}) = 100\%$, and $(\psi, \theta, \phi) = (0^\circ, 0^\circ, 0^\circ)$

3.6 Conclusion

In this chapter, twelve different cable suspended parallel robots were studied over a range of orientations as noted in Table 3.1 and Table 3.2. The different

design variations among the robots included the geometric angle γ and the percent ratio (r_{end}/r_{base}) of the MP to the BP. The workspace and GCI value were analyzed for each robot and compared to determine the “best” design. The data presented general trends that were acknowledged in the preceding sections and for some trends, supplementary case studies have been added for a deeper understanding. It is noted that the case studies presented in the sections provide only additional insight and support.

The preferred design is generally one with the largest workspace, the highest GCI, and the largest range of orientations. It was found that the workspace volume increases as the geometric γ angle decreases and/or the (r_{end}/r_{base}) percent ratio increases. In general, the GCI followed the same trends as the workspace volume, that is, it increases as the γ angle decreases and/or the (r_{end}/r_{base}) percent ratio increases.

The complete set of Constant Orientation Workspace graphs displaying the variation of the conditioning index and the shape of the workspace volume were not presented due to the extensive amount of data involved; however, selected trends were discussed. One trend that was noticed was that when the MP is close to the BP the robot Jacobian becomes ill conditioned. Another observation of the Constant Orientation Workspace shape was that the points that were reachable were generally located around the \mathbf{z}_O axis in a continuous volume. In addition, as the MP is rotated to different orientations, the Constant Orientation Workspace shape changes accordingly.

This chapter presented several useful trends and insights to the design selection and workspace behavior for cable suspended parallel robots. Cable suspended parallel robots have a smaller workspace when compared to traditional

parallel robots for the same size actuation lengths. However, cables can reasonably be extended to lengths far exceeding those of traditional parallel actuators but it is also noted that as the MP travels to distances far from the BP the robot Jacobian matrix becomes ill conditioned. From the analysis of all the data it appeared that the cable suspended parallel robot associated with $\gamma = 0^\circ$ and $(r_{end}/r_{base}) = 100\%$ had the largest workspace volume and the best GCI for the largest range of orientations.

Chapter 4

PRACTICAL DESIGN APPLICATIONS

4.1 Introduction

The workspace analysis is a tool used to compare one possible design of a robot against another. In the previous chapter, general trends relating several geometric parameters to the workspace were observed. In this chapter, specific design cases are presented for various robot geometries and sizes pertaining to cable suspended parallel robots. Each cable suspended robot is compared to observe how well one design is able to orient its MP perpendicular to a known surface versus another. The goal of this chapter is to verify that these trends are useful in considering the design of cable suspended parallel robots for practical applications.

A possible application where this particular design analysis may be valuable includes tasks such as welding, painting, washing, surface inspection, and pick and place tasks, etc. For such applications, it is desirable to choose a parallel robot that is able to manipulate itself over the largest surface area with the highest GCI value. Choosing a robot with the largest workspace volume is quite straightforward for it yields increased versatility. A design with a high GCI is one with a globally well-conditioned Jacobian. This directly correlates to the degree in which the robot is able to accurately position and orientate itself throughout the workspace and transmit forces and torques.

This chapter will begin by defining the problem statement and goals for the chapter, including a general definition of the surfaces considered and the performance indices used to evaluate the surfaces. In the next section, the various cable suspended parallel robots used and how they are defined is presented. The details of the specific surface cases are presented next along with the results. Finally, the chapter ends with a summary of the conclusions based on the design cases considered.

4.2 Problem Statement

The objective of this design problem is to determine which cable suspended parallel robot can orient itself perpendicular to the surface in question with the largest workspace and highest GCI. The workspace in this case will be measured by the amount of surface area in which the robot is able to reach. Three different surface conditions are considered for this design problem. Each surface is broken up into a discrete mesh of nodal points that define the particular surface. The first surface, Surface 1, is a half cylinder positioned with its longitudinal axis parallel to the \mathbf{x}_O axis and center located at some distance from the BP. The second surface, Surface 2, is also a half cylinder located at some distance from the BP though its longitudinal axis is parallel to the \mathbf{y}_O axis. For both cylinder surfaces the MP is not rotated about the \mathbf{z}_O axis but fixed to $\phi = 0^\circ$, in addition the dimensions of both surfaces are the same. The reason for using the same surface oriented in two different manners is to attempt to gain a deeper understanding of the workspace shape. The third surface, Surface 3, is a simple $(\mathbf{x}_O, \mathbf{y}_O)$ plane located at $\mathbf{z}_O = \text{constant}$. For this surface, each robot is evaluated at every node for a set of constant ϕ orientations. The detail of each surface case studied is given in the Case Study Results Section. In Table 4.1, the

surfaces are assigned a number, which will be used occasionally throughout the rest of the chapter for quick reference.

Table 4.1: Design Surfaces	
Surface #	Surface Description
1	Half cylinder with longitudinal axis parallel to \mathbf{x}_O
2	Half cylinder with longitudinal axis parallel to \mathbf{y}_O
3	Plane located at $\mathbf{z}_O = \text{constant}$

Table 4.1 Design Surfaces

A Matlab program was created to evaluate how well a particular cable suspended parallel robot is able to reach and orient itself perpendicularly to the discrete nodal points defining a surface. The inputs to this program are the robot geometry γ , the percentage of the MP to the BP, the surface and for the simple plane the MP orientation ϕ about the \mathbf{z}_O axis. The program evaluates whether or not the MP of a cable suspended parallel robot is able to locate itself perpendicular to the surface. The criteria used to deem a point on the surface reachable is that all the cables must be in tension under static conditions. No dynamic affects are considered for any of the examples presented in this chapter. The tools used for comparison include calculating the condition number for each reachable surface point, summing the total number of workspace volume or surface points and calculating the GCI.

4.3 Design Model

The cable suspended parallel robots selected will adhere to the same restrictions that were presented in the previous chapter on workspace. A brief review of these restrictions is mentioned again here for completeness. The base points (b_1 ,

\dots, b_6) are restricted to the ($\mathbf{z}_O = 0$) plane and the MP points (a_1, \dots, a_6) are restricted to the ($\mathbf{z}_E = 0$) plane. All BP points will be located at a common radius of r_{base} and similarly all MP points are located at a common radius of r_{end} . The radius of the BP is fixed to ($r_{base} = 6$) for every robot. For a chosen robot, the geometry for the BP and the MP are both defined by the same geometric γ value that is defined in the workspace chapter. Dissimilar geometric shapes of the BP and MP are not considered. Several different geometric shapes and sizes of the MP are chosen. The shapes included geometries for $\gamma = 0^\circ, 15^\circ, 30^\circ,$ and 45° where the same shape applies to both the MP as well as the BP. Fig. 4.1 presents a quick reference of these shapes. The exact values of the MP to BP ratios used are defined separately in the relevant sections for each surface.

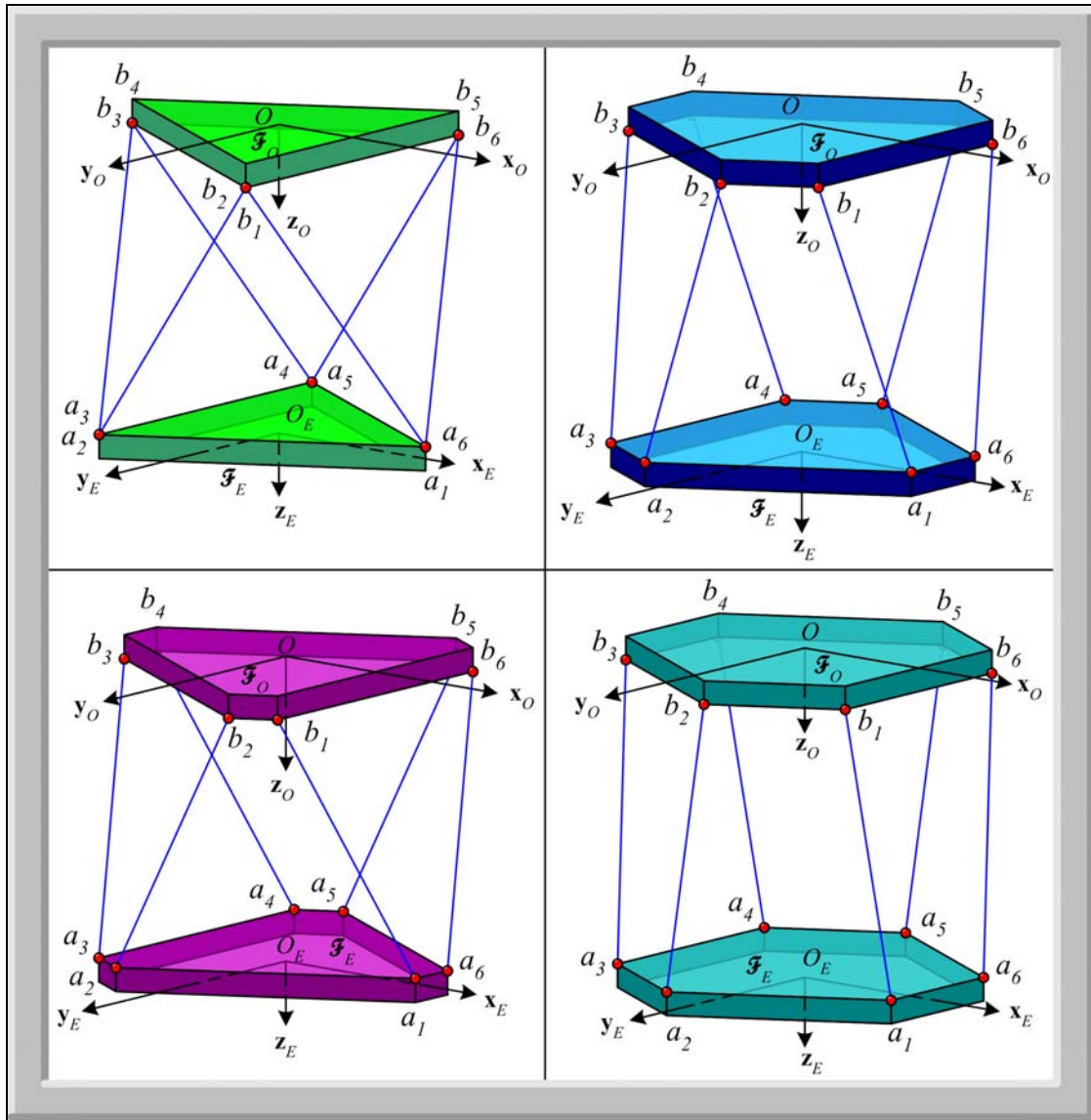


Fig. 4.1 Three Dimensional view of all four γ geometries

4.4 Case Study Results

The size of each surface used was chosen to be considerably larger than the BP and spanned to regions well beyond an area where the MP is able to reasonably

reach. The dimensions were based on preliminary sample runs where the surfaces were meshed with a large grid to compensate for computational time involved. The exact dimensions chosen were the ones that yielded the most perceptive results. In the next subsections, the cylinder surfaces 1 and 2 are presented together for obvious comparison reasons, followed by the case study for the plane surface.

4.4.1 Surface 1 and 2: Cylinder

Surface 1 is a half cylinder with its longitudinal axis parallel to the \mathbf{x}_O axis, and Surface 2 is a half cylinder with its longitudinal axis parallel to the \mathbf{y}_O axis. For comparison purposes, the dimensions of both half cylinders are fixed to the same values with a radius of ($r_{cyl} = 2$), length of ($L_{cyl} = 16$) and center located at the point ($\mathbf{x}_O = 0, \mathbf{y}_O = 0, \mathbf{z}_O = 10$). To insure consistency the mesh step size along the longitudinal axis of the half cylinder is fixed to 0.1 and the angular step size fixed to 2° for every run.

The cable suspended parallel robots chosen include four different γ geometries and eleven different ratios of the MP to the BP for forty-four different robots for this analysis. The values for γ and the percentages for (r_{end}/r_{base}) are shown in Table 4.2.

Table 4.2: Cable Suspended Parallel Robots Considered for Surfaces 1& 2	
Parameter	Value
γ	$0^\circ, 15^\circ, 30^\circ, 45^\circ$
$(r_{end}/r_{base}) \%$	100%, 90%, 80%, 70%, 60%, 50%, 40%, 30%, 20%, 10%, 1%

Table 4.2 Cable Suspended Parallel Robots Considered for Surfaces 1 & 2

Each cable suspended parallel robot is evaluated at every point that defines the half cylinder surface to determine if the point in question will yield tension in all the cables. If the point does yield positive tensions for all the cables then the condition number is calculated for that point. When the entire surface is checked the GCI is calculated. As previously mentioned, the MP is fixed to $\phi = 0^\circ$ and not rotated about the \mathbf{z}_O axis as it is positioned at each point on either of the half cylinder surfaces.

A plot of the workspace volume versus the (r_{end}/r_{base}) percent ratio is displayed in Fig. 4.2 for Surface 1. It is observed for all γ geometry values, that the workspace decreases as (r_{end}/r_{base}) decreases. In addition, as γ increases the workspace volume decreases. A plot of GCI versus (r_{end}/r_{base}) for Surface 1 is shown in Fig. 4.3. The GCI value increases as (r_{end}/r_{base}) increases and γ decreases.

Surface 2 yielded similar trends, as is observed from Fig. 4.4 and Fig. 4.5, to Surface 1. That is, the workspace decreases as (r_{end}/r_{base}) decreases for all geometries and as γ increases the workspace decreases. However, changing the orientation of the longitudinal axis of the half cylinder surface from the \mathbf{x}_O axis for Surface 1, to the \mathbf{y}_O axis for Surface 2, the workspace increases but the GCI decreases and becomes slightly worse. The shape maximum workspace is in Fig. 4.6 and Fig. 4.7 displaying the conditioning index distribution for the cable suspended parallel robot with $\gamma = 0^\circ$ and $(r_{end}/r_{base}) = 100\%$ for Surfaces 1 and 2 respectively.

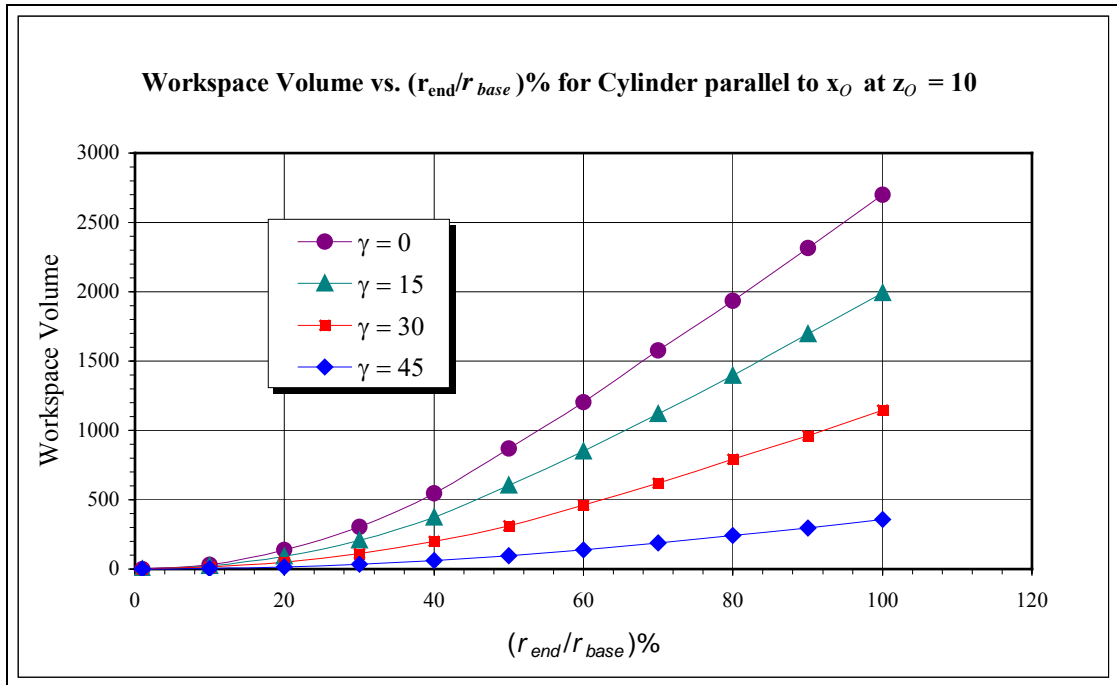


Fig. 4.2 Workspace Volume vs. $(r_{end}/r_{base})\%$ for Surface 1

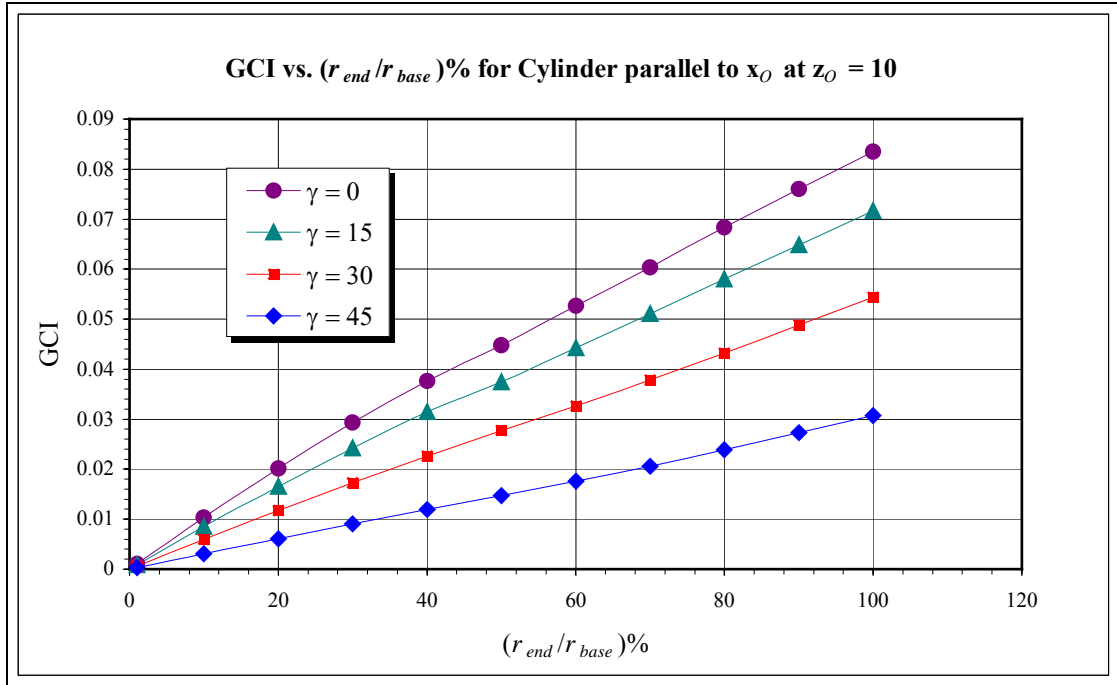


Fig. 4.3 GCI vs. $(r_{end}/r_{base})\%$ for Surface 1

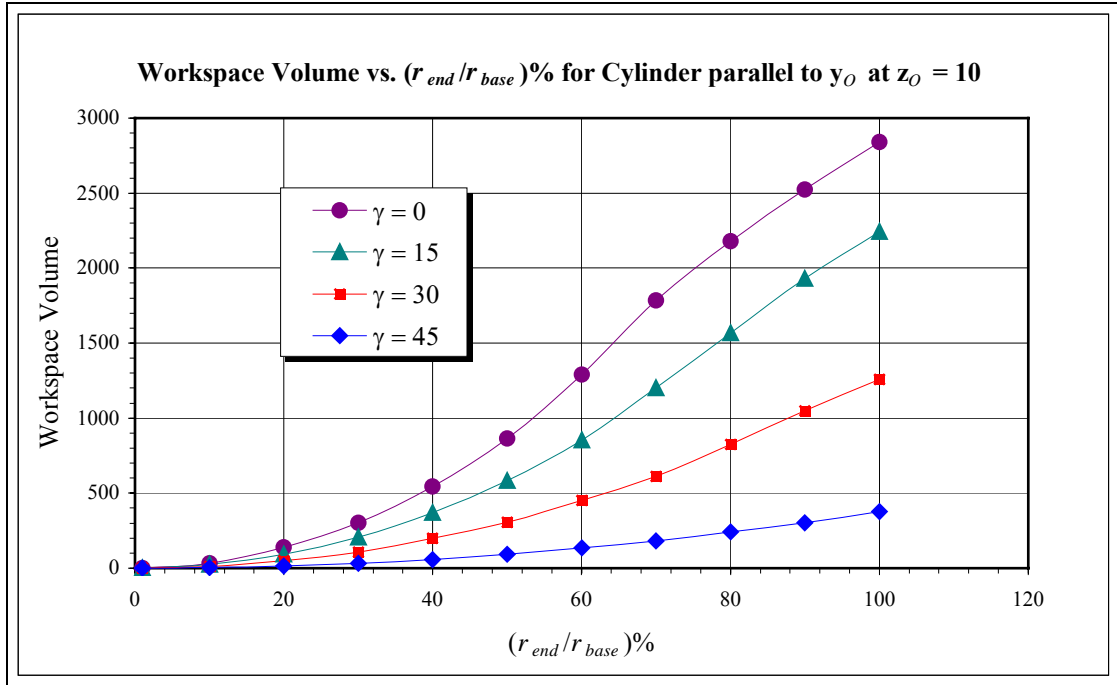


Fig. 4.4 Workspace Volume vs. $(r_{end}/r_{base})\%$ for Surface 2

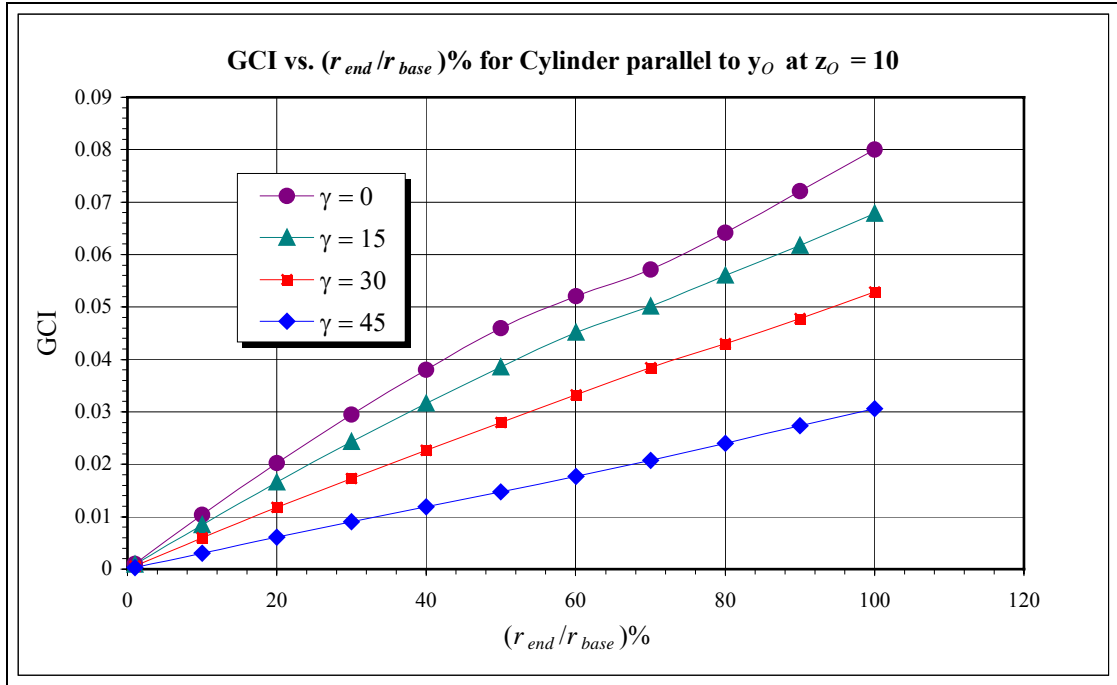


Fig. 4.5 GCI vs. $(r_{end}/r_{base})\%$ for Surface 2

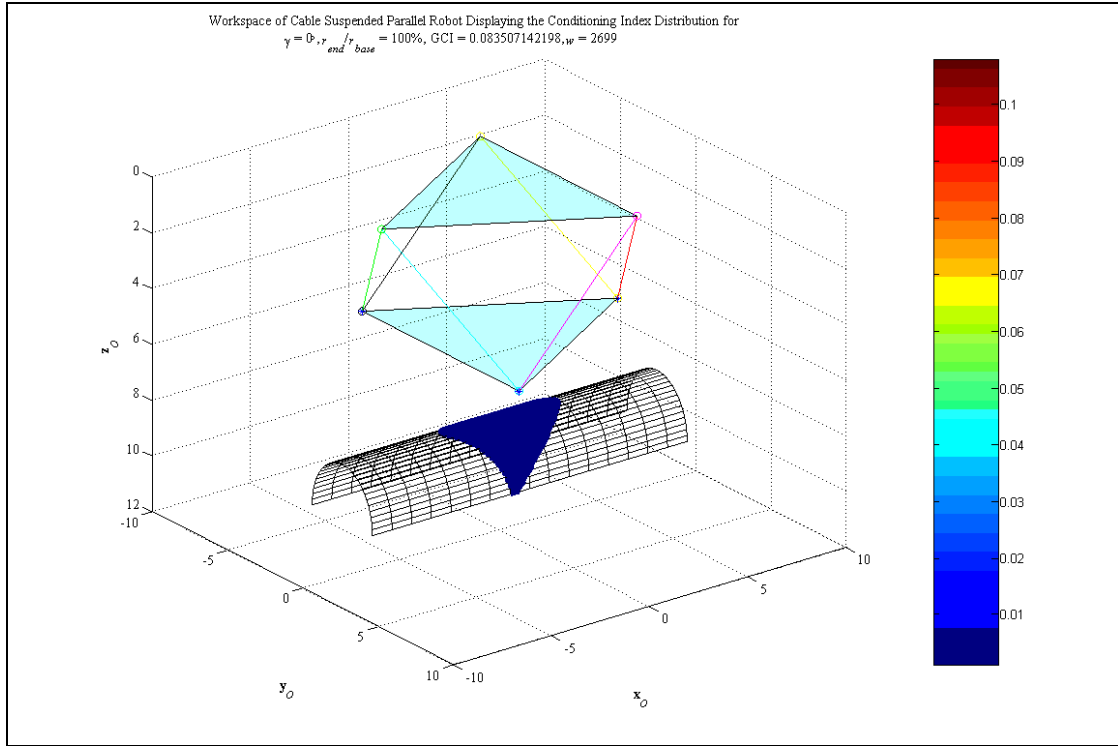


Fig. 4.6 Workspace Volume displaying the conditioning index distribution for Surface 1

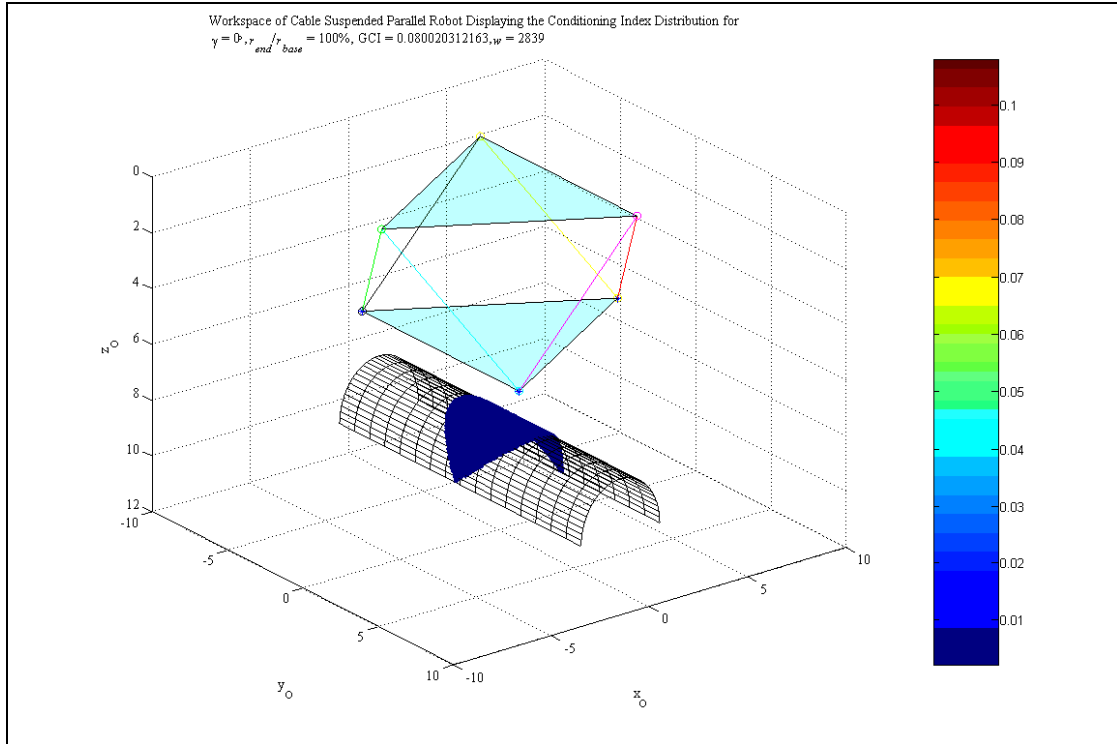


Fig. 4.7 Workspace Volume displaying the conditioning index distribution for Surface 2

4.4.2 Surface 3: Simple Plane

The third surface considered, Surface 3, is a simple plane defined as $(-8 \leq x_o \leq 8, -8 \leq y_o \leq 8, z_o = 5)$. The surface is represented by a mesh of grid points with a step size of 0.1 along each of the x_o and y_o axes. The cable suspended parallel robots considered for this surface include all combinations of the four values of γ and five ratios of (r_{end}/r_{base}) shown in Table 4.3.

Table 4.3: Cable Suspended Parallel Robots Considered for Surface 3	
Parameter	Values Used
γ	$0^\circ, 15^\circ, 30^\circ, 45^\circ$
$(r_{end}/r_{base}) \%$	100%, 80%, 50%, 20%, 1%

Table 4.3 Cable Suspended Parallel Robots Considered for Surfaces 3

The MP for each robot is rotated through a discrete set of constant orientations about the \mathbf{z}_O axis defined by $(-60^\circ \leq \phi \leq 60^\circ)$ with a step size of 10° . These values are presented in Table 4.4 for quick reference. It is understood that $(\psi = 0^\circ, \theta = 0^\circ)$ must be true for the MP to be perpendicular to the plane.

Table 4.4: Set of Orientations Used for Robots Encountering Surface 3	
	Degrees
ψ	0°
θ	0°
ϕ	$0^\circ, 10^\circ, 20^\circ, 30^\circ, 40^\circ, 50^\circ, 60^\circ, 300^\circ, 320^\circ, 330^\circ, 340^\circ, 350^\circ$

Table 4.4 Set of Orientations Used for Robots Encountering Surface 3

The graphs of the reachable workspace points versus the range of ϕ orientations for all the ratios of (r_{end}/r_{base}) are shown in figures Fig. 4.8, Fig. 4.9, Fig. 4.10 and Fig. 4.11 for the geometric values $\gamma = 0^\circ, 15^\circ, 30^\circ, \text{ and } 45^\circ$ respectively for Surface 3. The reachable workspace refers to the number of point locations on the surface that the MP is able to encounter with tension in all the cables.

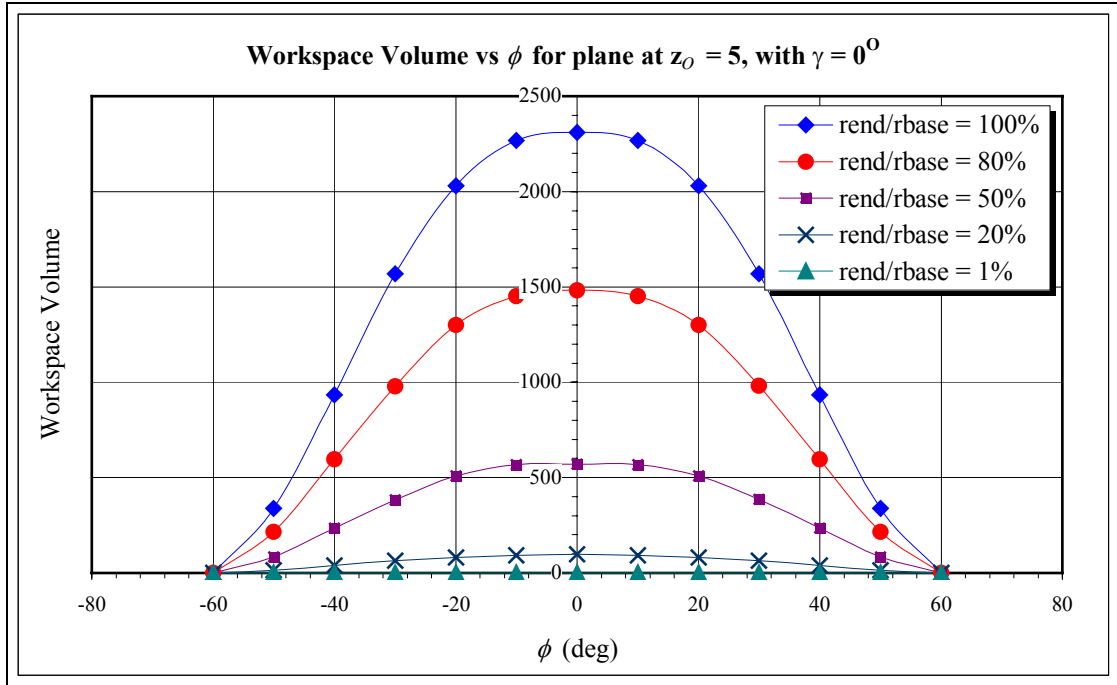


Fig. 4.8 Workspace vs. ϕ for $\gamma = 0^\circ$, Surface 3

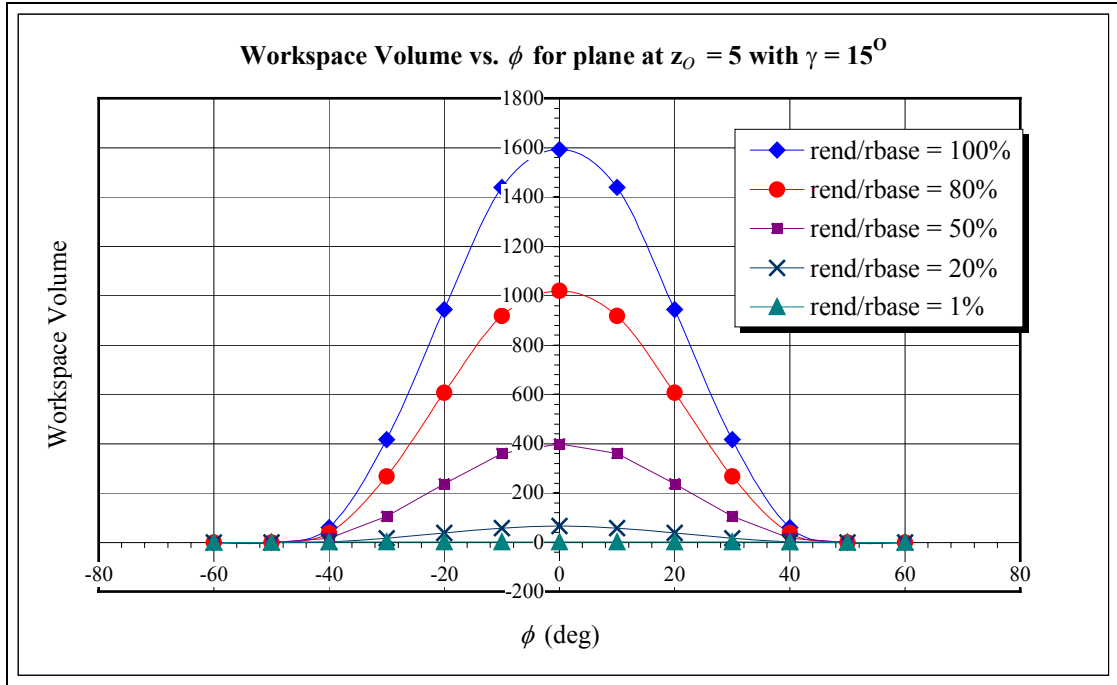


Fig. 4.9 Workspace vs. ϕ for $\gamma = 15^\circ$, Surface 3

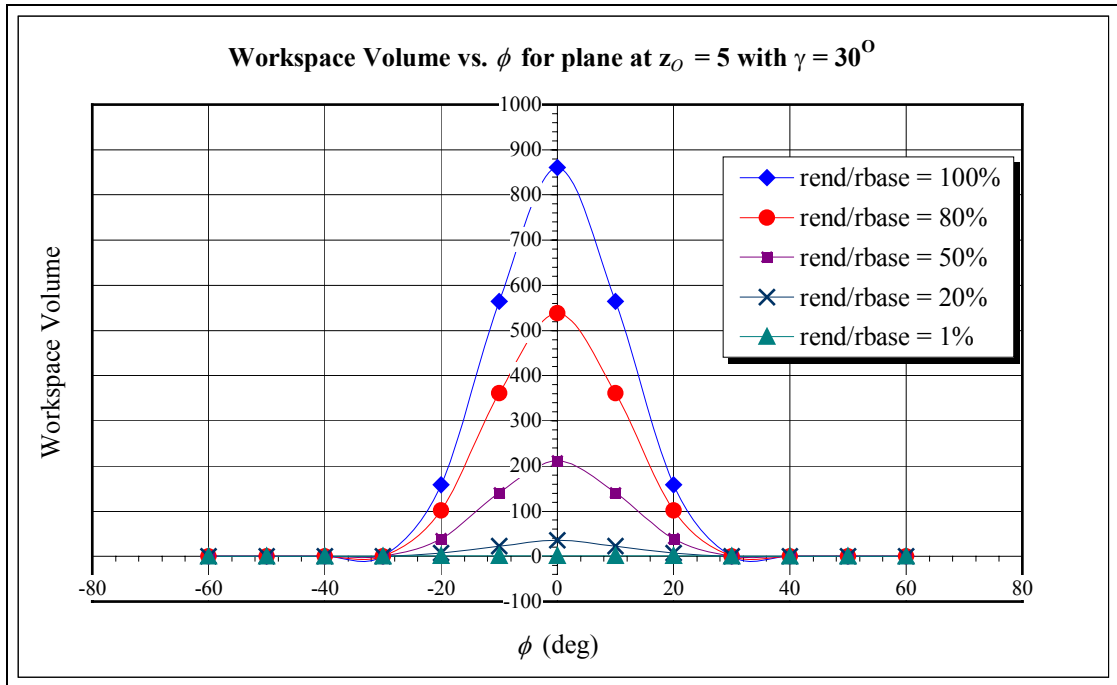


Fig. 4.10 Workspace vs. ϕ for $\gamma = 30^\circ$, Surface 3

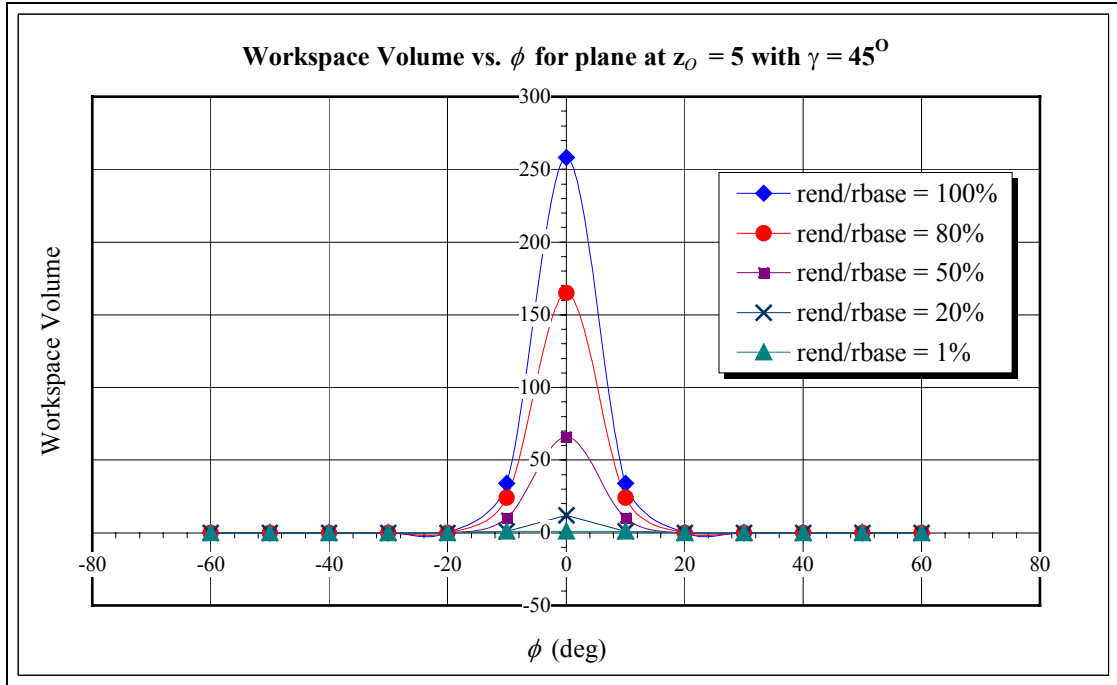


Fig. 4.11 Workspace vs. ϕ for $\gamma = 45^\circ$, Surface 3

As observed from the graphs of the workspace volume vs. ϕ shown in Fig. 4.8, Fig. 4.9, Fig. 4.10 and Fig. 4.11, as γ increases the workspace decreases. In addition, as (r_{end}/r_{base}) decreases the workspace decreases for each γ value. These results directly support the trends relayed in the Workspace and Analytical Design Chapter 3. The behavior of the GCI values versus the ϕ orientations is similarly displayed in Fig. 4.12, Fig. 4.13, Fig. 4.14, and Fig. 4.15 for $\gamma = 0^\circ, 15^\circ, 30^\circ$, and 45° respectively. It is noted that the abrupt end of the curves is where no points exist at that orientation and therefore no values for the GCI exist. It can be seen that the $\gamma = 0^\circ$ geometry has the highest GCI for comparative orientations and (r_{end}/r_{base}) ratios. However, for the three robots $\{\gamma = 0^\circ, (r_{end}/r_{base}) = 100\%\}$, $\{\gamma = 0^\circ, (r_{end}/r_{base}) =$

80%} and $\{\gamma = 15^\circ, (r_{end}/r_{base}) = 100\%\}$ the GCI values are fairly close to one another for small orientations away from $\phi = 0^\circ$. In addition, the workspace is relative the same for $\{\gamma = 0^\circ, (r_{end}/r_{base}) = 80\%\}$ and $\{\gamma = 15^\circ, (r_{end}/r_{base}) = 100\%\}$ for these same small range of orientations about $\phi = 0^\circ$. The workspace for $\gamma = 0^\circ$ and $(r_{end}/r_{base}) = 100\%$ at the orientation $\phi = 0^\circ$ is drawn in Fig. 4.16 to see the distribution of workspace points with the corresponding values of the conditioning index.

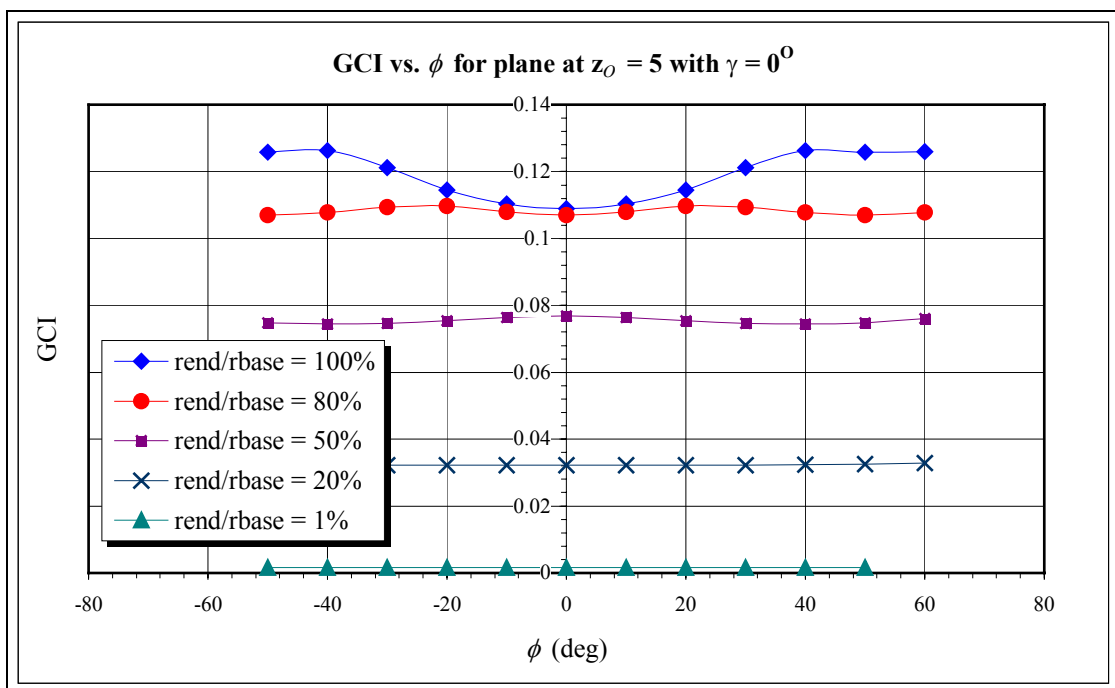


Fig. 4.12 GCI vs. ϕ for $\gamma = 0^\circ$, Surface 3

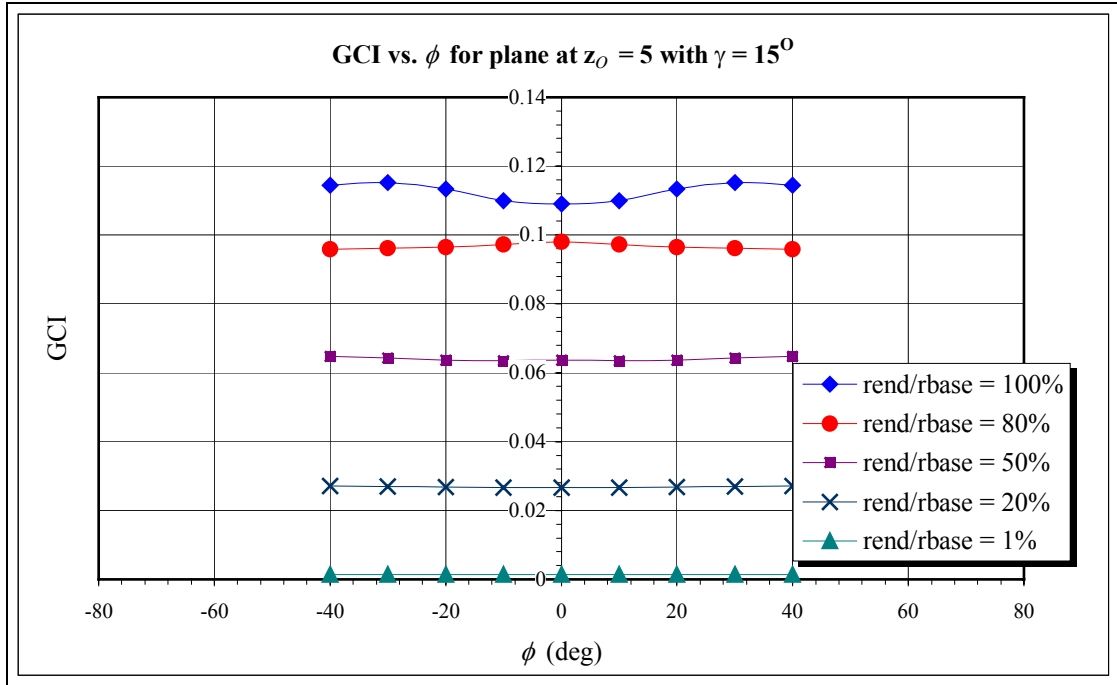


Fig. 4.13 GCI vs. ϕ for $\gamma = 15^\circ$, Surface 3

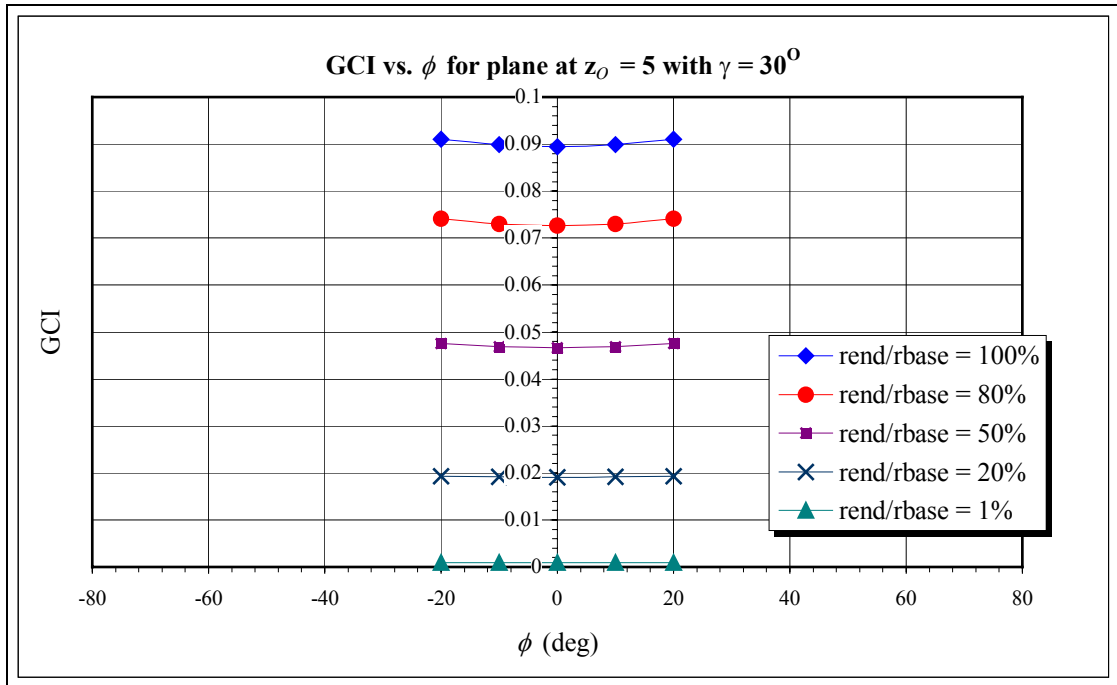


Fig. 4.14 GCI vs. ϕ for $\gamma = 30^\circ$, Surface 3

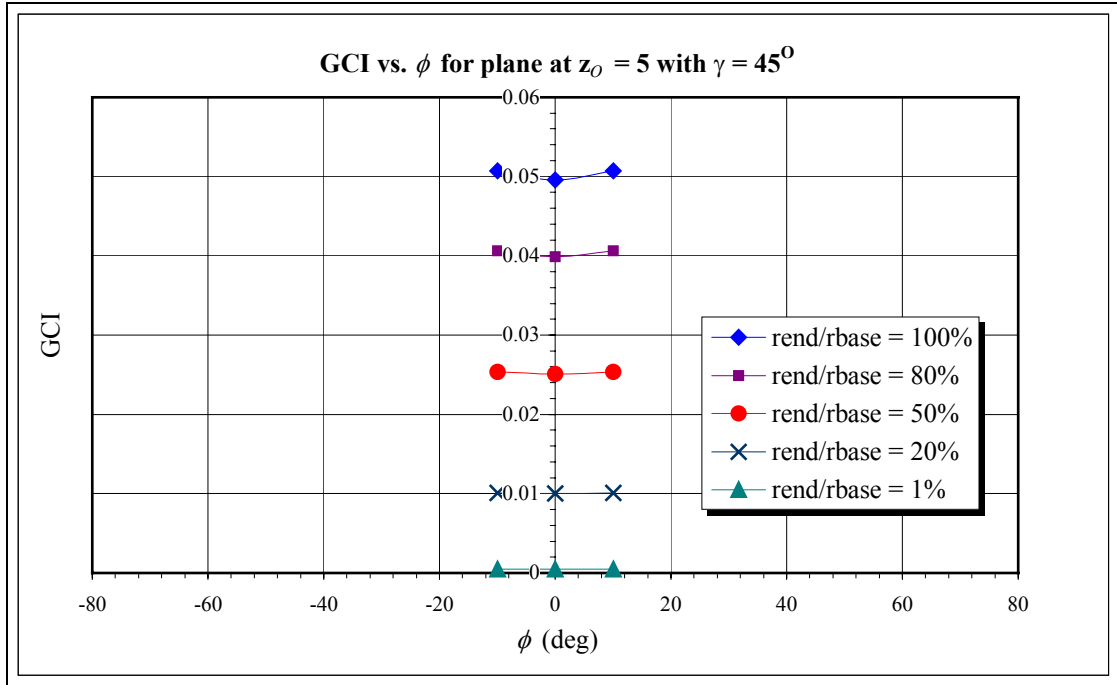


Fig. 4.15 GCI vs. ϕ for $\gamma = 45^\circ$, Surface 3

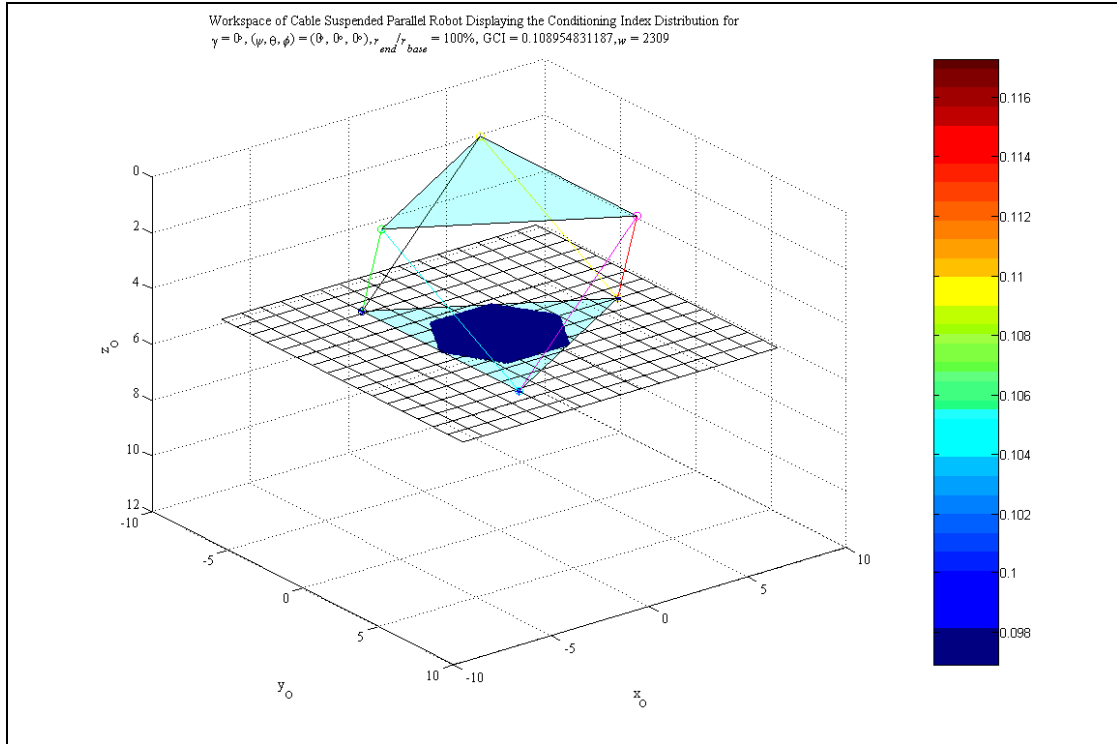


Fig. 4.16 Workspace Conditioning Index Distribution for $(\psi, \theta, \phi) = (0^\circ, 0^\circ, 0^\circ)$, $\gamma = 0^\circ$, $(r_{end}/r_{base}) = 100\%$, Surface 3

4.5 Conclusion

For each surface studied, the best design is the one with the $(r_{end}/r_{base}) = 100\%$ and the geometry $\gamma = 0^\circ$. This confirms the trends presented in the previous chapter. However, it is noted from the comparison of Surface 1 and 2 that the orientation of the MP with respect to the object it is to encounter does make a difference in its ability to maneuver over the surface and how much surface the MP is able to reach. The results obtained for Surface 2 where the longitudinal axis of the half cylinder was parallel to the y_O axis displayed a slightly larger workspace and a lower GCI when compared to Surface 1. This revealed that for Surface 2 the MP is

able to reach a larger number of points on the half cylinder but now has a globally increased error in it's ability to reach these points.

Therefore, from the results of three surface case studies, it is concluded that the trends presented in Chapter 3 regarding the behavior of the workspace volume and GCI are valuable tools for design. However, these tools present only guidelines in the design process and it is seen that the location and orientation of the object or surface that is to be manipulated does influence the performance of the robot chosen.

Chapter 5

FORCE CONTROL

5.1 Introduction

The control of a robotic manipulator is an important field in robotics. The controllers implemented on robots today have become more sophisticated with the growth of computer technology. A robotic manipulator is designed to perform certain tasks executed by a controller. Several control techniques are available for numerous robotic applications. Position controllers are commonly designed for tasks where the manipulator is to follow a trajectory through space. However, when the manipulator's end effector is in contact with its environment, position controllers may not be sufficient. In this case, it may be more appropriate to employ some level of force control. For example, consider a task where the manipulator is to wash a window surface. If the manipulator is to use a sponge, then a position controller may be adequate. However, the environment must be known accurately and/or the sponge must be compliant enough to help regulate the force applied to the window. Note that when mentioning position controllers it is meant to refer to both position and orientation control of the manipulator. Similarly, when indicating force control it is understood to generally imply both force and moment control of the manipulator. These references will be used throughout the chapter with clarifications as needed.

If the environment and the tool on the end effector possess high stiffness, the complexity of the task increases significantly. Consider a case where the

manipulator is to scrape paint off a glass window with a metal scraper. In this situation, any small error in the map of the environment (glass window) could cause the manipulator to either break the window or wave the scraper in front of the window without any contact. In situations similar to the window washing or scraping, the use of force control may be more reasonable. As a manipulator interacts with its environment it becomes very important that this interaction is controlled especially when precise movement is needed. When assembling two parts together using a position controller the accuracy of aligning the mating parts must be on the order of magnitude greater than the tolerance of the two fitting parts. If this cannot be guaranteed then the position error may result in unwanted contact forces causing the end effector to deviate from the desired trajectory. As a result, the position controller continually supplies commands to reduce such error, which in many instances leads to critical failure of the parts being assembled or the robot manipulator itself. In addition, if a large amount of friction exists between the parts then the contact force interaction between the manipulator and the environment becomes greatly complicated. Although detailed knowledge of the environment is not always known or available, the bounds related to the critical failure limits between the manipulator and the environment is usually known to some extent. Through the use of a force controller, the precision of assembly tasks can be greatly increased because the force controller provides relative measurements between the end effector and the environment. This information can be used to prevent failure and reduce the relative error [465].

Many applications currently exist where force controllers are or can be used. These applications include tasks such as grinding, deburring [466], fettling,

polishing, machining, weighing, pick, place, grasping, and assembly. Some types of force controllers are integral force control with robustness [426], simultaneous position and force control ([467 - 468]), sliding mode force control ([169], [396], [401 - 404]), impedance force control ([372], [374], [379], [386 - 400]), switching control [405], active compliance force control ([54], [407 - 410]), passive compliance force control [7], parallel force/position control ([52], [398 - 399], [424 - 425]), force control with inner position loop [398], force control with inner velocity loop [398], force control using passive velocity field control approach [469], hybrid force/vision control ([427 - 428]), robust hybrid force/position control [30], dynamic hybrid position/force control [422], dynamic hybrid velocity/force control [431], adaptive force control of position/velocity controlled robots [430], hybrid impedance control [423], and hybrid force/position control ([10], [12], [16], [17], [23], [398], [411 - 421]) just to name a few.

The implementation of a force controller for a cable suspended parallel robot is slightly more difficult because the MP is suspended under the influence of gravity by the cables. A cable suspended parallel robot cannot endure any disturbance forces that cause the cables become slack and the cables can only submit tension forces i.e. pulling forces to the MP and not pushing forces. This limits the tasks that are possible for the robot. On the other hand, if the cable robot is designed in such a way that some of the cables could act in the direction of gravity preventing the cables from becoming slack then, the force controller may be more useful. One application where force controllers could be more useful is in the two dimensional cable suspended parallel robots. However, these robots were not investigated within the scope of the present work.

This chapter will present an analytical model of a force controller that can be used on robotic manipulators. Due to the additional restriction that the cables must always be in tension, this chapter will only present preliminary ideas on the notion of a force controller for a cable suspended parallel robot. The difficulty relating to the tension requirement and incorporating these constraints into a feasible force control law has inhibited further investigation due to time. Further refinement and real time implementation of the force controller for cable suspended parallel robots is left for future work. This chapter will discuss some basic force control concepts including the simulation of a hybrid force/position control used on both a six degree-of-freedom traditional actuated parallel robot and a cable actuated parallel robot. The traditional parallel robots refer to those that are able to push and pull on their environment with the MP and a cable actuated parallel robot can only interact with the environment in situations when all the cables possess tension.

The chapter begins with a brief introduction on the control law-partitioning concept defined by Craig [465]. Then the following section presents a logical explanation for the selection of a practical force controller that is applicable to various robotic manipulators. The section considers the model of traditional parallel robots with a brief reference to cable suspended parallel robots. The next section discusses the design of a hybrid force/position controller [465]. This section will also present a hybrid force/position controller for the cable suspended parallel robot with an additional decision making block. The decision making block is used to ensure that all the cables will remain in tension throughout the execution of the desired task. The chapter continues with the implementation of the hybrid force/position controller on both the traditional parallel robot and cable suspended parallel robot through several

simulated task trajectories. A Matlab Simulink program was created to test the performance of the controller and observe the behavior of the each parallel robot in a virtual environment. The individual results of each simulation are included and discussed in the relevant section. The following section presents general discussion and analysis of the results. Finally, the chapter ends with a summary of the ideas presented throughout the chapter and results of the simulation.

5.2 Control Law Partitioning

In this section, a brief description of the control law partitioning [465] technique is presented which is similar to the computed torque method ([21], [470]) and the dynamic model-based compensation method ([8], [429], [449 - 450]) for nonlinear control theory. The goal of these methods is to decouple the nonlinear dynamics of the system through modeling the nonlinearities and incorporating these equations as part of the control law. This section will explain this method from the viewpoint of the control law partitioning method.

When creating a controller for a system generally the first step is to determine the kinematic and dynamic equations of motion for the system. These equations are used to understand the behavior of the system such that the selection of an appropriate control law can be determined. The controller usually incorporates some aspect of these equations into their design law. If the dynamic equations derived describe the system exactly then the system can be controlled completely. However, every physical real world system naturally possesses some level of nonlinear behavior. Due to this complex nonlinear behavior and the intrusion of higher order disturbances, the system's dynamic equations are never known perfectly. In spite of this, real world

systems are controlled with the precision needed using various approximation techniques.

Nonlinear behavior within a system is difficult to control and it is common for many control designers to try to apply some linearization method to the system. For systems that do not portray severe nonlinearities, a local linearization method may be used to simplify the nonlinear system equations in the neighborhood of an operating point to a linear approximate model ([465], [471]). However, for most robotic systems, this method is not well suited because the manipulator generally moves through gross motions to separate regions all over its workspace, preventing a valid linearization encompassing all the regions. In this case, another method may be considered where the local operating point continuously moves with the manipulator constantly linearizing within the vicinity of the desired position of the manipulator. This method is referred to as a moving linearization where the linearization takes place on a time varying system ([465], [472]). Although both of these linearization techniques are exploited for control purposes in real world applications, they will not be employed in the current control law. Instead, the nonlinear equations of motion are dealt with directly and the mathematical expressions are incorporated into the control law definition without using linearizations.

The control law partitioning is a simple scheme devised to separate the model-based portion of a system from the servo portion for more complex systems [465]. The model-based portion contains the mathematical expressions that describe the system including any nonlinear terms. These terms are used to cancel all the linear and/or nonlinearities in the system such that the resulting system is ideally linear. The remaining portion of the system is then controlled the by servo or error part. This

method obviously requires the complete knowledge of the nonlinear behavior and the corresponding parameters that form them in order to create the mathematical expressions for the model portion. This is often a problem in practical real world implementations of this method. For example, the model of frictional effects is extremely difficult to accurately derive let alone the parameters that influence them. However, if the system model is reasonably close to the actual system then the difference between the two can be controlled by the servo/error portion. To gain a better understanding of how the control law partitioning method is applied, consider the simple example of a one dimensional spring mass system exposed to frictional damping as shown in Fig. 5.1.

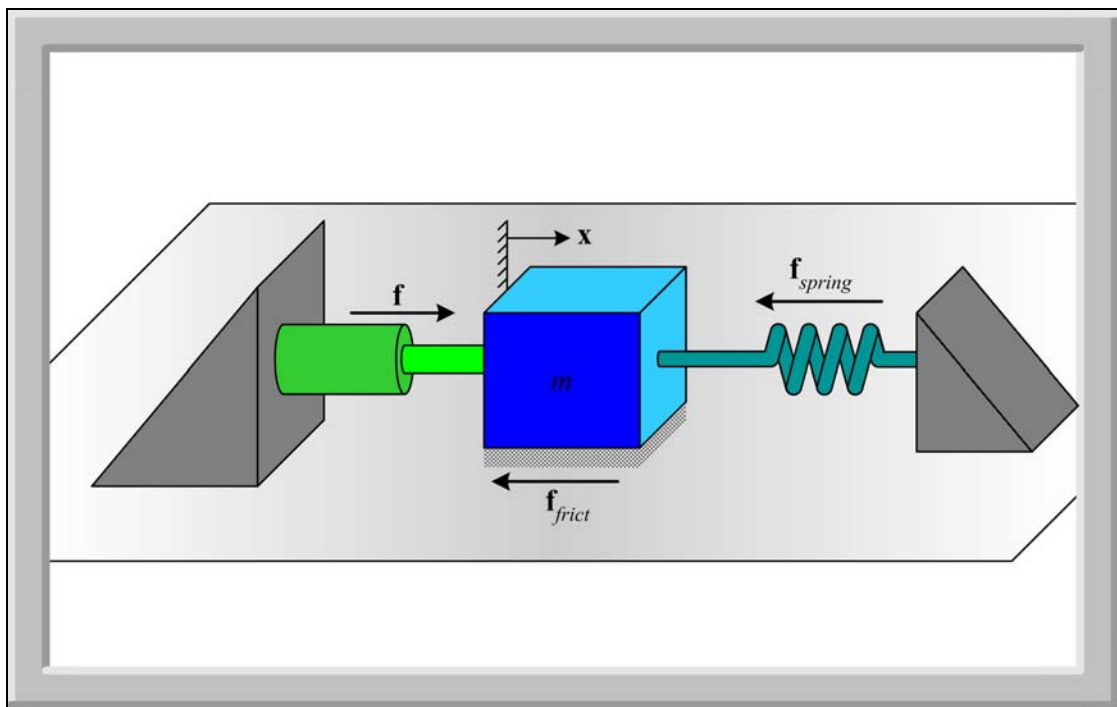


Fig. 5.1 Spring Mass System exposed to friction damping

The dynamic equations of motion for the system are found by summing the forces on the block and are given by the following equation.

$$\sum \mathbf{F} = \mathbf{f} - \mathbf{f}_{frict} - \mathbf{f}_{spring} = m\ddot{\mathbf{x}} \quad (5.1)$$

The input force supplied by the prismatic actuator is represented as \mathbf{f} , the friction force and spring force acting against the block is denoted by \mathbf{f}_{frict} and \mathbf{f}_{spring} respectively and m is the uniform mass of the block. For the sake of discussion, consider the expressions for the friction and spring force as defined in subsequent equations.

$$\mathbf{f}_{frict} = b_c \operatorname{sgn}(\dot{\mathbf{x}}) \quad (5.2)$$

$$\mathbf{f}_{spring} = k\mathbf{x}^3 \quad (5.3)$$

The friction function represents the coulomb friction where b_c is the coulomb friction constant multiplied by the sign of the velocity. The spring force is represented by a cubic function pre-multiplied by k the spring constant. Substituting Eq. (5.2) and Eq. (5.3) into Eq. (5.1) and solving for the input force, the dynamic equations of motion become

$$\mathbf{f} = m\ddot{\mathbf{x}} + b_c \operatorname{sgn}(\dot{\mathbf{x}}) + k\mathbf{x}^3. \quad (5.4)$$

The equations of motion are nonlinear because of the spring and frictional force terms. A simple linear mathematical representation could have been chosen but in many cases, the nonlinear expression more accurately models the dynamic behavior of the

system especially for the case of coulomb friction. Now using the control law partitioning technique the model-based portion of the control law is chosen in the form

$$\mathbf{f} = \alpha \mathbf{f}' + \beta. \quad (5.5)$$

The terms α and β are constant or nonlinear functions chosen such that the system appears as a simple unit mass or unit mass matrix for multi-input multi-output systems. The term \mathbf{f}' represents the new system inputs at the next time instant and is the servo portion of the control law. For the system given by Eq. (5.4) the values α and β of the model-based portion are chosen as

$$\alpha = m, \quad (5.6)$$

$$\beta = b_c \operatorname{sgn}(\dot{\mathbf{x}}) + k\mathbf{x}^3. \quad (5.7)$$

In addition, the servo portion of the control law is selected as

$$\mathbf{f}' = \ddot{\mathbf{x}}_d + k_v(\dot{\mathbf{x}}_d - \dot{\mathbf{x}}) + k_p(\mathbf{x}_d - \mathbf{x}). \quad (5.8)$$

Eq. (5.8) represents a classic proportional derivative (PD) controller where k_p is the proportional gain constant and k_v is the derivative gain constant. The variables $\ddot{\mathbf{x}}_d$, $\dot{\mathbf{x}}_d$ and \mathbf{x}_d are the desired acceleration, velocity and position respectively which are predefined for all time. The servo error is defined as the difference between the desired trajectory and the actual trajectory as

$$\mathbf{e} = (\mathbf{x}_d - \mathbf{x}) \quad (5.9)$$

which is the position and orientation servo error. It is noted that the actual trajectory is subtracted from the desired trajectory. This is done for the reason that as the actual trajectory veers away from the desired trajectory, the difference causes the servo error portion to excite with a signal that opposes the deviation and forces the actual trajectory to follow the desired trajectory.

In Chapter 2, the equations governing the motion of a six-degree-of-freedom cable suspended parallel robot were derived. Inherent in these equations are nonlinear terms for which some mathematical expressions are already given such as the Coriolis and centrifugal forces. Rather than considering linear approximations for the nonlinear terms that are already modeled, the mathematical expressions are directly used as part of the control law. The details of the control law used for the parallel robot are described in the next section when the selection of a well-defined force controller is discussed.

5.3 Selection of a Force Control Law

The popularity of the force controllers in industrial applications is slowly increasing due to the improvement of force sensors and force control schemes. Several different force control laws are available as previously mentioned. In order to derive a feasible control law, the interaction between the manipulator's end effector and the environment must be modeled. The dynamic equations of motion for a general cable suspended parallel robot are derived in Chapter 2 and rewritten again here for convenience in Eq. (5.10).

$$-\mathbf{J}^T \mathbf{u} = \mathbf{D}(x) \ddot{\mathbf{X}} + \mathbf{C}(x, \dot{x}) \dot{\mathbf{X}} - \mathbf{G}(x) + \mathbf{f}_{ext} \quad (5.10)$$

This equation can also represent a simplified model of a traditional parallel robot that is able to push and pull on the environment with its MP. It is noted that Eq. (5.10) does not include the dynamic effects of the input actuating links on the system because of the assumption that the actuating links possess no mass or inertial properties. This assumption may hold if the mass of the MP is much greater than that of the actuating links. The active links in this case are either the cables or traditional prismatic actuators connecting the BP to the MP.

To help obtain a better understanding of the forces and their relative signs, consider the following practical example where a block is being lowered into a body of water to assemble some structure that is presently under water as shown in Fig. 5.2. In the bottom right hand corner of Fig. 5.2 is a free body diagram of the MP.

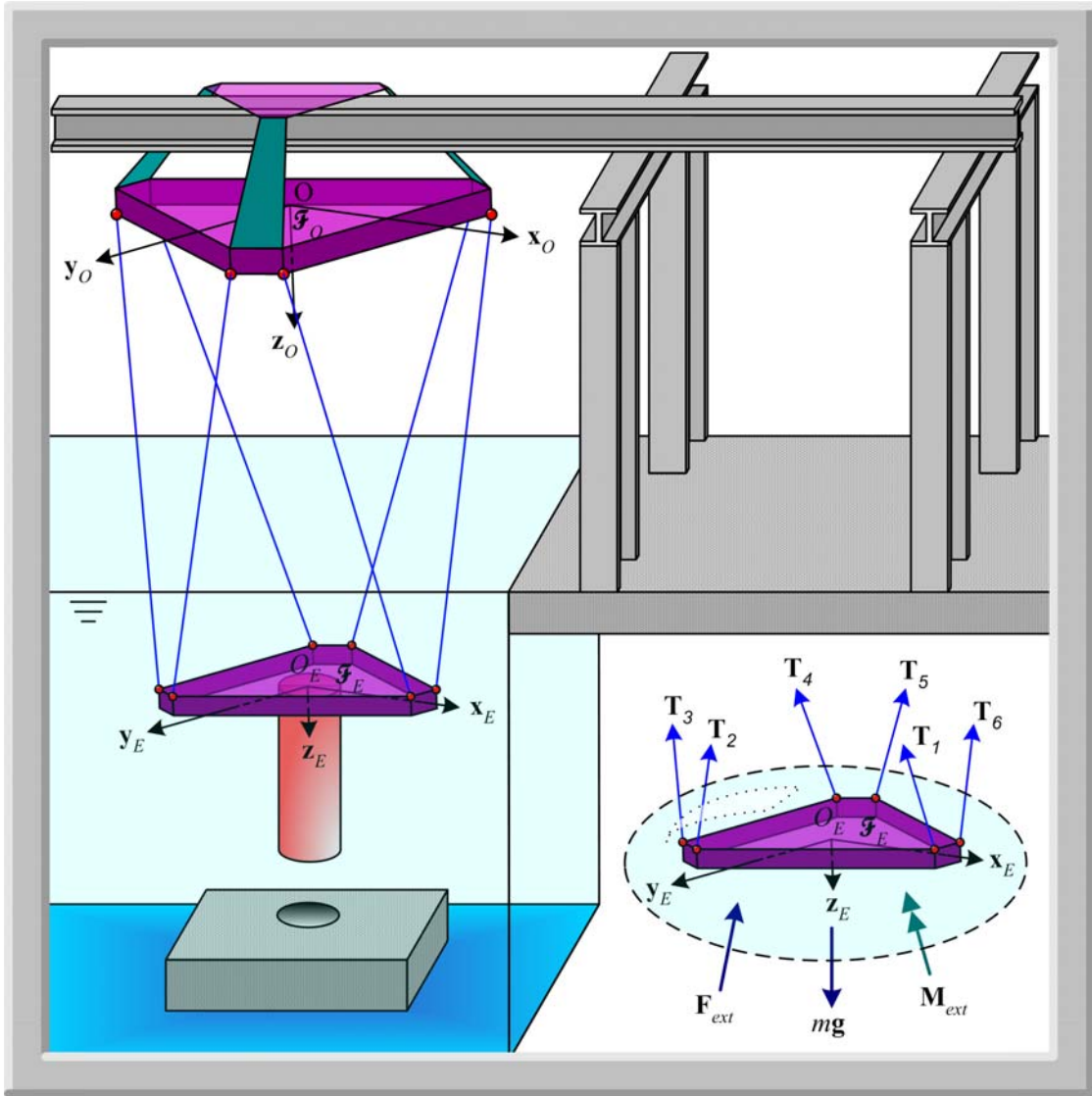


Fig. 5.2 Parallel robot assembling a peg into a hole

The robot lowering the block into the water is a parallel robot that is rigidly fixed to the dock or solid ground. The block is securely fixed to the MP and as the block (and MP) is lowered into the water, it experiences a number of forces. Some of the forces that the block may experience will be the gravitational force $\mathbf{G}(x)$, the

centripetal and centrifugal forces $\mathbf{C}(x, \dot{x})\dot{\mathbf{X}}$, the inertial forces $\mathbf{D}(x)\ddot{\mathbf{X}}$, the external forces and moments \mathbf{f}_{ext} resulting from the environment contact and any other unknown disturbance forces, and finally the input force from the manipulator's actuators given by $\mathbf{J}^T \mathbf{u}$. If the parallel robot is actuated by cables then the block cannot be lowered into the water too fast otherwise the drag forces experienced by the block will cause the cables to loose tension and become slack. However, if the parallel robot is actuated by traditional prismatic actuators then the drag force can be overcome by increasing the actuator force in the direction that opposes the drag force. For ease of writing and explanation purposes, consider the following new representations for the terms $\mathbf{J}^T \mathbf{u}$ and \mathbf{f}_{ext} given by Eq. (5.11) and Eq. (5.12) respectively.

$$\mathbf{f} = \mathbf{J}^T \mathbf{u} \quad (5.11)$$

$$\mathbf{f}_{ext} = \mathbf{f}_{dist} + \mathbf{f}_{env} \quad (5.12)$$

The external forces are separated into a set of disturbance forces given as \mathbf{f}_{dist} , and another set of environmental forces \mathbf{f}_{env} . The disturbance forces include the forces such as friction, gear cogging, inherent system vibrations, and any other unknown disruptive forces and moments. The environmental forces include the forces and moments due to physical contact with the environment. For the current discussion, it will be assumed that the environmental forces are much greater than the disturbance forces. These forces are sensed by the force transducer placed between the manipulator and the environment. The force sensor is usually attached to the manipulator's end effector or MP. After applying these substitutions to Eq. (5.10) the equations of motion become

$$-\mathbf{f} = \mathbf{D}\ddot{\mathbf{X}} + \mathbf{C}\dot{\mathbf{X}} - \mathbf{G} + \mathbf{f}_{dist} + \mathbf{f}_{env}, \quad (5.13)$$

$$\mathbf{f} = -\mathbf{D}\ddot{\mathbf{X}} - \mathbf{C}\dot{\mathbf{X}} + \mathbf{G} - \mathbf{f}_{dist} - \mathbf{f}_{env}. \quad (5.14)$$

The individual arguments of each term are omitted to simplify the writing. The environmental force can be written as

$$\mathbf{f}_{env} = \mathbf{K}_{env}\mathbf{X} \quad (5.15)$$

where \mathbf{K}_{env} is a constant environmental stiffness matrix. Now Eq. (5.15) can be rewritten as

$$\mathbf{X} = \mathbf{K}_{env}^{-1}\mathbf{f}_{env}. \quad (5.16)$$

In addition, upon taking the first and second derivatives of Eq. (5.16) with respect to time yields the relationships given in Eq. (5.17) and Eq. (5.18) respectively.

$$\dot{\mathbf{X}} = \mathbf{K}_{env}^{-1}\dot{\mathbf{f}}_{env} \quad (5.17)$$

$$\ddot{\mathbf{X}} = \mathbf{K}_{env}^{-1}\ddot{\mathbf{f}}_{env} \quad (5.18)$$

Substituting Eq. (5.16), Eq. (5.17), and Eq. (5.18) into Eq. (5.14), the system dynamic equations of motion become

$$\mathbf{f} = -\mathbf{D}\mathbf{K}_{env}^{-1}\ddot{\mathbf{f}}_{env} - \mathbf{C}\mathbf{K}_{env}^{-1}\dot{\mathbf{f}}_{env} + \mathbf{G} - \mathbf{f}_{dist} - \mathbf{f}_{env}. \quad (5.19)$$

To obtain a force control law using the partitioned controller concept, a logical choice leads to the following

$$\mathbf{f} = -\mathbf{f}_{dist} - \mathbf{f}_{env} - \mathbf{CK}_{env}^{-1}\dot{\mathbf{f}}_{env} + \mathbf{G} - \mathbf{DK}_{env}^{-1} \left\{ \ddot{\mathbf{f}}_d + \mathbf{k}_{fv} (\dot{\mathbf{f}}_d - \dot{\mathbf{f}}_{env}) + \mathbf{k}_{fp} (\mathbf{f}_d - \mathbf{f}_{env}) \right\}. \quad (5.20)$$

The column vectors \mathbf{f}_d , $\dot{\mathbf{f}}_d$, and $\ddot{\mathbf{f}}_d$ represent the desired force trajectory and the rates at which they are applied. In mentioning the desired force, it is understood that this refers to the force and moments in general. The model portion of the controller according to Eq. (5.5) is defined for Eq. (5.20) by the variables

$$\alpha = -\mathbf{DK}_{env}^{-1}, \quad (5.21)$$

$$\beta = -\mathbf{f}_{dist} - \mathbf{f}_{env} - \mathbf{CK}_{env}^{-1}\dot{\mathbf{f}}_{env} + \mathbf{G}. \quad (5.22)$$

The servo portion of the controller is defined by the terms within the curly brackets $\{\}$ as

$$\mathbf{f}' = \ddot{\mathbf{f}}_{env} = \ddot{\mathbf{f}}_d + \mathbf{k}_{fv} (\dot{\mathbf{f}}_d - \dot{\mathbf{f}}_{env}) + \mathbf{k}_{fp} (\mathbf{f}_d - \mathbf{f}_{env}). \quad (5.23)$$

For discussion purposes, Eq. (5.20) will be referred to as force controller (\mathcal{A}). To study the closed loop dynamics of the system subject to force controller (\mathcal{A}), Eq. (5.20) is equated to the system dynamics given by Eq. (5.19), which yields

$$-\mathbf{DK}_{env}^{-1}\ddot{\mathbf{f}}_{env} - \mathbf{CK}_{env}^{-1}\dot{\mathbf{f}}_{env} + \mathbf{G} - \mathbf{f}_{dist} - \mathbf{f}_{env} = -\mathbf{CK}_{env}^{-1}\dot{\mathbf{f}}_{env} + \mathbf{G} - \mathbf{f}_{dist} - \mathbf{f}_{env} - \mathbf{DK}_{env}^{-1} \left\{ \ddot{\mathbf{f}}_d + \mathbf{k}_{fv} (\dot{\mathbf{f}}_d - \dot{\mathbf{f}}_{env}) + \mathbf{k}_{fp} (\mathbf{f}_d - \mathbf{f}_{env}) \right\}. \quad (5.24)$$

After Eq. (5.24) is simplified and all terms are brought to one side the result is

$$\ddot{\mathbf{f}}_d - \ddot{\mathbf{f}}_{env} + \mathbf{k}_{fv} (\dot{\mathbf{f}}_d - \dot{\mathbf{f}}_{env}) + \mathbf{k}_{fp} (\mathbf{f}_d - \mathbf{f}_{env}) = \mathbf{0}. \quad (5.25)$$

Now, controller (\mathcal{A}) is not a realistic controller since it assumes that the disturbance force \mathbf{f}_{dist} is a known quantity. In real world applications, the behavior of \mathbf{f}_{dist} is usually not a well-known quantity. With this in mind, consider a new force controller that neglects the \mathbf{f}_{dist} term represented as

$$\mathbf{f} = -\mathbf{f}_{env} - \mathbf{CK}_{env}^{-1} \dot{\mathbf{f}}_{env} + \mathbf{G} - \mathbf{DK}_{env}^{-1} \left\{ \ddot{\mathbf{f}}_d + \mathbf{k}_{fv} (\dot{\mathbf{f}}_d - \dot{\mathbf{f}}_{env}) + \mathbf{k}_{fp} (\mathbf{f}_d - \mathbf{f}_{env}) \right\}. \quad (5.26)$$

The controller given by Eq. (5.26) will be referred to as force controller (\mathcal{B}). Again, to observe the closed loop dynamics by equating force controller (\mathcal{B}), i.e. Eq. (5.26) to the dynamic equations of motion given by Eq. (5.19) yields the following

$$\begin{aligned} -\mathbf{DK}_{env}^{-1} \ddot{\mathbf{f}}_{env} - \mathbf{CK}_{env}^{-1} \dot{\mathbf{f}}_{env} + \mathbf{G} - \mathbf{f}_{dist} - \mathbf{f}_{env} &= -\mathbf{f}_{env} - \mathbf{CK}_{env}^{-1} \dot{\mathbf{f}}_{env} + \mathbf{G} \\ &\quad - \mathbf{DK}_{env}^{-1} \left\{ \ddot{\mathbf{f}}_d + \mathbf{k}_{fv} (\dot{\mathbf{f}}_d - \dot{\mathbf{f}}_{env}) + \mathbf{k}_{fp} (\mathbf{f}_d - \mathbf{f}_{env}) \right\}. \end{aligned} \quad (5.27)$$

After simplifying Eq. (5.27) and rearranging terms, the equation becomes

$$\mathbf{f}_{dist} = \mathbf{DK}_{env}^{-1} \left\{ (\ddot{\mathbf{f}}_d - \ddot{\mathbf{f}}_{env}) + \mathbf{k}_{fv} (\dot{\mathbf{f}}_d - \dot{\mathbf{f}}_{env}) + \mathbf{k}_{fp} (\mathbf{f}_d - \mathbf{f}_{env}) \right\}. \quad (5.28)$$

Now the steady state analysis of Eq. (5.28) is found by setting all time derivatives equal to zero. In doing so Eq. (5.28) simplifies to

$$\mathbf{f}_{dist} = \mathbf{DK}_{env}^{-1} \left\{ \mathbf{k}_{fp} (\mathbf{f}_d - \mathbf{f}_{env}) \right\}. \quad (5.29)$$

Rearranging Eq. (5.29) in terms of the steady state error yields the expression

$$\mathbf{f}_d - \mathbf{f}_{env} = \left(\frac{\mathbf{f}_{dist}}{\mathbf{DK}_{env}^{-1} \mathbf{k}_{fp}} \right). \quad (5.30)$$

Eq. (5.30) represents the steady state error in the force when the force controller (\mathcal{B}) is applied to the system. Now suppose \mathbf{f}_d is chosen in place of the terms $(\mathbf{f}_{env} + \mathbf{f}_{dist})$ then the controller becomes

$$\mathbf{f} = -\mathbf{f}_d - \mathbf{CK}_{env}^{-1} \dot{\mathbf{f}}_{env} + \mathbf{G} - \mathbf{DK}_{env}^{-1} \left\{ \ddot{\mathbf{f}}_d + \mathbf{k}_{fv} (\dot{\mathbf{f}}_d - \dot{\mathbf{f}}_{env}) + \mathbf{k}_{fp} (\mathbf{f}_d - \mathbf{f}_{env}) \right\} \quad (5.31)$$

where Eq. (5.31) will be referred to as force controller (\mathcal{C}). Now, equating force controller (\mathcal{C}), Eq. (5.31) with the system dynamic equations given by Eq. (5.19) results in

$$\begin{aligned} -\mathbf{DK}_{env}^{-1} \ddot{\mathbf{f}}_{env} - \mathbf{CK}_{env}^{-1} \dot{\mathbf{f}}_{env} + \mathbf{G} - \mathbf{f}_{dist} - \mathbf{f}_{env} = & -\mathbf{f}_d - \mathbf{CK}_{env}^{-1} \dot{\mathbf{f}}_{env} + \mathbf{G} \\ & - \mathbf{DK}_{env}^{-1} \left\{ \ddot{\mathbf{f}}_d + \mathbf{k}_{fv} (\dot{\mathbf{f}}_d - \dot{\mathbf{f}}_{env}) + \mathbf{k}_{fp} (\mathbf{f}_d - \mathbf{f}_{env}) \right\}. \end{aligned} \quad (5.32)$$

After simplifying and rearranging terms, the equation becomes

$$\mathbf{f}_{dist} = \mathbf{f}_d - \mathbf{f}_{env} + \mathbf{DK}_{env}^{-1} \left\{ (\ddot{\mathbf{f}}_d - \ddot{\mathbf{f}}_{env}) + \mathbf{k}_{fv} (\dot{\mathbf{f}}_d - \dot{\mathbf{f}}_{env}) + \mathbf{k}_{fp} (\mathbf{f}_d - \mathbf{f}_{env}) \right\}. \quad (5.33)$$

The steady state analysis of Eq. (5.33) again is found by setting all the time derivative terms equal to zero. In doing so, Eq. (5.33) ends up as

$$\mathbf{f}_{dist} = \mathbf{f}_d - \mathbf{f}_{env} + \mathbf{DK}_{env}^{-1} \{ \mathbf{k}_{fp} (\mathbf{f}_d - \mathbf{f}_{env}) \}, \quad (5.34)$$

or, alternatively in the form as

$$\mathbf{f}_d - \mathbf{f}_{env} = \left(\frac{\mathbf{f}_{dist}}{1 + \mathbf{DK}_{env}^{-1} \mathbf{k}_{fp}} \right). \quad (5.35)$$

Eq. (5.35) represents the force error when force controller (\mathcal{C}) is applied to the system. Comparing the steady state analysis results for controllers (\mathcal{B}) and (\mathcal{C}), given by Eq. (5.30) and Eq. (5.35) respectively, it is observed that the force control law (\mathcal{C}) is a better choice. If the environment is stiff then \mathbf{K}_{env}^{-1} is small (usually the case) then the steady state error for controller (\mathcal{C}) is much smaller than that for controller (\mathcal{B}). This suggests in theory that control law (\mathcal{C}) is a good controller, however, the real world implementation of a control scheme of this nature is usually not practical. Applications where force trajectories are functions of time are not commonly encountered, i.e., the force trajectories are usually constant over time. In this case, $\dot{\mathbf{f}}_d$ and $\ddot{\mathbf{f}}_d$ are permanently set to zero. Another common problem is that the force sensor designs used today tend to be noisy and numerical differentiation of a noisy signal only amplifies the problem. In an attempt to avoid the complications that arise from noisy differentiation, a different approach is sought out. Returning to Eq. (5.15), it is observed that the environmental force signal is directly related to the displacement. This equation and its derivatives are rewritten here as follows

$$\mathbf{f}_{env} = \mathbf{K}_{env} \mathbf{X}, \quad (5.36)$$

$$\dot{\mathbf{f}}_{env} = \mathbf{K}_{env} \dot{\mathbf{X}}, \quad (5.37)$$

$$\ddot{\mathbf{f}}_{env} = \mathbf{K}_{env} \ddot{\mathbf{X}}. \quad (5.38)$$

The expressions given by Eq. (5.37) and (5.38) relate the force derivatives to the velocity and acceleration of the end effector. The velocity $\dot{\mathbf{X}}$ and acceleration $\ddot{\mathbf{X}}$ are signals that are easily measured since most robotic manipulator acquire adequate means of obtaining these signals with reasonable accuracy. In the design of this next controller, consider the use of the kinematic displacement signals instead of using the force signals as part of the force controller. The sensor placed on the manipulator already senses the environmental forces and moments \mathbf{f}_{env} and the representation given by Eq. (5.36) is preformed at the sensor level. Force sensors are designed to measure the deformation or displacements of an elastic material inside the sensor. Many force sensors use the stress strain relationships of precision-machined material to gain the force and moment signals needed. When the sensor is subjected to environmental forces and moments, the resulting strains directly influence the resistive properties of the material inside the sensor. This relationship between the sensor strain and the forces and moments applied is calibrated and converted into electrical signals. Other more accurate sensors use photoelectric displacement transducers that measure the change in light flow, or the change in magnetic flux used in inductive and capacitive force sensors. However, theses sensors become more sensitive to noise. In any case, the force sensor itself already measures the environmental forces and moments. Substituting Eq. (5.37) into the force control law (\mathcal{C}) i.e. Eq. (5.31), the new control law becomes

$$\mathbf{f} = -\mathbf{f}_d - \mathbf{C}\mathbf{K}_{env}^{-1}\mathbf{K}_{env}\dot{\mathbf{X}} + \mathbf{G} - \mathbf{D}\mathbf{K}_{env}^{-1} \left\{ \ddot{\mathbf{f}}_d + \mathbf{k}_{fv} (\dot{\mathbf{f}}_d - \mathbf{K}_{env}\dot{\mathbf{X}}) + \mathbf{k}_{fp} (\mathbf{f}_d - \mathbf{f}_{env}) \right\}. \quad (5.39)$$

Noting that $\mathbf{K}_{env}^{-1}\mathbf{K}_{env}$ is the identity matrix, Eq. (5.39) simplifies to

$$\mathbf{f} = -\mathbf{f}_d - \mathbf{C}\dot{\mathbf{X}} + \mathbf{G} - \mathbf{D}\mathbf{K}_{env}^{-1} \left\{ \ddot{\mathbf{f}}_d + \mathbf{k}_{fv} (\dot{\mathbf{f}}_d - \mathbf{K}_{env}\dot{\mathbf{X}}) + \mathbf{k}_{fp} (\mathbf{f}_d - \mathbf{f}_{env}) \right\}. \quad (5.40)$$

This will be referred to as force control law (\mathcal{D}). This control law results in the same steady state errors as those given by Eq. (5.35). To improve steady state errors, an integral term can be added to the servo portion of the force control law (\mathcal{D}). In doing so the force controller becomes

$$\mathbf{f} = -\mathbf{f}_d - \mathbf{C}\dot{\mathbf{X}} + \mathbf{G} - \mathbf{D}\mathbf{K}_{env}^{-1} \left\{ \ddot{\mathbf{f}}_d + \mathbf{k}_{fv} (\dot{\mathbf{f}}_d - \mathbf{K}_{env}\dot{\mathbf{X}}) + \mathbf{k}_{fp} (\mathbf{f}_d - \mathbf{f}_{env}) + \mathbf{k}_{fi} \int (\mathbf{f}_d - \mathbf{f}_{env}) dt \right\}. \quad (5.41)$$

The force controller given by Eq. (5.41) will be referred to as the force control law ($\mathcal{D2}$) for simplicity.

Now each controller given in this section assumes that the environmental stiffness matrix \mathbf{K}_{env} is known. This assumption may not always be valid for the manipulator could experience a changing environmental stiffness as it executes its task or the term is unknown completely. However, many tasks such as assembly include interactions with rigid bodies. Therefore, an approximate environmental stiffness matrix is usually guessed to incorporate the stiffness variations encountered. For the current simulations, the environmental stiffness is modeled as a known quantity and

held constant for each study. Variations of environments that are more complex are left for future work.

5.4 Hybrid Force/Position Controller

There are many tasks for robotic manipulators where the use of position and force control is needed. The type of tasks considered for the current discussion relates to situations where the end effector or MP physically interacts with the environment. For the current discussion, it is assumed that the disturbance forces and moments are relatively small compared to the forces and moments involved when contacting the surface. These tasks are referred to as constrained or partially constrained tasks because the environment, with which the manipulator interacts, inhibits the motion in some defined direction. For instance, when a manipulator is to turn a crank, insert a peg, or turn a screw there are certain directions in which a controlled force is needed while other directions require position control. The direction in which the desired force or position control action is to be taken is defined by a constraint frame \mathcal{F}_C . According to this frame, there exist directions that are restrained by natural constraints. *Natural constraints* are the set of constraints that prohibit motion due to physical or mechanical obstacles. Consider the case where a manipulator is to apply a certain amount of force to scrape paint off a rigid glass surface. The direction perpendicular to the surface is a natural position constraint because the manipulator is not able to go through the surface. In addition, if the surface is smooth enough such that the frictional forces are negligible then a natural force constraint arises because the manipulator is not able to apply arbitrary forces tangent to the surface. Generally, when a manipulator is interacting with a rigid surface the directions perpendicular to the surface are defined as *natural position*

constraints and the directions tangent to the surface are defined as *natural force constraints*. As a result, the directions of control are divided into two separate sets of control schemes that are orthogonal to each other and defined by different control law criteria. Note that when indicating a position constraint, this includes position and/or orientation constraints and when indicating a force constraint, it is meant to include force and/or moment constraints.

The directions that are to be controlled are sometimes referred to as the *artificial constraints* because in these directions the task is defined by the desired trajectories and virtual environments. The artificial constraints are defined along the same directions as the natural constraints. For instance, in the case where the manipulator is to scrape paint from the rigid glass surface, the direction perpendicular to the surface has a defined natural position constraint and hence there must be an artificial force constraint to control the force task in that direction. Similarly, in the directions tangent to the surface exists a natural force constraint and therefore an artificial position constraint must be instilled to control the position task. In summary, for every direction with a natural force constraint, there is a defined artificial position constraint and vice versa for every natural position constraint, there exists an artificial force constraint. The constraint definitions just mentioned still hold for surfaces with friction because in many cases frictional effects are compensated through position control laws. It is noted again for completeness, that when referring to force control it is understood to include the control of the forces and moments, and when referring to position control this includes the control of both the position and orientation.

Each of these directions, as previously mentioned, is defined according to the constraint frame \mathcal{F}_C . The appropriate placement of the constraint frame depends

on the desired task. For some tasks, as in the case of turning a crank, it is more appropriate to attach the constraint frame to the environment. In other situations, attaching the constraint frame directly on the end effector is more suitable such as the task of turning a screw or inserting a peg. During the execution of a task, the controlled directions can switch from force control to position control (or vice versa) due to a sensed threshold signal. These complex tasks are broken up into subtasks with separate constraint directions defined according to each separate subtask.

The following example will be used to gain a clearer understanding of some of the terms discussed in this section. The example is an assembly task where a parallel robot is to insert a peg into a surface with a hole. The peg is modeled as part of the MP with a force/moment sensor placed between the peg and the MP. The constraint frame \mathcal{F}_C coincides with the frame \mathcal{F}_E , rigidly attached to the MP. The number of subtasks depends on where the manipulator is initially positioned with the peg. Each of the subtasks is shown in Fig. 5.3 with a table defining the natural and artificial constraints. The position constraints are acknowledged by using the translational and angular velocity variables. The position variables could have been used, however, the description of the desired motion becomes more complicated. The force constraints are described using the force and moment components.

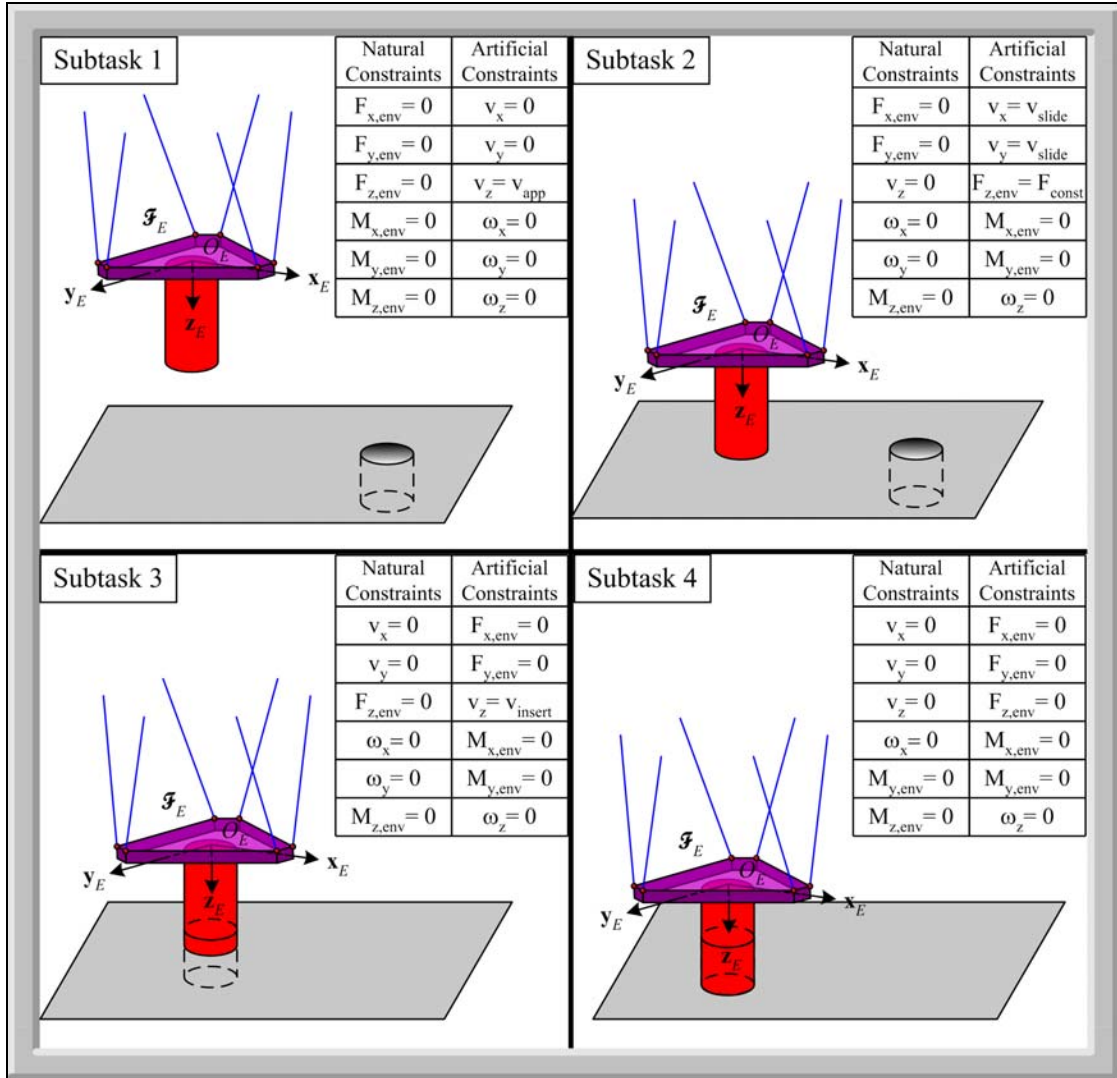


Fig. 5.3 Subtasks of a parallel robot assembling a peg into a hole

The peg is initially above the surface, at this location, the manipulator is in pure position control because it is not in contact with the surface environment and thus the natural force constraints are all zero. The position control is to move towards the surface with an approach velocity of v_{app} . The switch from the first subtask to the second is enabled when a force sensitivity threshold is exceeded which is initiated

when the peg is in contact with the surface. The force sensitivity threshold is a low-end force bound that the sensor is able to accurately read. Most force sensors are generally corrupted by level of noise resulting from several sources. Some of the possible sources of the noise may be a result of vibrations within the system, thermal changes, electronic error, etc. In the second subtask, the MP is not able to go through the surface in the \mathbf{z}_C direction or able to rotate about the \mathbf{x}_C and \mathbf{y}_C axes, which define the natural position constraints. The natural force constraints arise because the surface is modeled as frictionless thus preventing the MP to freely apply forces tangent to the surface. The artificial force constraints are to apply a constant force \mathbf{F}_{const} along the \mathbf{z}_C direction and maintain a zero moment about the \mathbf{x}_C and \mathbf{y}_C axes. The artificial position constraints are defined to move the peg towards the hole with a velocity trajectory \mathbf{v}_{slide} and prevent any angular velocity about the \mathbf{z}_C axis. The trajectory tangent to the surface depends on where the peg is located relative to the hole. It will be assumed for the example that this trajectory is known. The third subtask is enabled through the sensed change in velocity in the \mathbf{z}_C direction and observing the force sensor decreasing to zero or below the force sensitivity threshold. At this stage in the task, the peg is not able to translate or rotate about the \mathbf{x}_C and \mathbf{y}_C axes and the natural position constraints are defined for these directions as shown in Fig. 5.3. The peg cannot apply forces along the \mathbf{z}_C axis or any moments about the \mathbf{z}_C axis if the walls of the hole are frictionless and as a result natural force constraints are defined. The artificial force constraints are to maintain zero forces and moments along and about the \mathbf{x}_C and \mathbf{y}_C axes. The artificial position constraints are to insert the peg with a velocity trajectory along the \mathbf{z}_C direction as represented by \mathbf{v}_{insert} and to keep the peg from spinning about the \mathbf{z}_C axis. Finally, the fourth subtask is enabled when the peg contacts the bottom of

the hole and a force greater than the force threshold sensitivity is sensed along the \mathbf{z}_C axis while observing the velocity decreasing to zero.

A *hybrid force/position* controller is used in situations where in one direction the task may require force control, and in separate direction, the task may require position control. These directions may be changed while the task is being executed but a single direction never requires the force and position control simultaneously executed at the same time. Along each axis or in each direction defined by the constraint frame \mathcal{F}_C , the hybrid controller supplies either a force controller or a position controller at any one instant. This type of controller assumes that the interaction forces and moments between the manipulator and the environment are the dominant forces. Reference [406], provides a further discussion of the placement of coordinate systems for force controlled manipulation.

The hybrid force/position controller will be implemented and studied on a traditional parallel robot where the actuators can pull and push on its environment and on a cable suspended parallel robot where the MP can interact with the environment with only the pulling forces of its cables and the weight of its MP. The control law used for the *hybrid force/position* controller is defined as

$$-\mathbf{u} = (\mathbf{J}^T)^{-1} \left[\mathbf{C}(x, \dot{x}) \dot{\mathbf{X}} - \mathbf{G}(x) + \mathbf{S} \left\{ \mathbf{D}(x) \left[\ddot{\mathbf{X}}_d + \mathbf{k}_v (\dot{\mathbf{X}}_d - \dot{\mathbf{X}}) + \mathbf{k}_p (\mathbf{X}_d - \mathbf{X}) \right] \right\} + \right. \\ \left. (\mathbf{I} - \mathbf{S}) \left\{ \mathbf{D}(x) \mathbf{K}_{env}^{-1} \left[\ddot{\mathbf{f}}_d + \mathbf{k}_{fv} (\dot{\mathbf{f}}_d - \mathbf{K}_{env} \dot{\mathbf{X}}) + \mathbf{k}_{fp} (\mathbf{f}_d - \mathbf{f}_{env}) \right] + \mathbf{f}_d \right\} \right]. \quad (5.42)$$

The matrix \mathbf{S} is a diagonal matrix known as the selection matrix. The selection matrix contains all zeros except for the entries along its diagonal, which can be either zero or one. The selection matrix is used to switch the controller to the force

controller mode or position controller mode. If the diagonal entry of the selection matrix is one, then that axis is in position control mode and the force controller is turned off. Conversely, if the entry is zero the position mode is off and the force controller is activated. A block diagram of the hybrid force/position controller is given by Eq. (5.42) is shown in Fig. 5.4.

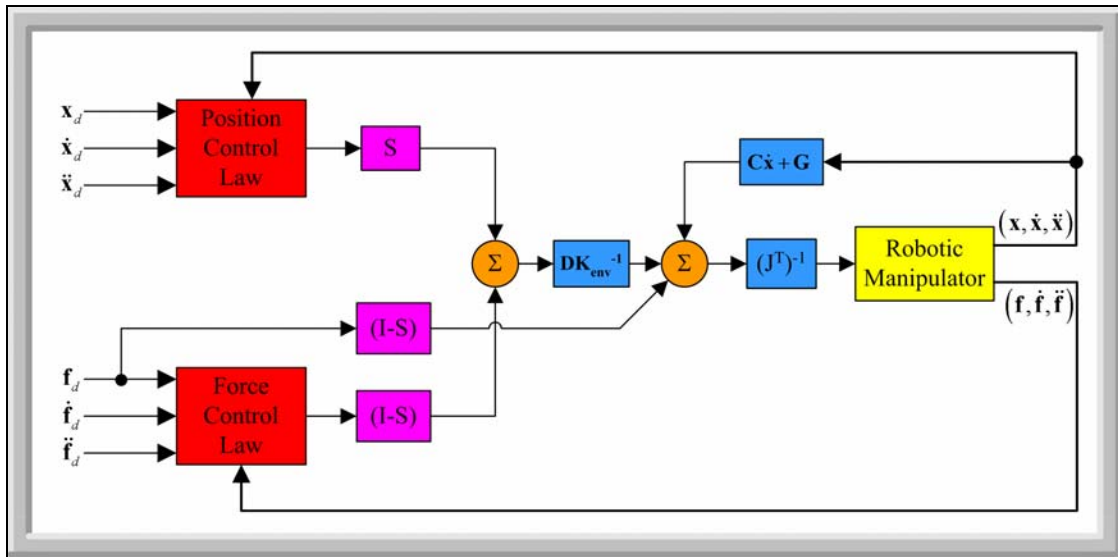


Fig. 5.4 Hybrid Force/Position Controller

The position control law of the hybrid controller used for these specific cases implements a proportional derivative (PD) controller and the force control law (\mathcal{D}) derived in the previous section is used to control the desired force/moment trajectory.

The cable suspended parallel robot uses an additional decision making block that checks the tensions in the cables to ensure that all the tensions are positive and not slack. The block intercepts the input control signal that is sent to the robot

and if all the tensions are positive, meaning none of the cables are slack, then the signal is passed through the block without any modification. However, if any of the cable tensions are not positive then new tension values are calculated so the desired trajectory can be completed if possible. The block diagram of the hybrid force/position controller showing the location of the decision making block is given in Fig. 5.5.

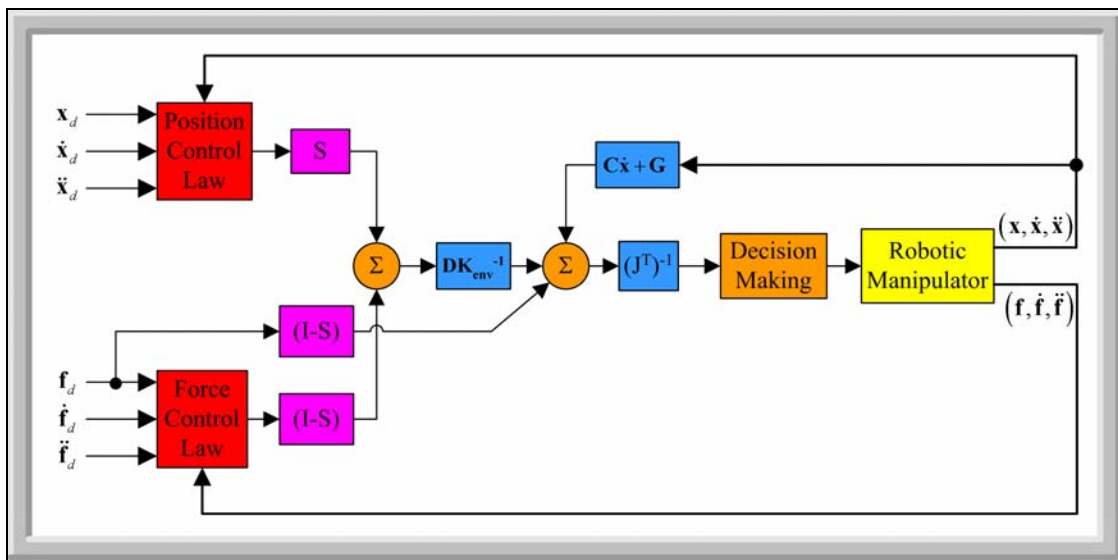


Fig. 5.5 Hybrid Force/Position Controller with Decision Making Block

Two methods have been previously implemented on the University of Delaware cable suspended parallel robot for position control law ([194 - 196]). These methods include the Lyapunov and feedback linearization method. For the current study, a modified version of the feedback linearization method will be used. In order to ensure the new variables are positive a Matlab function (lsqnonneg.m) is used. This function performs the nonnegative least squares solution. Additional articles written

on the Lyapunov controller are addressed in references ([194 - 196], [465], [473 - 475]) and feedback linearization methods are addressed in references ([472], [476 - 478]).

The selection matrix in the hybrid force/position controller does not always have to be either one or zero. In some cases the tasks requires a force and a position control along the same direction. For these cases, the selection matrix can choose a number between one and zero depending on the degree of force or position control that is desired. This type of control is referred to as the mechanical impedance control. Further investigation of this particular type of controller is left for future work.

5.5 Simulation Studies

The hybrid force/position controller given by Eq. (5.42) is implemented on two 6-DOF parallel robots. The first parallel robot is actuated by traditional prismatic actuators that can both push and pull on the environment with its MP such as hydraulic pistons or lead screws. The second parallel robot is the cable suspended parallel robot that uses cables for actuation. The cable suspended parallel robot will include the decision making block shown in Fig. 5.5 as an additional part of its controller. Both parallel manipulators will execute each simulation case study and the results are compared together. Some of the properties selected for the both parallel manipulators along with other constants used in the simulation are given in Table 5.1.

Table 5.1: Values used in Simulation		
Variable	Value	Description
\mathbf{K}_{env}	100000 (N/m)	Environmental stiffness matrix for surfaces
r_{end}	0.54594241454571 m	Radius of MP connection points
r_{base}	0.54594241454571 m	Radius of BP connection points
$(r_{end}/r_{base})\%$	100%	Percent ratio of MP to BP
γ	0°	Geometric Constant See Chapter 3
\mathbf{I}_{xx}	0.494815599734625 (kg m ²)	Moment of Inertia about the \mathbf{x}_E axis
\mathbf{I}_{yy}	0.494815599734625 (kg m ²)	Moment of Inertia about the \mathbf{y}_E axis
\mathbf{I}_{zz}	0.98927430547503 (kg m ²)	Moment of Inertia about the \mathbf{z}_E axis
m	13.2756 kg	Mass of MP
g	9.81 (m/sec ²)	Gravitational constant
mg	130.242 N	Weight of MP
Thickness	0.0127 m	Thickness of MP
ρ_{Al}	2700 (kg/m ³)	Density of Aluminum MP

Table 5.1 Values used in Simulation

The dimensions of both parallel manipulators are based on the idealized measurements of the University of Delaware Cable Suspended Parallel Robot. One idealization includes the assumption that the MP and BP are equilateral triangles with the connection points coinciding as defined by the geometric value $\gamma = 0^\circ$ stated in Chapter 3. The University of Delaware cable suspended parallel robot is close to the $\gamma = 0^\circ$ which is the ideal 3-3 configuration. The mass and inertia of each actuating prismatic link is neglected and the MP is defined as a rigid body with a uniformly distributed mass for both manipulators. Neglecting the mass and inertia properties of the legs greatly simplifies the dynamic equations of motion considerably. If the mass and inertia properties of the legs are included in the dynamic equations, then the solutions to the dynamic equations of motion must be sought out through numerical

techniques such as the natural orthogonal complement (NOC) method ([246 - 247], [302], [361]). The gravity vector in the inertial frame \mathcal{F}_O is defined in the same manner presented in Chapter 2 and Chapter 3. In addition, no frictional effects between the joints are considered.

A Matlab Simulink program was created to simulate the parallel robot influenced by the hybrid force/position controller in the modeled environment. The simulations included five simple cases to verify the functionality of the controller and to observe the behavior of the both parallel manipulators. For each case, the environment is modeled as a fixed rigid body defined by an infinite plane according to the \mathcal{F}_O frame with a smooth frictionless profile. The surface is modeled as an elastic spring with a large linear constant stiffness \mathbf{K}_{env} . No additional disturbance forces are considered in any of the case studies. An ideal force and moment sensing probe is attached to the MP and is used to apply the desired force trajectory to the surface. The probe is small enough that the environmental moments are negligible and have no effect on the MP. The mass of the probe is considered negligible compared to the mass of the MP. The MP is initially positioned directly above the surface such that ideally there is no distance between the surface and the probe attached to the MP. This is done to prevent initial impact forces resulting from displacement between the environment and the MP and to avoid switching the control direction between the force and position. For each case described in the following sections the position trajectory is displayed the \mathcal{F}_O frame while the forces and moments are described according to the \mathcal{F}_E frame or \mathcal{F}_C frame. The forces for each simulation are measured in Newtons and the moments are measured in Newton-meters. The position and orientation of the MP are measured in meters and radians respectively. All the cases

are planned so that the position trajectory is within the workspace boundaries defined according to the cable suspended parallel robot and an attempt is made to come as close to the boundaries as possible while maintaining the prescribed force trajectory. This was done obviously to make the simulations more interesting and provide better insight to the true capabilities of the parallel manipulators especially for the cable suspended parallel robot.

The idealizations considered for the following studies are presented to simplify the analysis. Each case is chosen to provide preliminary source of information for future work on cable suspended parallel robot control. Additional realistic and/or complex parameters can be explored as future work for a more complete investigation if desired. The following sections will present each case individually and display the results for each parallel robot with an analysis of the results for that particular case. After each case is presented, an additional discussion and analysis is given summarizing all the results supporting explanations.

5.5.1 Case 1

The task for this case is for each parallel robot to push the MP against a planar surface along the \mathbf{z}_O axis with a constant force and no additional motion along any other direction. The parallel robot is to exert a force that is slightly less than the weight of the MP. The parallel robot is force controlled along the \mathbf{z}_E axis and position controlled along the remaining directions. The simulation was run for 10 seconds. The natural and artificial constraints for the Case 1 task are given in Table 5.2.

Table 5.2: Natural and Artificial Constraints for Case 1	
Natural Constraints	Artificial Constraints
$\mathbf{F}_{x,env} = 0$	$\mathbf{v}_x = 0$
$\mathbf{F}_{y,env} = 0$	$\mathbf{v}_y = 0$
$\mathbf{v}_z = 0$	$\mathbf{F}_{z,env} = 129N$
$\mathbf{M}_{x,env} = 0$	$\boldsymbol{\omega}_x = 0$
$\mathbf{M}_{y,env} = 0$	$\boldsymbol{\omega}_y = 0$
$\mathbf{M}_{z,env} = 0$	$\boldsymbol{\omega}_z = 0$

Table 5.2 Natural and Artificial Constraints for Case 1

The position and orientation of the MP for the traditional parallel robot are shown in Fig. 5.6, the forces and moments experienced by the MP are shown by Fig. 5.7, and the input forces given to the actuating prismatic links are shown in Fig. 5.8. The cable suspended parallel robot's position and orientation of the MP are given in Fig. 5.9, the forces and moments the MP experiences are given in Fig. 5.10 and the tensions in each cable are given in Fig. 5.11.

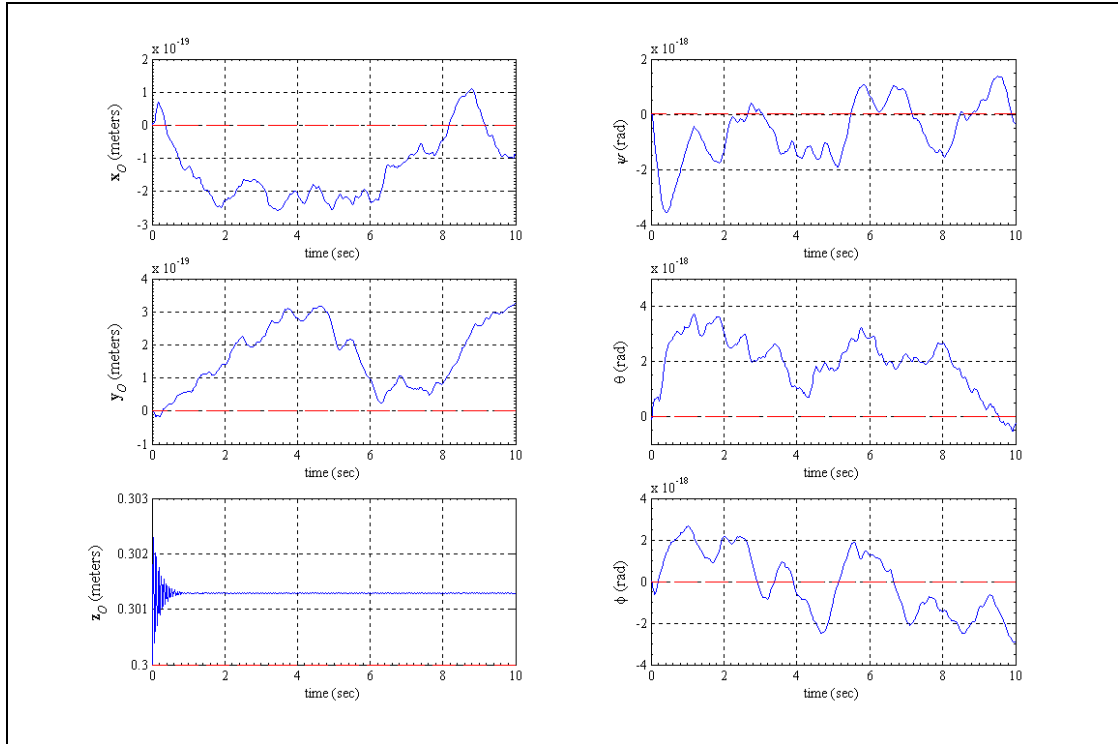


Fig. 5.6 Plot of the position and orientation of the MP as the Case 1 task is executed for the traditional parallel manipulator

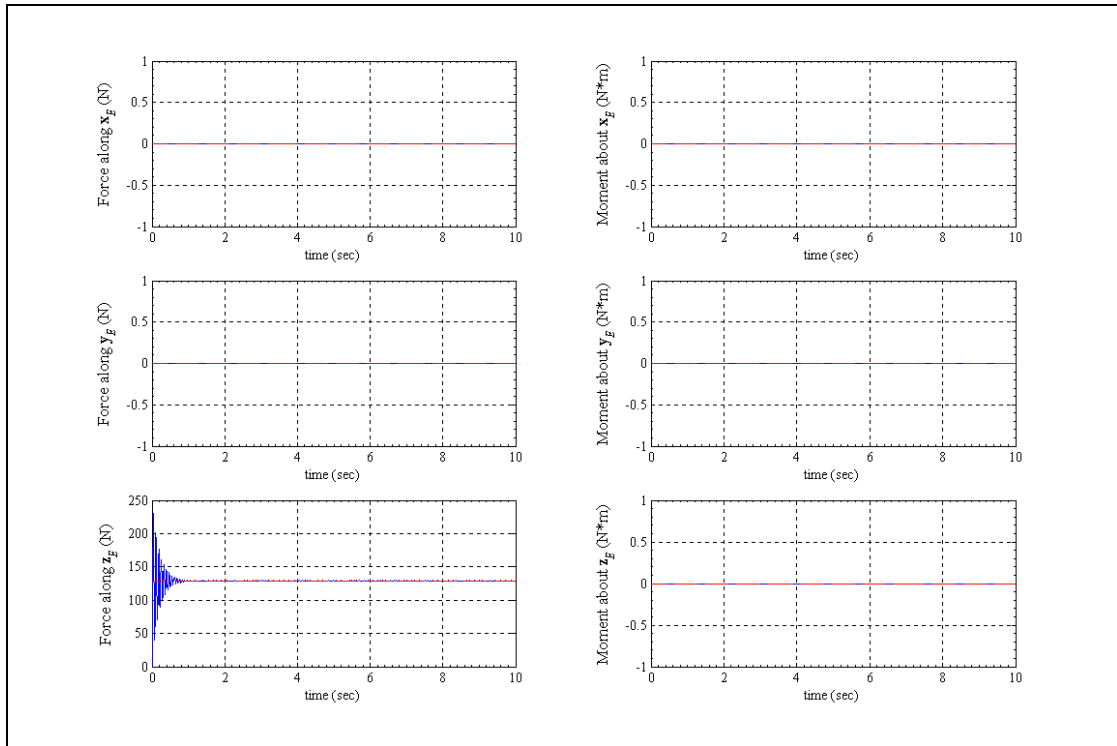


Fig. 5.7 Plots of the forces and moments acting on the MP as the Case 1 task is executed for the traditional parallel manipulator

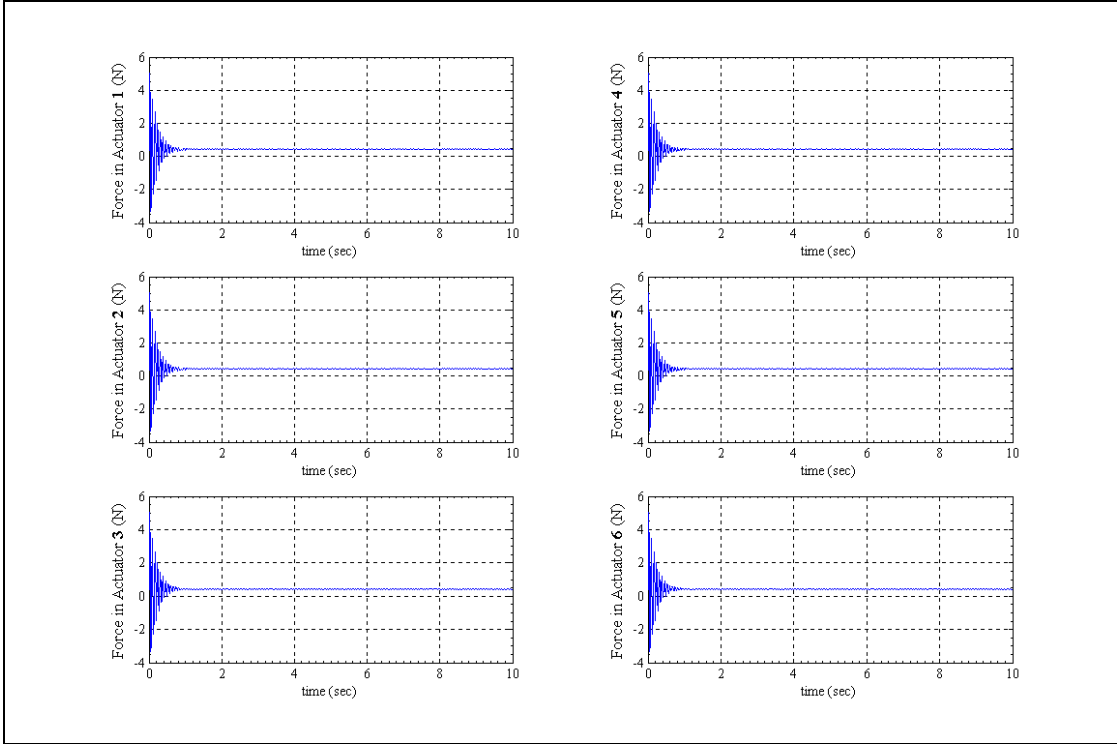


Fig. 5.8 Plots of the input force experienced by each actuator as the Case 1 task is executed for the traditional parallel manipulator

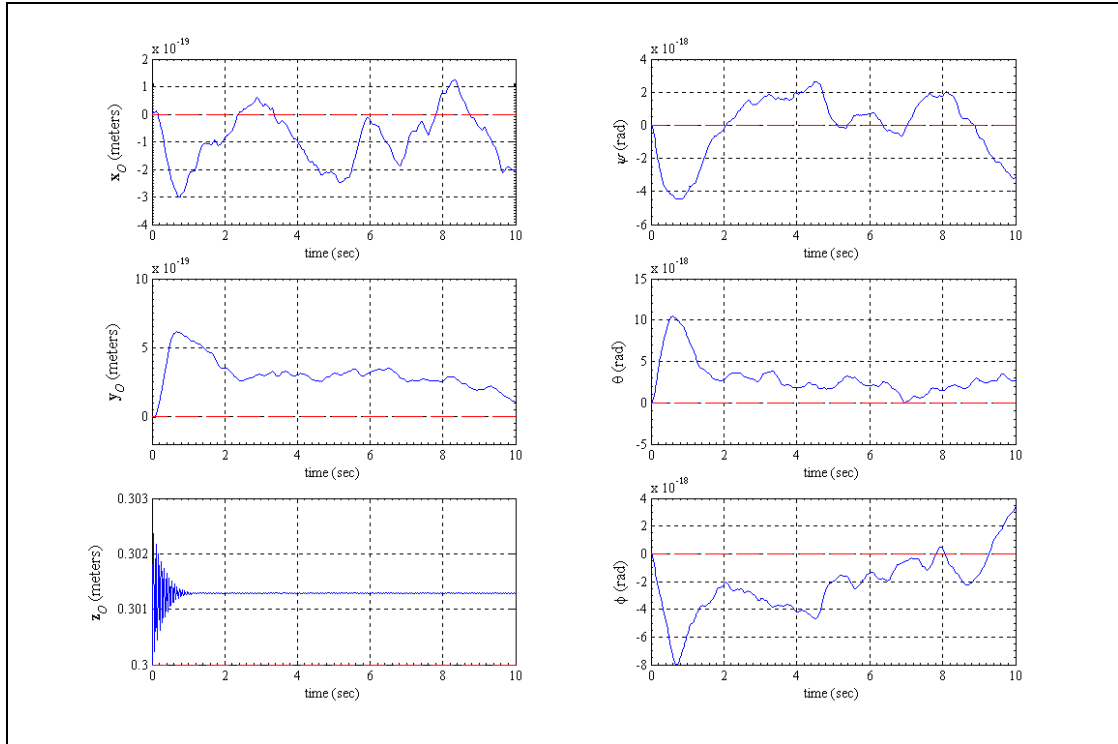


Fig. 5.9 Plot of the position and orientation of the MP as the Case 1 task is executed for the cable suspended parallel manipulator

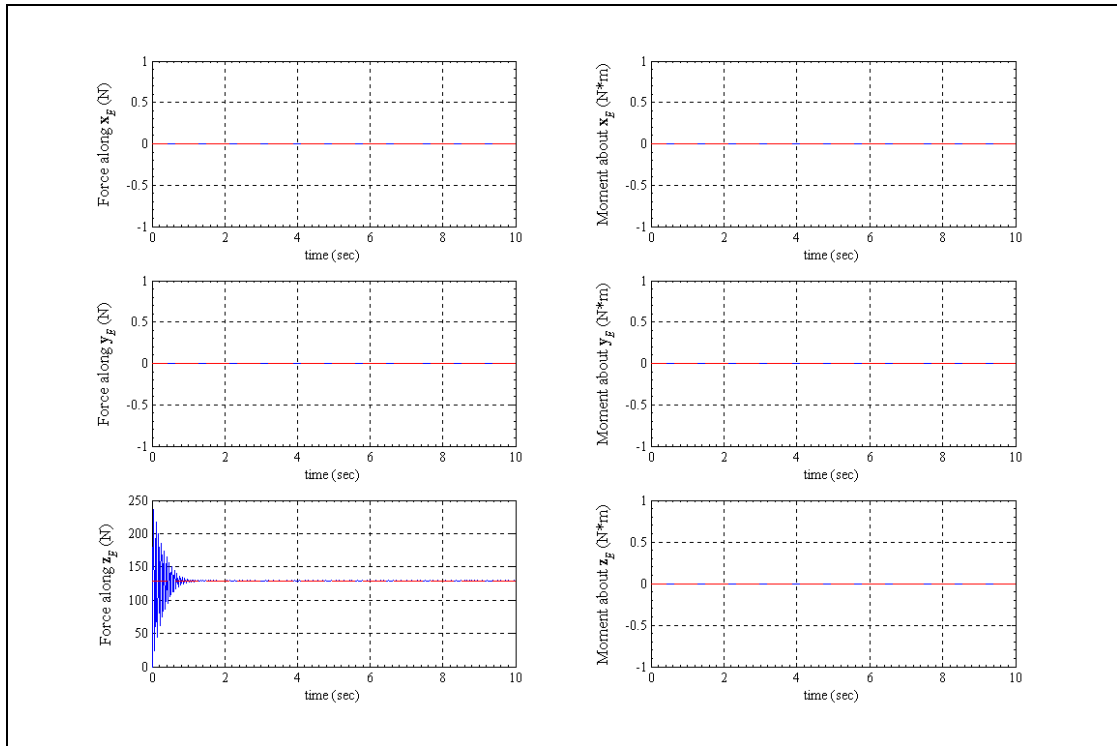


Fig. 5.10 Plots of the forces and moments acting on the MP as the Case 1 task is executed for the cable suspended parallel manipulator

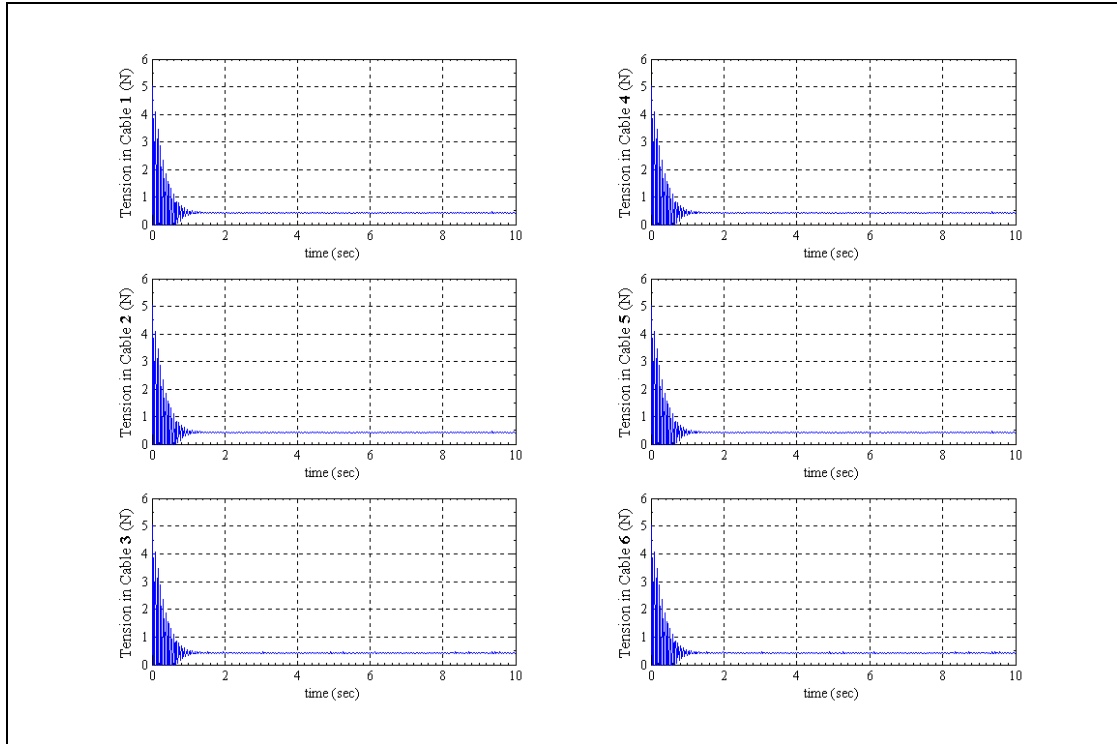


Fig. 5.11 Plots of the tensions experienced by each cable as the Case 1 task is executed for the cable suspended parallel manipulator

The cable suspended parallel robot can only push on the environment in the positive \mathbf{z}_O direction with a force equal to the weight of its MP, as expected. The traditional parallel robot is able to push on the environment with as much force as the actuators can supply. In either case, when the MP exerted force on the environment the initial force resulted in large vibrations with amplitude nearly double the desired force value. In some situations, unsteady motion results if the desired force exerted by the MP on the environment in the direction of gravity is too close to the weight of the MP for the cable suspended parallel robot.

For the traditional parallel robot, the initial actuator inputs called for pushing forces as seen by the negative input force values shown in Fig. 5.7. During

the instances where pushing forces were needed the decision-making block was enabled for the cable suspended parallel robot to recalculate the cable input forces so that only positive pulling input forces were sent to the cables as seen in Fig. 5.11. As a result, the force variation appeared denser initially but the maximum amplitude of the cable forces are not that much different from the maximum forces for the traditional parallel robot except that the cable forces contained all pulling (positive) forces.

To satisfy curiosity, additional simulations were run for Case 1 where the desired force was varied over a large range of values. It was found that if the desired force is less than the weight of the MP then the force could be applied. However, the desired force has a lower bound. This lower bound is obviously limited in the real world application by the force sensitivity threshold of the sensor, but these noise disturbances are not considered in the simulation. The controller revealed to possess an extremely small noise disturbance due most likely to computer calculation limitations. This limitation is in general much smaller than the force sensitivity threshold of common force/torque sensors. This result was observed to be common in both parallel manipulators.

What appeared more interesting is when the desired force was chosen to be equal or very close to the weight of the MP for the cable suspended parallel robot. When the desired force is equal to the weight of the MP for the traditional parallel robot, the initial actuator forces will oscillate between pushing and pulling forces and ideally result in a zero force within the actuators and the MP will simply rest on the surface. When the cable suspended parallel robot applies a desired force that is equal to the weight of the MP, the initial cable tensions are extremely large and vibratory.

At this initial stage, the decision making block is enabled and is seeking new input tension values that are neither negative nor zero. However, in this particular case the best value for the cables is simply zero. As observed from the results in Fig. 5.9, Fig. 5.10 and Fig. 5.11, the cable suspended parallel robot is able to apply relatively large forces on the environment compared to the weight of its MP.

5.5.2 Case 2

The task presented in this case is for the MP to translate along the \mathbf{x}_O axis with a defined trajectory while maintaining a constant force on the environment in the \mathbf{z}_O direction. The total simulation was run for 40 seconds for each parallel robot. The natural and artificial constraints for the Case 2 task are given in Table 5.3.

Table 5.3: Natural and Artificial Constraints for Case 2	
Natural Constraints	Artificial Constraints
$\mathbf{F}_{x,env} = 0$	$\mathbf{v}_x = \mathbf{v}_{x,trajectory}$
$\mathbf{F}_{y,env} = 0$	$\mathbf{v}_y = 0$
$\mathbf{v}_z = 0$	$\mathbf{F}_{z,env} = 110N$
$\mathbf{M}_{x,env} = 0$	$\boldsymbol{\omega}_x = 0$
$\mathbf{M}_{y,env} = 0$	$\boldsymbol{\omega}_y = 0$
$\mathbf{M}_{z,env} = 0$	$\boldsymbol{\omega}_z = 0$

Table 5.3 Natural and Artificial Constraints for Case 2

The graphs for the position and orientation of the MP, forces and moments acting on the MP, and forces in each actuating link are given in Fig. 5.12, Fig. 5.13 and Fig. 5.14 respectively for the traditional parallel robot. The cable suspended parallel robot position and orientation are given in Fig. 5.15, the forces and moments

experienced by the MP are shown in Fig. 5.16, and the tensions in each cable are shown in Fig. 5.17.

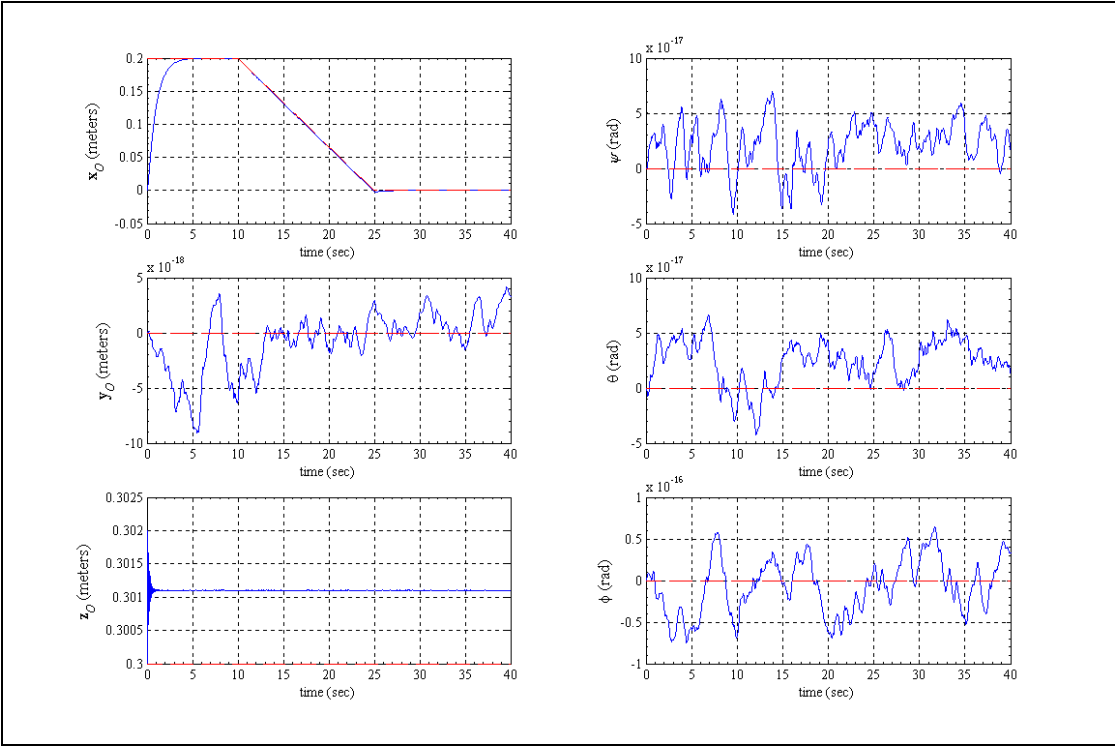


Fig. 5.12 Plot of the position and orientation of the MP as the Case 2 task is executed for the traditional parallel manipulator

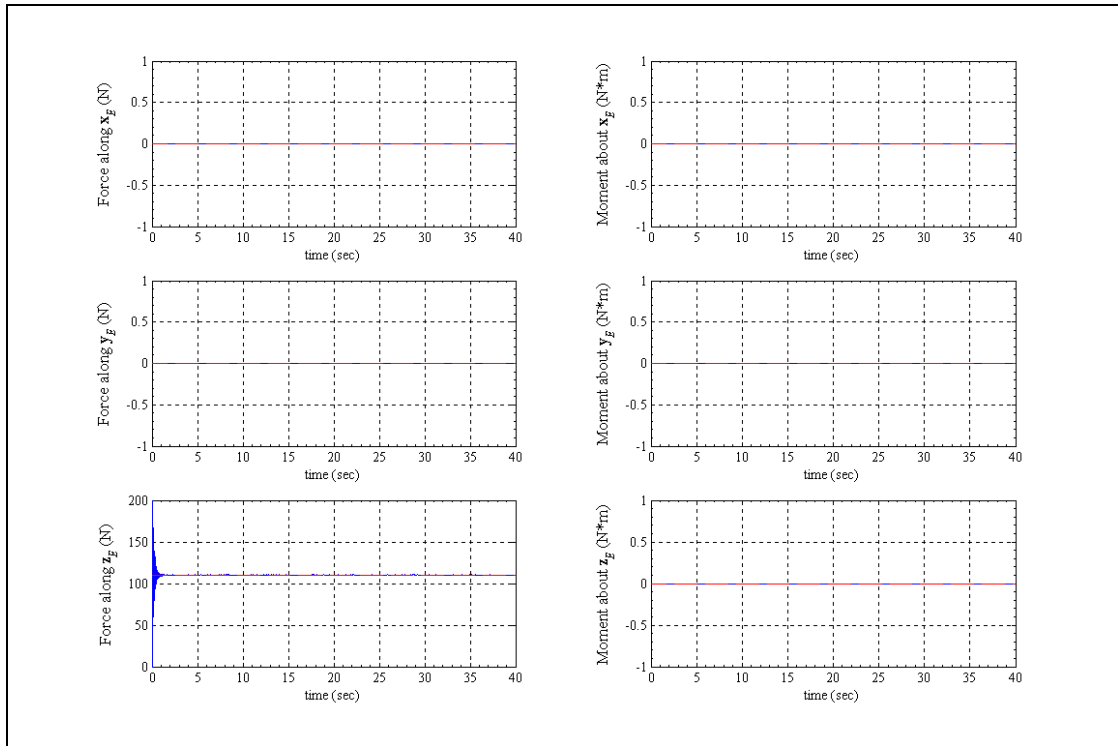


Fig. 5.13 Plots of the forces and moments acting on the MP as the Case 2 task is executed for the traditional parallel manipulator

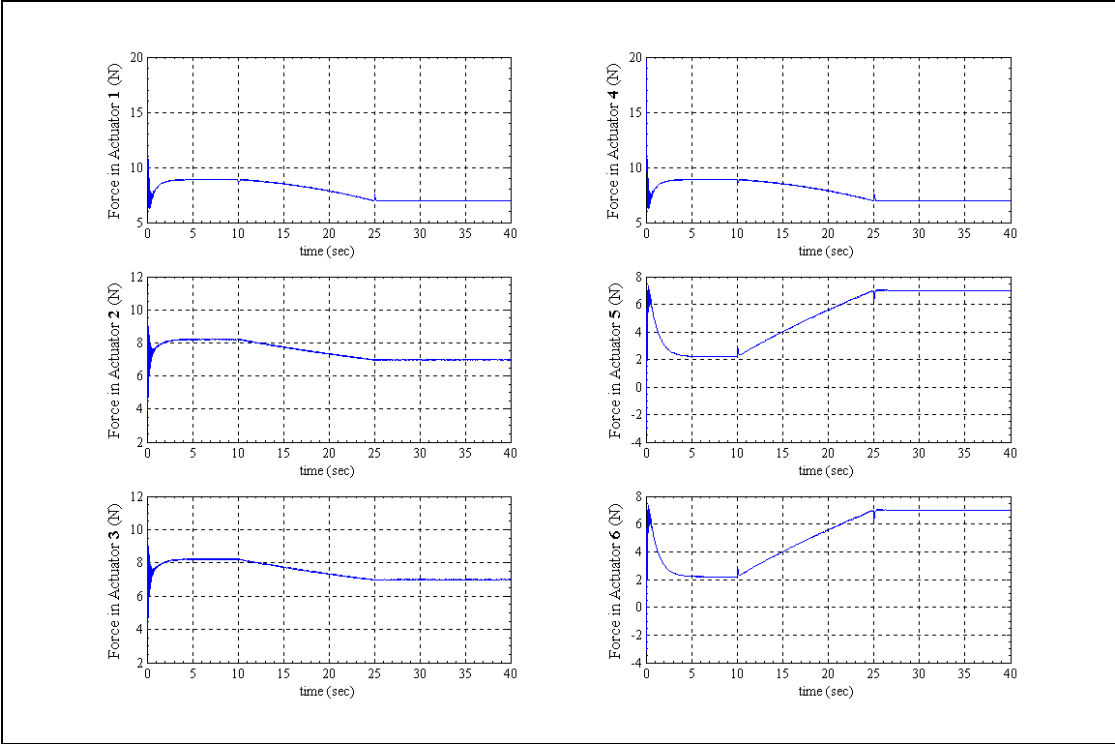


Fig. 5.14 Plots of the input force experienced by each actuator as the Case 2 task is executed for the traditional parallel manipulator

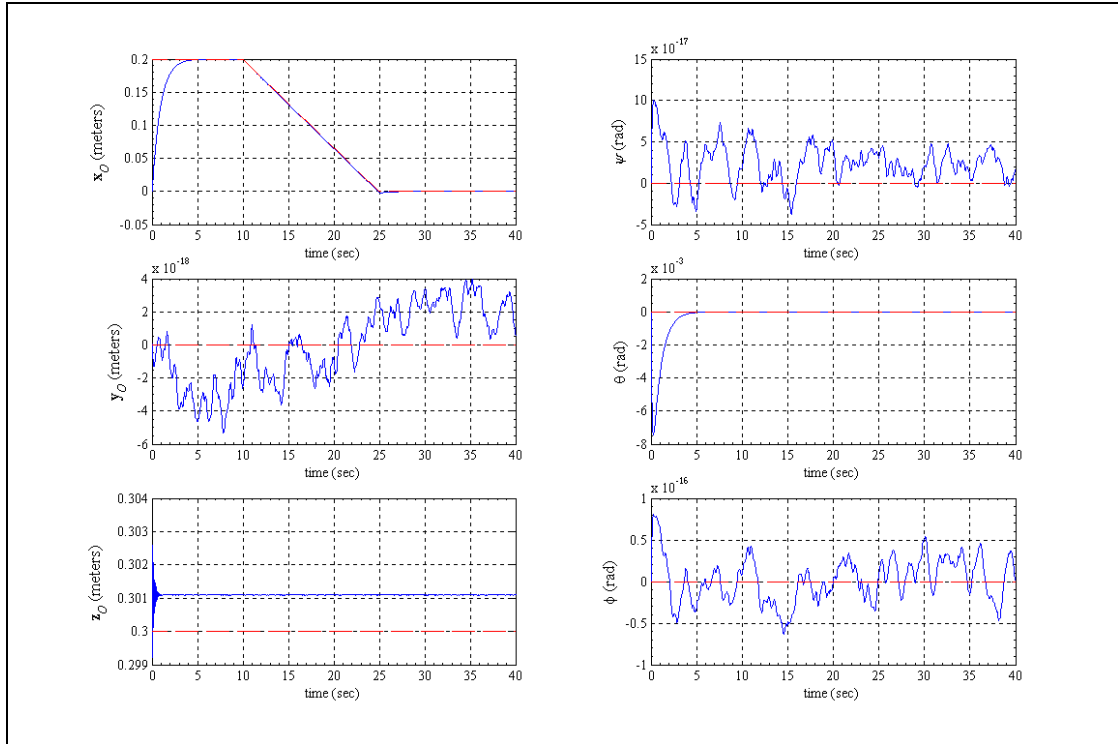


Fig. 5.15 Plot of the position and orientation of the MP as the Case 2 task is executed for the cable suspended parallel manipulator

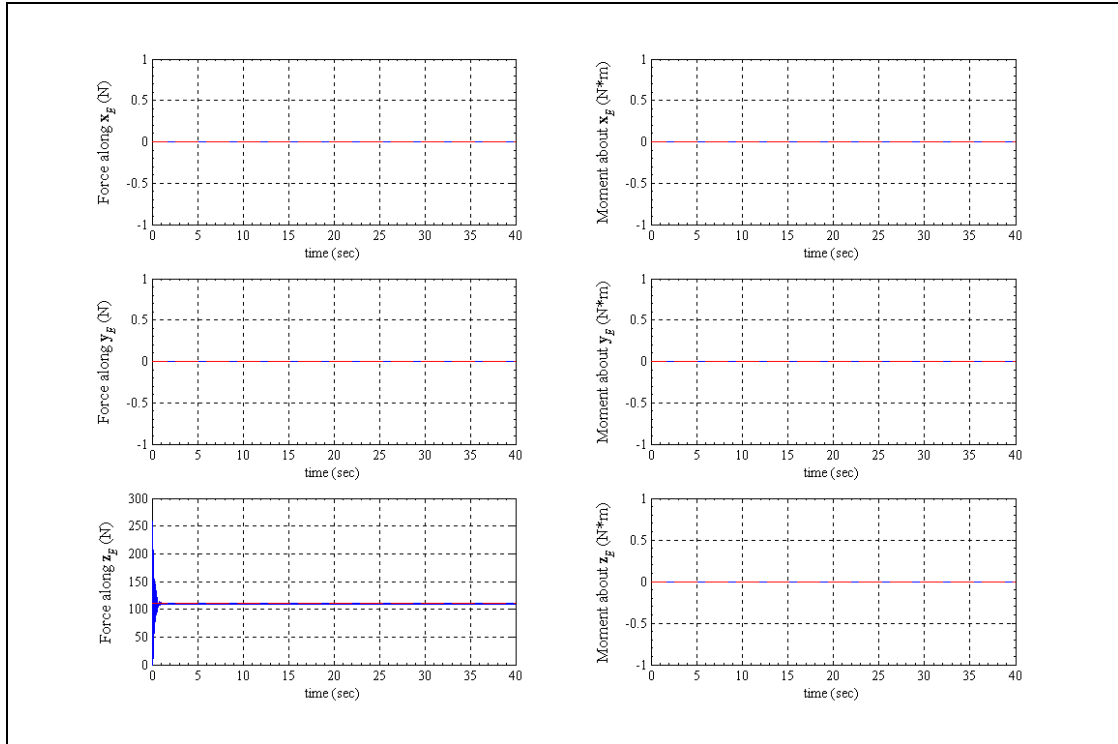


Fig. 5.16 Plots of the forces and moments acting on the MP as the Case 2 task is executed for the cable suspended parallel manipulator

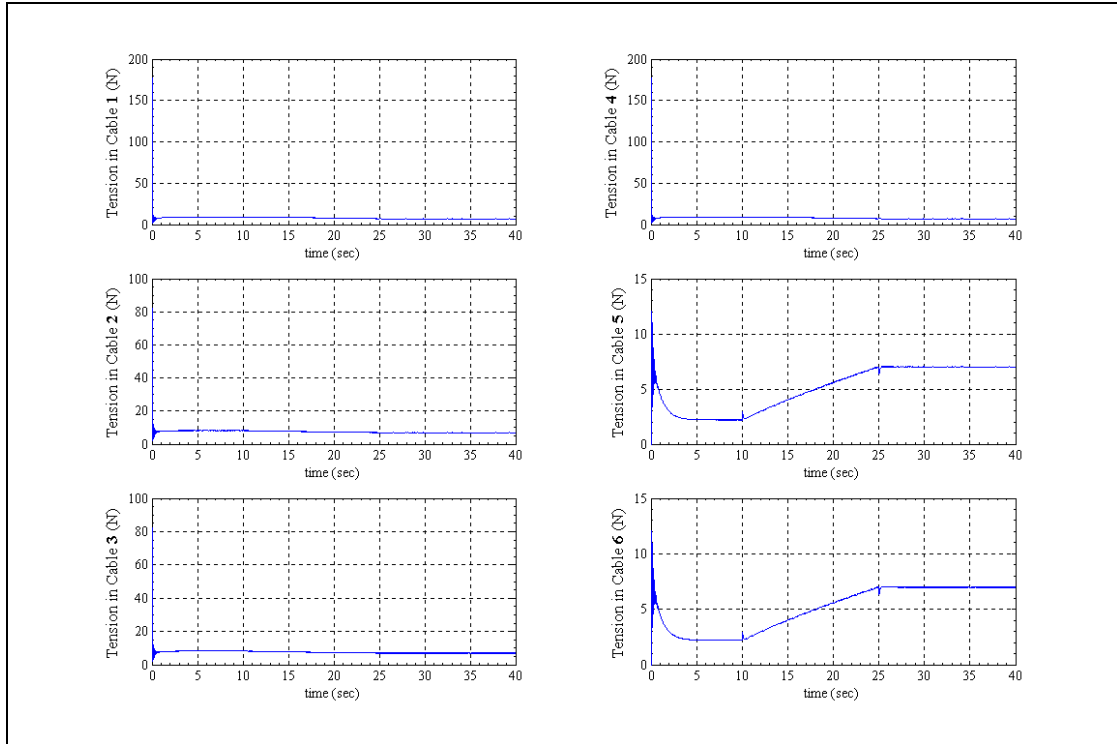


Fig. 5.17 Plots of the tensions experienced by each cable as the Case 2 task is executed for the cable suspended parallel manipulator

The traditional parallel robot initially required pushing forces (negative) for the input actuators 5 and 6 as shown in Fig. 5.14. In this case, the decision-making block compensated for the pushing forces by drastically increasing the tension values for the cables 1, 2, 3 and 4 as seen in Fig. 5.17. In addition, it is noted that at this instant the θ rotation about the y_o axis is also affected by the output of the decision making block. For this case the decision making block found new tension values that are all positive and the new values caused the MP to compensate for the needed negative pushing forces from its cables by reorienting its MP.

5.5.3 Case 3

In this task, the MP is to push against a planar surface along the \mathbf{z}_O axis with a constant force and translate the MP in a square motion pattern as if washing the surface as shown in Fig. 5.18. This case is to provide insight to the performance of the controller when executing multiple task trajectories along different directions. The motion is chosen such that the MP will translate very close to its workspace boundaries. The extremes that the MP translates to include $\mathbf{x}_O = \mathbf{y}_O = \pm 0.165$ meters. The entire simulation takes 40 seconds to complete the task and the natural and artificial constraints for the task are given in Table 5.4.

The position and orientation of the MP for the traditional parallel manipulator are given in Fig. 5.19, the forces and moments acting on the MP are given in Fig. 5.20, and the input forces within the actuators are given in Fig. 5.21. For the cable suspended parallel manipulator the position and orientation of the MP are shown in Fig. 5.22, the forces and moments experiences by the MP are displayed in Fig. 5.23, and the tension forces with in the cables are given in Fig. 5.24.

Table 5.4: Natural and Artificial Constraints for Case 3	
Natural Constraints	Artificial Constraints
$\mathbf{F}_{x,env} = 0$	$\mathbf{v}_x = \mathbf{v}_{x,trajectory}$
$\mathbf{F}_{y,env} = 0$	$\mathbf{v}_y = \mathbf{v}_{y,trajectory}$
$\mathbf{v}_z = 0$	$\mathbf{F}_{z,env} = 110N$
$\mathbf{M}_{x,env} = 0$	$\boldsymbol{\omega}_x = 0$
$\mathbf{M}_{y,env} = 0$	$\boldsymbol{\omega}_y = 0$
$\mathbf{M}_{z,env} = 0$	$\boldsymbol{\omega}_z = 0$

Table 5.4 Natural and Artificial Constraints for Case 3

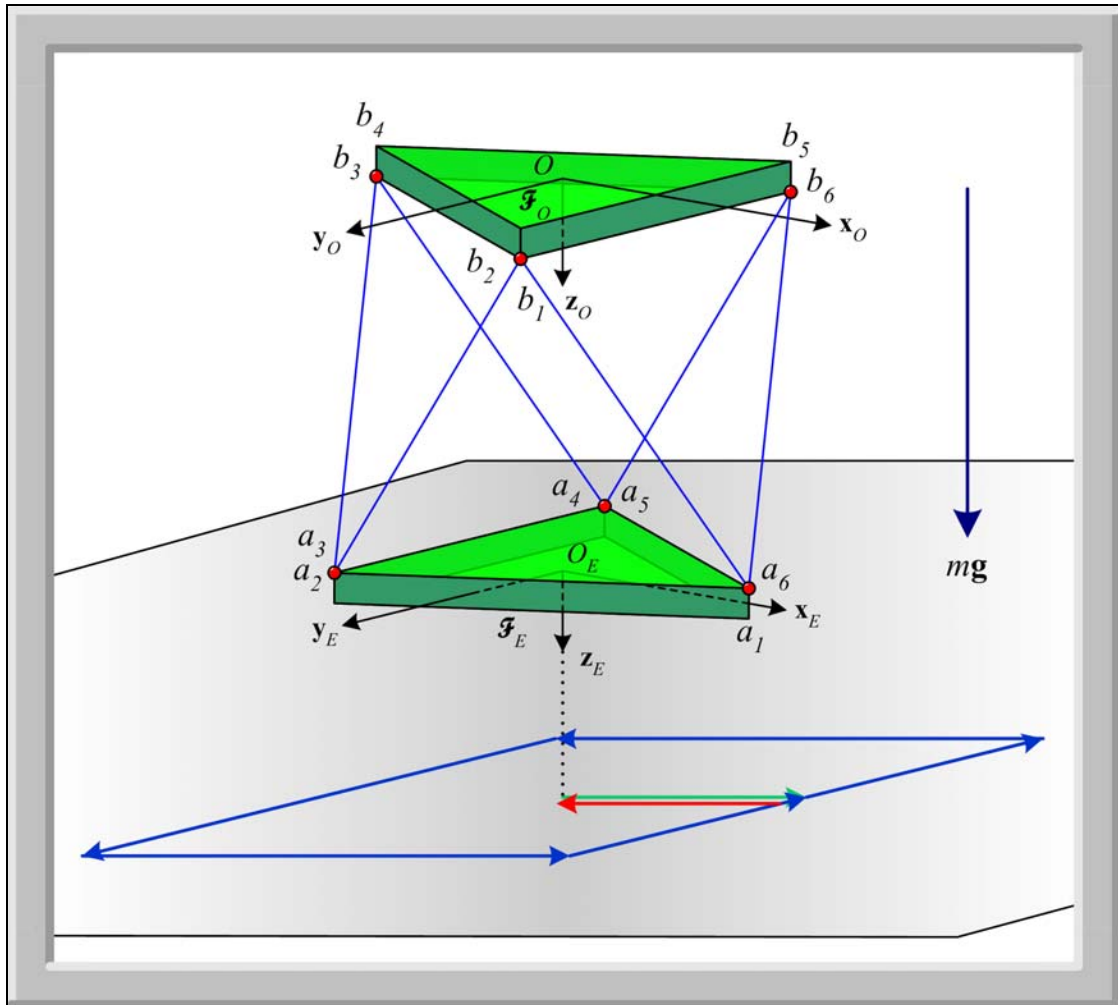


Fig. 5.18 Desired trajectory of the MP for Case 3 task

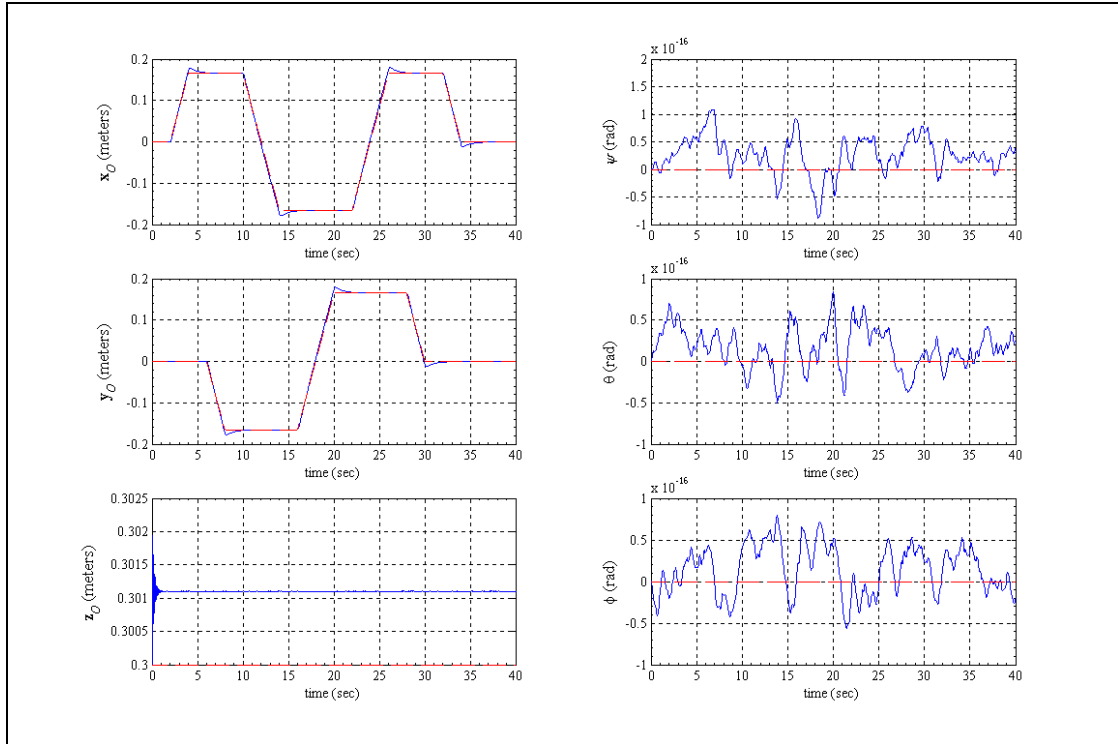


Fig. 5.19 Plot of the position and orientation of the MP as the Case 3 task is executed for the traditional parallel manipulator

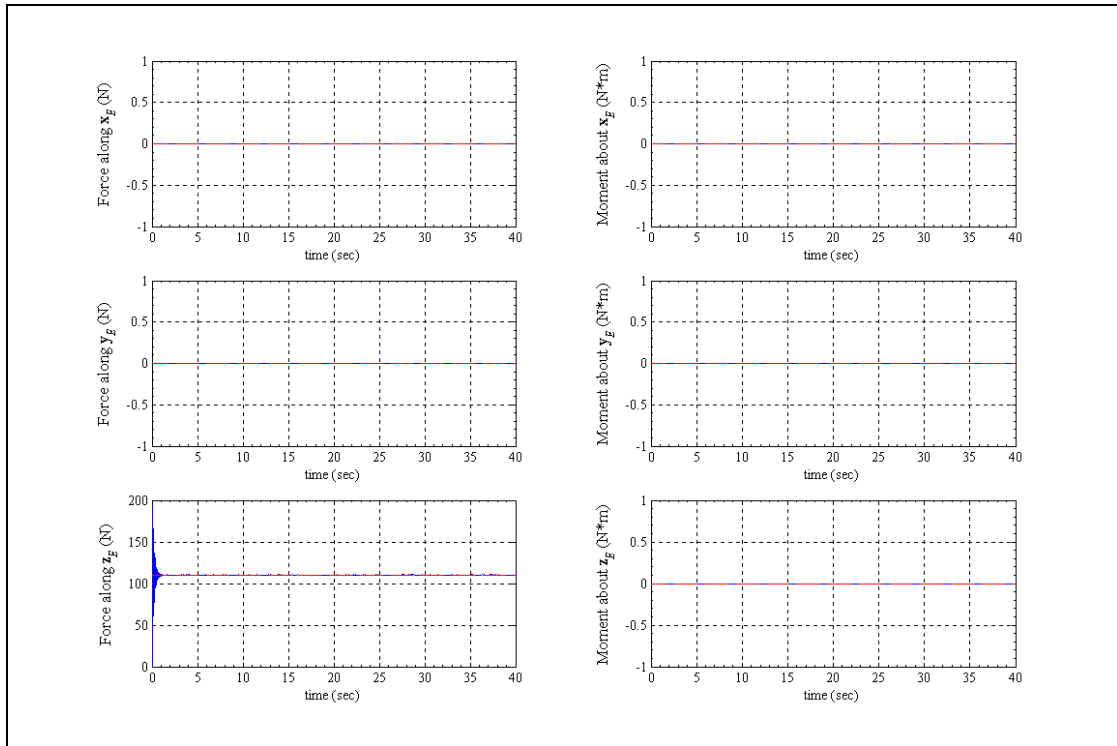


Fig. 5.20 Plots of the forces and moments acting on the MP as the Case 3 task is executed for the traditional parallel manipulator

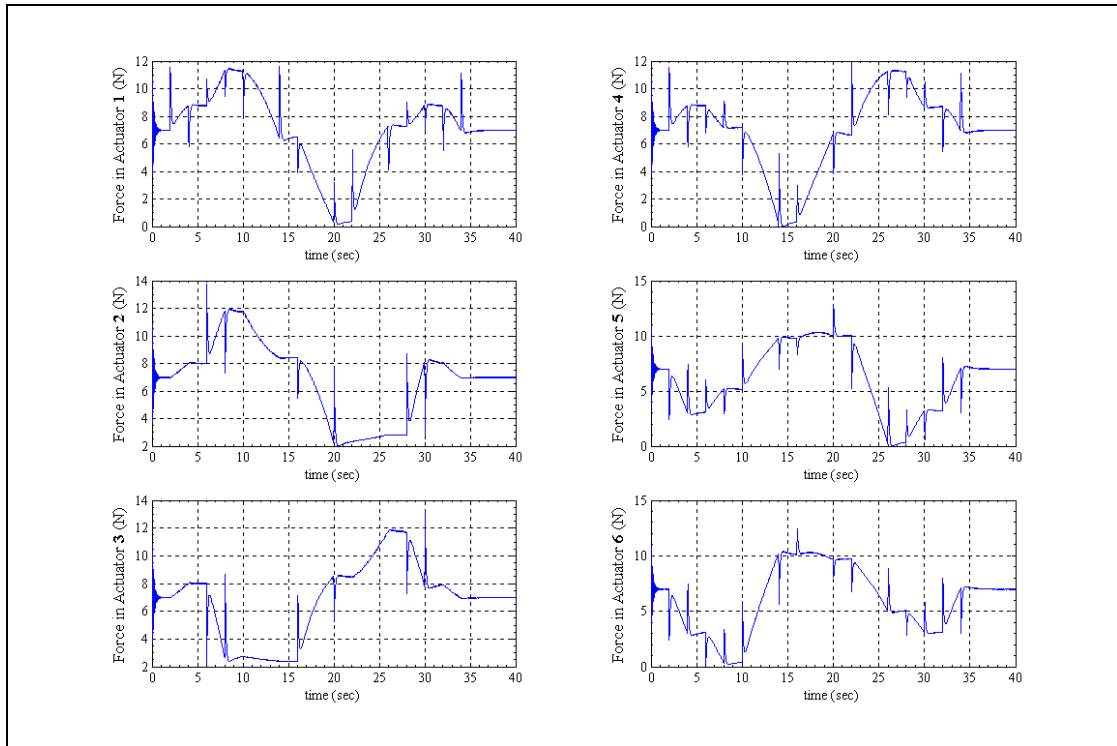


Fig. 5.21 Plots of the input force experienced by each actuator as the Case 3 task is executed for the traditional parallel manipulator

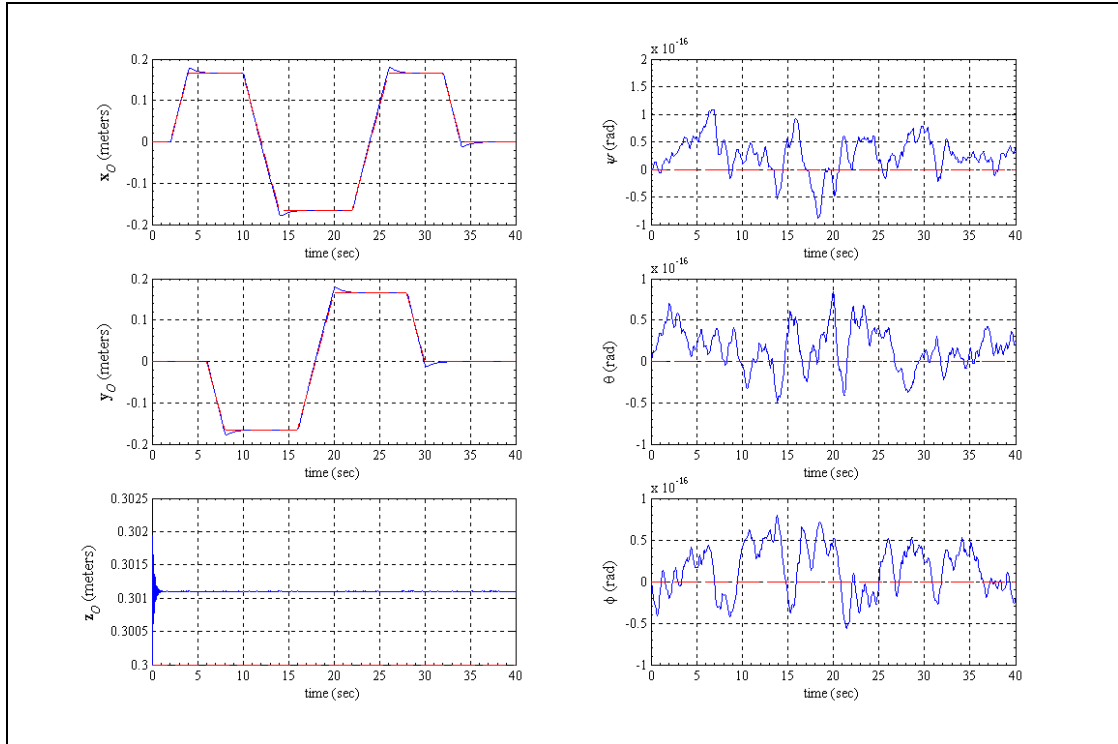


Fig. 5.22 Plot of the position and orientation of the MP as the Case 3 task is executed for the cable suspended parallel manipulator

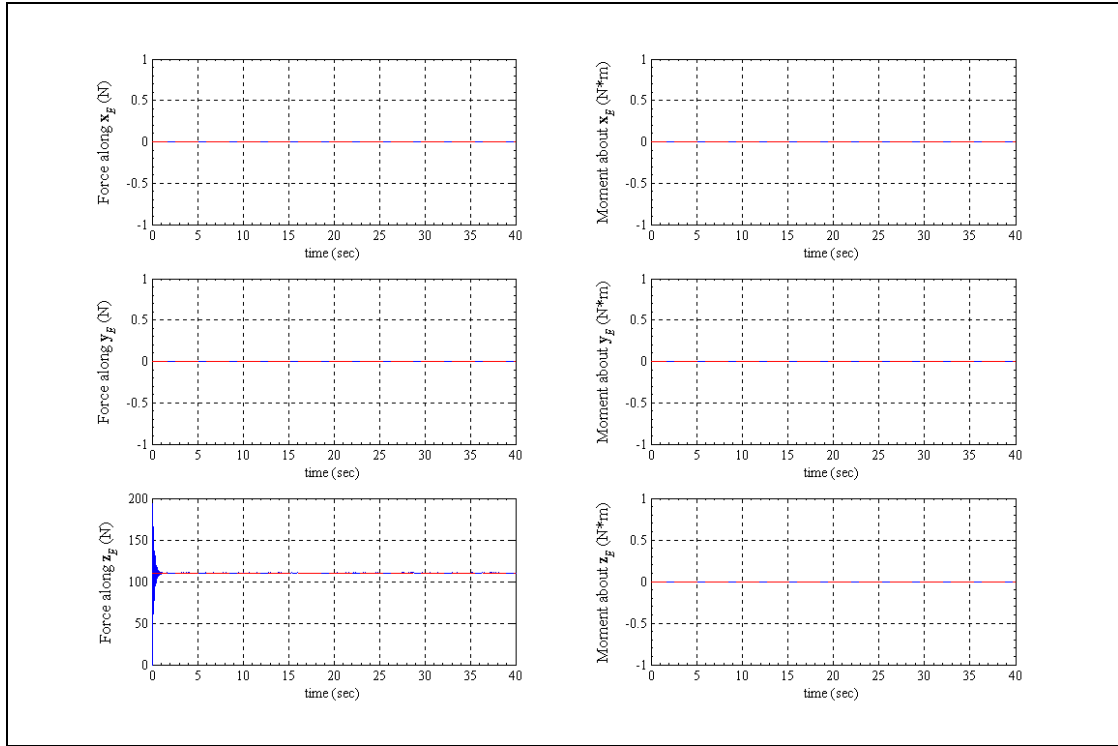


Fig. 5.23 Plots of the forces and moments acting on the MP as the Case 3 task is executed for the cable suspended parallel manipulator

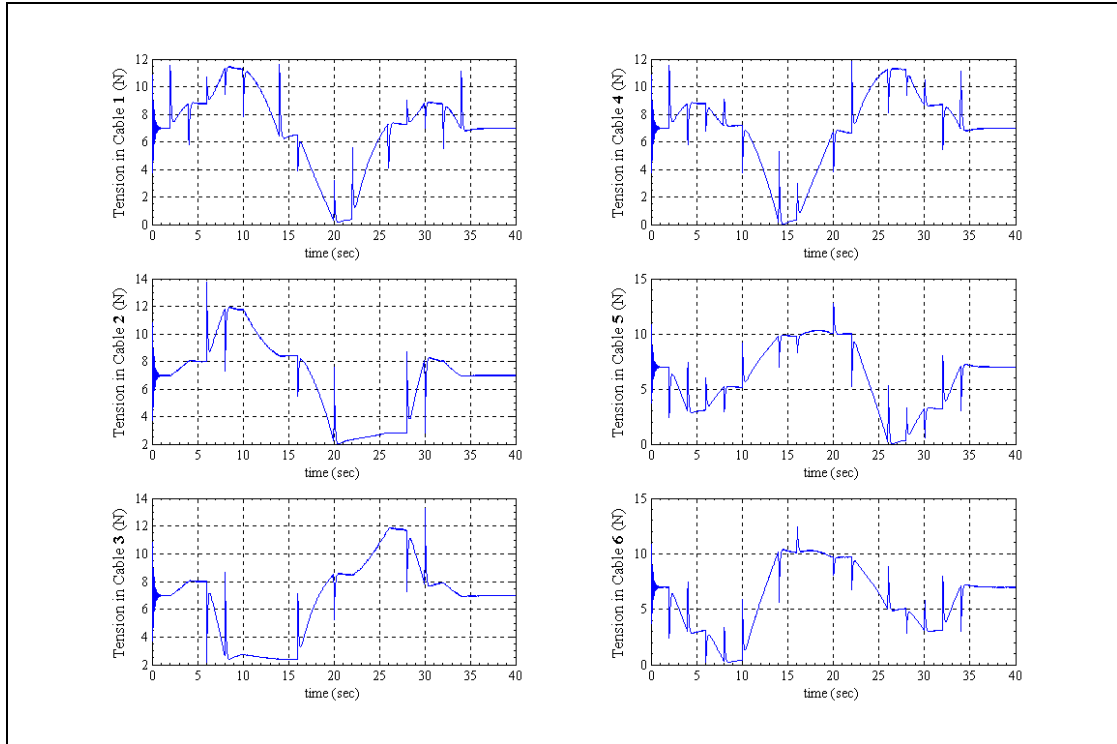


Fig. 5.24 Plots of the tensions experienced by each cable as the Case 3 task is executed for the cable suspended parallel manipulator

For this case, the trajectory for the traditional and cable suspended parallel manipulator appear to be very similar. The differences between the two manipulators are minor if any at all. It is noted that the MP of the cable suspended parallel robot is not able to translate to large distances along the x_o and y_o axes relative to the size of its MP and BP when compared to the capabilities of the traditional parallel manipulator. However, the cable suspended parallel is able to reasonably reach much greater distances along the z_o axis than the traditional parallel robot, which will be observed and discussed in the following case.

5.5.4 Case 4

This specific example is used to provide insight into the behavior of the hybrid force/position controller with a varying force and position trajectory. For this particular simulation, the MP is to apply varying force trajectory against a wall located in the (y_o, z_o) plane defined by $x_o = \text{constant}$ and translated along the z_o axis. The probe attached to the MP is extended past the edge of the MP allowing the center of the MP to remain somewhere near $x_o = 0$. The simulation takes 40 seconds to run and the natural and artificial constraints are given in Table 5.5.

Table 5.5: Natural and Artificial Constraints for Case 4	
Natural Constraints	Artificial Constraints
$\mathbf{v}_x = 0$	$\mathbf{F}_{x,env} = \mathbf{F}_{x,trajectory}$
$\mathbf{F}_{y,env} = 0$	$\mathbf{v}_y = 0$
$\mathbf{F}_{z,env} = 0$	$\mathbf{v}_z = \mathbf{v}_{z,trajectory}$
$\mathbf{M}_{x,env} = 0$	$\boldsymbol{\omega}_x = 0$
$\mathbf{M}_{y,env} = 0$	$\boldsymbol{\omega}_y = 0$
$\mathbf{M}_{z,env} = 0$	$\boldsymbol{\omega}_z = 0$

Table 5.5 Natural and Artificial Constraints for Case 4

The position and orientation of the MP are given in Fig. 5.25 for the traditional parallel robot and Fig. 5.28 for the cable suspended parallel robot, the forces and moments experienced by the MP are shown in Fig. 5.26 for the traditional parallel robot and Fig. 5.29 for the cable suspended parallel robot. The forces exerted by the input prismatic actuators of the traditional parallel robot are shown in Fig. 5.27 and the tensions in the cables are shown in Fig. 5.30 for the cable suspended parallel robot.

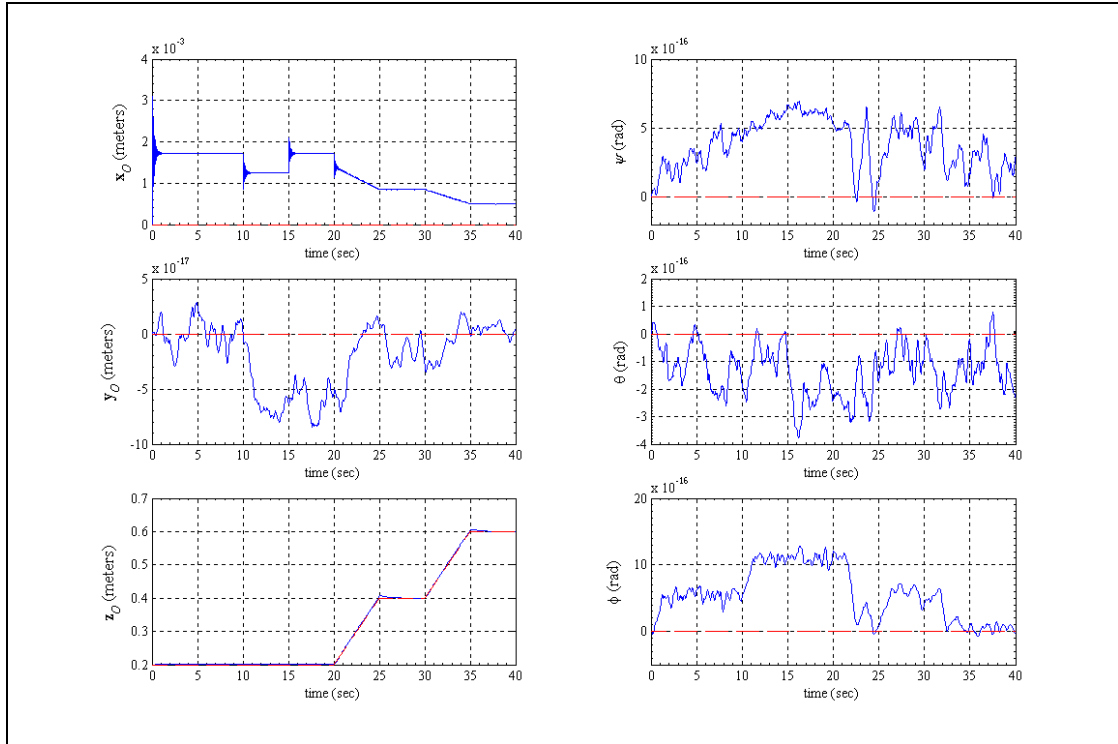


Fig. 5.25 Plot of the position and orientation of the MP as the Case 4 task is executed for the traditional parallel manipulator

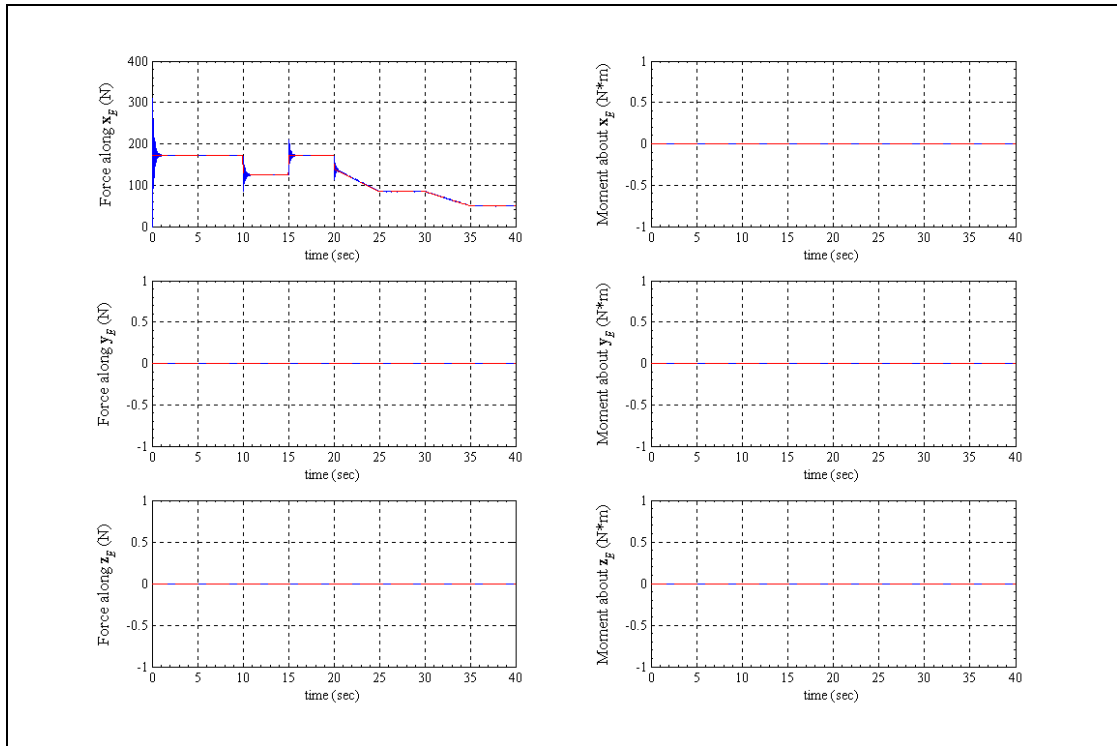


Fig. 5.26 Plots of the forces and moments acting on the MP as the Case 4 task is executed for the traditional parallel manipulator

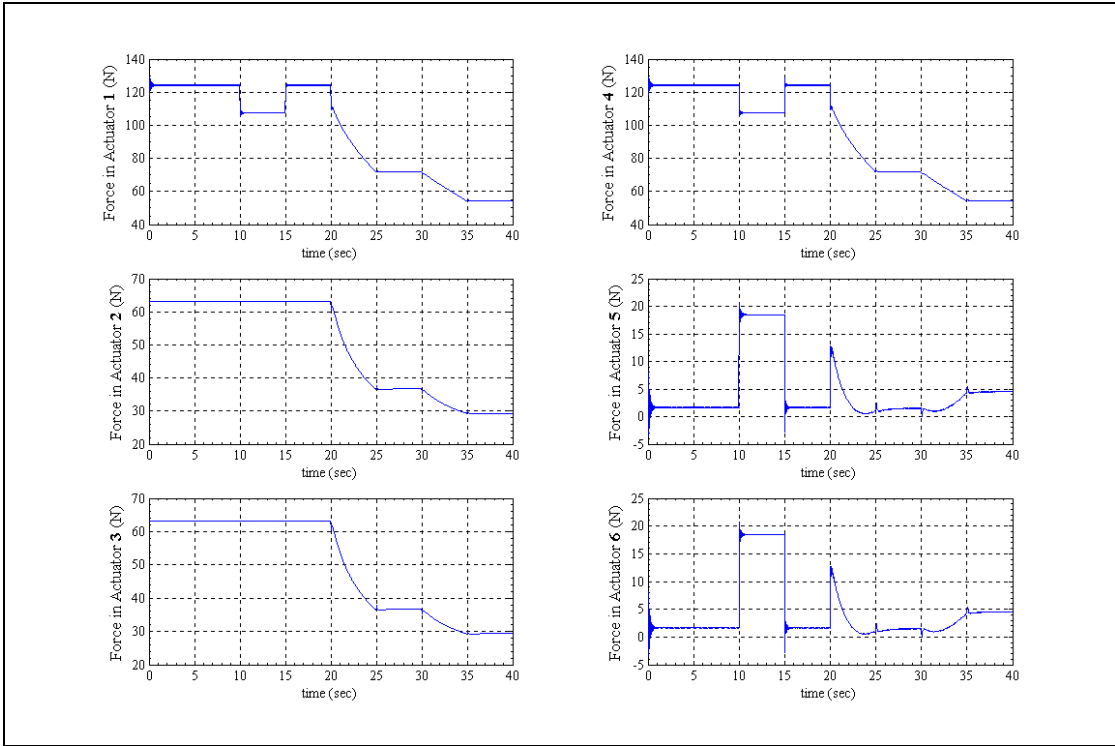


Fig. 5.27 Plots of the input force experienced by each actuator as the Case 4 task is executed for the traditional parallel manipulator

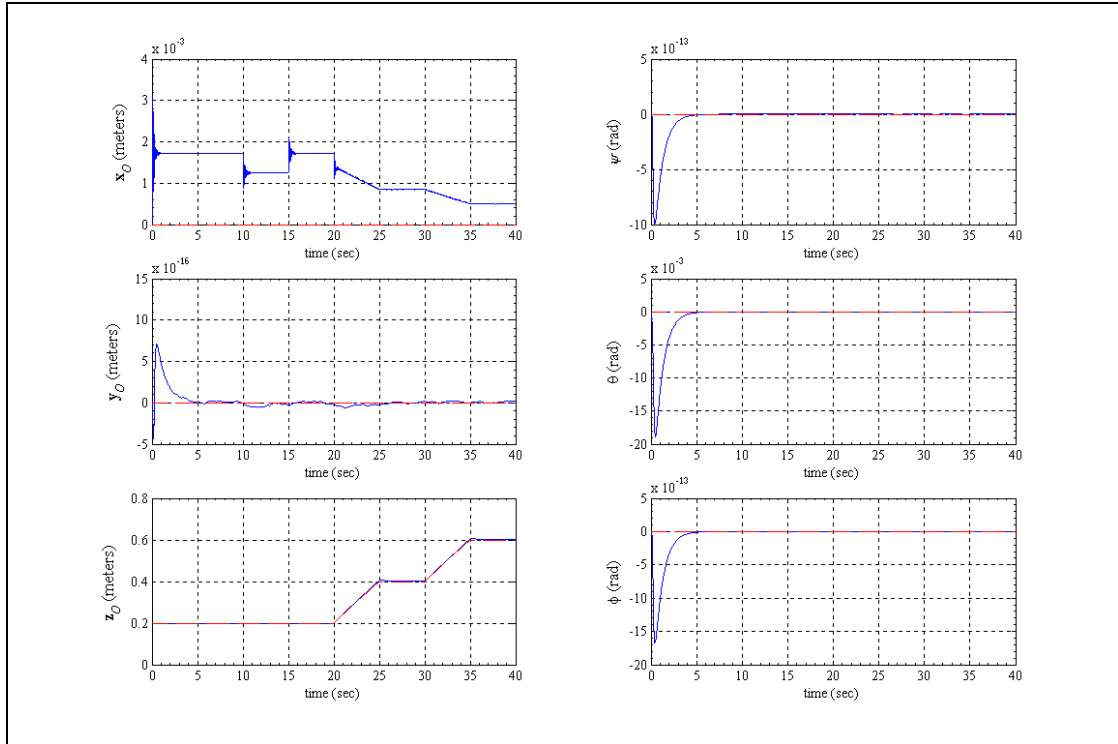


Fig. 5.28 Plot of the position and orientation of the MP as the Case 4 task is executed for the cable suspended parallel manipulator

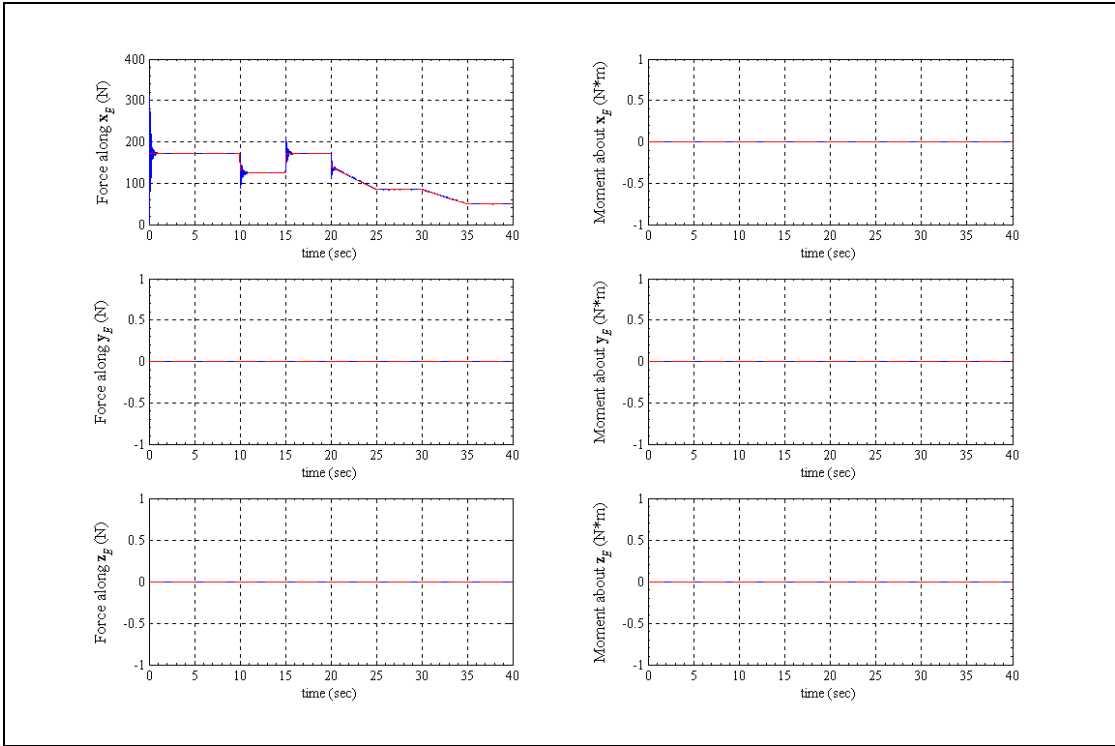


Fig. 5.29 Plots of the forces and moments acting on the MP as the Case 4 task is executed for the cable suspended parallel manipulator

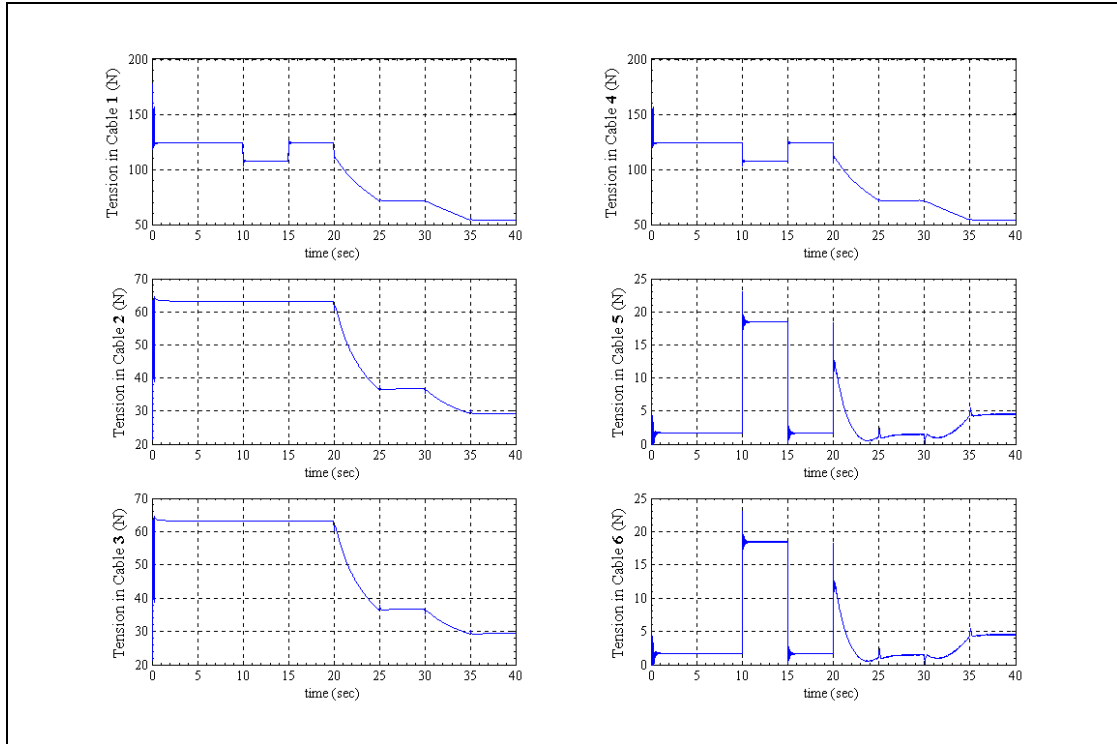


Fig. 5.30 Plots of the tensions experienced by each cable as the Case 4 task is executed for the cable suspended parallel manipulator

In the simulation actuators 5 and 6 required negative forces at $t = 0$ seconds and $t = 15$ seconds as observed in Fig. 5.27 for the traditional parallel robot. At these two times, the decision making block for the cable suspended parallel robot is activated to generate new positive cable tensions. The new tensions caused the MP to have increased orientation errors about each axis with the largest error being only slightly larger than one degree for θ , the rotation about the y_o axis. At the points where the decision making block is engaged the cable tensions show a sudden increase in tension. There was also a very small error in the y_o position but this error is hardly noticeable. In addition, the cable suspended parallel robot's ability to transmit forces at several different elevations along the z_o axis is observed in Fig. 5.30 by noting how

close the cable tensions come to zero. Overall, both parallel manipulators were able to execute the desired task with reasonable input actuator forces.

5.5.5 Case 5

In this simulation the MP is to apply a constant force to a planar surface defined by $x_o = \text{constant}$ while translating along the y_o axis. The probe extends past the edge of the MP and contacts the surface allowing the center of the MP to remain near $x_o = 0$. The simulation is run for a total of $t = 40$ seconds and the natural and artificial constraints for the task are shown in Table 5.6. The position and orientation of the MP for the traditional parallel robot are given in Fig. 5.31 and the forces experienced by the MP are shown in Fig. 5.32. The forces residing in the prismatic actuators for the traditional parallel robot are given in Fig. 5.33. The cable suspended parallel robot's position and orientation are shown in Fig. 5.34, the forces and moments acting on the MP are displayed in Fig. 5.35, and the tensions in each cable are given in Fig. 5.36.

Table 5.6: Natural and Artificial Constraints for Case 5	
Natural Constraints	Artificial Constraints
$\mathbf{v}_x = 0$	$\mathbf{F}_{x,env} = \mathbf{F}_{x,trajectory}$
$\mathbf{F}_{y,env} = 0$	$\mathbf{v}_y = \mathbf{v}_{y,trajectory}$
$\mathbf{F}_{z,env} = 0$	$\mathbf{v}_z = 0$
$\mathbf{M}_{x,env} = 0$	$\boldsymbol{\omega}_x = 0$
$\mathbf{M}_{y,env} = 0$	$\boldsymbol{\omega}_y = 0$
$\mathbf{M}_{z,env} = 0$	$\boldsymbol{\omega}_z = 0$

Table 5.6 Natural and Artificial Constraints for Case 5

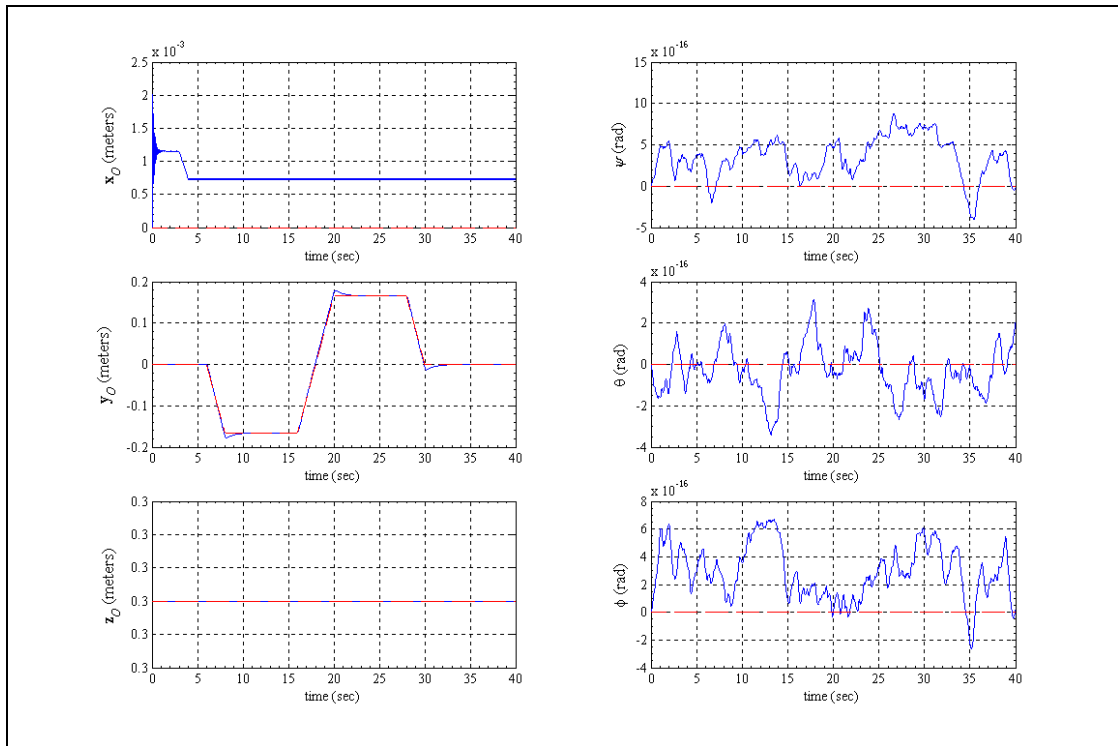


Fig. 5.31 Plot of the position and orientation of the MP as the Case 5 task is executed for the traditional parallel manipulator

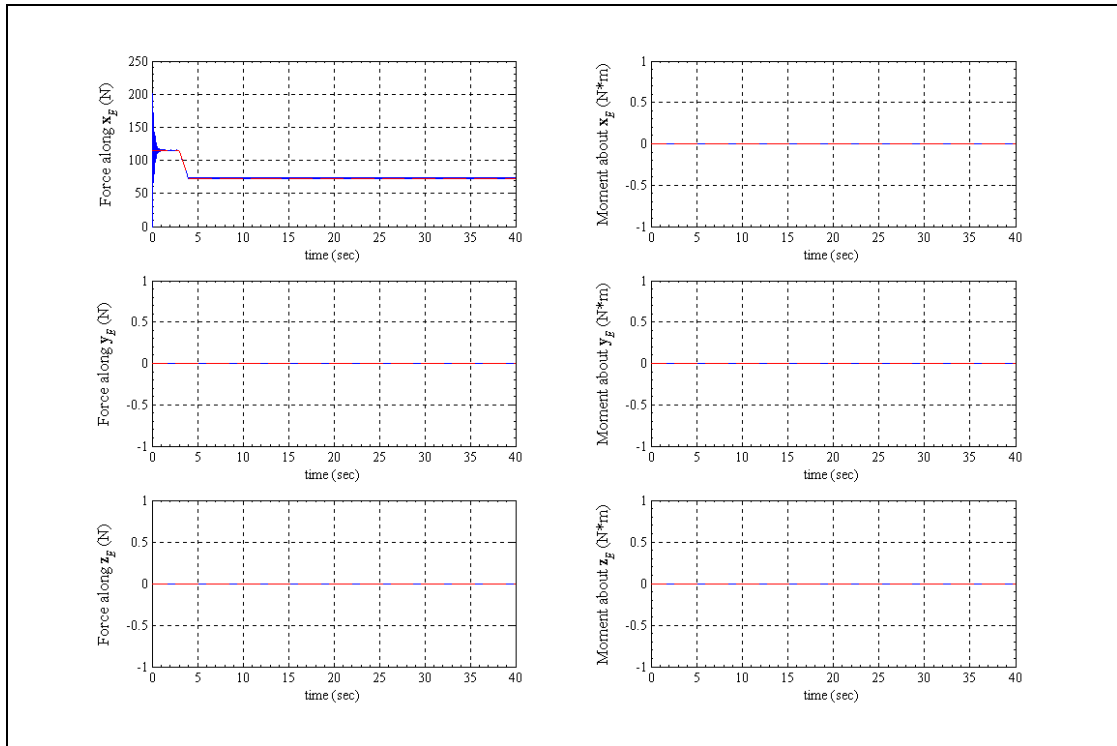


Fig. 5.32 Plots of the forces and moments acting on the MP as the Case 5 task is executed for the traditional parallel manipulator

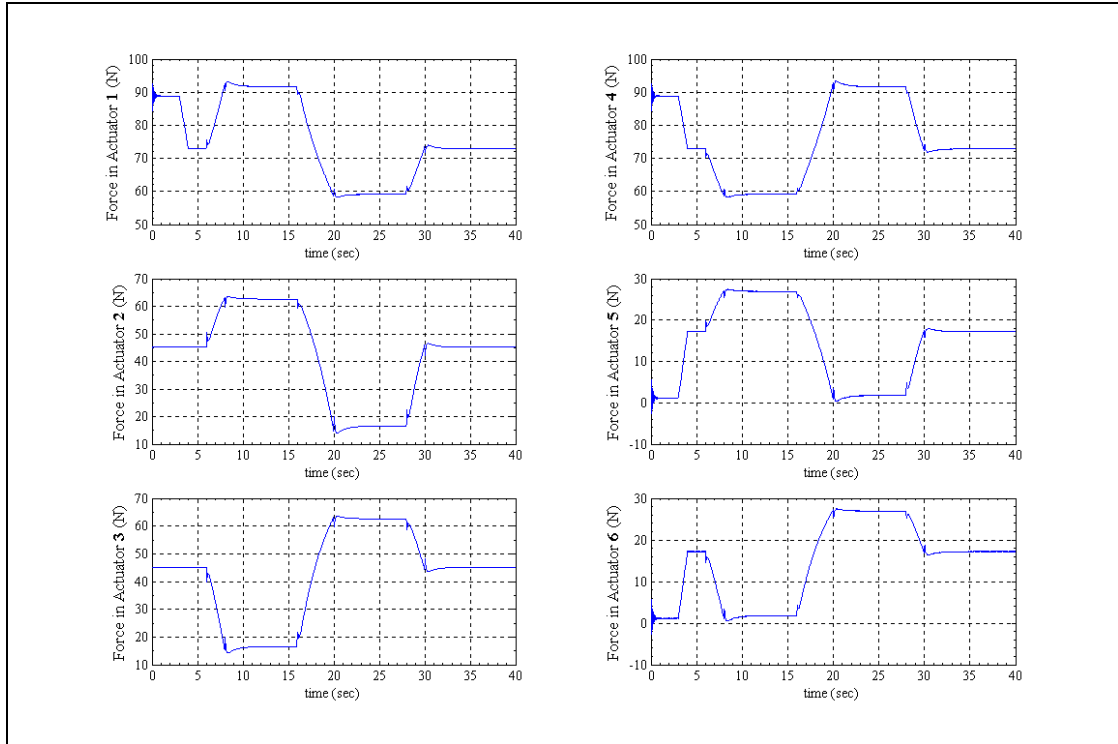


Fig. 5.33 Plots of the input force experienced by each actuator as the Case 5 task is executed for the traditional parallel manipulator

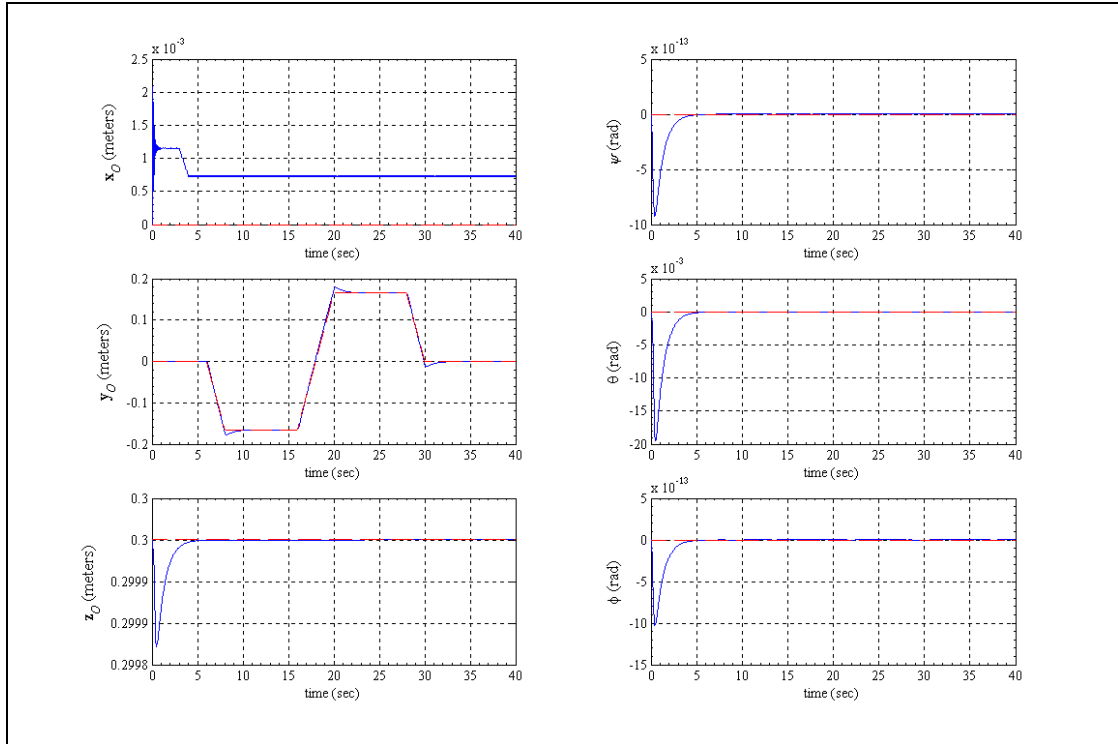


Fig. 5.34 Plot of the position and orientation of the MP as the Case 5 task is executed for the cable suspended parallel manipulator

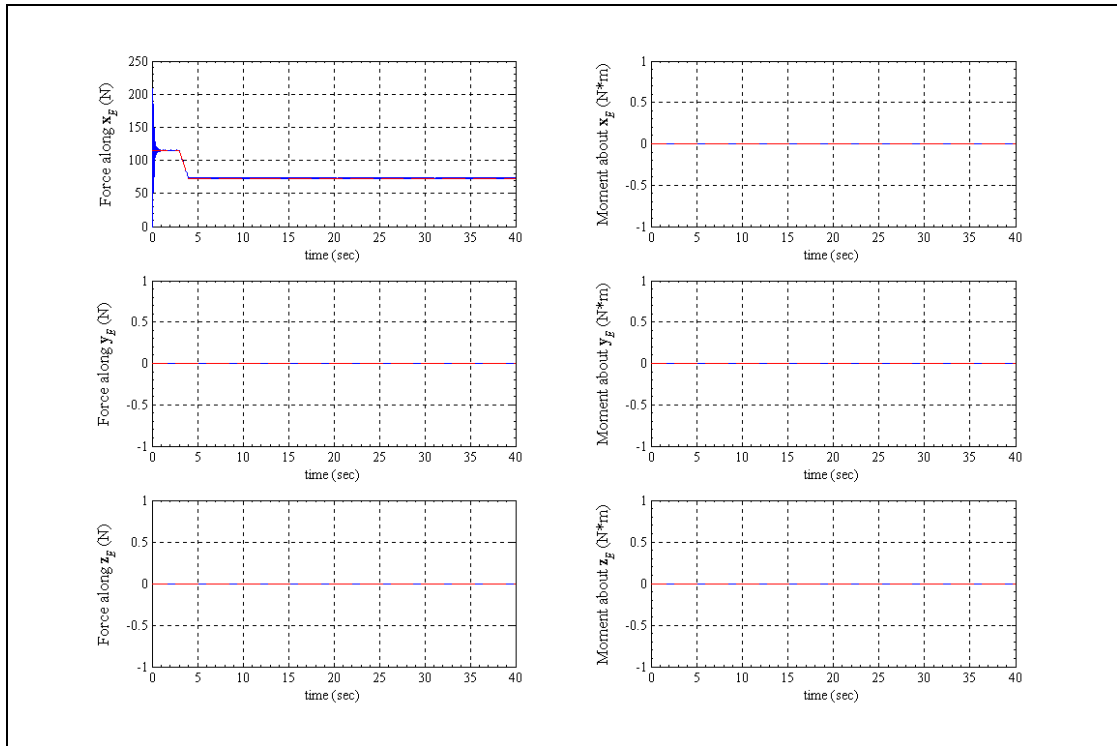


Fig. 5.35 Plots of the forces and moments acting on the MP as the Case 5 task is executed for the cable suspended parallel manipulator

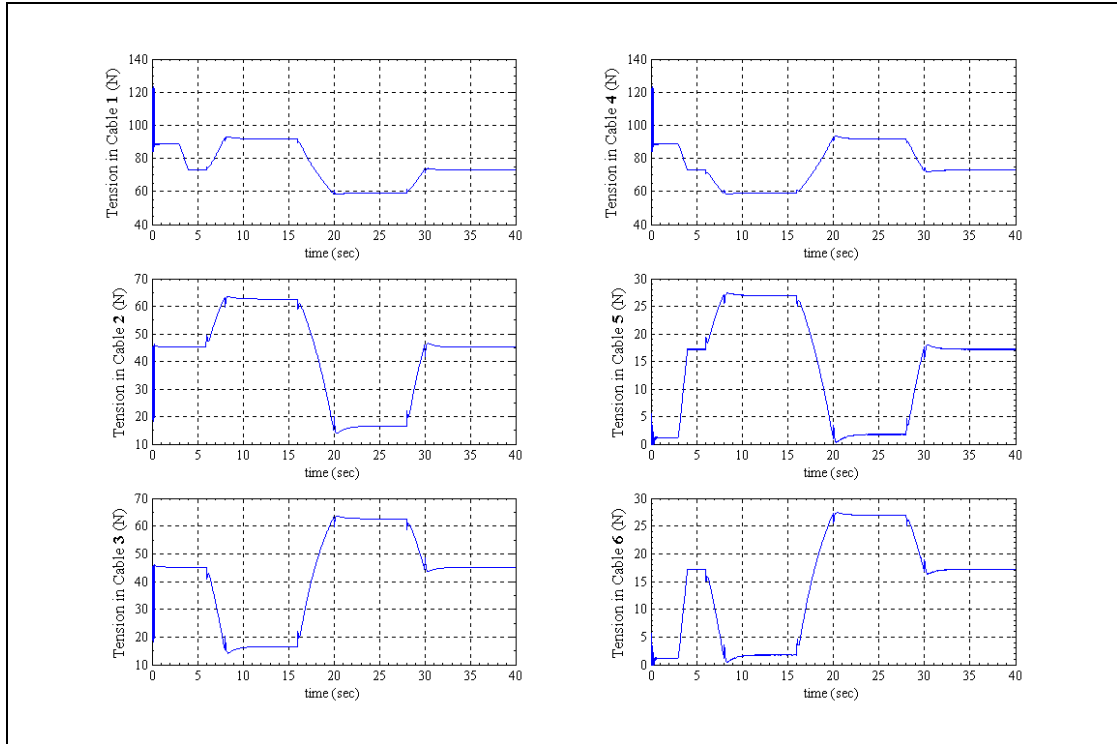


Fig. 5.36 Plots of the tensions experienced by each cable as the Case 5 task is executed for the cable suspended parallel manipulator

For this case, the task initially required negative pushing forces from actuators 5 and 6 for the traditional parallel robot. At this same time the cable suspended parallel robot enabled the decision making block and which found new positive tensions for the cables. The new tension values caused the MP to move slightly closer to the BP and orientation error. In study of the workspace volume for cable suspended parallel robots done in Chapter 3, it was found that the workspace volume slowly becomes ill conditioned when the MP is farther away from the BP along the z_o axis. The results suggested for this particular simulation tend to follow this trend. One last observation noted is that the force applied is relatively small

compared to the weight of the MP for the cable suspended parallel robot. The traditional parallel robot is able to apply as much force as its actuators allow.

5.6 Discussion and Analysis of Results

In each of the case simulations, the hybrid force/position controller was able to effectively control the parallel robot through the desired task. From the cases, several useful points were revealed. This section will give a general summary of the simulation results and present additional discussion on certain topics that were observed in extra simulations not presented. Since the traditional parallel robot can push and pull with its actuators, many of the comments discussed are directed towards the control of the cable suspended parallel robot. This section will also present some information and guidelines for future work and modifications.

Both parallel manipulators employed the hybrid force/position control law given in Eq. (5.42). This controller makes use of the control law partitioning method to compensate for the nonlinearities inherent within the system. The disadvantage of the control law partitioning method for an actual system is that the implementation can become computationally intensive. However, the speed and capacity of the computer is rapidly growing which makes this particular controller more attractive. The cable suspended parallel robot included an additional decision-making block used to ensure that the cable tensions never become slack. However, the new tensions that are suggested, even though they are positive, are not always practical. Some of the new tension signals for instance, may be extremely large or require high frequency pulsating tensions within the cables. In simulation, it was found that this sometimes resulted in larger error in the desired position and orientation of the MP and/or loss of the desired contact force or moment. In addition, the decision making block can be

computationally time consuming especially if the strict error tolerance is not relaxed. When the block did converge to a solution, after some time, the resulting solution presented interesting behavior. The decision-making block engaged when any one of the cables became slack. This occurred when the MP exceeded the workspace or stiffness map boundary. For these instances, it was found that the decision-making block converged to solutions that included orientations of the MP more suited for the needed task. Future work could include the search for algorithms that converge to a solution quicker.

For each trajectory task, the control gains are all fixed to the same value. For some cases, this revealed to be acceptable. However, if the strict gains on all the directions are not needed then lowering them to allow more variation may result in better performance and agility. It may be especially resourceful to consider allowing the orientation gains to be relaxed for the tasks where only forces are applied and the environmental moments acting on the MP are negligible. This is with the understanding that the rotational displacements are still kept as small as possible so that the applied force is not affected to drastically.

The cable suspended parallel robot is not able to exceed its workspace boundaries for a particular position and orientation of the MP except for unique situations where the dynamic motion of the MP is able to provide positive tensions for all the cables. When the cable suspended parallel robot is near the boundaries of its workspace, the control of the manipulator slowly begins to deteriorate, resulting in poor control behavior. The farther away the MP is from the BP along the z_0 axis the more ill conditioned the robot Jacobian becomes. This can be realized by observing the forces and moments acting on the MP at distances far from the BP. As the MP

increases its distance from the BP, the acute angle between the directional gravity vector and the cable vector diminishes. With this decrease in angle comes a decrease in potential stiffness. The limitations of the manipulator are observed by noting the points where the cables near zero tension. The task for Case 4 gives an example of the force capabilities of the cable suspended parallel robot as the MP translates to various altitudes along the z_0 axis and the remaining cases give different perspectives for the translational capabilities along the remaining two axes. The tasks given in each case are all executed at locations where the MP is fairly close to the BP.

The MP of the cable suspended parallel robot is restricted by the amount of forces it can apply or receive when interacting with the environment. Some of these restrictions as previously discussed are related to the workspace volume and the value of the conditioning index throughout the workspace. An additional restriction is governed by the weight of the MP. Increasing the weight of the MP of a cable suspended parallel robot will allow larger forces and moments to be applied within the workspace. This is because gravity acts as an additional actuator and provides the MP with an additional pushing force that typically assists the cables within its workspace. It is noted that the gravitational force is a body force providing this additional pushing force and acts only in one direction regardless of the task.

The workspace defined in Chapter 3 for the cable suspended parallel robot is a statically derived workspace. However, the dynamic effects of motion for any task influence the cable tensions even within the workspace. For instance, if the MP is to move from a point on the z_0 axis say, $z_0 = 10$ to a point $z_0 = 2$ instantaneously, then the desired abrupt stop at the second point may cause the cables to become slack if the rate of approach is not appropriately reduced first. Similarly, if the MP approaches

the surface too fast the impact could cause the cables to become slack and possibly send the MP erratically free flying in the air. Several problems result when the MP loses contact with the environment while remaining in force control mode. One problem is that the MP tends to travel erratically above the surface and in order to compensate the cable tensions are reduced as low as possible to allow the MP to resume the desired contact force with the environment. This usually results in a large impact to the environment that in turn sends MP drifting away again. Another problem is that when the MP is randomly traveling because of the undesirable impact the desired position trajectory is also influenced, usually resulting in large error. This is because the MP can only pull with the cables and not push. The only pushing force the MP possesses is the gravitational weight of the MP. Many of these problems are avoided using some level of switching control as briefly mentioned in a previous section. Consequently, when planning the task trajectory for a cable suspended parallel robot careful consideration must be taken to ensure that there are no sudden directional changes or undesirable impacts between the MP and the environment that cause the cables to loose tensions.

The traditional parallel robot is able to perform more complex force/moment and position/orientation trajectories than the cable suspended parallel robot with reasonable input force signals to the actuating links. Additional characteristics such as the stiffness and/or elasticity properties of the cables or traditional actuators were not included in the model of either parallel robot. These factors can influence the behavior of the controller especially when vibrations are present in the motion, which is often the case in the force-controlled directions. Several methods were found in the literature discussing various techniques applied to

reduce the initial vibrations generally found in force control tasks. Gradually applying the force on the environment helps to significantly reduce the initial vibrations between the MP and the environment. Other methods suggested to use passive attachments placed on the end effector so that when the manipulator interacts with the environment the attachment absorbs the impact shock from the stiff manipulator motion ([465], [479 - 480]).

5.7 Additional Comments

The tasks considered for each case are simplified so that the force and position control laws can be observed independently to ensure that they work. Future work may consider the addition of a switching mechanism allowing smooth transitions between the force and position control laws. In addition, all the cases included the interaction with a fixed environment. Future control laws may consider the interaction of the MP with objects that can move or are already in motion.

The end effector can guarantee to stay in contact with a stationary object by applying a constant force. This constant force depends on whether it is desired to keep the object at rest or to put it into motion. If it is preferred to keep the object at rest then the manipulator must apply a desired force larger than some sensitivity threshold force and smaller than the frictional forces acting on the object that keep it at rest. The sensitivity threshold force is the low-end force bound that the sensor is able to accurately read force signals. This bound may incorporate noise disturbances and/or physical limitations of the sensor due to its design. Now if the manipulator is to keep in contact with an object that is in motion then slightly more sophisticated controllers must be developed.

The hybrid force/position control law applied to the parallel robot actuated by traditional prismatic links revealed several interesting observations. If the environment encountered in the force controlled direction possessed low stiffness, i.e. was soft and compliant, then the force controller behaved fairly well. However, as the environmental stiffness increased the manipulator responded with high force vibrations at the surface in the force controller direction. It is better to have a force controller that has a compliant end effector in the direction of a stiff environment so that it can taper the intensity of the interaction through a suitable choice of a desired position. The actual implementation of the hybrid force/position controller would require additional modification to the control law to compensate for real world environmental interaction. Environmental parameters that will affect the controller behavior will be factors such as friction between the MP and the surface of contact and within the robot itself. The proposed hybrid position/force controller did not address the notion of friction be it within the system or resulting from the interaction with the environment. Some articles that discuss methods of identifying and estimating friction within systems are found in ([316 - 317], [437], [439 - 440], [442], [444]). Other articles presenting friction models are given in ([12], [438], [441], [443], [449 - 450], [481]), and articles that address the control of friction are presented in ([12], [43], [381], [437], [442 - 443], [445 - 450]). Other factors that could influence the control of the robot may be the deflection of the cables [318]. Incorporating flexible link models into the model-based portion of the control law may also increase the precision and accuracy of the cable suspended parallel robot. Additional research into the topics just mentioned and its implementation on the cable suspended parallel robot is left to another ambitious engineer.

5.8 Conclusion

This chapter presented the groundwork for the design of a hybrid force/position controller for a cable suspended parallel robot. The performance of the controller was evaluated through virtual simulations of various desired tasks. The tasks encompassed a variety of force and position trajectories. For each case, the moments experienced by the MP and the mass and inertia properties of the cable/traditional actuator are not modeled in the simulation. Therefore, small discrepancies in the results are to be expected when compared to a real world environment, however, for a preliminary study, this is acceptable. Overall, the hybrid force/position controller successfully controlled the parallel manipulator and with the decision making block, the cable suspended parallel robot was able to ensure positive tensions for all the cables throughout the desired task. In addition, the basis for the application of the hybrid force/position controller on a cable suspended parallel robot is given as well as tips for future modifications and implementation in a real world environment.

Chapter 6

CONCLUSION

6.1 Summary

A cable suspended parallel robot exploits the fundamental idea of the traditional Stewart-Gough platform. The traditional parallel manipulator commonly uses hydraulic or pneumatic pistons, or lead screws for its input actuators that are able to push and pull with its MP. The cable suspended parallel manipulator replaces these traditional actuators with cable actuators. The cables can be physically actuated with a simple winch system. Cables are only capable of supplying pulling tension forces but no pushing compressive forces. The attractive features related to the use of cables, as opposed to traditional actuators, are that cables have a large strength to weight ratio, are lightweight and can reasonably reach large distances far away from the BP along the z_0 axis. Since cables can only pull and not push, the existing theory on parallel robots is slightly modified to incorporate the additional characteristic pertaining to the cables. The current work includes some existing theory on cable-actuated robots and parallel manipulators to form additional ideas about the workspace, design, and control of a 6-degree-of-freedom cable suspended parallel robot.

The author designed a cable suspended parallel robot at the University of Delaware Robotics and Control Laboratory. The MP is connected to the BP by six steel wire cables actuated by a direct drive winch system. Every cable contains an

inline tension sensor used to feedback the force within each cable to the controller. The BP is equipped with an adjustable lead screw system that changes the radial cable connection points, r_{base} , to dimensions that are larger or smaller than the MP radius, r_{end} . To increase the workspace of the robot the BP is rigidly fastened to a two-dimensional gantry system.

This thesis investigated several different topics related to the workspace, design and control of the cable suspended parallel robot. A number of useful trends resulted from the workspace analysis of twelve different cable robot designs. These trends were then verified in practical design applications and deemed valuable tools of reference. The preliminary analysis of a hybrid force/position controller for a cable suspended parallel robot was then derived. Several successful simulated tasks proved the controller worked and gave additional insight to future modifications.

6.2 Future Work

For future research, the rotation angles ψ about the \mathbf{x}_O axis and θ about the \mathbf{y}_O axis could be increased to incorporate angles greater than $\pm 30^\circ$ possibly up to $\pm 90^\circ$. The step size taken for the angles considered were at 10° increments for the workspace analysis. The discrete step size chosen was relatively large for the set of orientations; however, the results portrayed by the data appeared to still reveal acceptable and useful results. The reduction of this step size should again be included in future studies. Similarly, the translational step size along the \mathbf{x}_O , \mathbf{y}_O , \mathbf{z}_O axis was set to 0.4 units. The reduction of this would help in better defining the shape of the workspace for the constant orientation or translational workspace study as well as providing a more accurate GCI value. The range of search region for each robot considered was fixed to a set volume to ensure consistency. The search region limits

placed on the x_O and y_O axes appeared to be selected generously, however, the behavior of the MP for the set of parameters at large distances along the z_O axis were only briefly considered. Future analysis could incorporate the behavior of the MP at these large distances for completeness.

The robotic designs included four different geometric γ angles used to define the shape of both the MP and BP and, for each γ value, three different ratios of the MP to BP were chosen. The mismatching of the MP and BP γ values for different ratios was not considered in the present work and can be considered to add another level of complexity to workspace analysis.

The work pertaining to the hybrid force/position controller could be extended to include a more sophisticated and realistic virtual environment and robot model. The robotic model chosen did not take into account the stiffness, inertia or mass properties of the cables and the environment was greatly simplified. An enhanced simulation model may be possible with the assistance of supplementary software that is further advanced and better suited for this type of computational complexity such as SolidWorks. Nevertheless, the simulation revealed very interesting and useful results for a preliminary model. The future work could investigate the refinement of the decision making block to one which is computationally more efficient and include a switching scheme that allows the hybrid force/position controller to smoothly transition between the force and position control laws. In addition, the simulation results showed that the dynamic effects have a large influence on the tasks even when the desired trajectories were within the workspace. To further extend the research, the future work should include a comprehensive study of the dynamic workspace of the cable suspended parallel robot.

The hybrid force/position controller was not implemented on the current University of Delaware Cable Suspended Parallel Robot because of some problems with accuracy. The position control scheme presently used on the robot implements a discrete numerical approximation in order to compute the forward kinematic motion of the MP. As a result, error accumulates as the run time increases, naturally affecting the performance of the robot. The computer that controls the robot is not fast enough to accurately compute a small enough step size. One method sought to correct this problem includes the addition of three extra cables used solely as a displacement sensor that will allow a closed form solution as previously mentioned in Chapter 2. Other improvements presently under consideration include upgrading the winding mechanisms and adding different attachments to the MP.

Appendix A: Plots of Workspace Volume

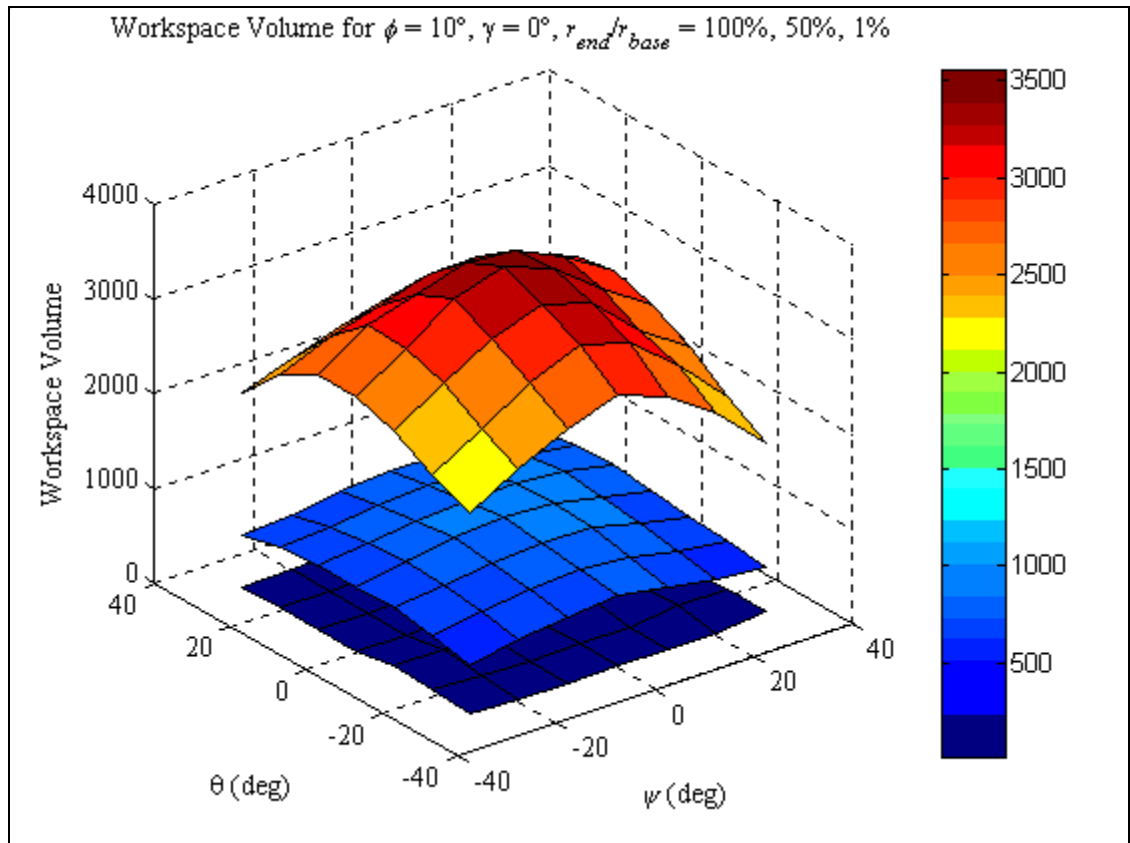


Fig. 3.4a Workspace Volume for $\gamma = 0^\circ$, $(r_{end}/r_{base}) = 100\%$, 50% , 1% and $\phi = 10^\circ$

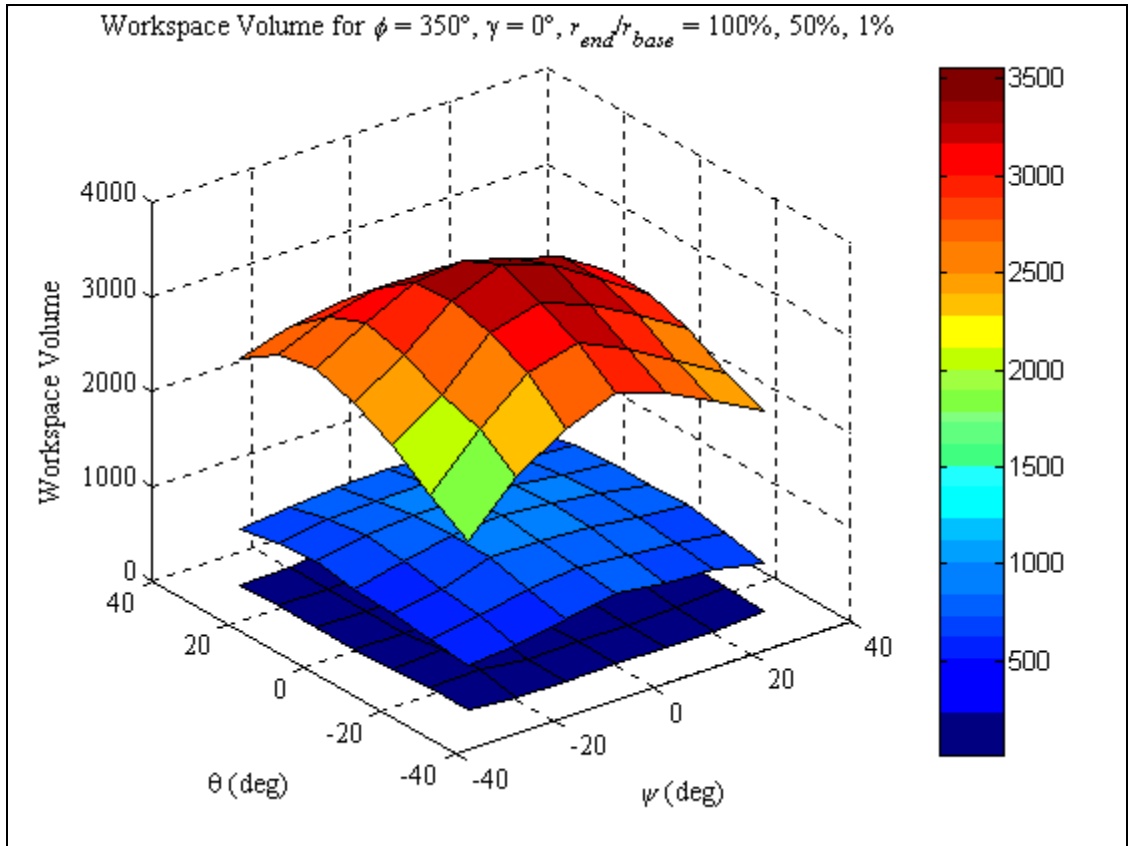


Fig. 3.4b Workspace Volume for $\gamma = 0^\circ$, $(r_{end}/r_{base}) = 100\%$, 50% , 1% and $\phi = 350^\circ$

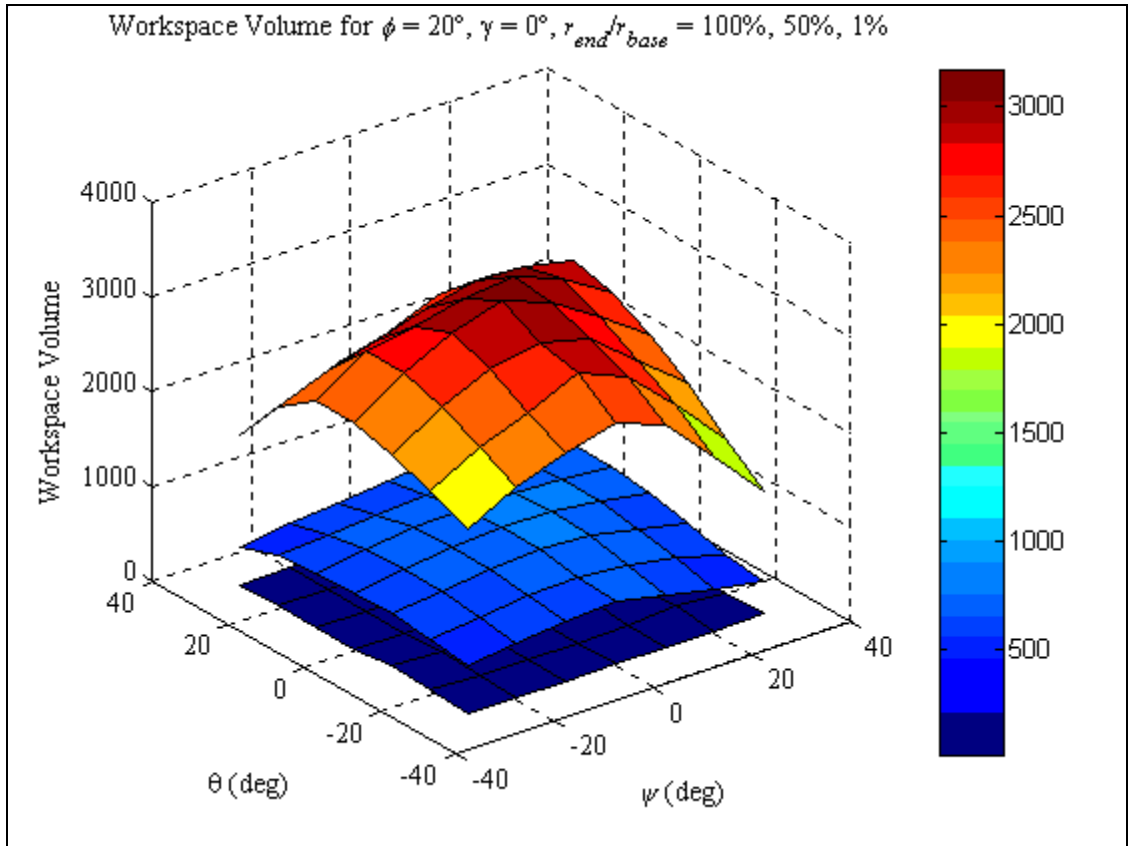


Fig. 3.4c Workspace Volume for $\gamma = 0^\circ, (r_{end}/r_{base}) = 100\%, 50\%, 1\%$ and $\phi = 20^\circ$

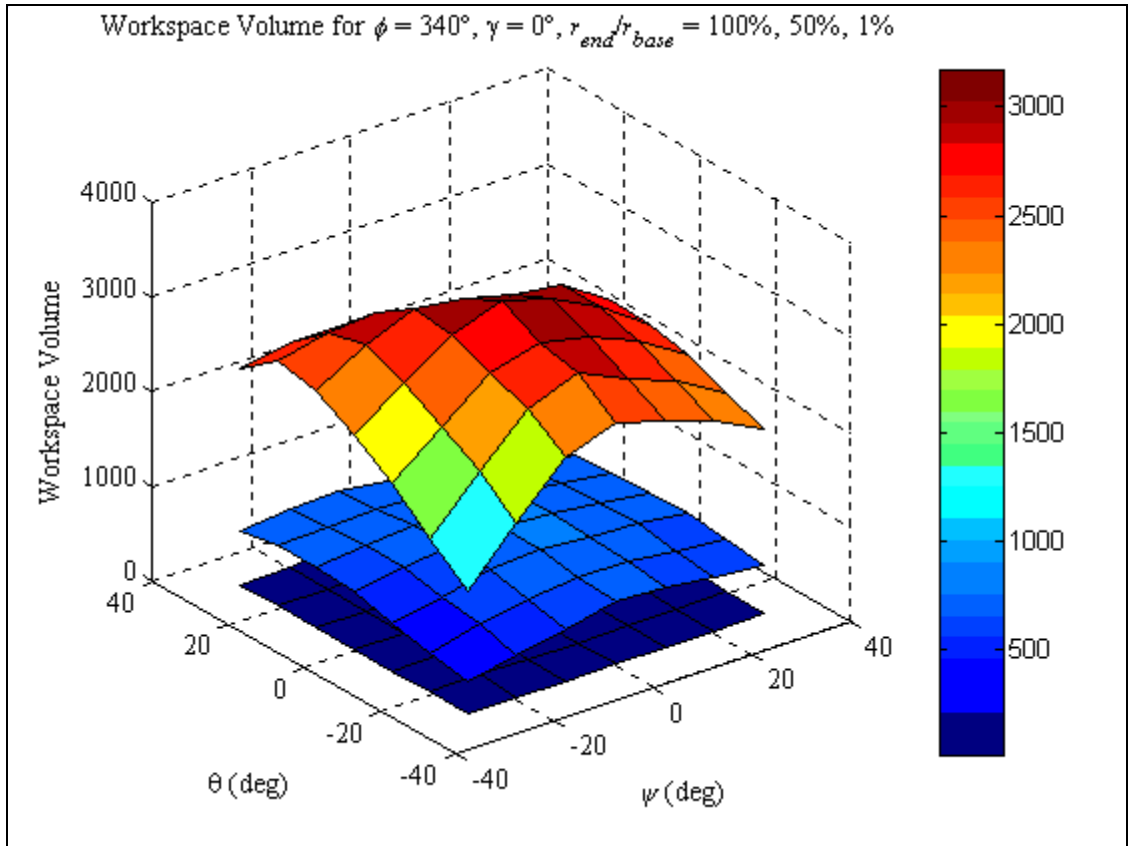


Fig. 3.4d Workspace Volume for $\gamma = 0^\circ$, $(r_{end}/r_{base}) = 100\%$, 50% , 1% and $\phi = 340^\circ$

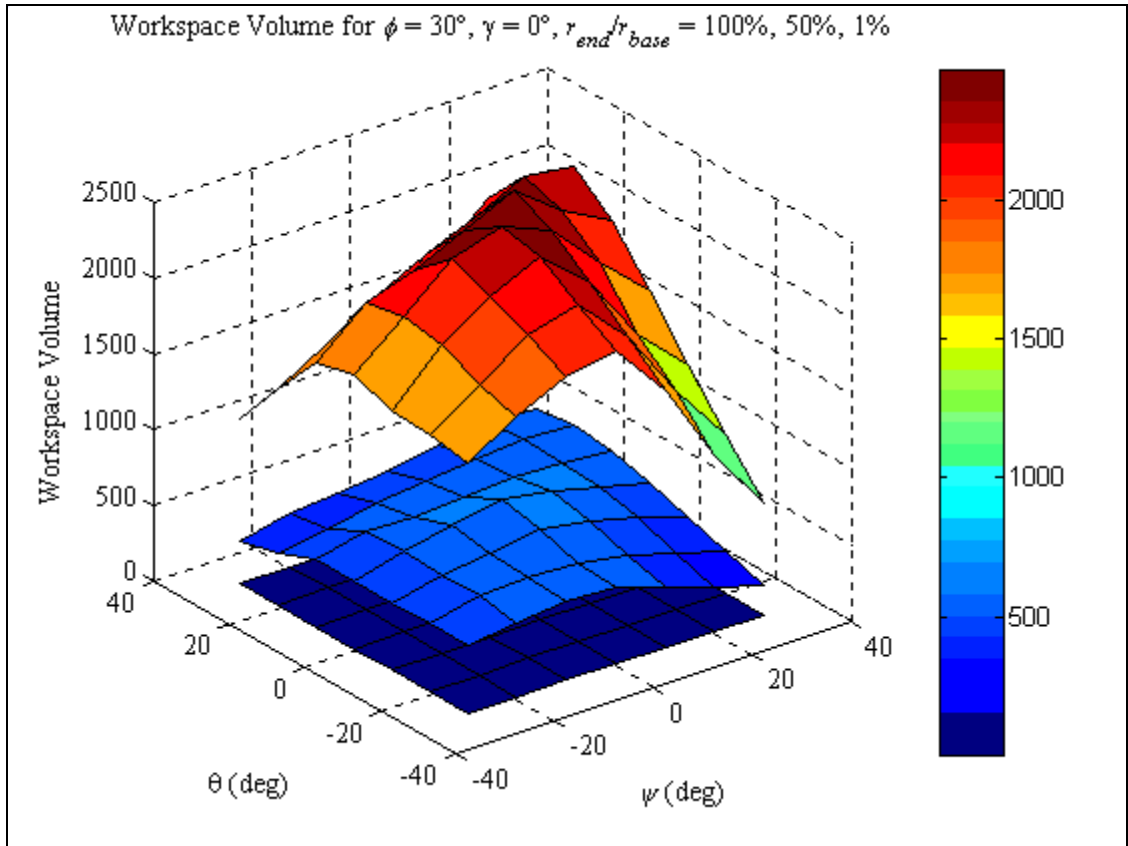


Fig. 3.4e Workspace Volume for $\gamma = 0^\circ$, $(r_{end}/r_{base}) = 100\%$, 50% , 1% and $\phi = 30^\circ$

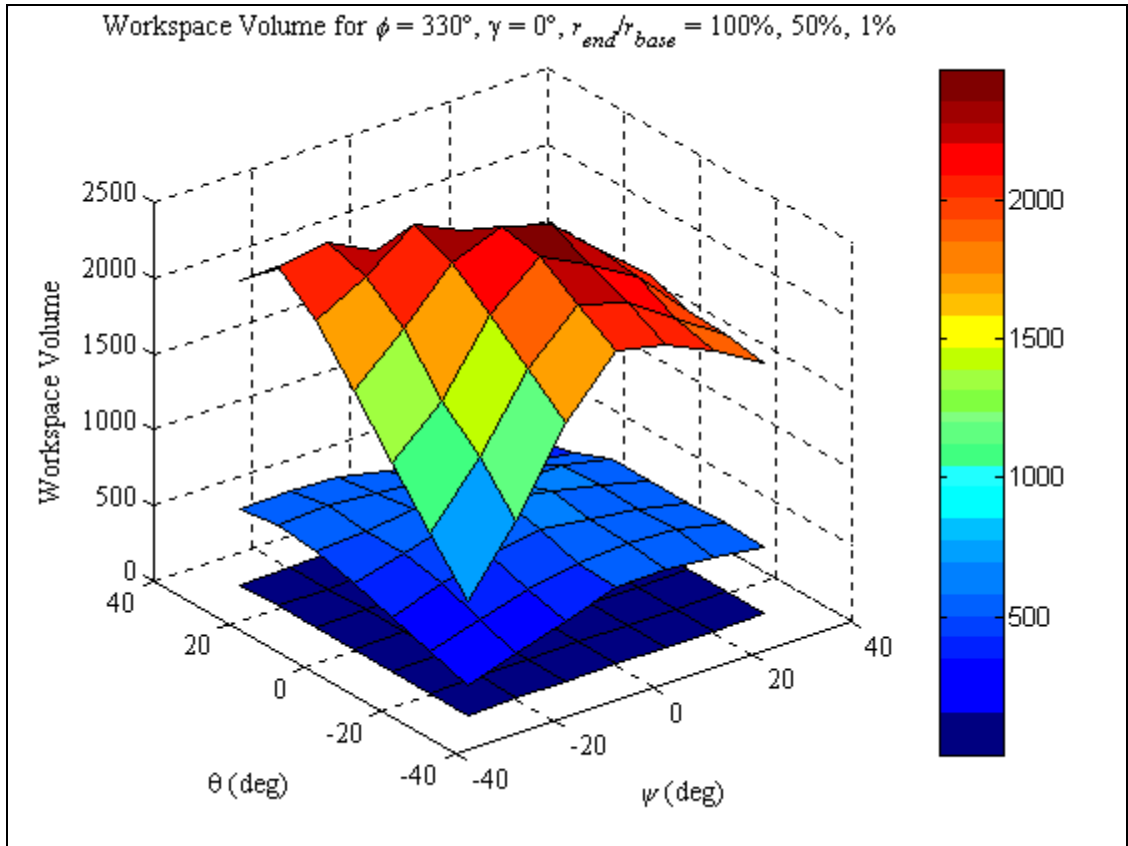


Fig. 3.4f Workspace Volume for $\gamma = 0^\circ$, $(r_{end}/r_{base}) = 100\%$, 50% , 1% and $\phi = 330^\circ$

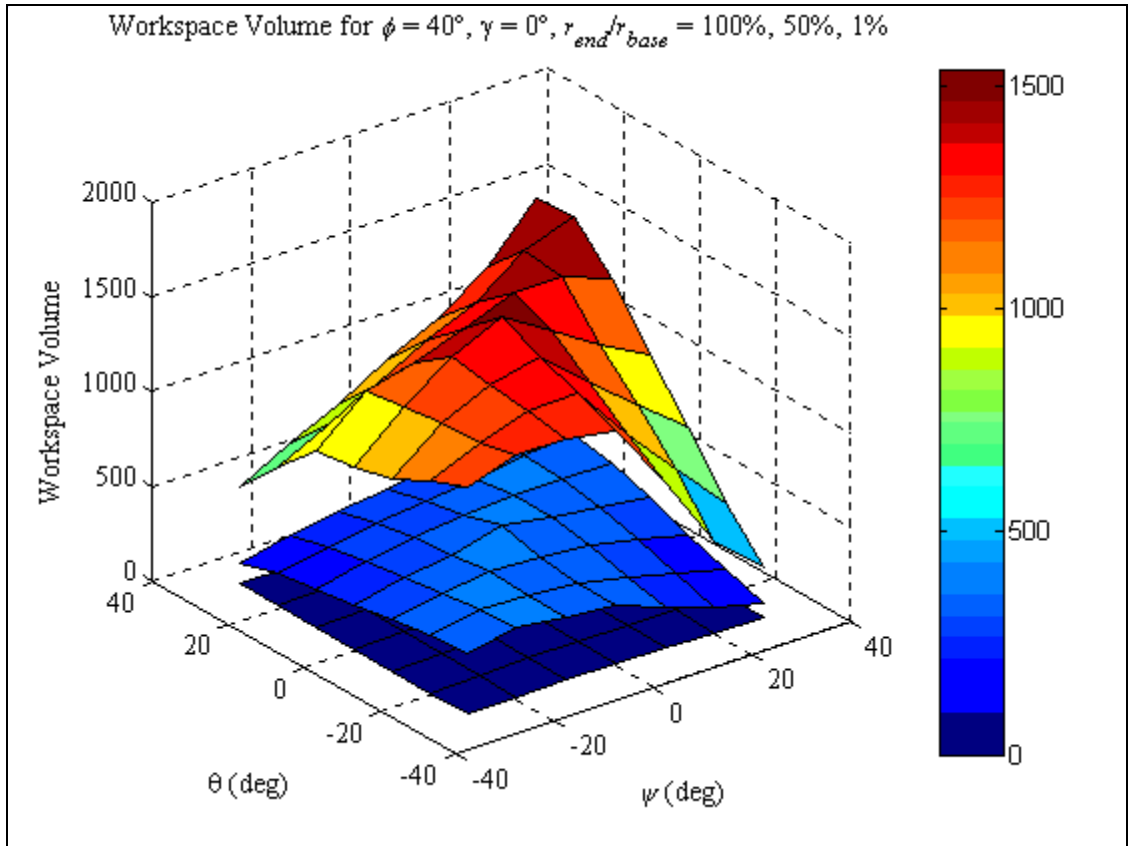


Fig. 3.4g Workspace Volume for $\gamma = 0^\circ, (r_{end}/r_{base}) = 100\%, 50\%, 1\%$ and $\phi = 40^\circ$

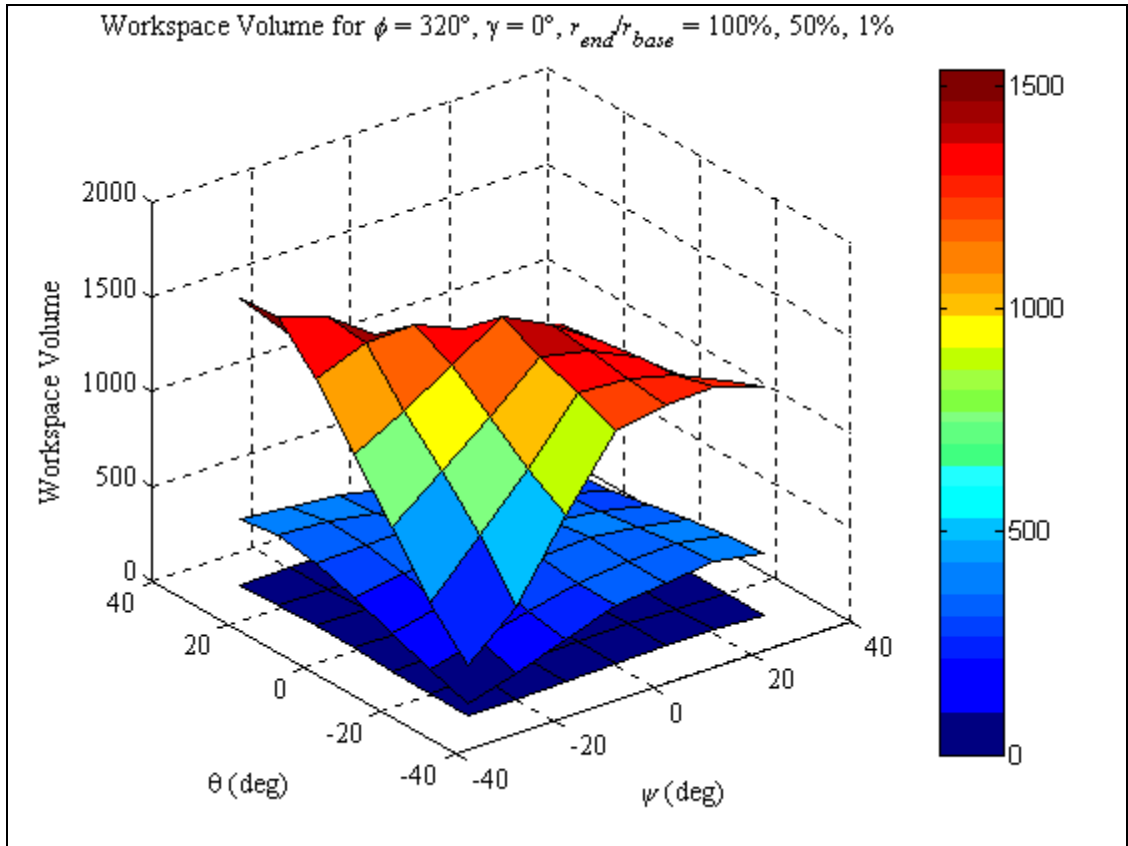


Fig. 3.4h Workspace Volume for $\gamma = 0^\circ$, $(r_{end}/r_{base}) = 100\%$, 50% , 1% and $\phi = 320^\circ$

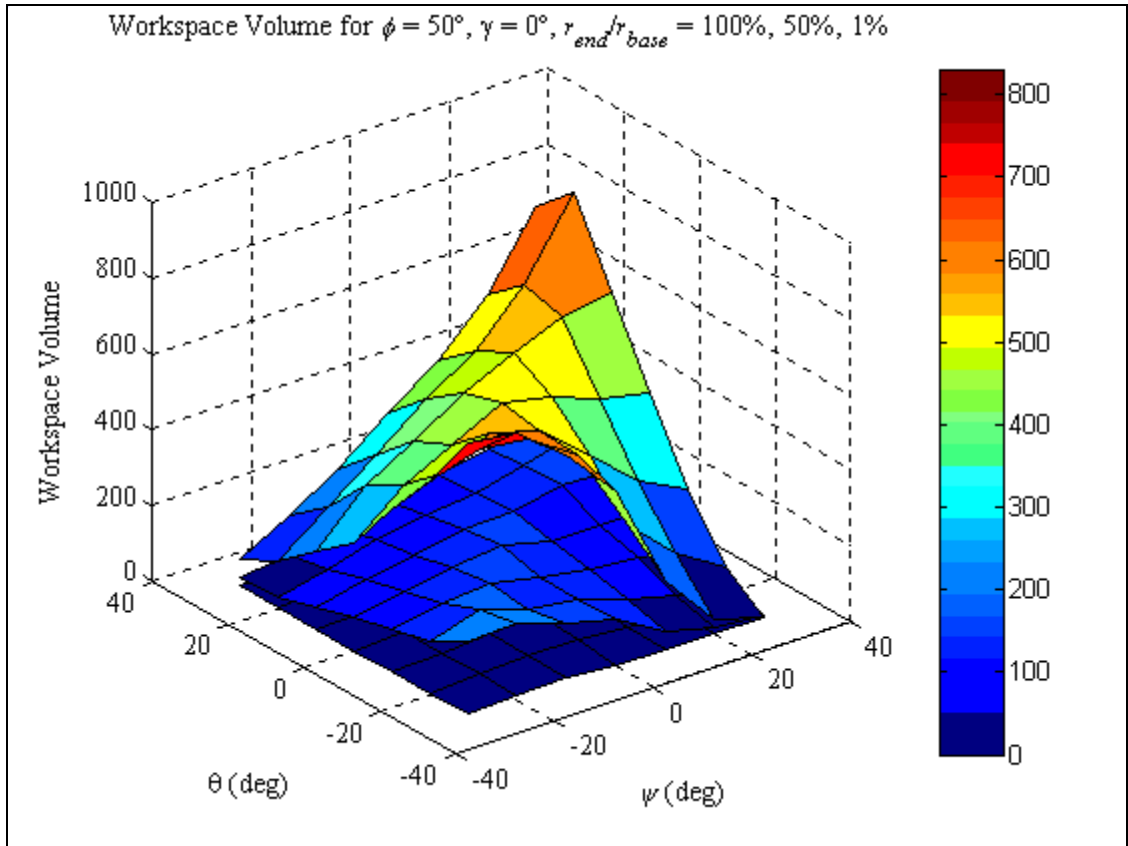


Fig. 3.4i Workspace Volume for $\gamma = 0^\circ, (r_{end}/r_{base}) = 100\%, 50\%, 1\%$ and $\phi = 50^\circ$

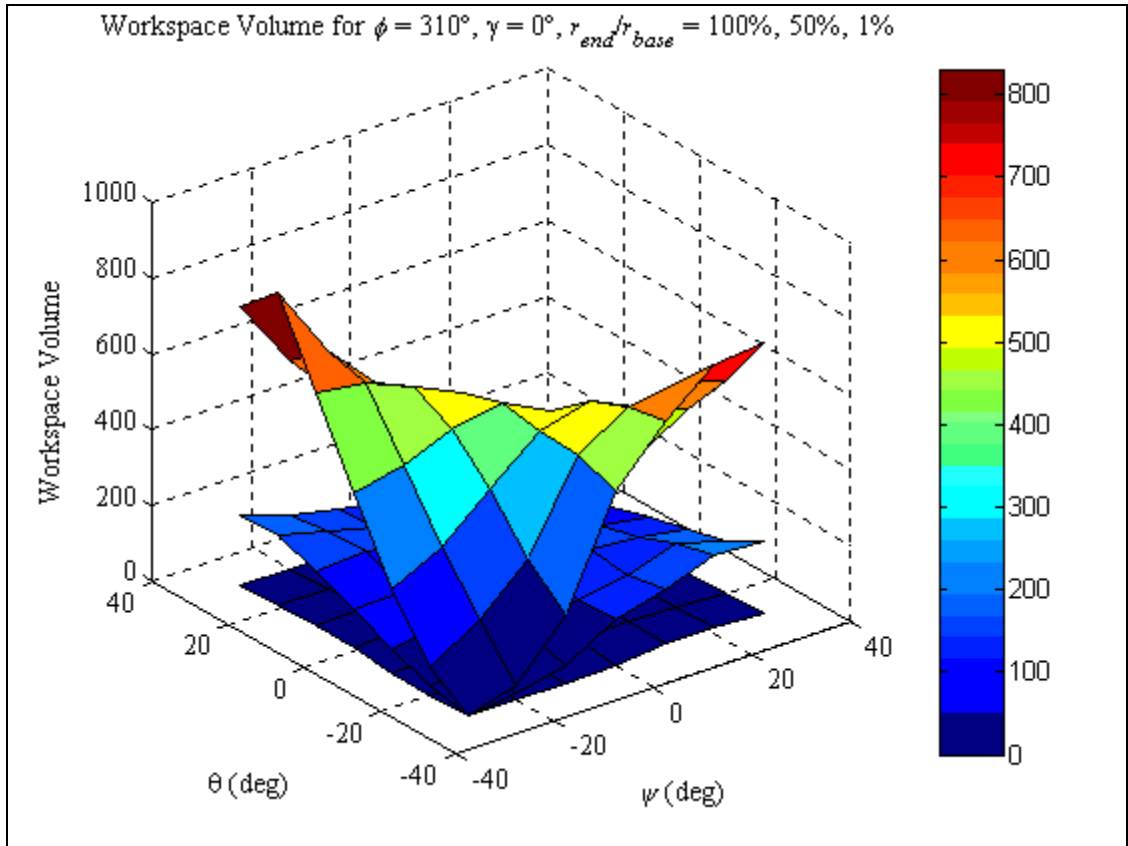


Fig. 3.4j Workspace Volume for $\gamma = 0^\circ$, $(r_{end}/r_{base}) = 100\%$, 50% , 1% and $\phi = 310^\circ$

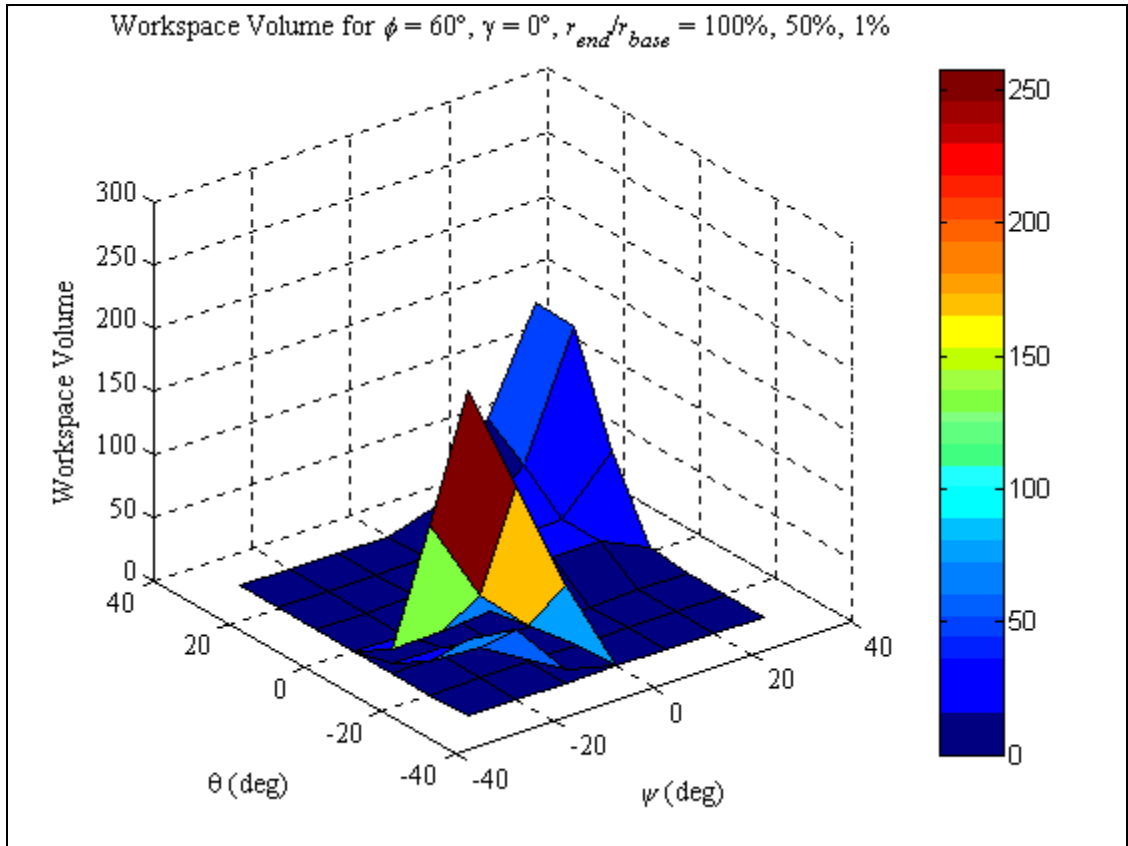


Fig. 3.4k Workspace Volume for $\gamma = 0^\circ$, $(r_{end}/r_{base}) = 100\%$, 50% , 1% and $\phi = 60^\circ$

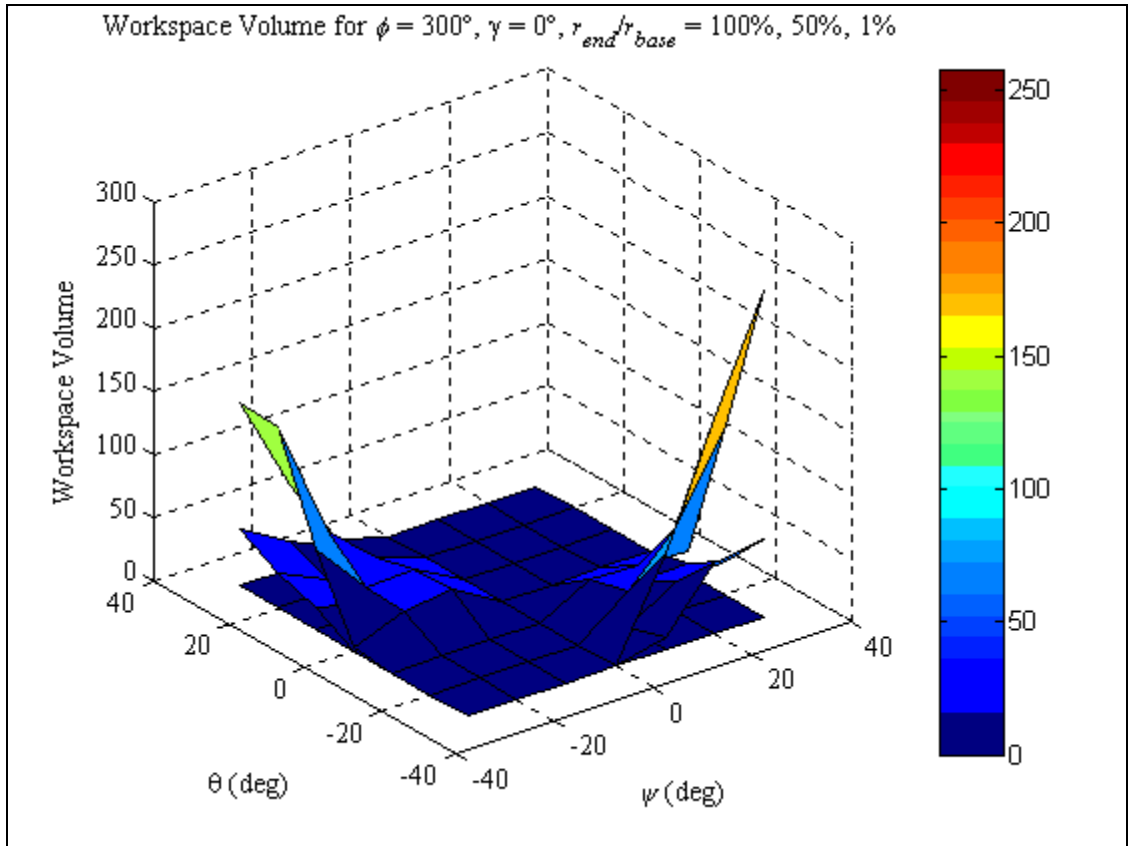


Fig. 3.4l Workspace Volume for $\gamma = 0^\circ$, $(r_{end}/r_{base}) = 100\%$, 50% , 1% and $\phi = 300^\circ$

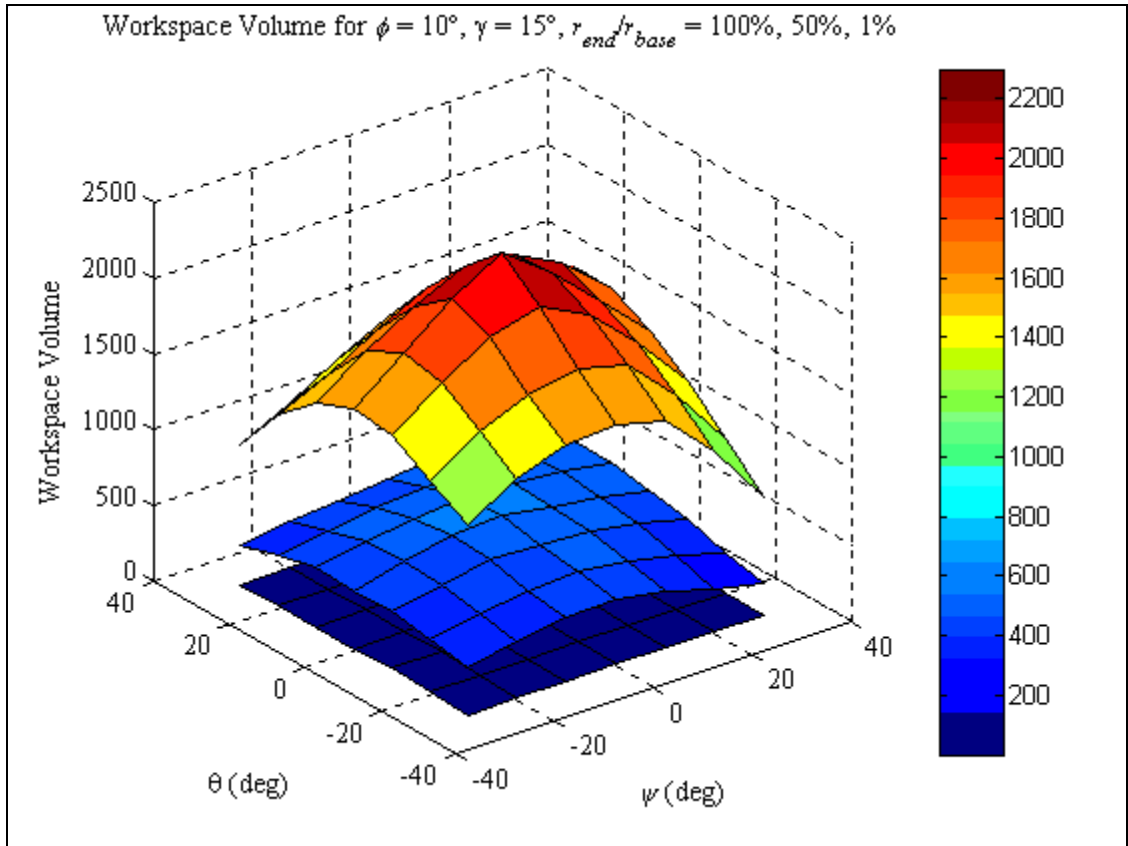


Fig. 3.5a Workspace Volume for $\gamma = 15^\circ$, $(r_{end}/r_{base}) = 100\%$, 50% , 1% and $\phi = 10^\circ$

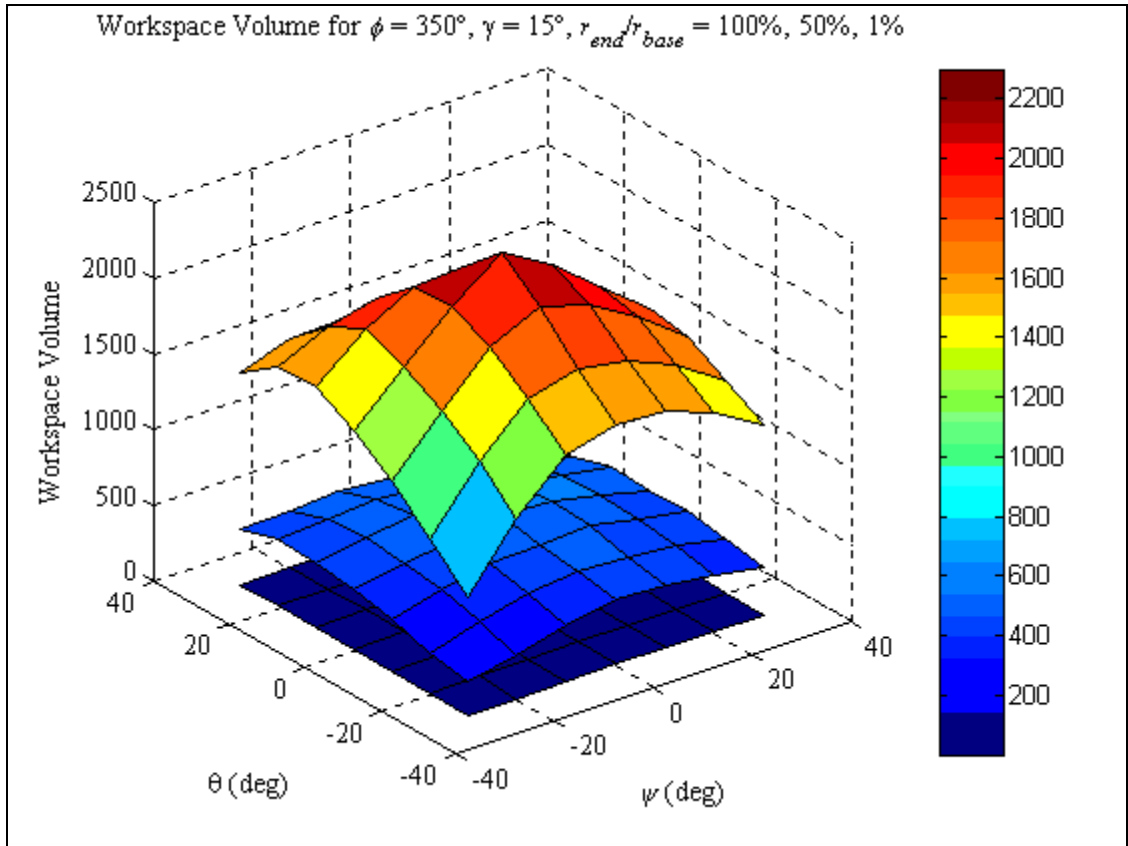


Fig. 3.5b Workspace Volume for $\gamma = 15^\circ$, $(r_{end}/r_{base}) = 100\%$, 50% , 1% and $\phi = 350^\circ$

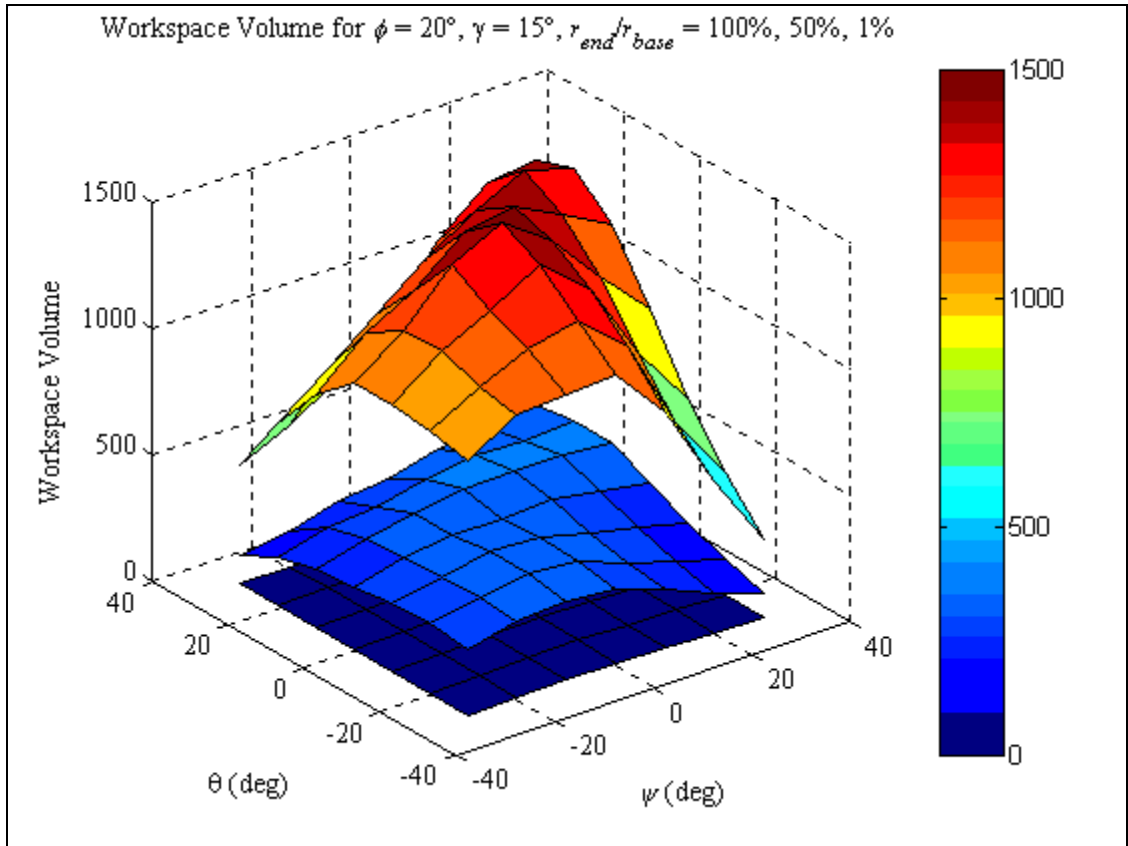


Fig. 3.5c Workspace Volume for $\gamma = 15^\circ$, $(r_{end}/r_{base}) = 100\%, 50\%, 1\%$ and $\phi = 20^\circ$

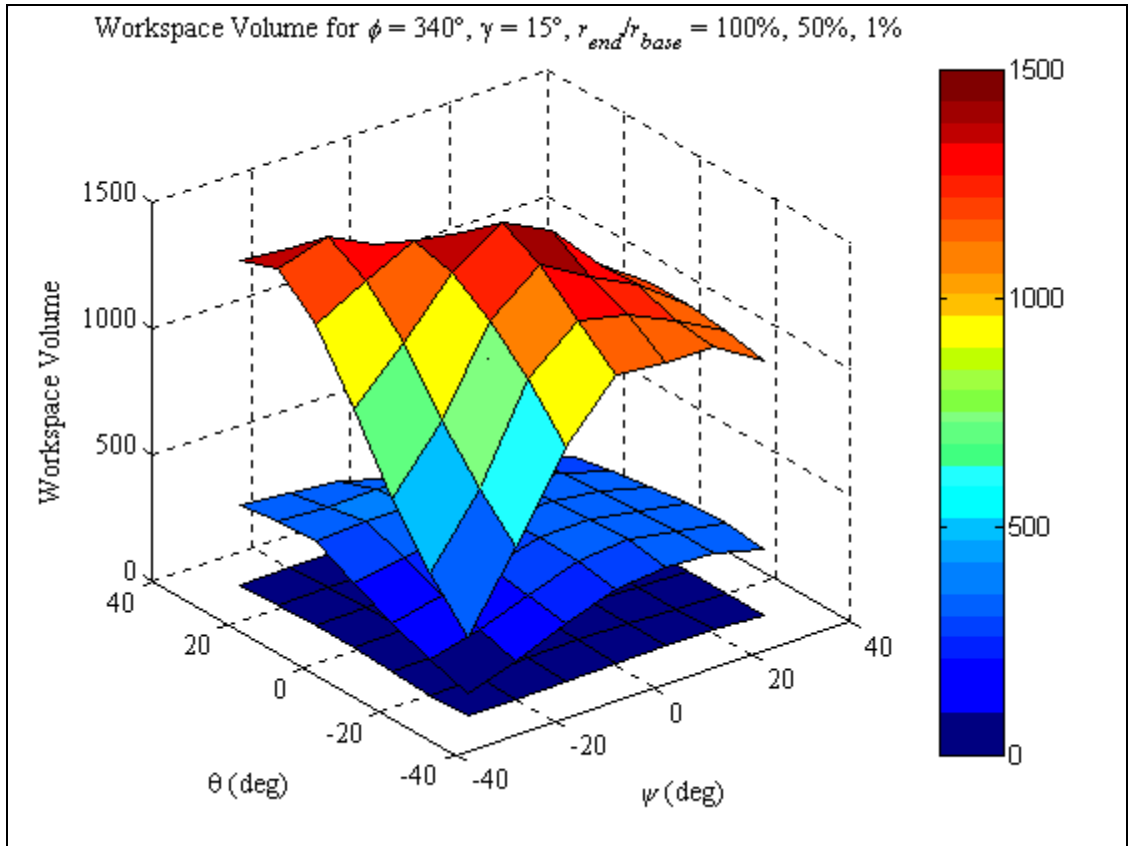


Fig. 3.5d Workspace Volume for $\gamma = 15^\circ$, $(r_{end}/r_{base}) = 100\%, 50\%, 1\%$ and $\phi = 340^\circ$

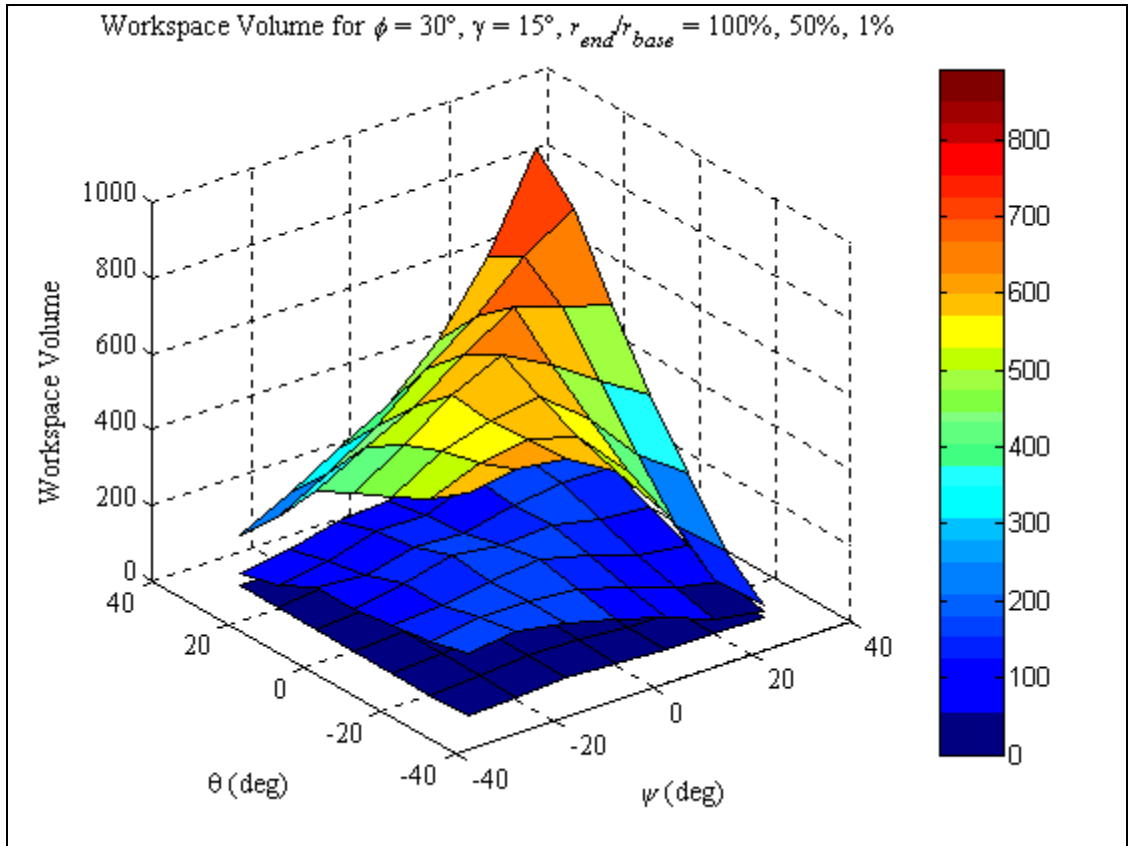


Fig. 3.5e Workspace Volume for $\gamma = 15^\circ$, $(r_{end}/r_{base}) = 100\%, 50\%, 1\%$ and $\phi = 30^\circ$

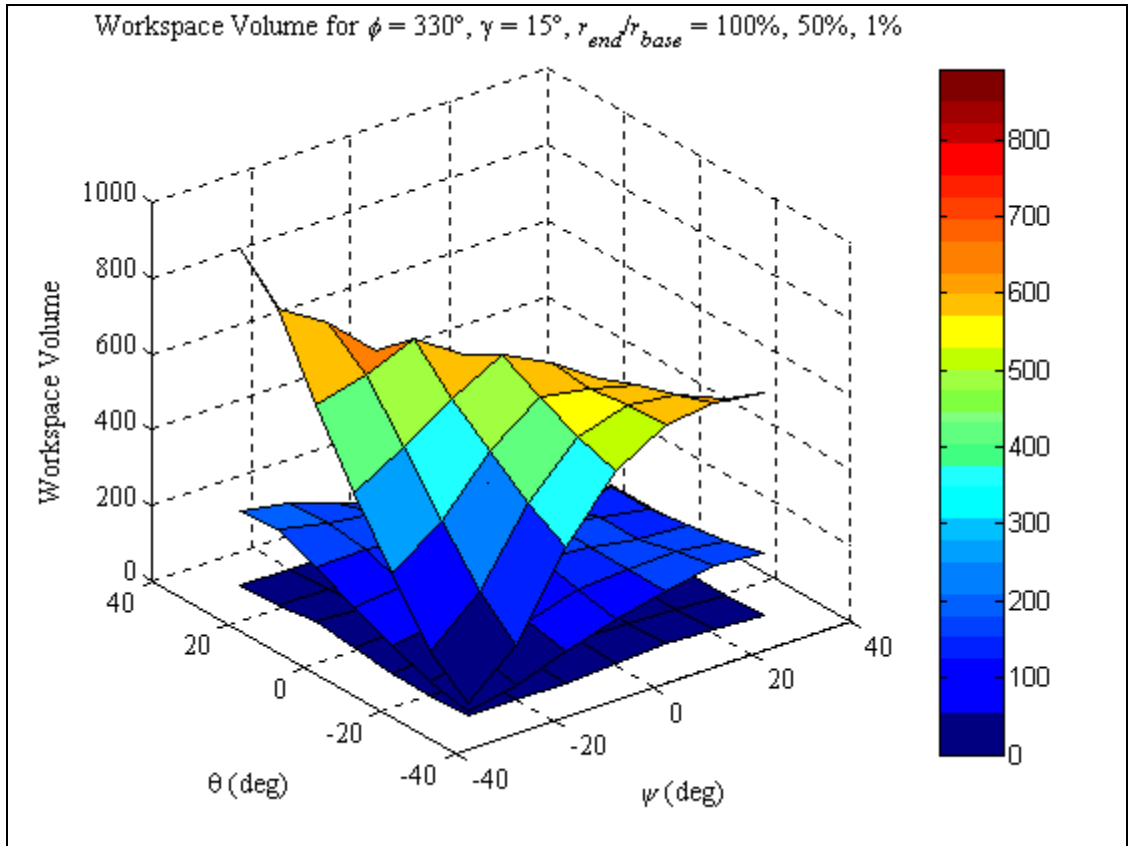


Fig. 3.5f Workspace Volume for $\gamma = 15^\circ, (r_{end}/r_{base}) = 100\%, 50\%, 1\%$ and $\phi = 330^\circ$

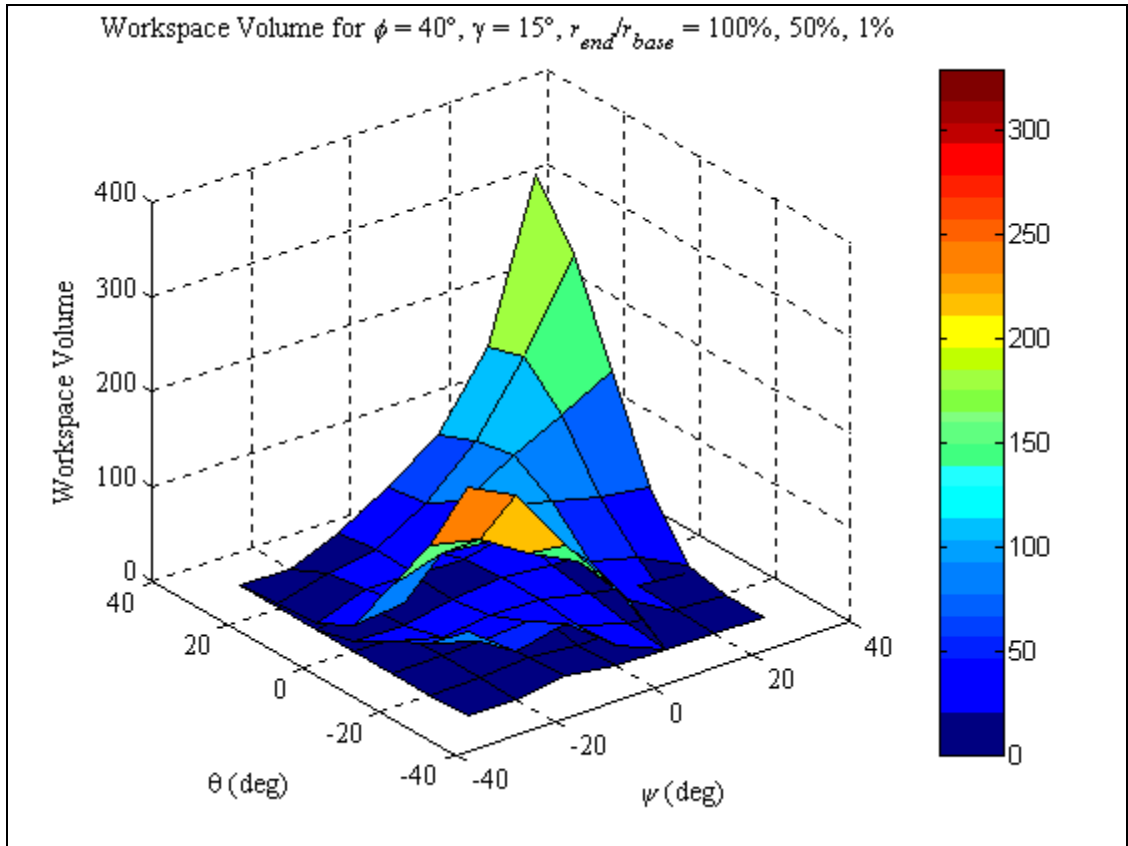


Fig. 3.5g Workspace Volume for $\gamma = 15^\circ$, $(r_{end}/r_{base}) = 100\%$, 50% , 1% and $\phi = 40^\circ$

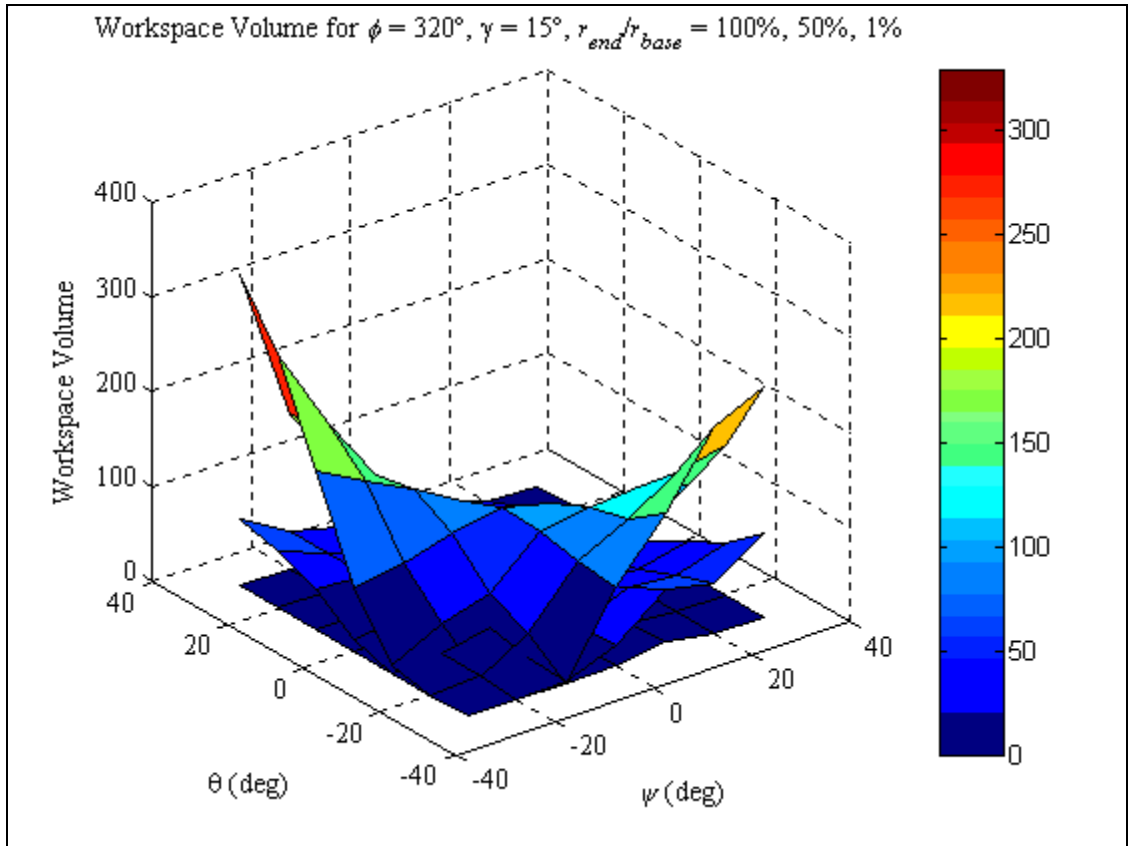


Fig. 3.5h Workspace Volume for $\gamma = 15^\circ$, $(r_{end}/r_{base}) = 100\%, 50\%, 1\%$ and $\phi = 320^\circ$

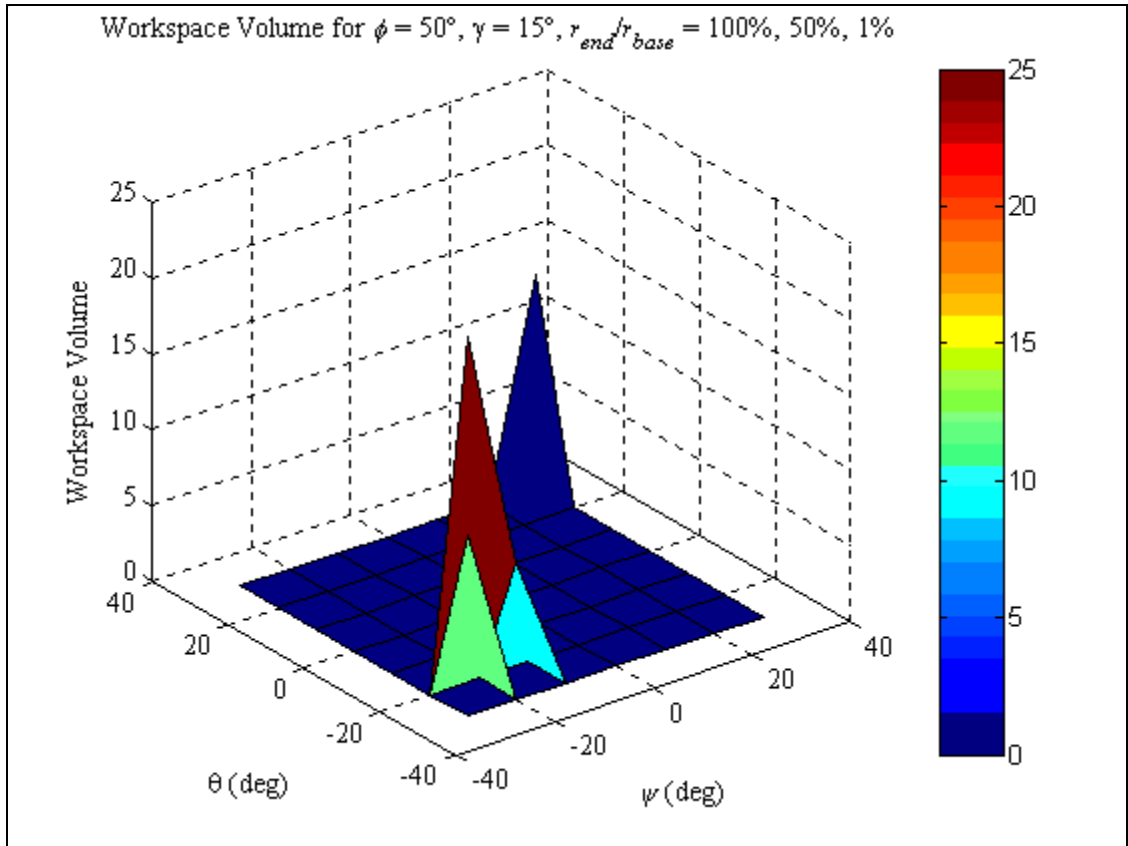


Fig. 3.5i Workspace Volume for $\gamma = 15^\circ$, $(r_{end}/r_{base}) = 100\%$, 50% , 1% and $\phi = 50^\circ$

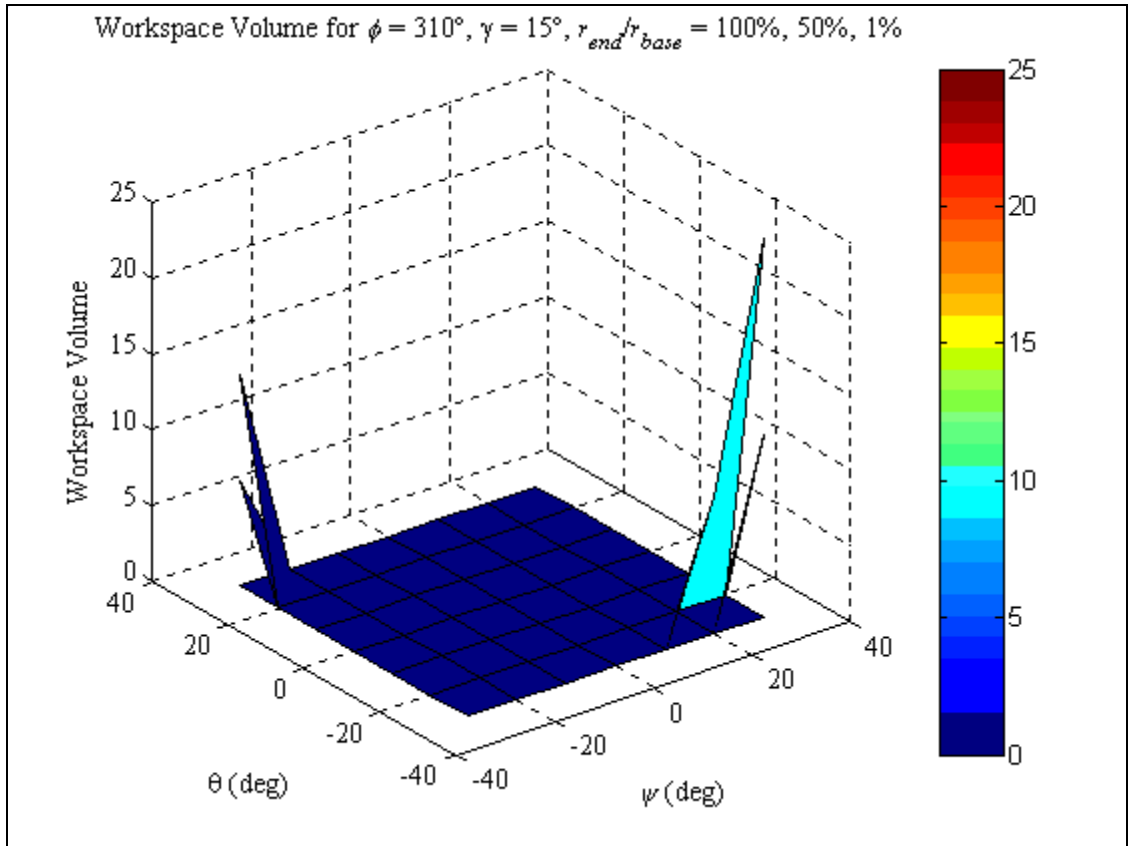


Fig. 3.5j Workspace Volume for $\gamma = 15^\circ$, $(r_{end}/r_{base}) = 100\%, 50\%, 1\%$ and $\phi = 310^\circ$

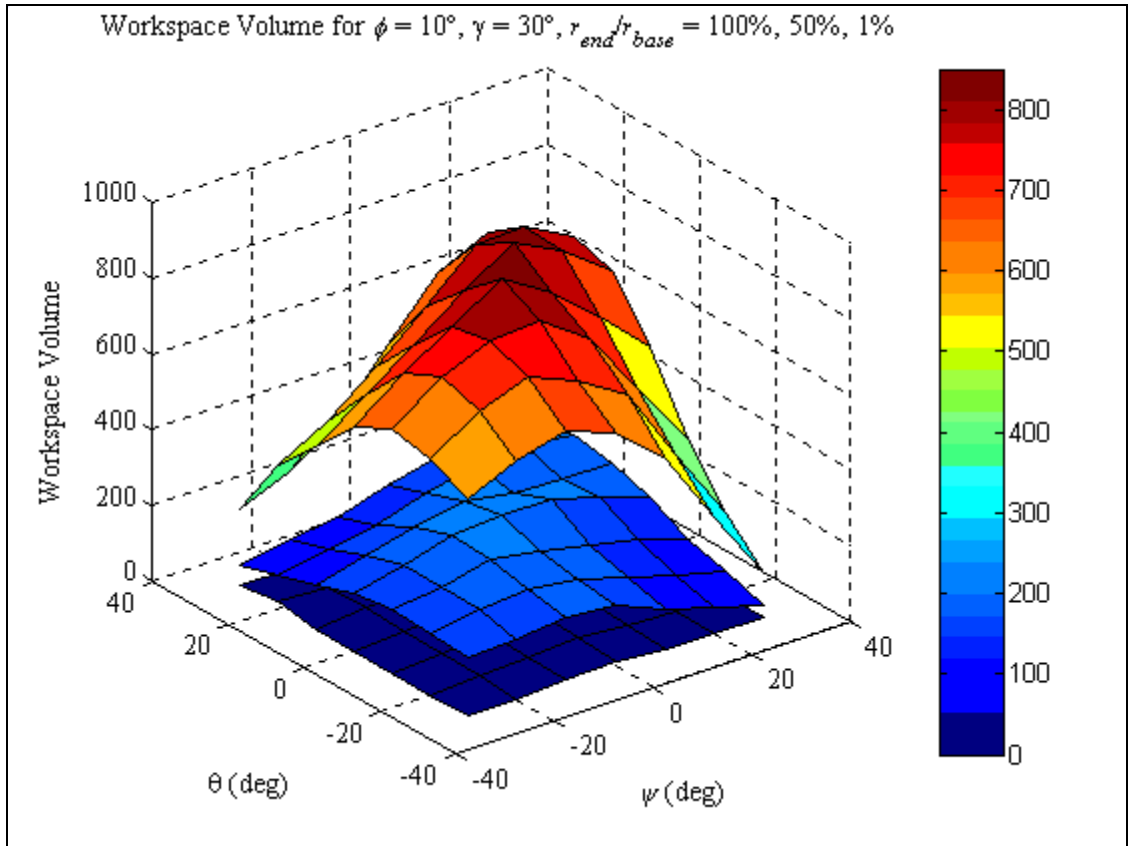


Fig. 3.6a Workspace Volume for $\gamma = 30^\circ$, $(r_{end}/r_{base}) = 100\%, 50\%, 1\%$ and $\phi = 10^\circ$

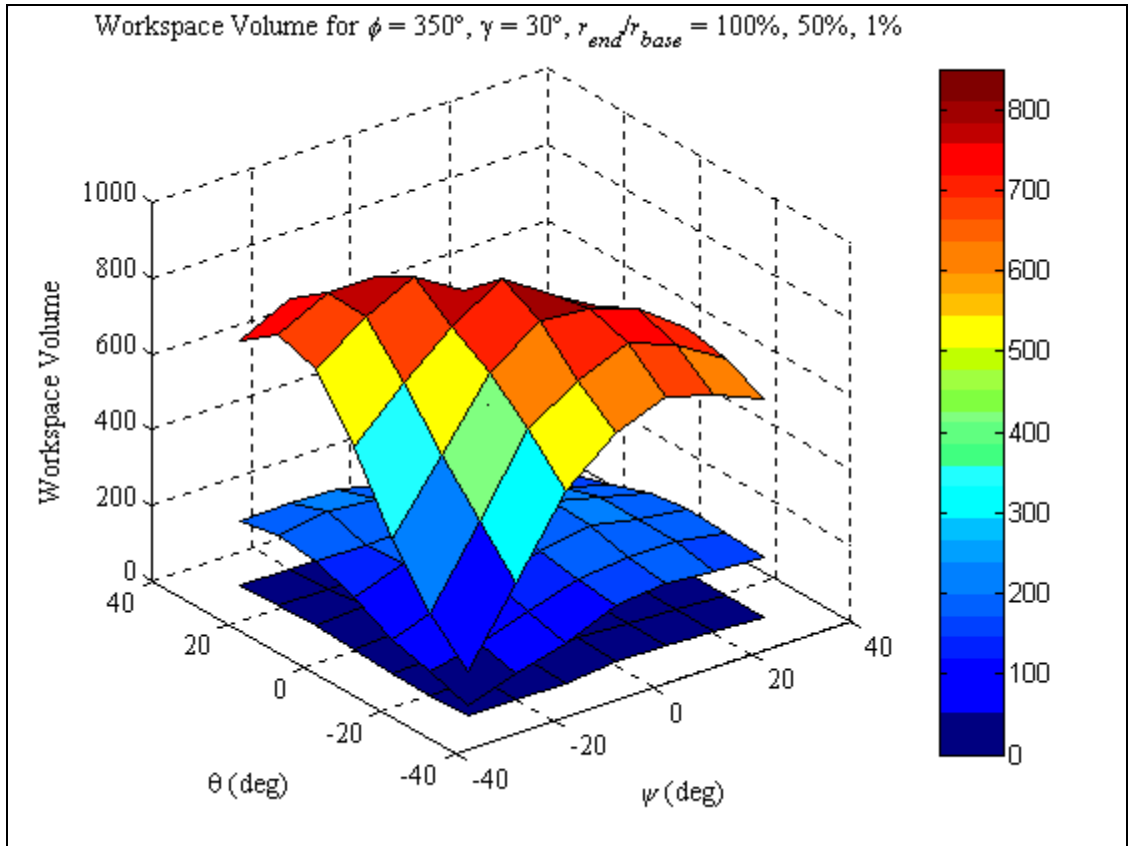


Fig. 3.6b Workspace Volume for $\gamma = 30^\circ$, $(r_{end}/r_{base}) = 100\%$, 50% , 1% and $\phi = 350^\circ$

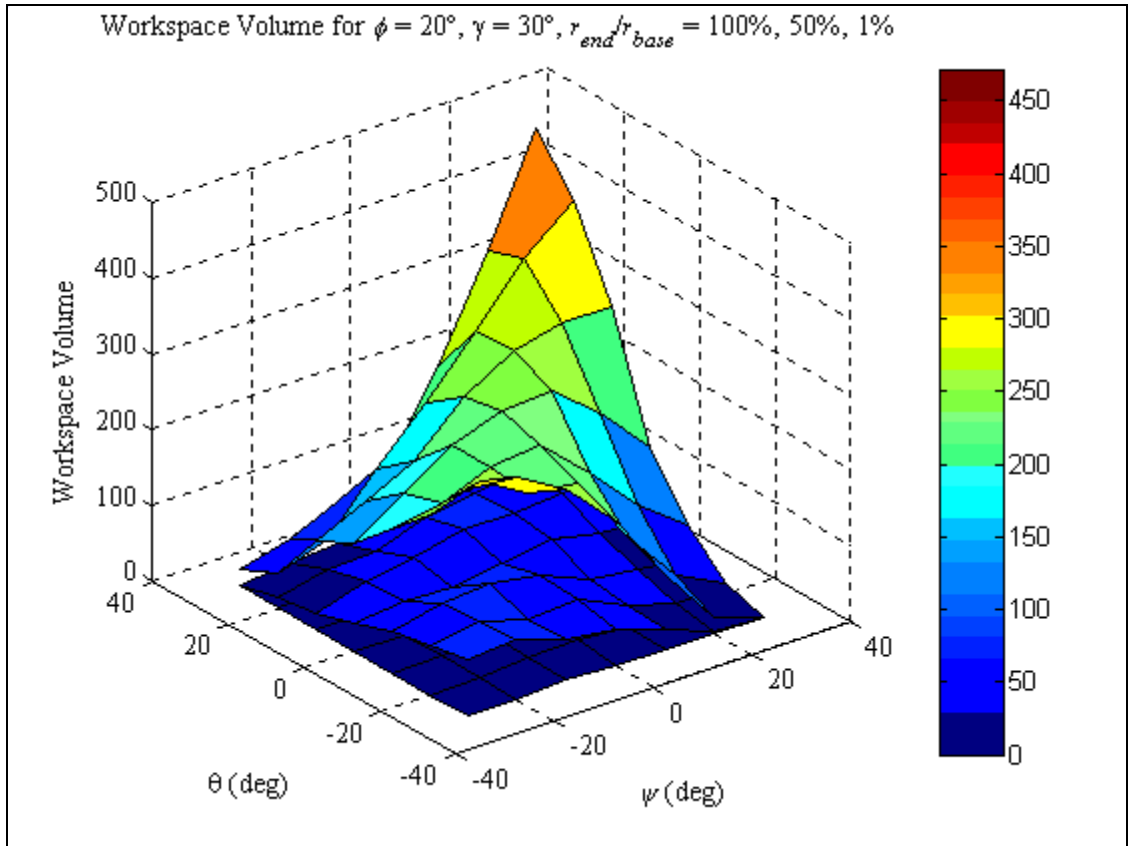


Fig. 3.6c Workspace Volume for $\gamma = 30^\circ$, $(r_{end}/r_{base}) = 100\%, 50\%, 1\%$ and $\phi = 20^\circ$

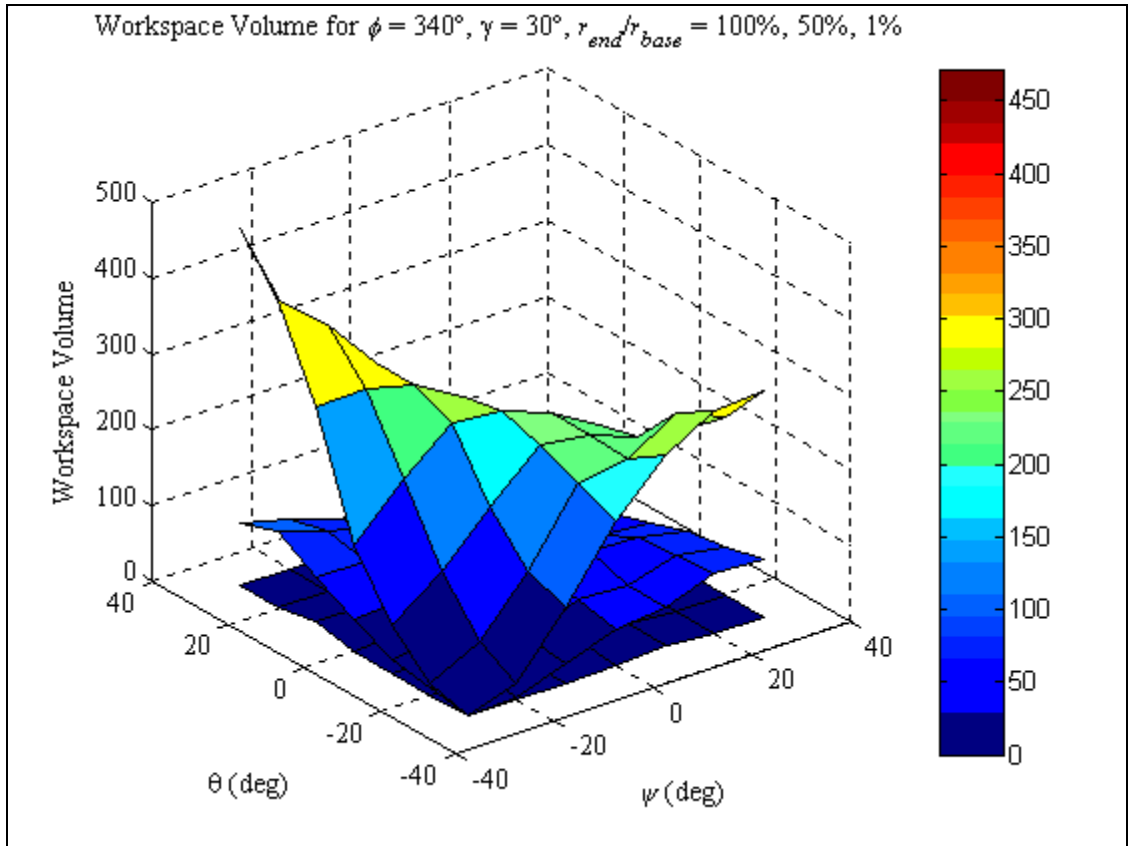


Fig. 3.6d Workspace Volume for $\gamma = 30^\circ, (r_{end}/r_{base}) = 100\%, 50\%, 1\%$ and $\phi = 340^\circ$

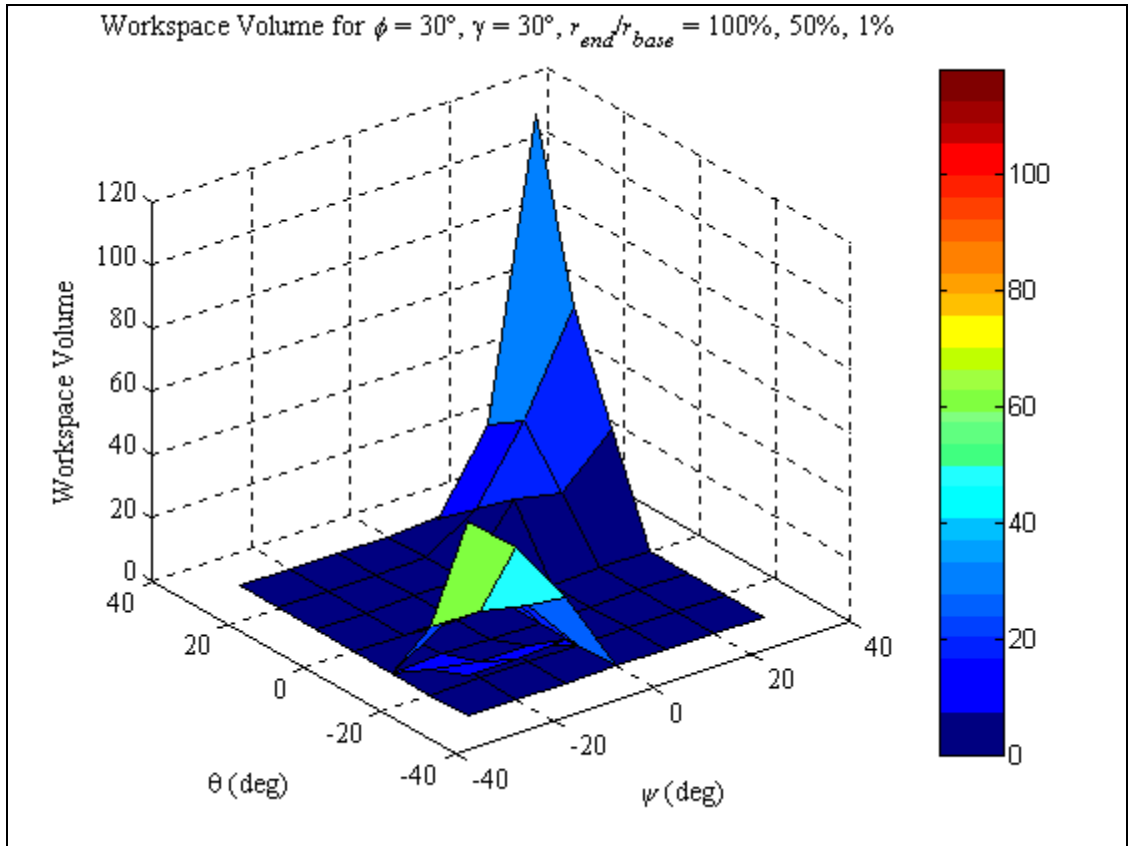


Fig. 3.6e Workspace Volume for $\gamma = 30^\circ$, $(r_{end}/r_{base}) = 100\%$, 50% , 1% and $\phi = 30^\circ$

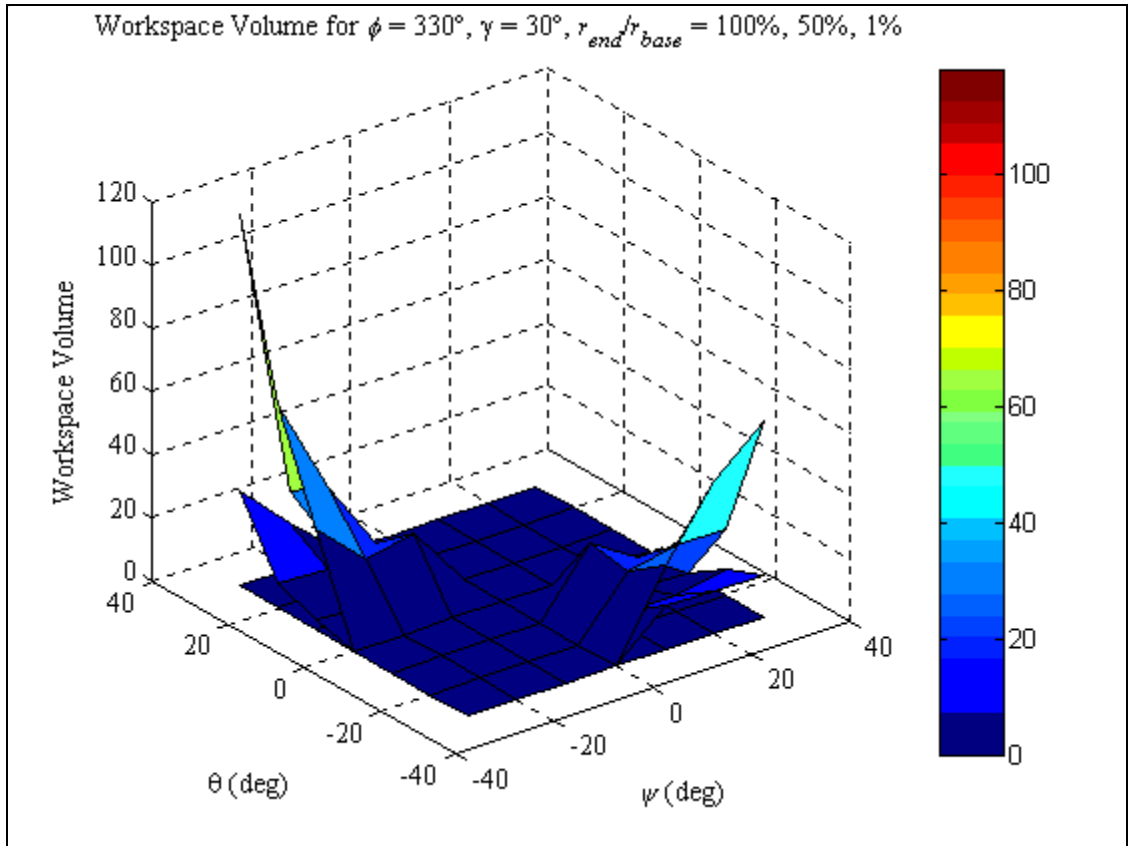


Fig. 3.6f Workspace Volume for $\gamma = 30^\circ$, $(r_{end}/r_{base}) = 100\%$, 50% , 1% and $\phi = 330^\circ$

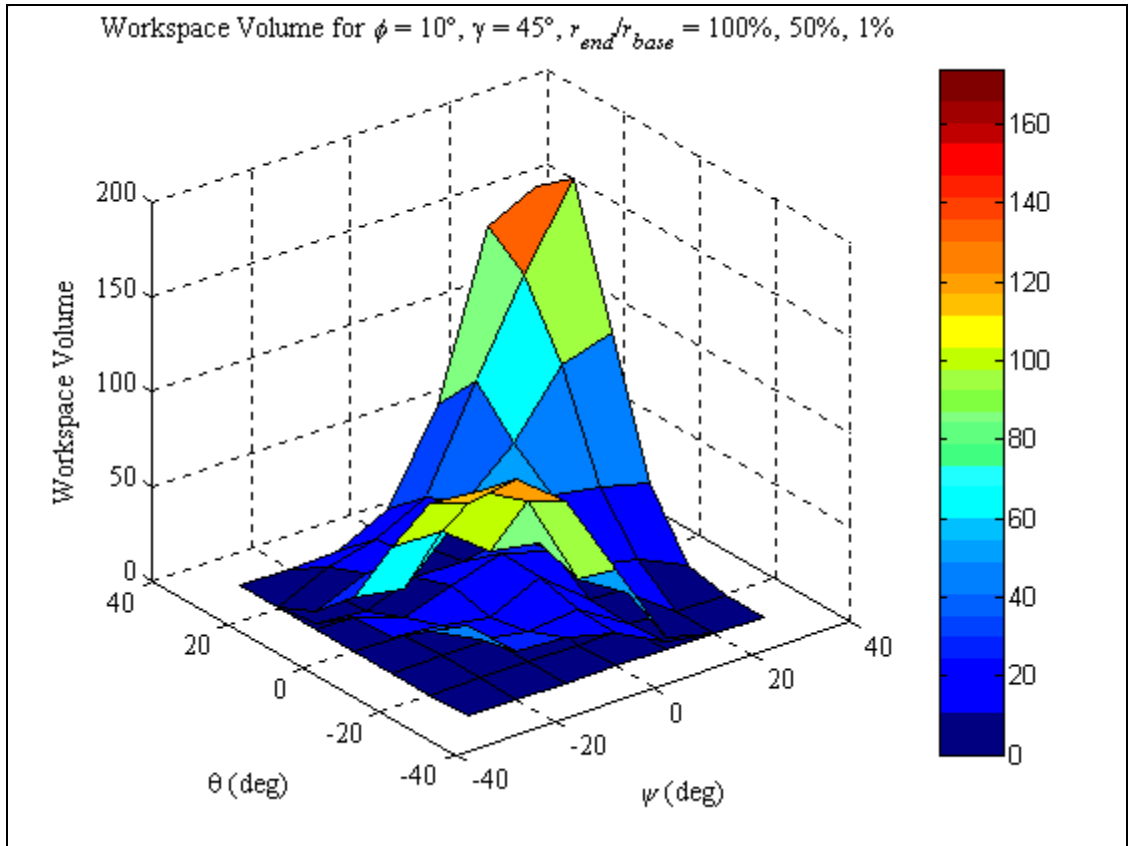


Fig. 3.7a Workspace Volume for $\gamma = 45^\circ$, $(r_{end}/r_{base}) = 100\%$, 50% , 1% and $\phi = 10^\circ$

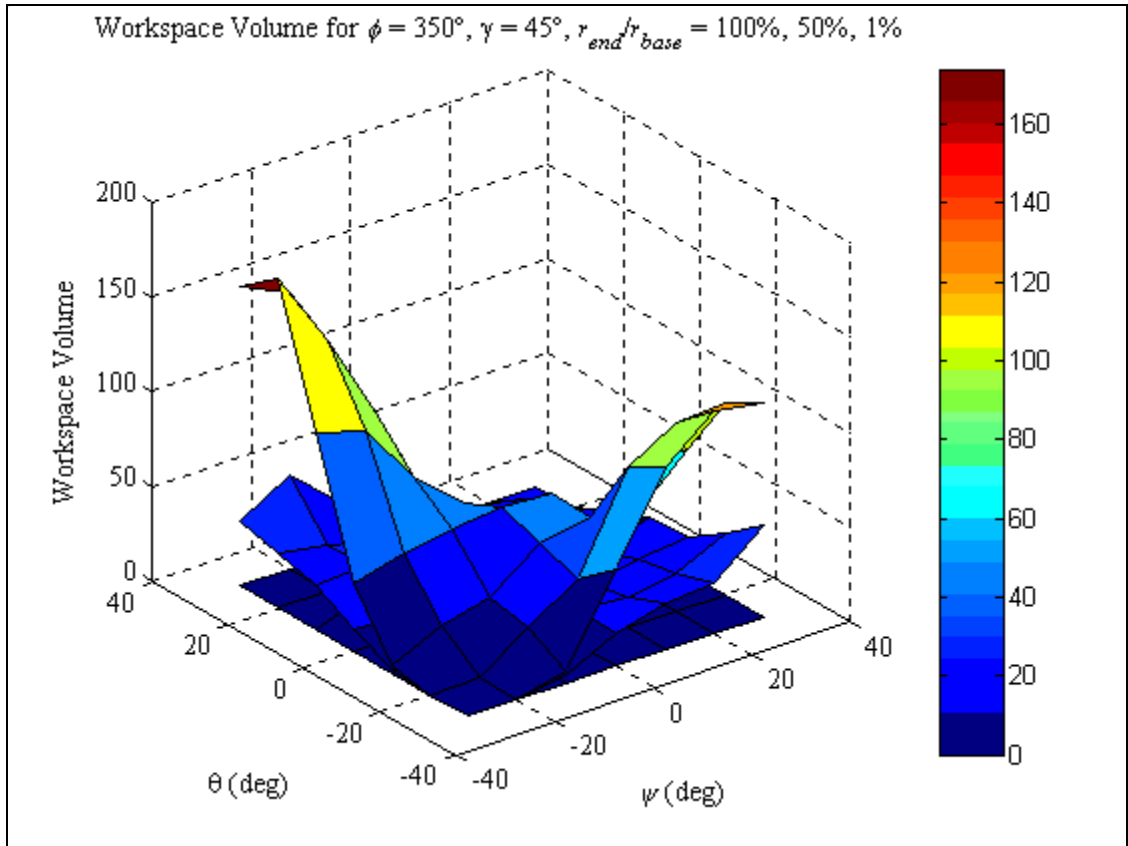


Fig. 3.7b Workspace Volume for $\gamma = 45^\circ$, $(r_{end}/r_{base}) = 100\%$, 50% , 1% and $\phi = 350^\circ$

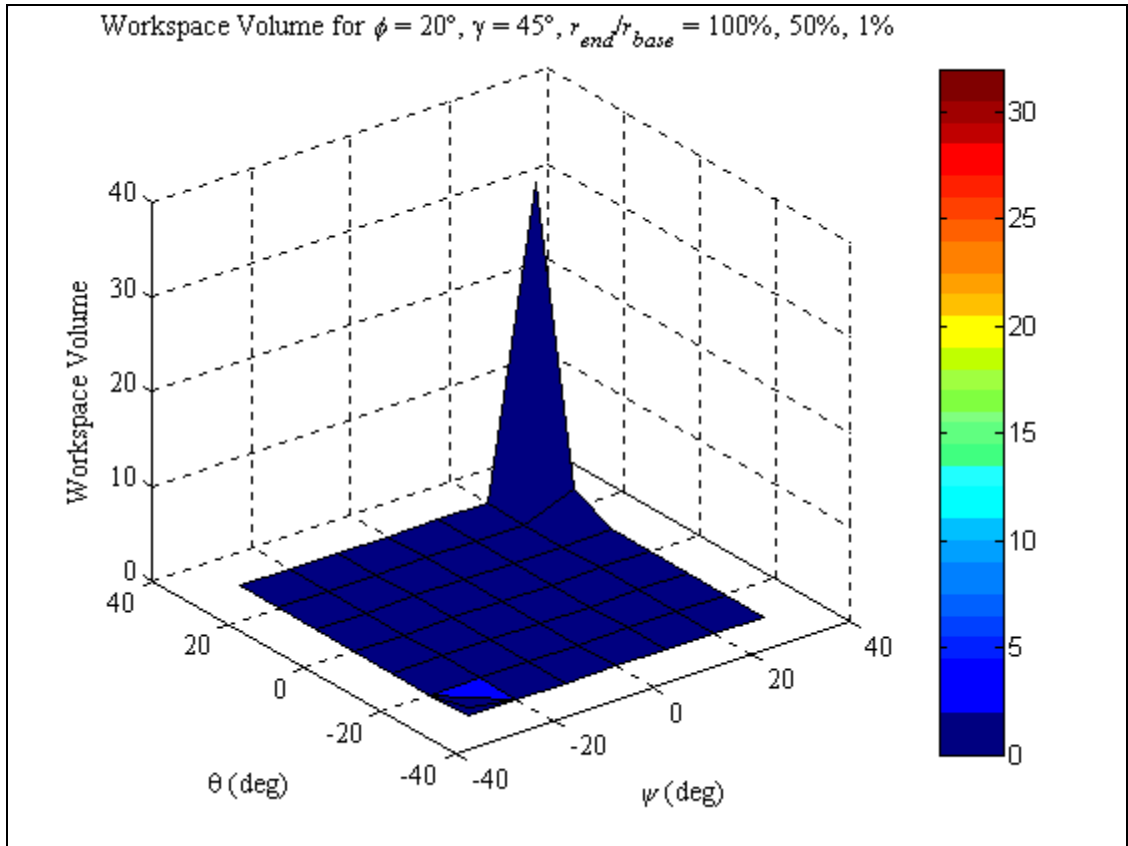


Fig. 3.7c Workspace Volume for $\gamma = 45^\circ$, $(r_{end}/r_{base}) = 100\%$, 50% , 1% and $\phi = 20^\circ$

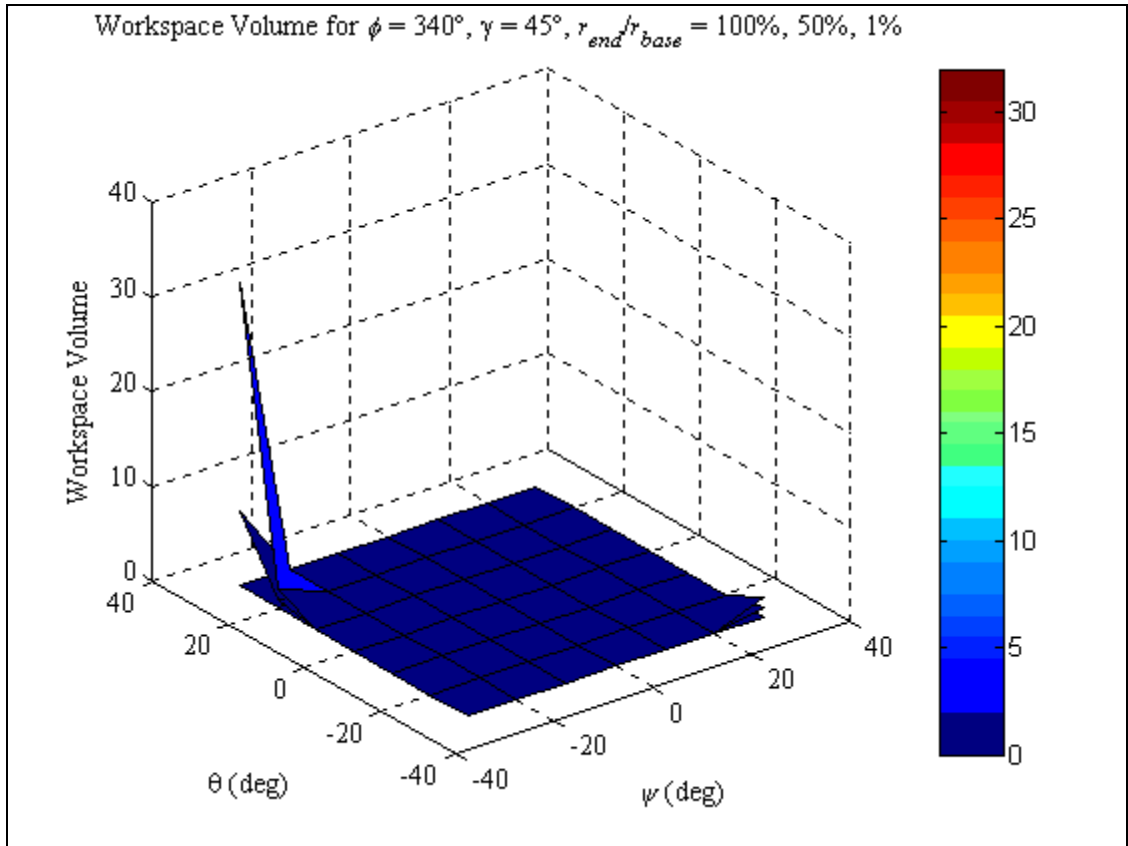


Fig. 3.7d Workspace Volume for $\gamma = 45^\circ, (r_{end}/r_{base}) = 100\%, 50\%, 1\%$ and $\phi = 340^\circ$

Appendix B: Plots of GCI

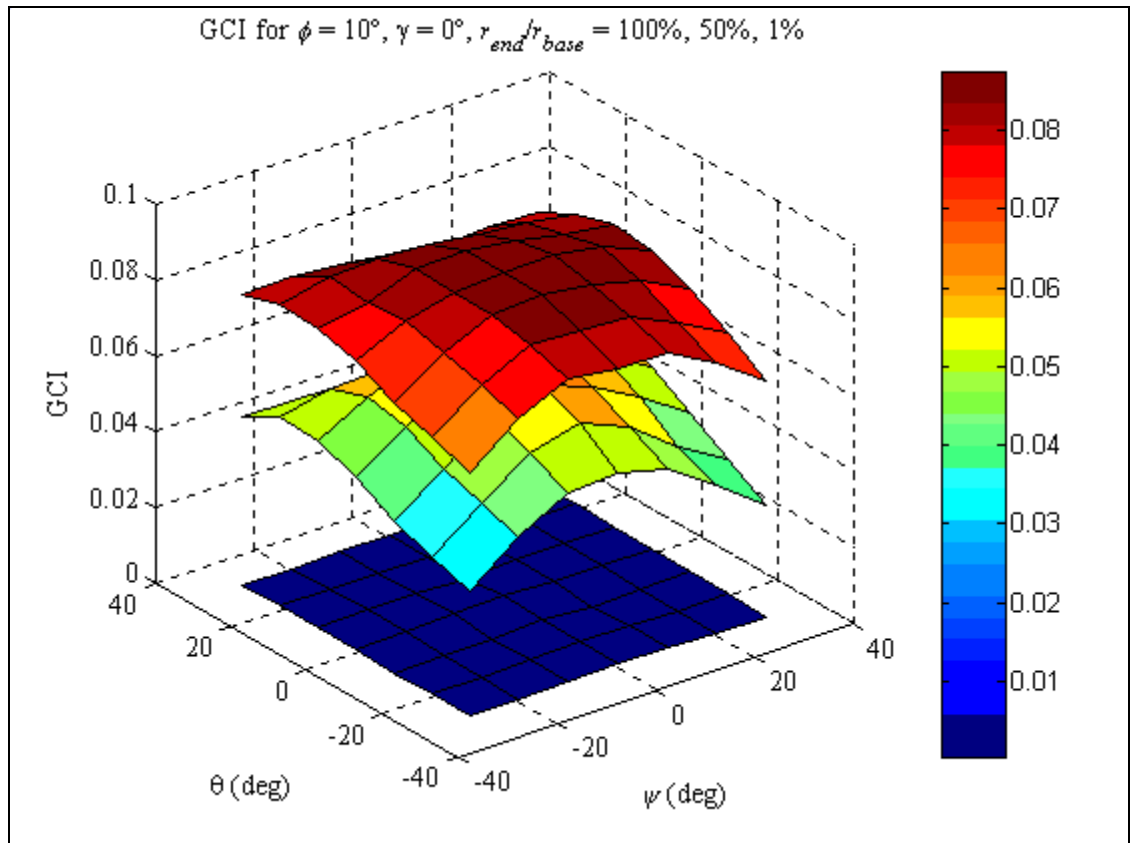


Fig. 3.18a GCI for $\gamma = 0^\circ$, $(r_{end}/r_{base}) = 100\%$, 50% , 1% , and $\phi = 10^\circ$

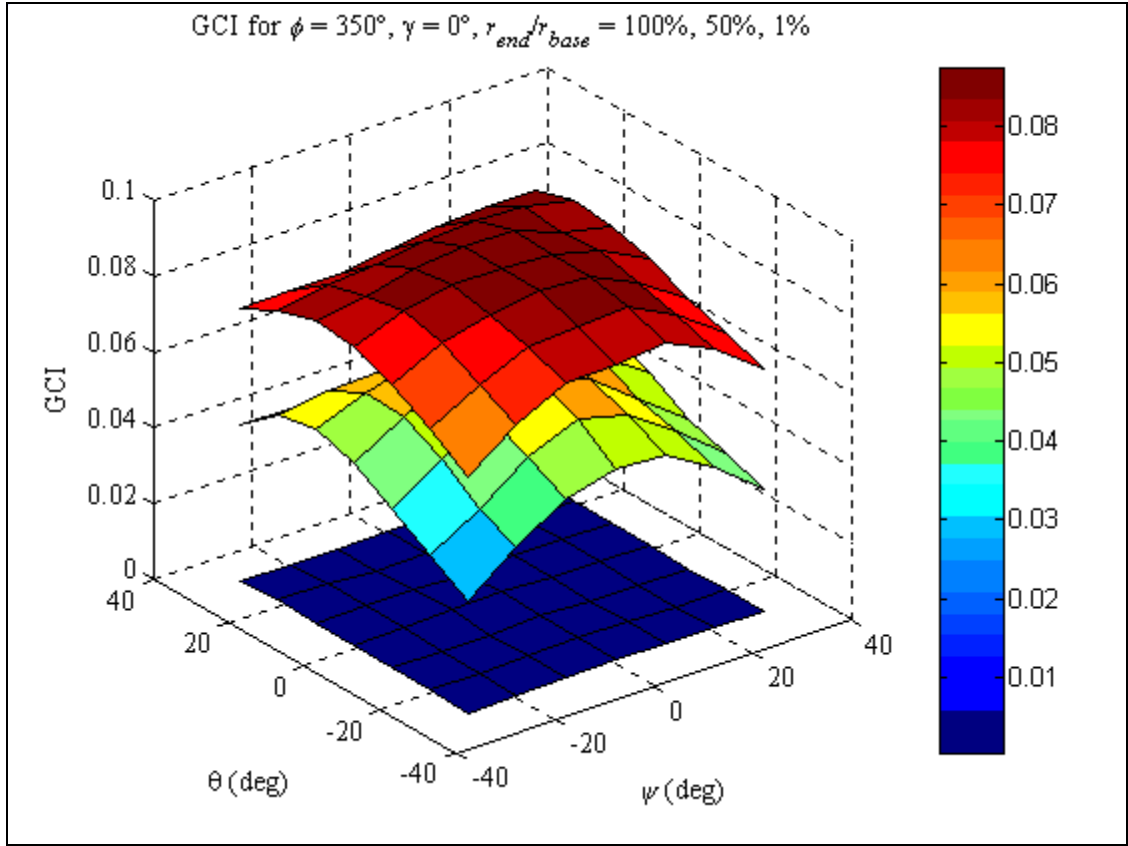


Fig. 3.18b GCI for $\gamma = 0^\circ$, $(r_{end}/r_{base}) = 100\%$, 50% , 1% , and $\phi = 350^\circ$

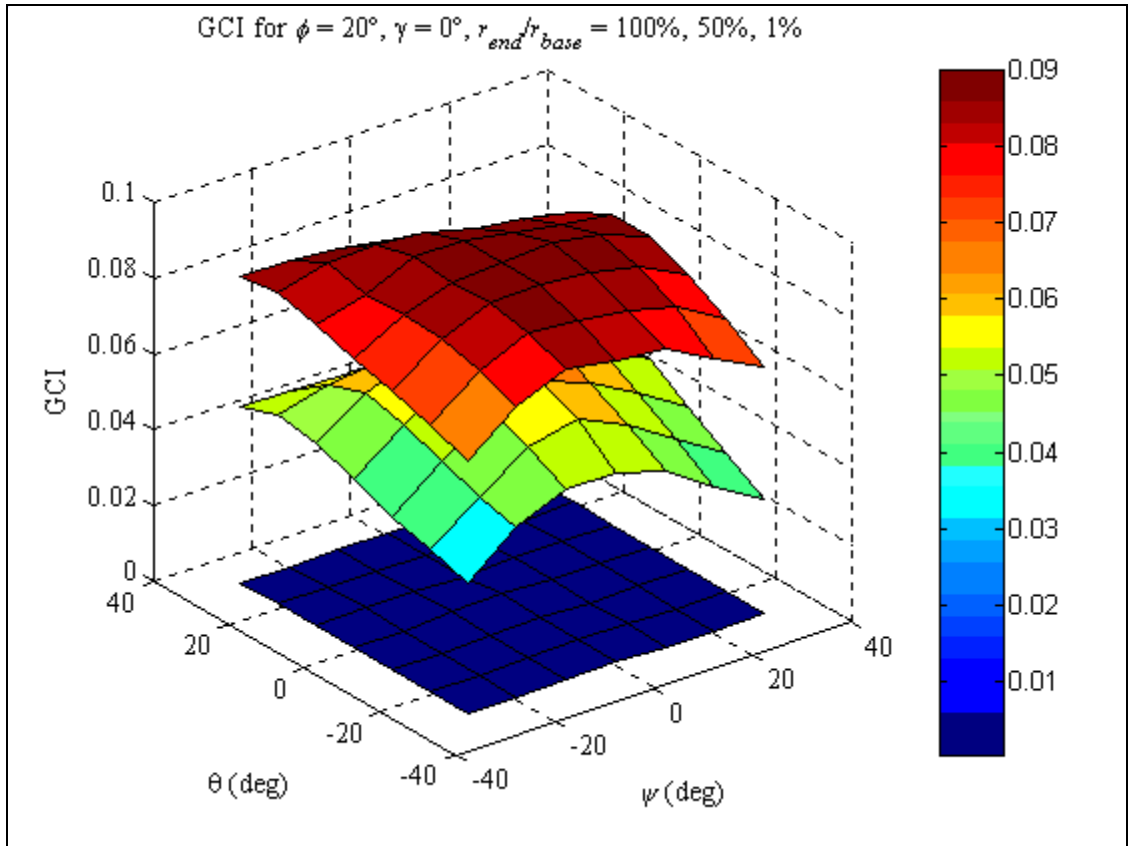


Fig. 3.18c GCI for $\gamma = 0^\circ, (r_{end}/r_{base}) = 100\%, 50\%, 1\%$, and $\phi = 20^\circ$

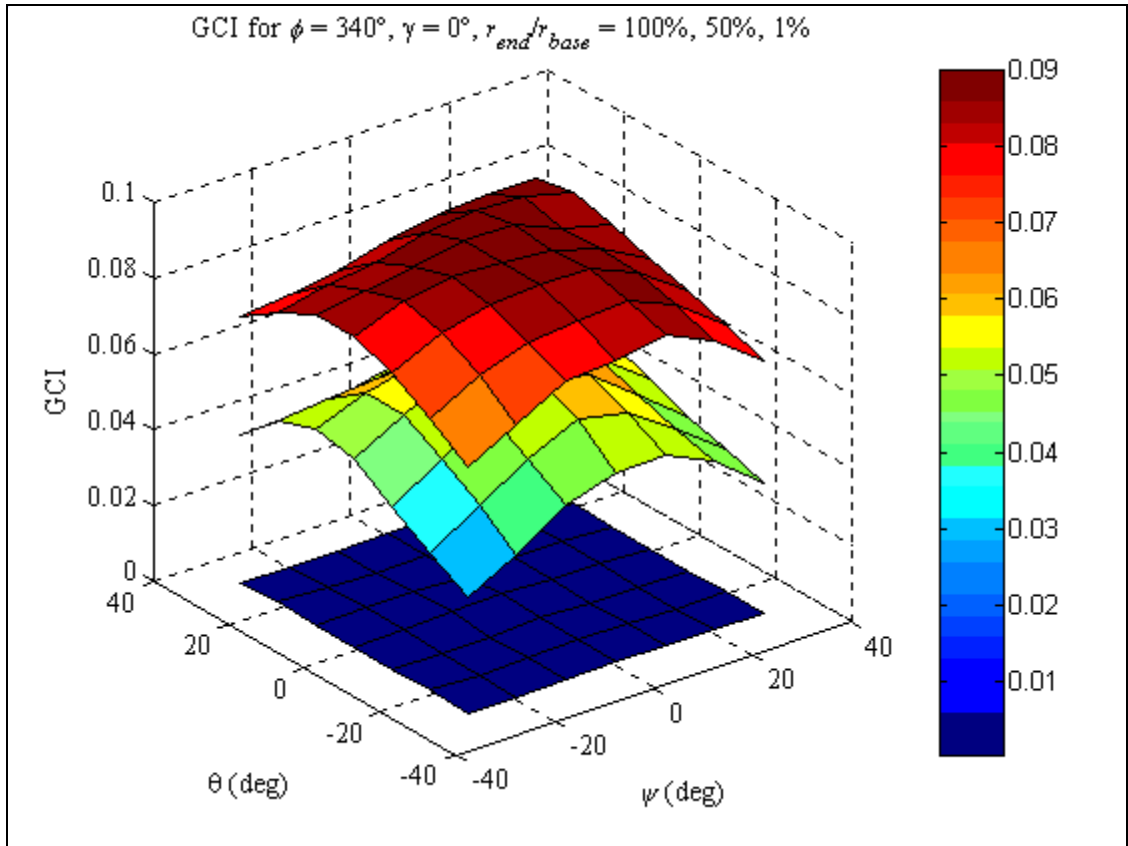


Fig. 3.18d GCI for $\gamma = 0^\circ$, $(r_{end}/r_{base}) = 100\%$, 50% , 1% , and $\phi = 340^\circ$

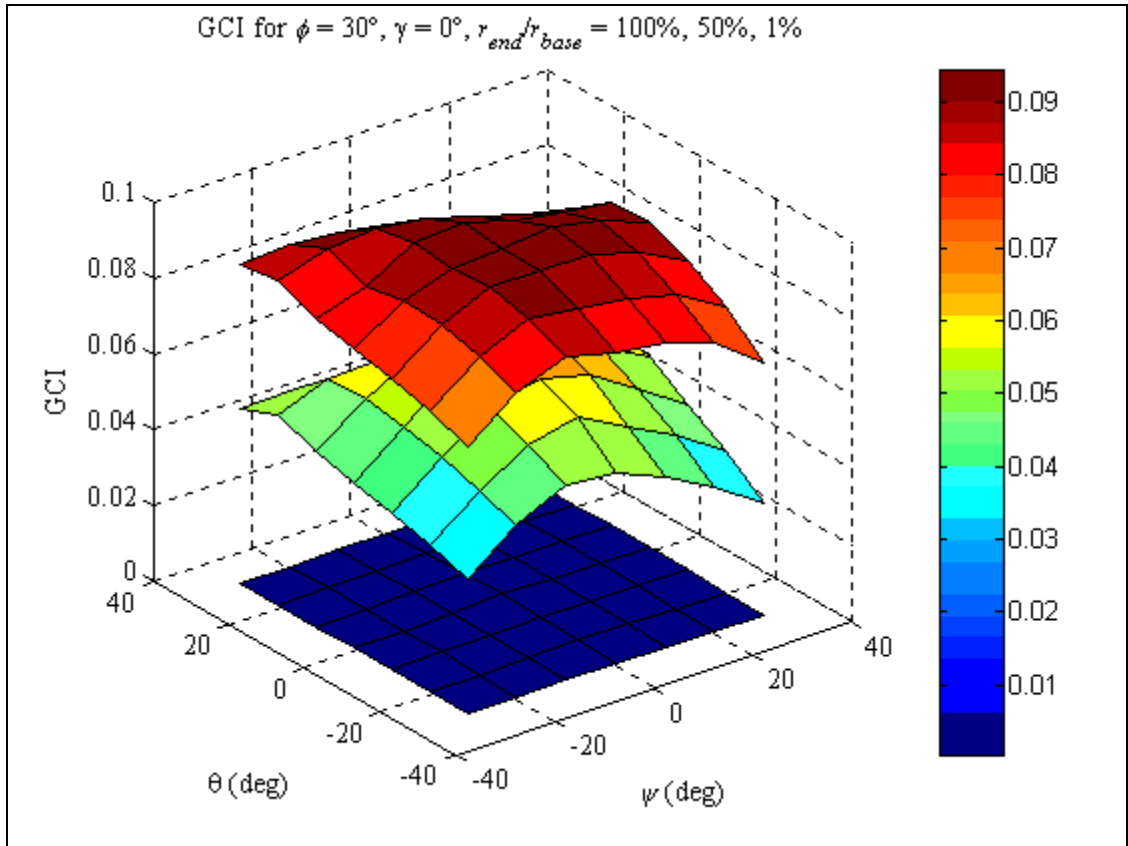


Fig. 3.18e GCI for $\gamma = 0^\circ$, $(r_{end}/r_{base}) = 100\%$, 50% , 1% , and $\phi = 30^\circ$

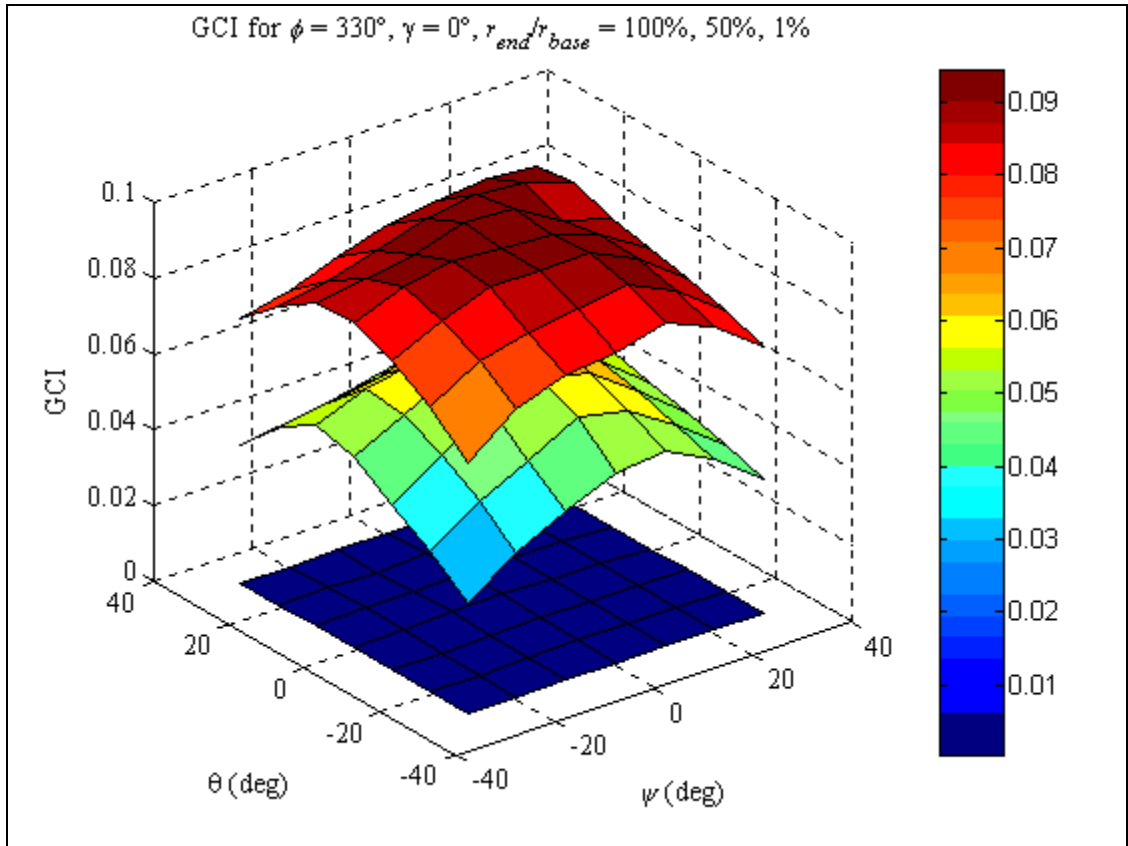


Fig. 3.18f GCI for $\gamma = 0^\circ$, $(r_{end}/r_{base}) = 100\%$, 50% , 1% , and $\phi = 330^\circ$

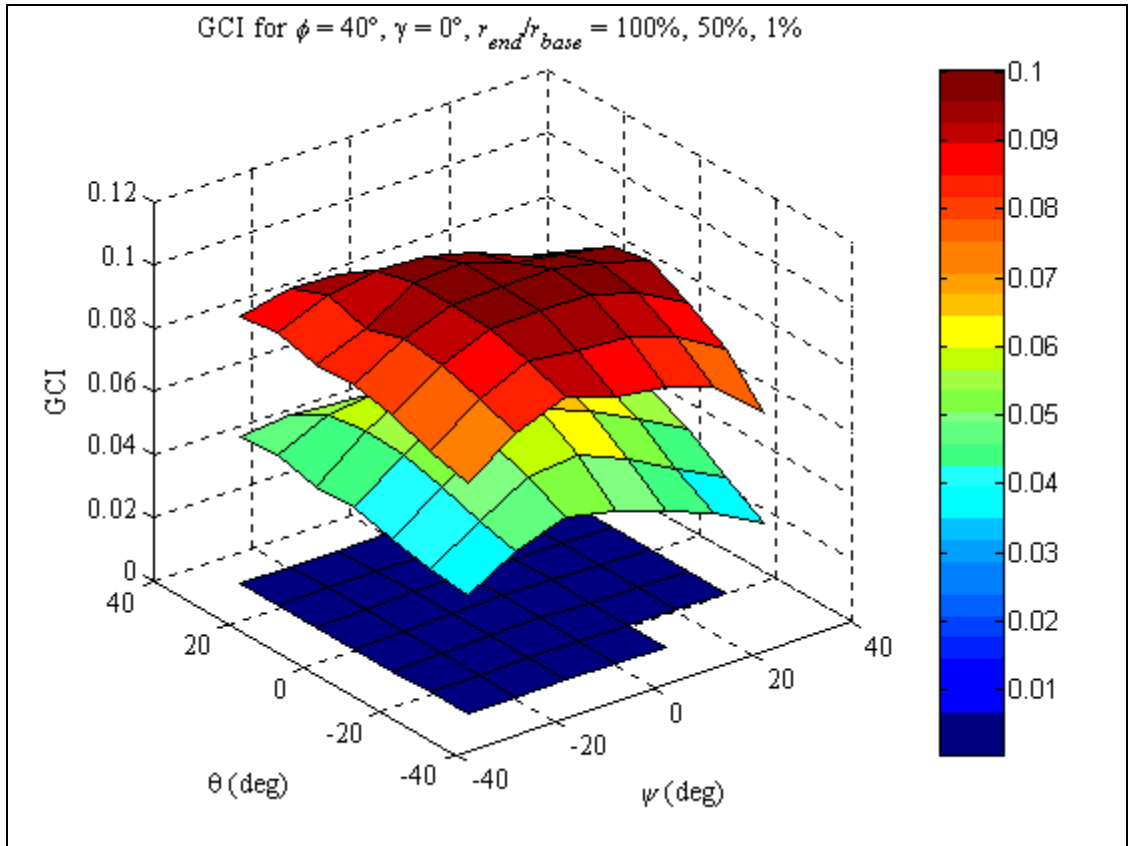


Fig. 3.18g GCI for $\gamma = 0^\circ$, $(r_{end}/r_{base}) = 100\%$, 50%, 1%, and $\phi = 40^\circ$

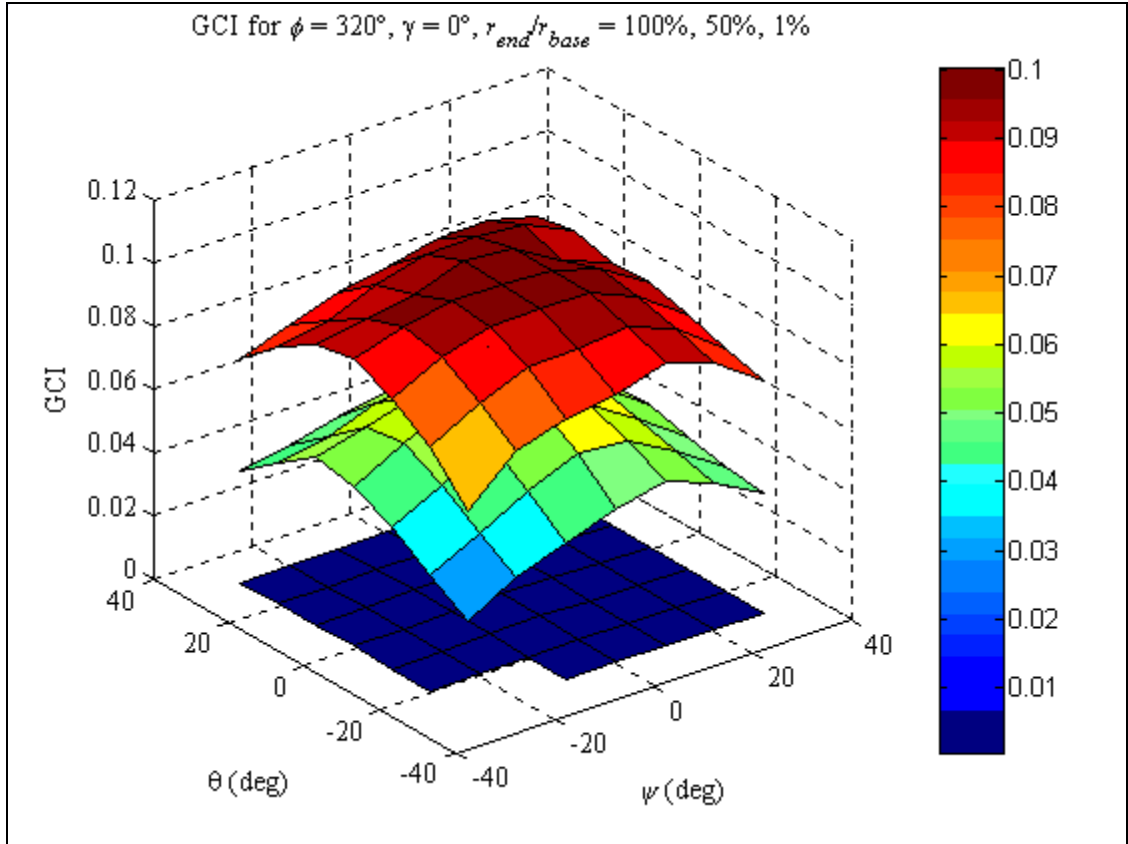


Fig. 3.18h GCI for $\gamma = 0^\circ$, $(r_{end}/r_{base}) = 100\%$, 50% , 1% , and $\phi = 320^\circ$

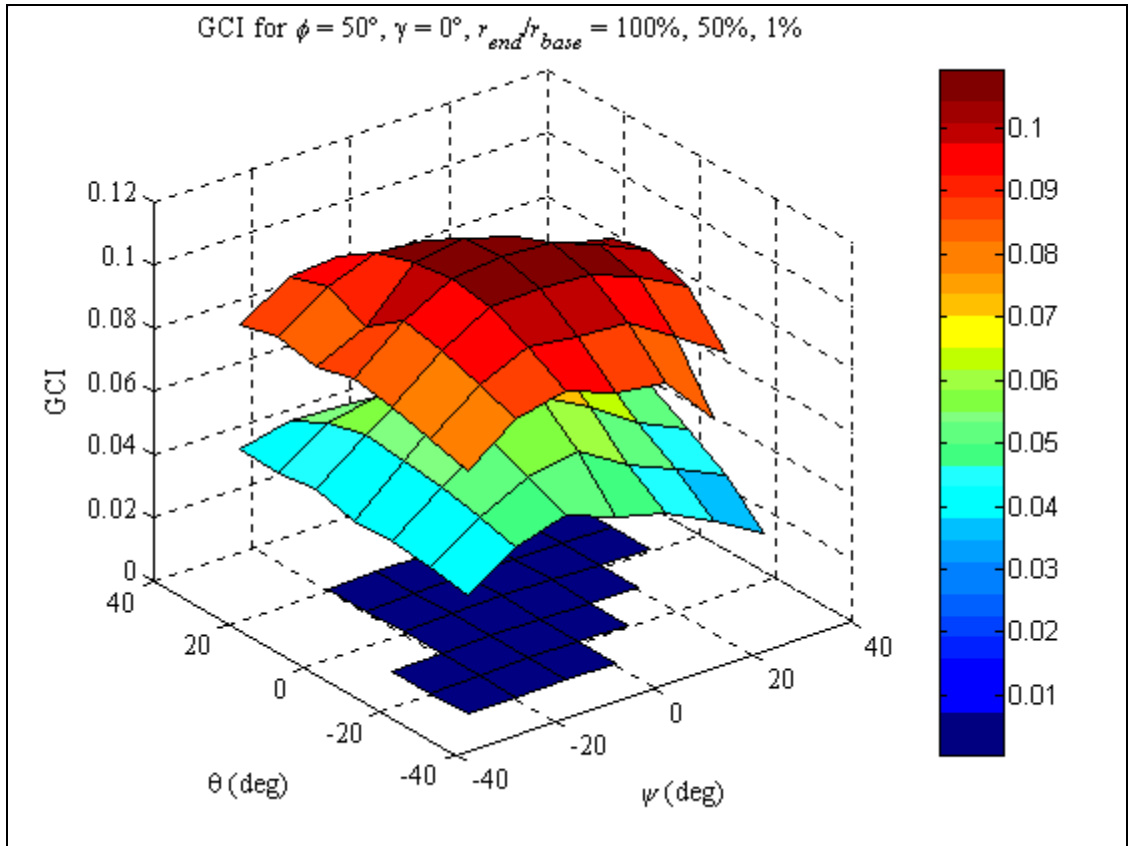


Fig. 3.18i GCI for $\gamma = 0^\circ$, $(r_{end}/r_{base}) = 100\%$, 50% , 1% , and $\phi = 50^\circ$

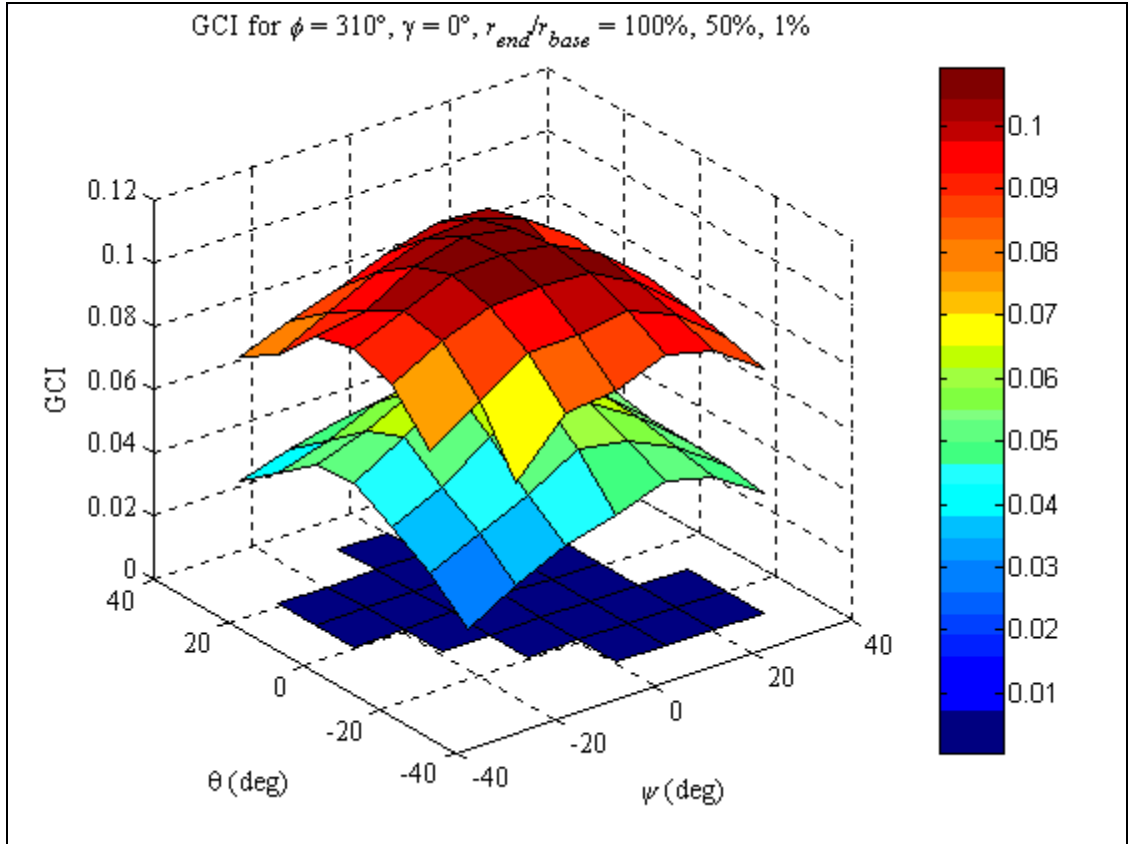


Fig. 3.18j GCI for $\gamma = 0^\circ$, $(r_{end}/r_{base}) = 100\%$, 50% , 1% , and $\phi = 310^\circ$

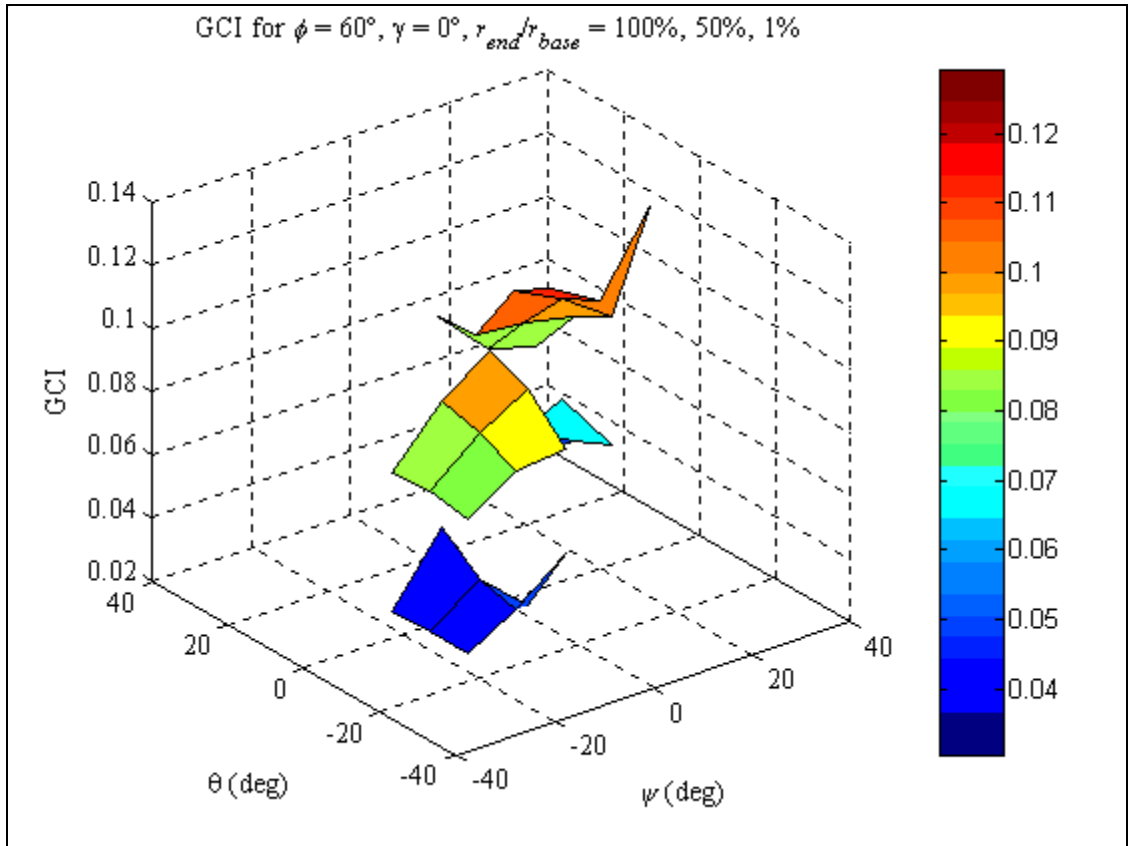


Fig. 3.18k GCI for $\gamma = 0^\circ$, $(r_{end}/r_{base}) = 100\%$, 50% , 1% , and $\phi = 60^\circ$

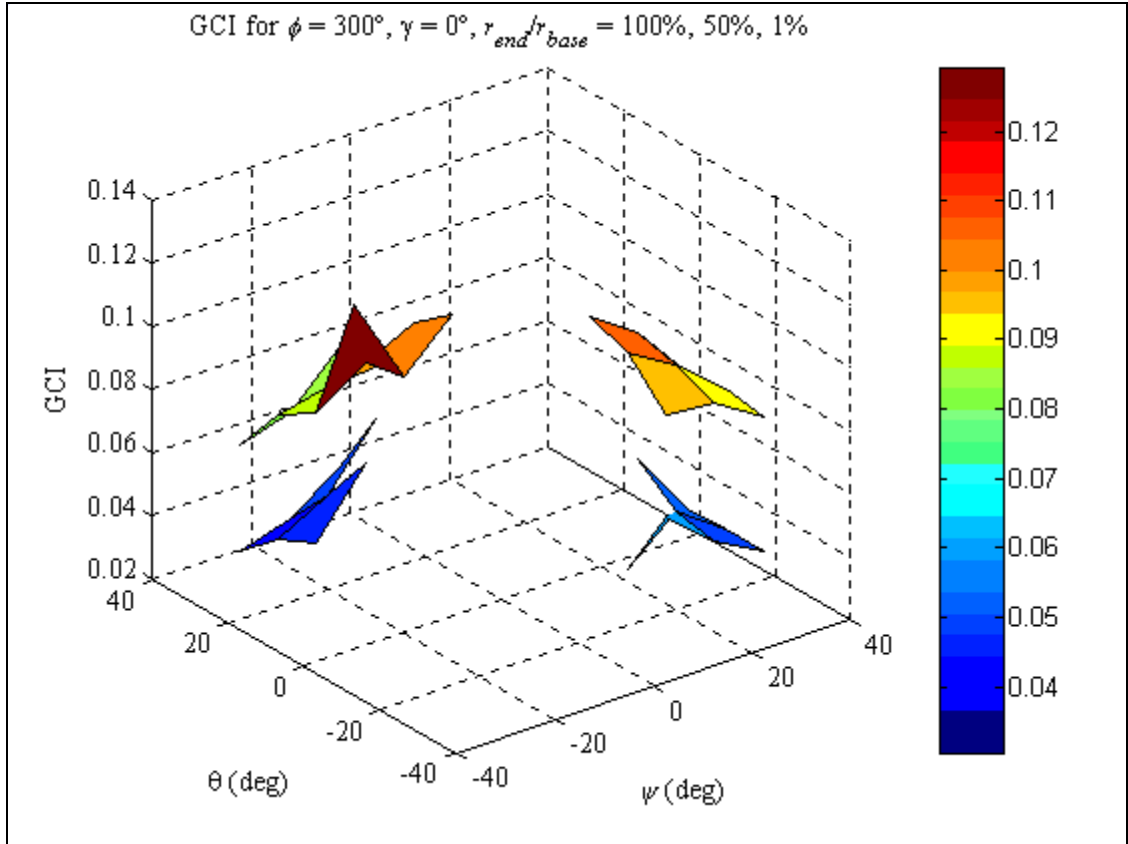


Fig. 3.18l GCI for $\gamma = 0^\circ$, $(r_{end}/r_{base}) = 100\%$, 50% , 1% , and $\phi = 300^\circ$

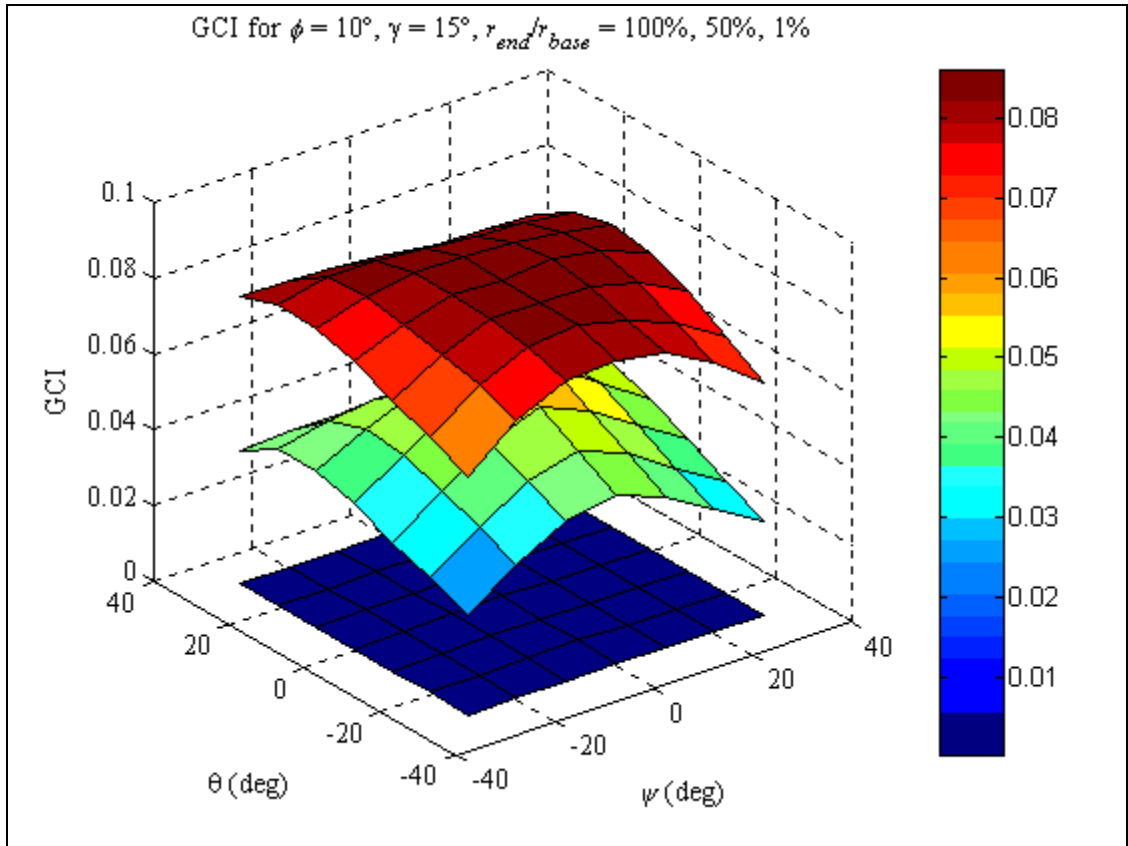


Fig. 3.19a GCI for $\gamma = 15^\circ$, $(r_{end}/r_{base}) = 100\%$, 50% , 1% , and $\phi = 10^\circ$

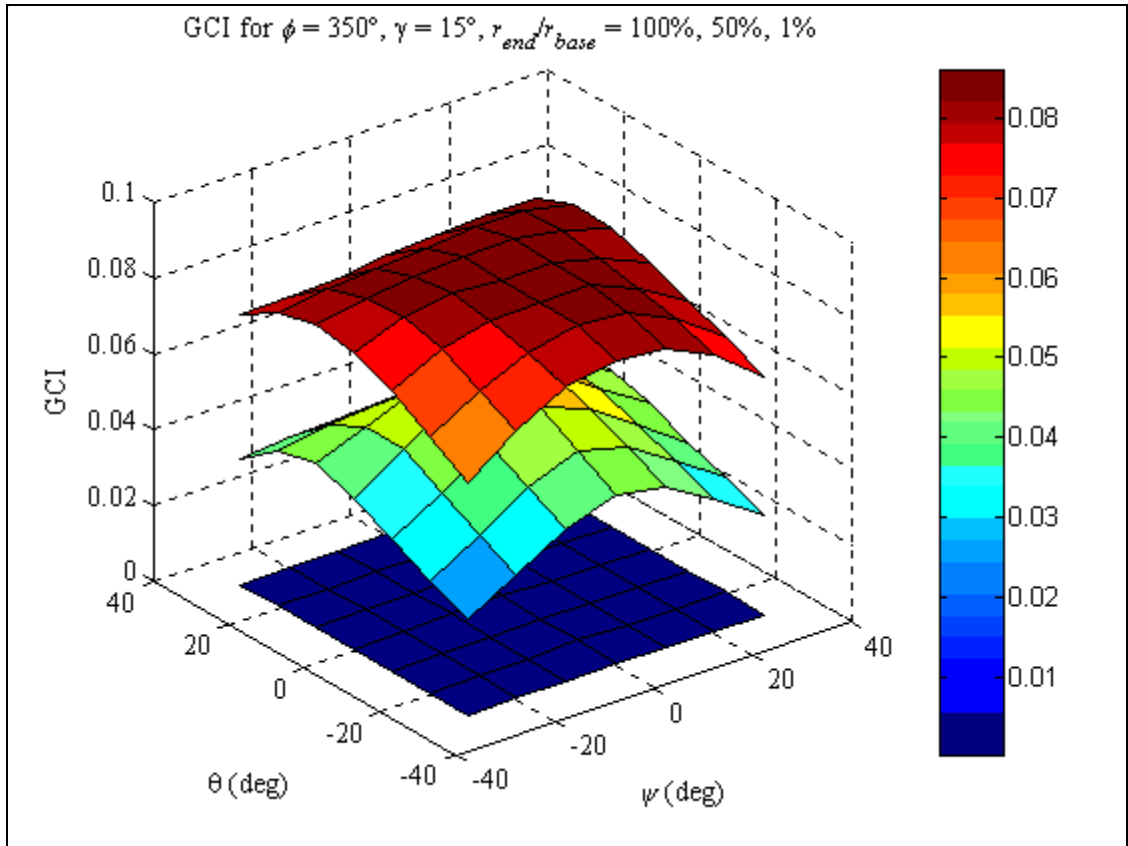


Fig. 3.19b GCI for $\gamma = 15^\circ$, $(r_{end}/r_{base}) = 100\%$, 50% , 1% , and $\phi = 350^\circ$

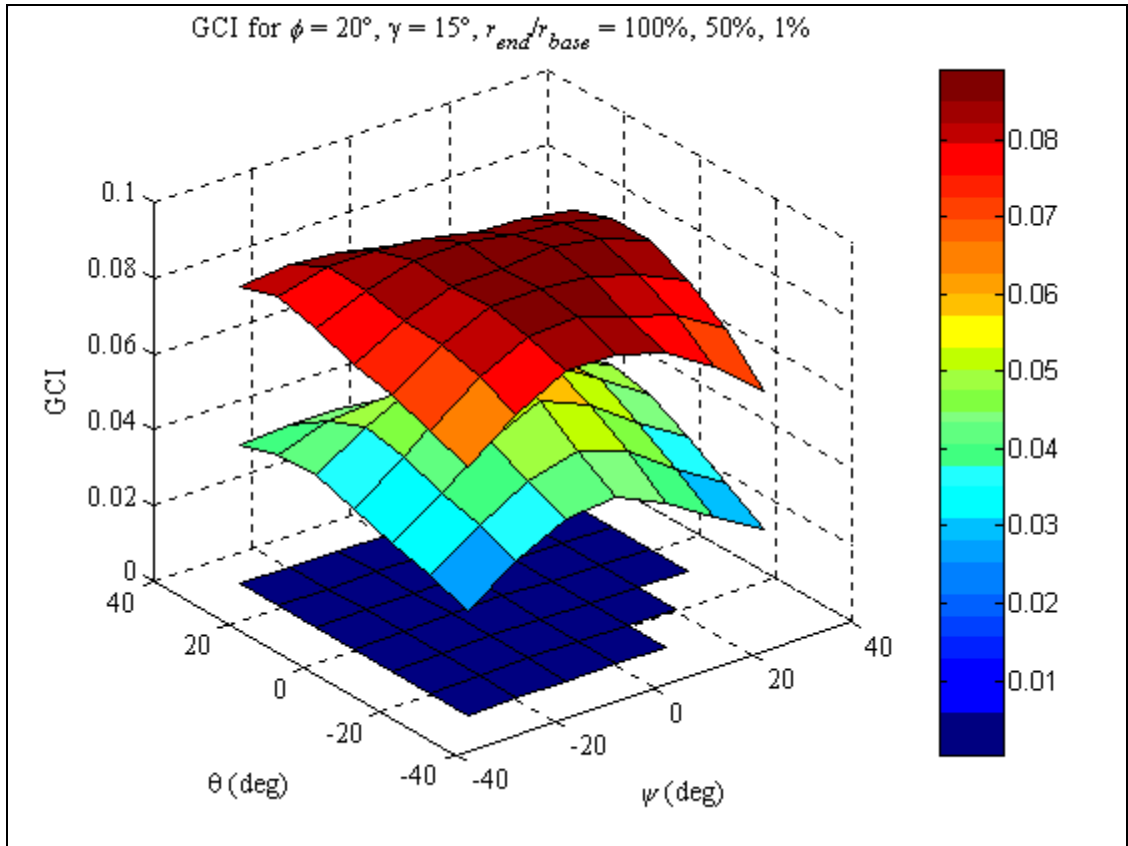


Fig. 3.19c GCI for $\gamma = 15^\circ$, $(r_{end}/r_{base}) = 100\%$, 50% , 1% , and $\phi = 20^\circ$

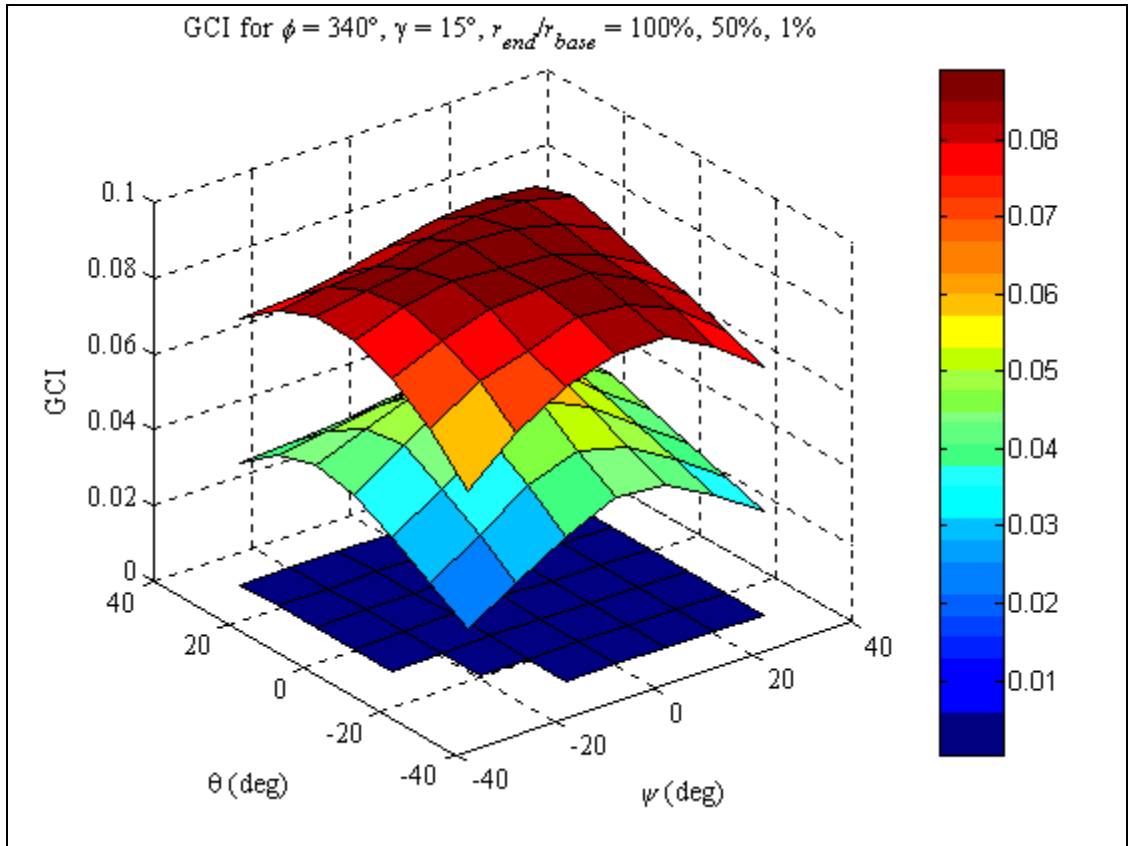


Fig. 3.19d GCI for $\gamma = 15^\circ$, $(r_{end}/r_{base}) = 100\%$, 50% , 1% , and $\phi = 340^\circ$

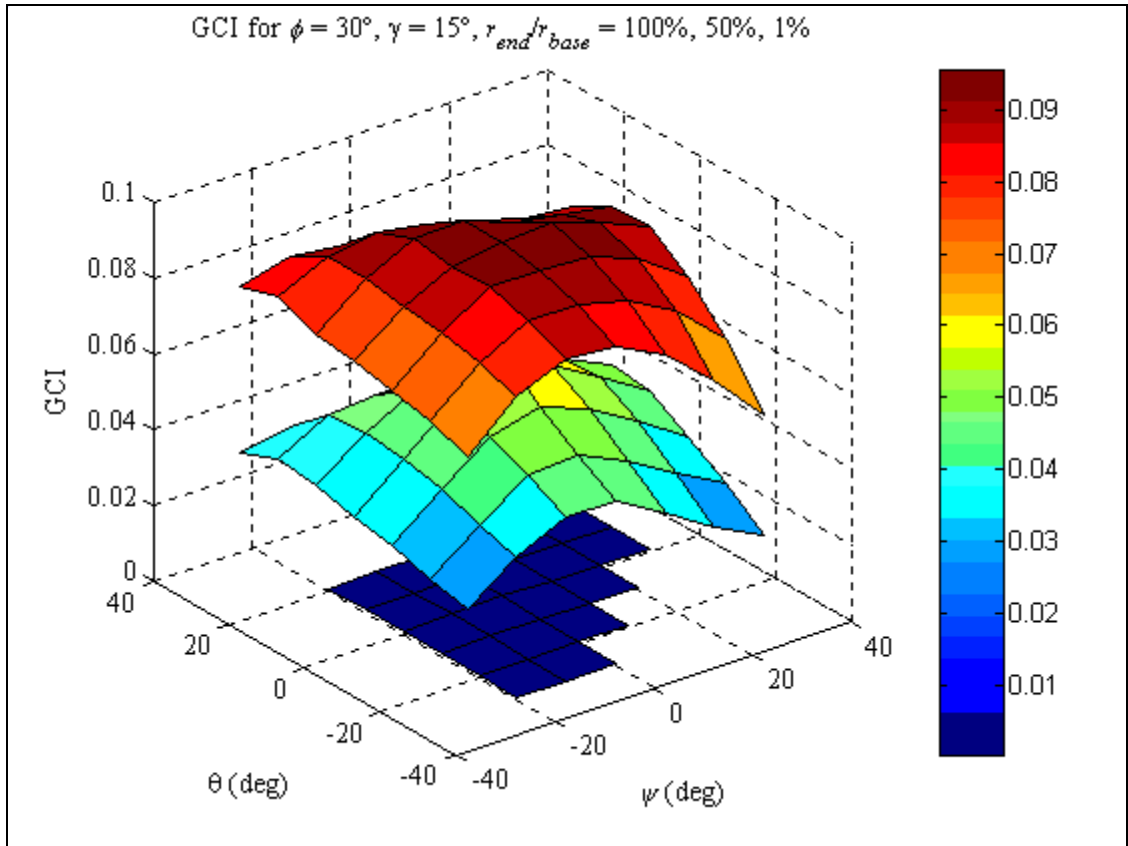


Fig. 3.19e GCI for $\gamma = 15^\circ$, $(r_{end}/r_{base}) = 100\%$, 50% , 1% , and $\phi = 30^\circ$

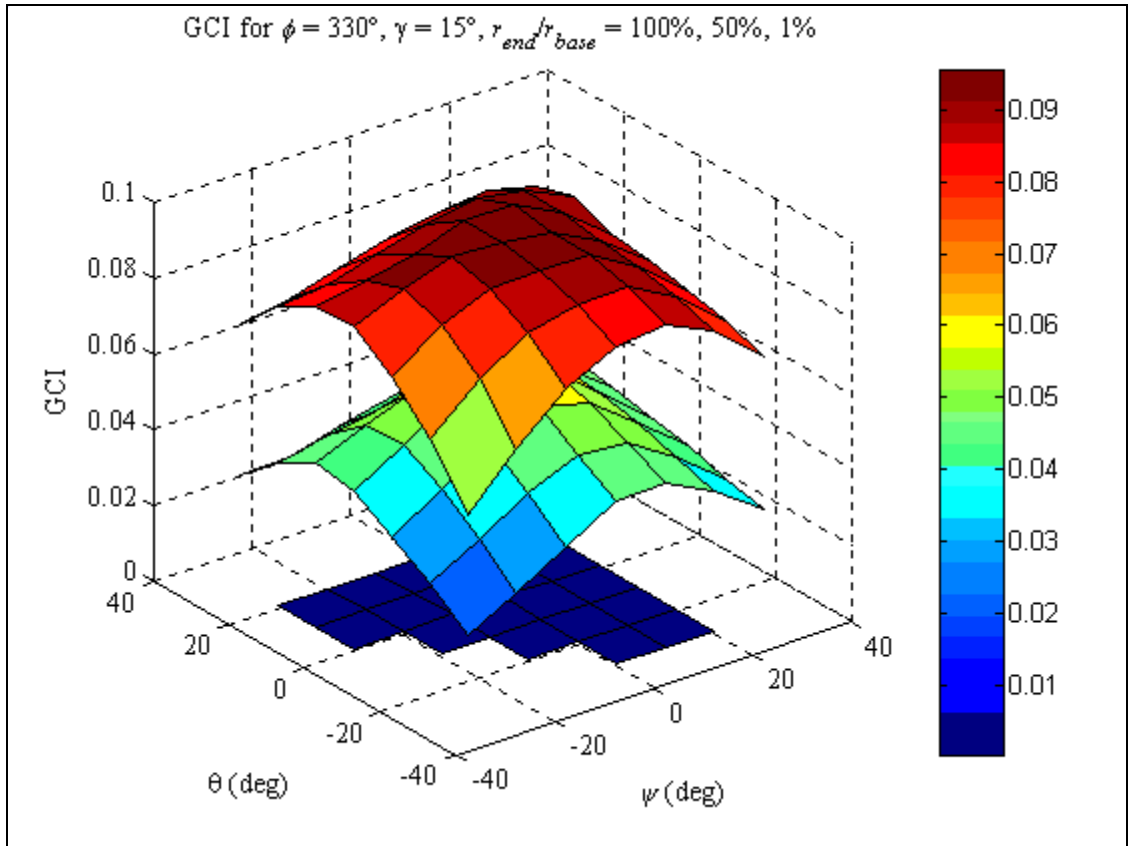


Fig. 3.19f GCI for $\gamma = 15^\circ$, $(r_{end}/r_{base}) = 100\%$, 50% , 1% , and $\phi = 330^\circ$

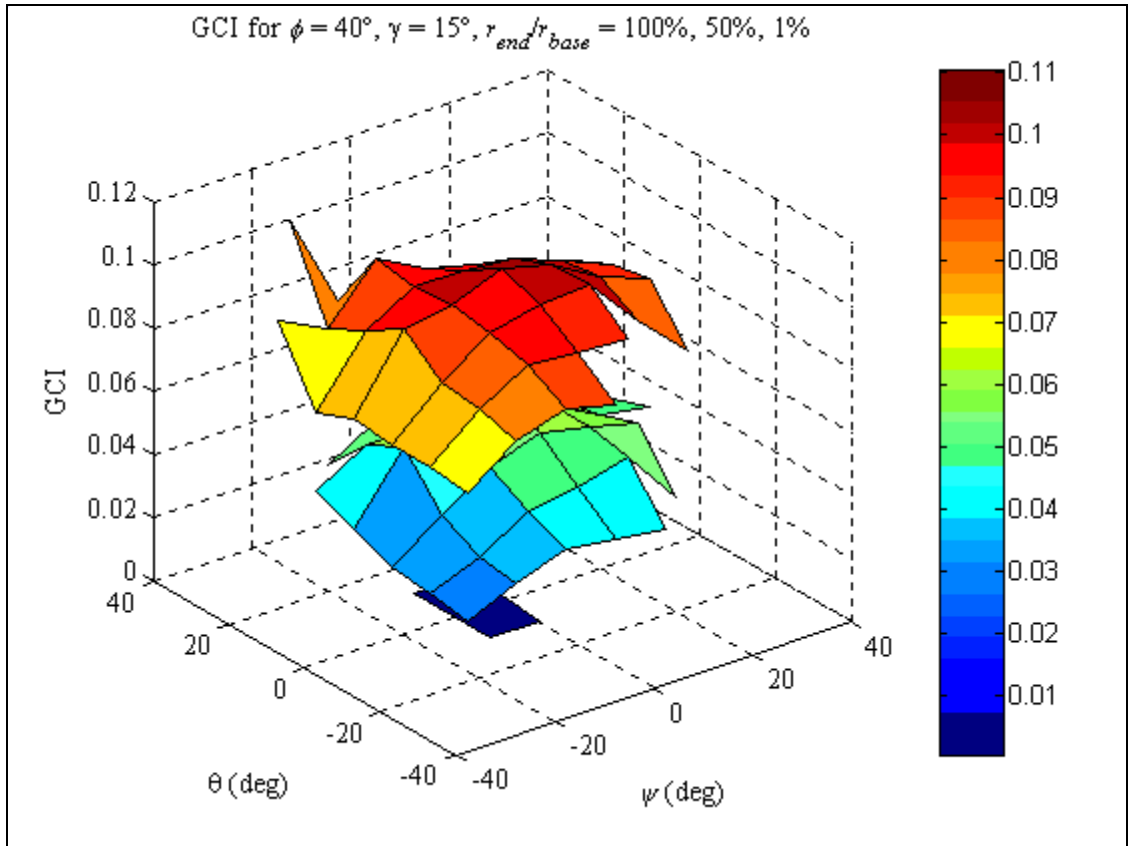


Fig. 3.19g GCI for $\gamma = 15^\circ$, $(r_{end}/r_{base}) = 100\%$, 50% , 1% , and $\phi = 40^\circ$

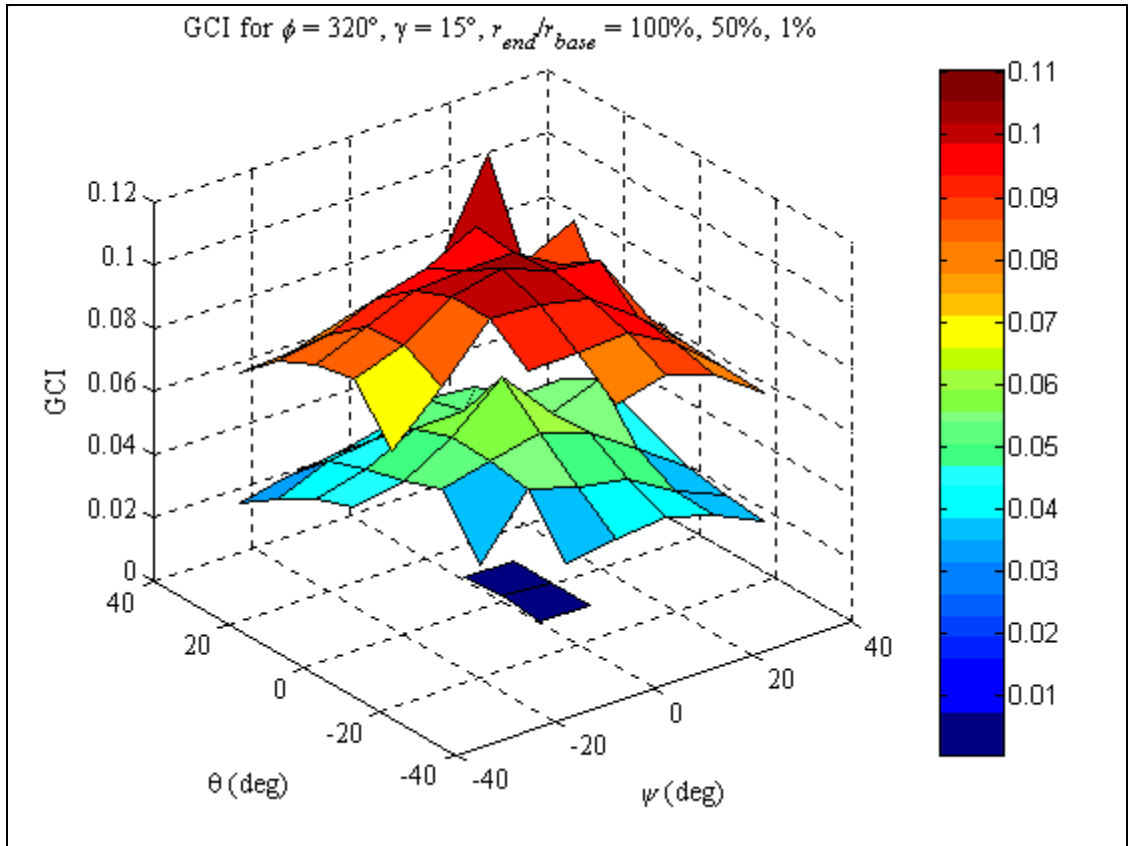


Fig. 3.19h GCI for $\gamma = 15^\circ$, $(r_{end}/r_{base}) = 100\%$, 50% , 1% , and $\phi = 320^\circ$

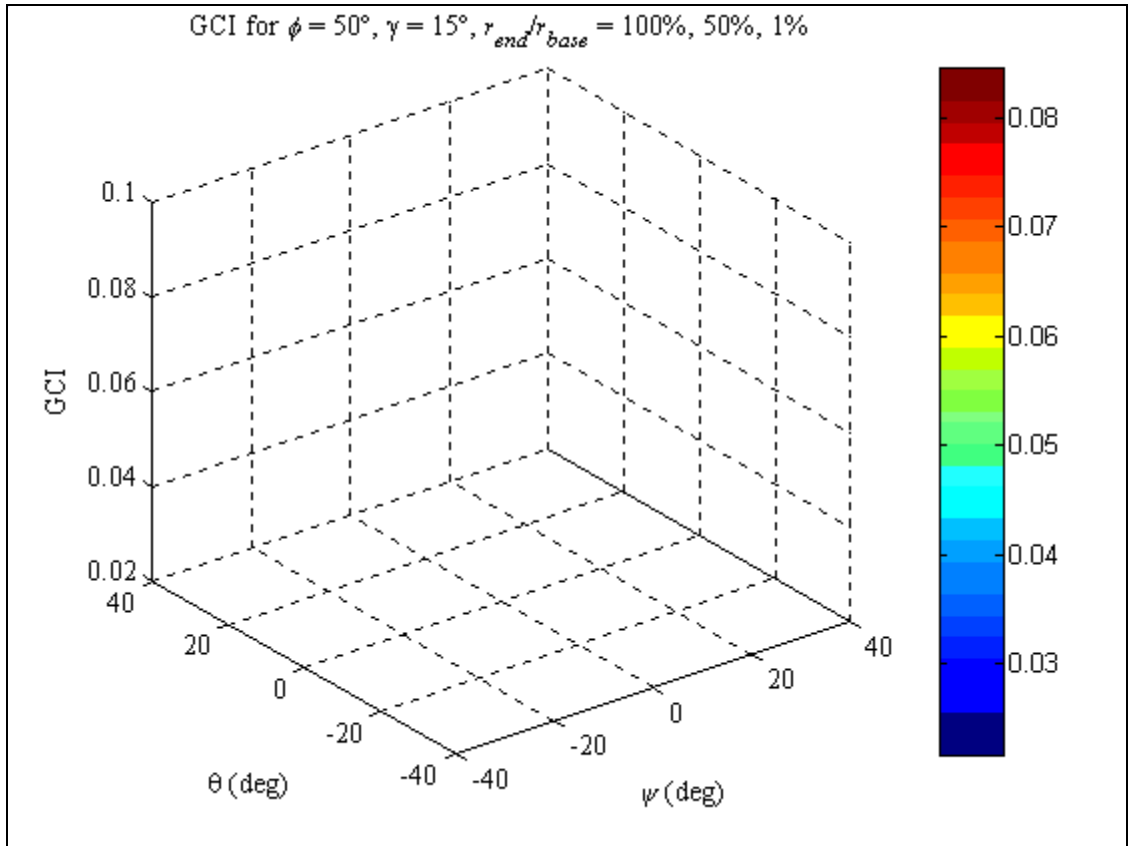


Fig. 3.19i GCI for $\gamma = 15^\circ$, $(r_{end}/r_{base}) = 100\%$, 50% , 1% , and $\phi = 50^\circ$

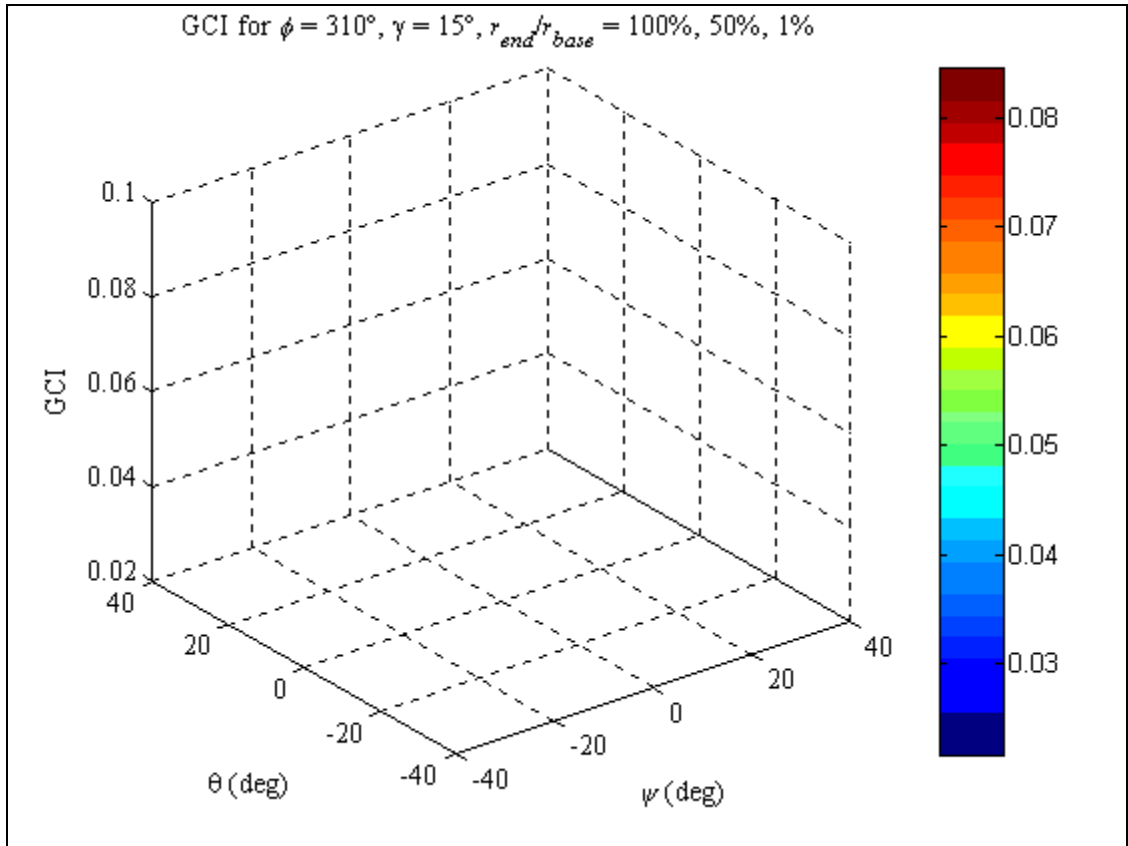


Fig. 3.19j GCI for $\gamma = 15^\circ$, $(r_{end}/r_{base}) = 100\%$, 50% , 1% , and $\phi = 310^\circ$

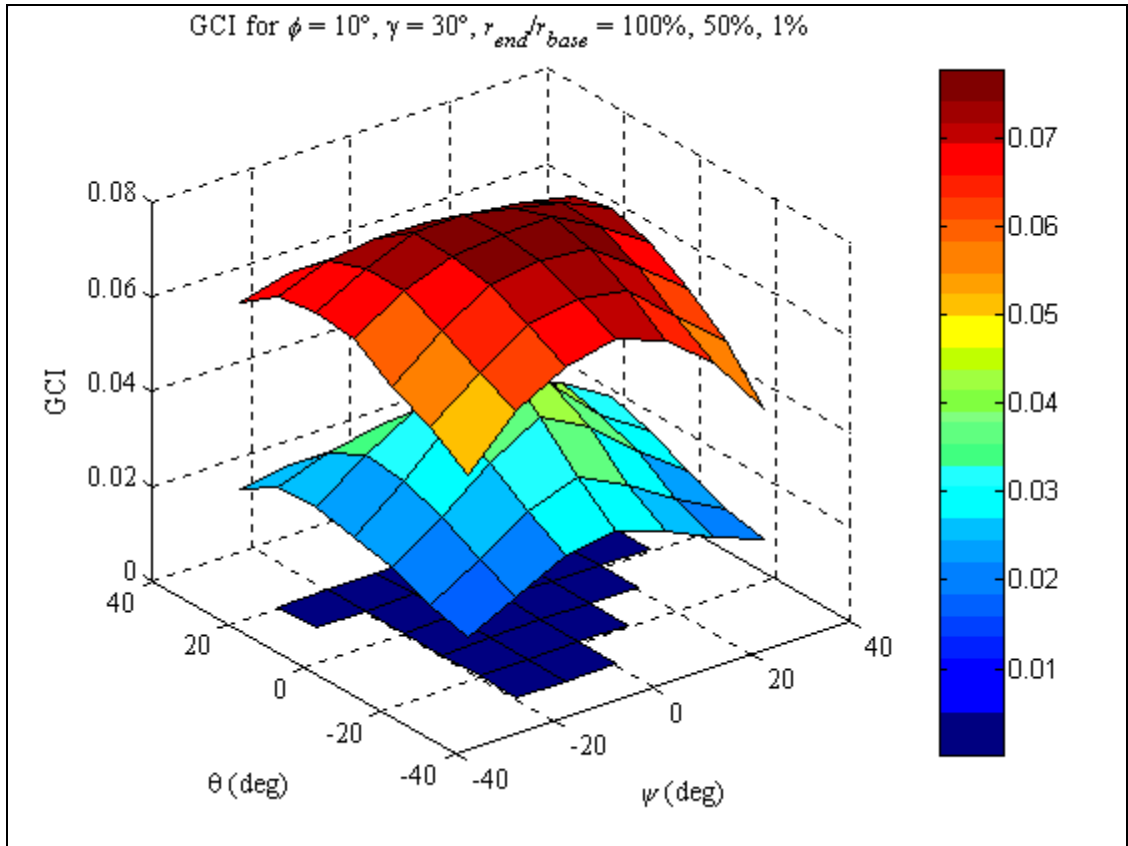


Fig. 3.20a GCI for $\gamma = 30^\circ$, $(r_{end}/r_{base}) = 100\%$, 50% , 1% , and $\phi = 10^\circ$

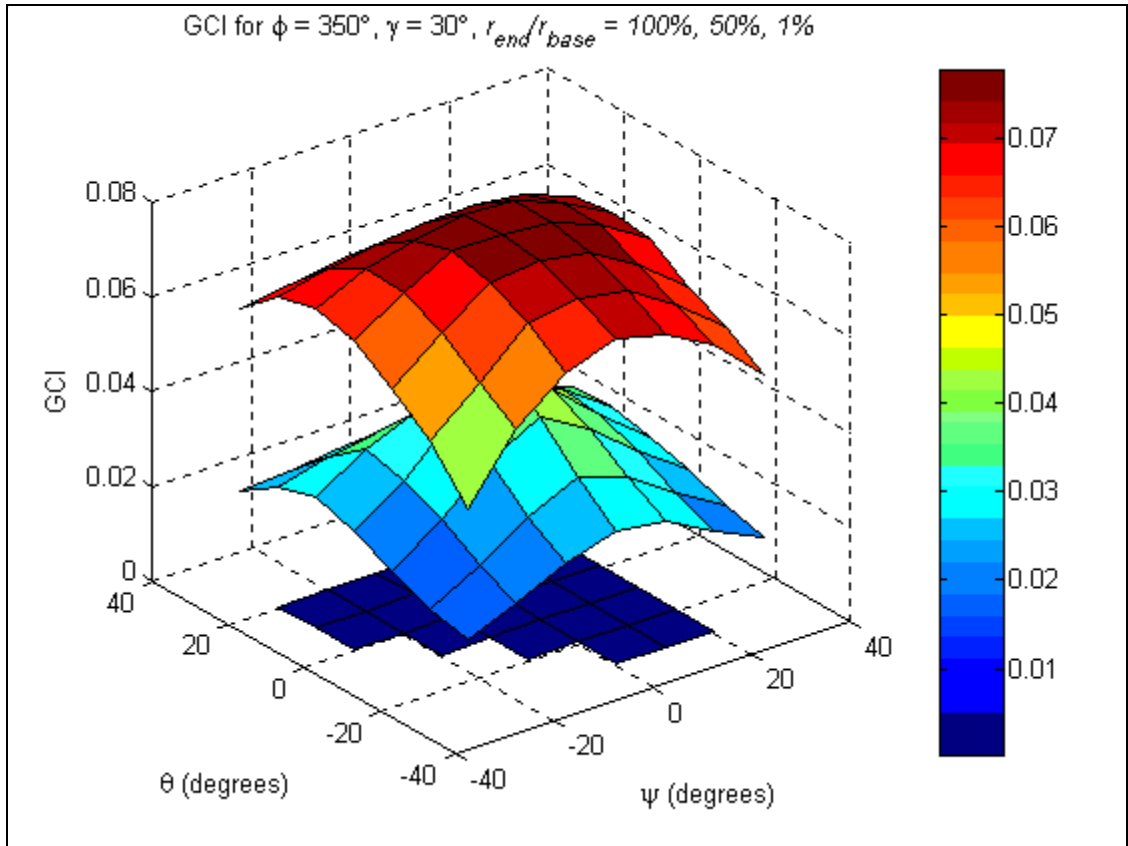


Fig. 3.20b GCI for $\gamma = 30^\circ$, $(r_{end}/r_{base}) = 100\%$, 50% , 1% , and $\phi = 350^\circ$

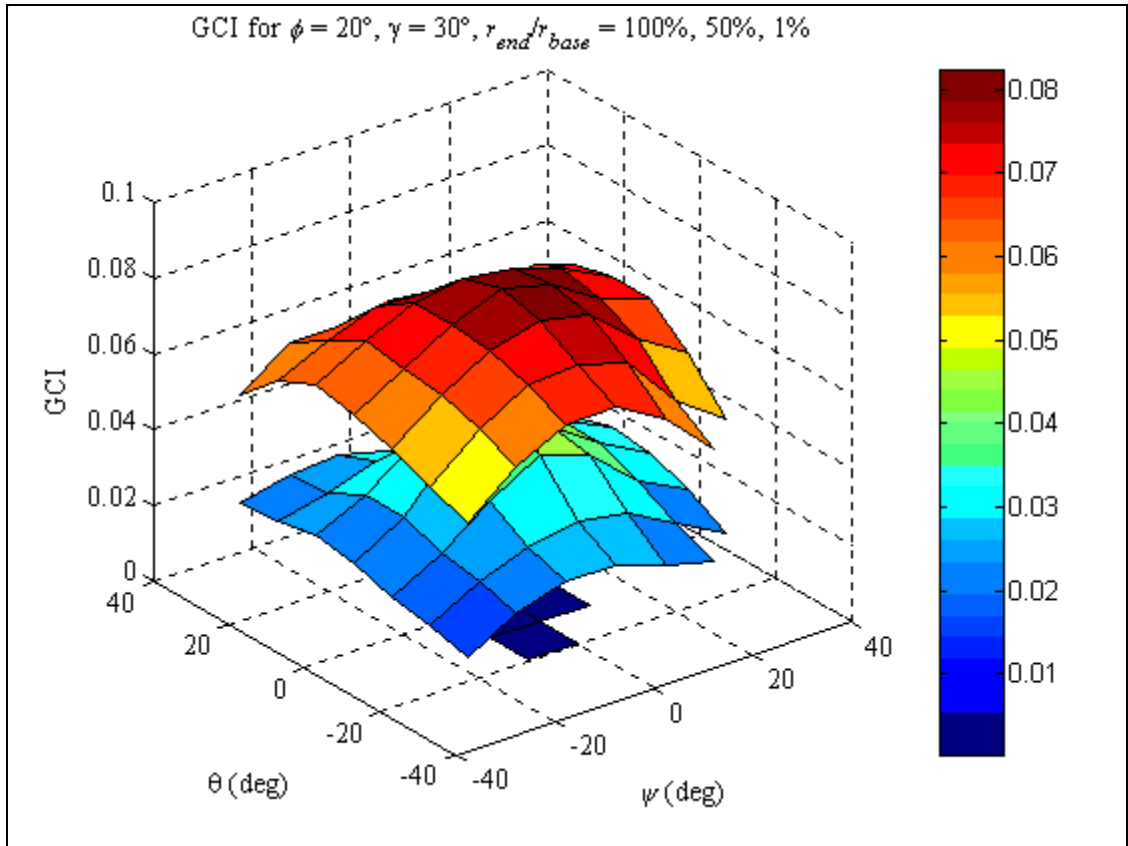


Fig. 3.20c GCI for $\gamma = 30^\circ$, $(r_{end}/r_{base}) = 100\%$, 50% , 1% , and $\phi = 20^\circ$

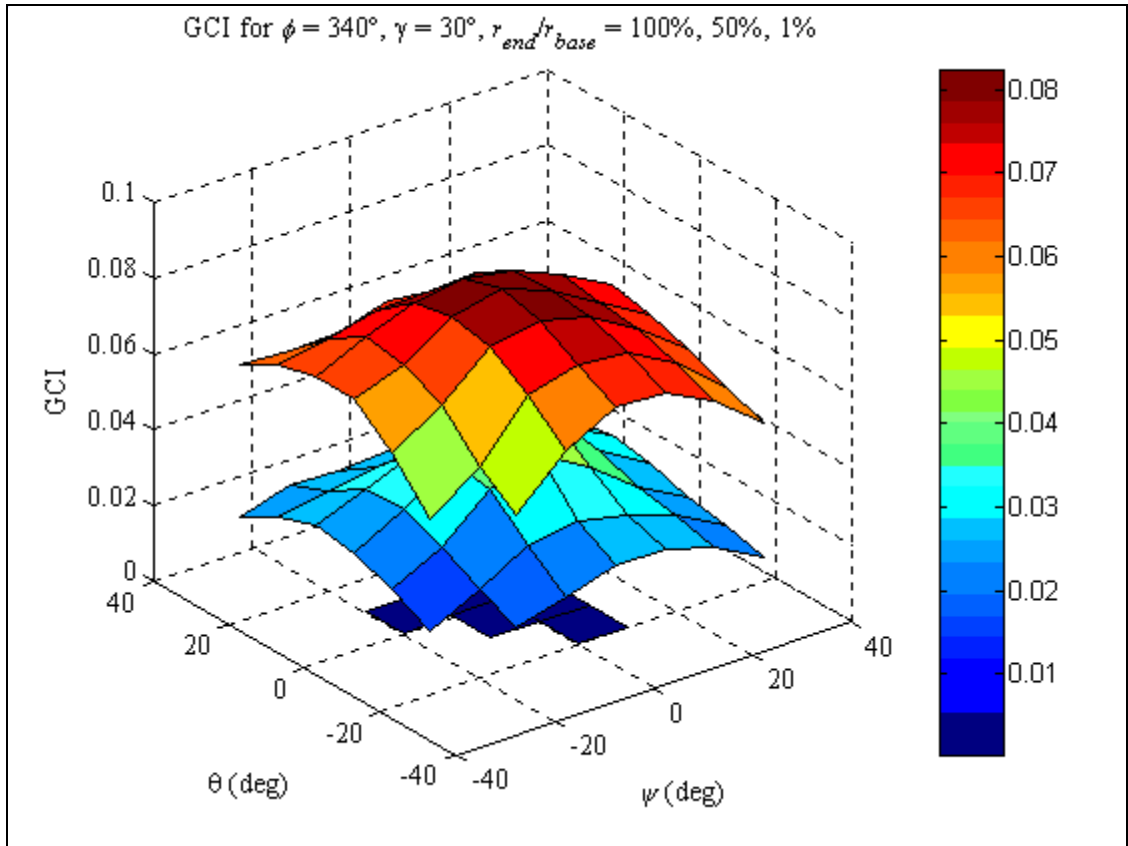


Fig. 3.20d GCI for $\gamma = 30^\circ$, $(r_{end}/r_{base}) = 100\%, 50\%, 1\%$, and $\phi = 340^\circ$

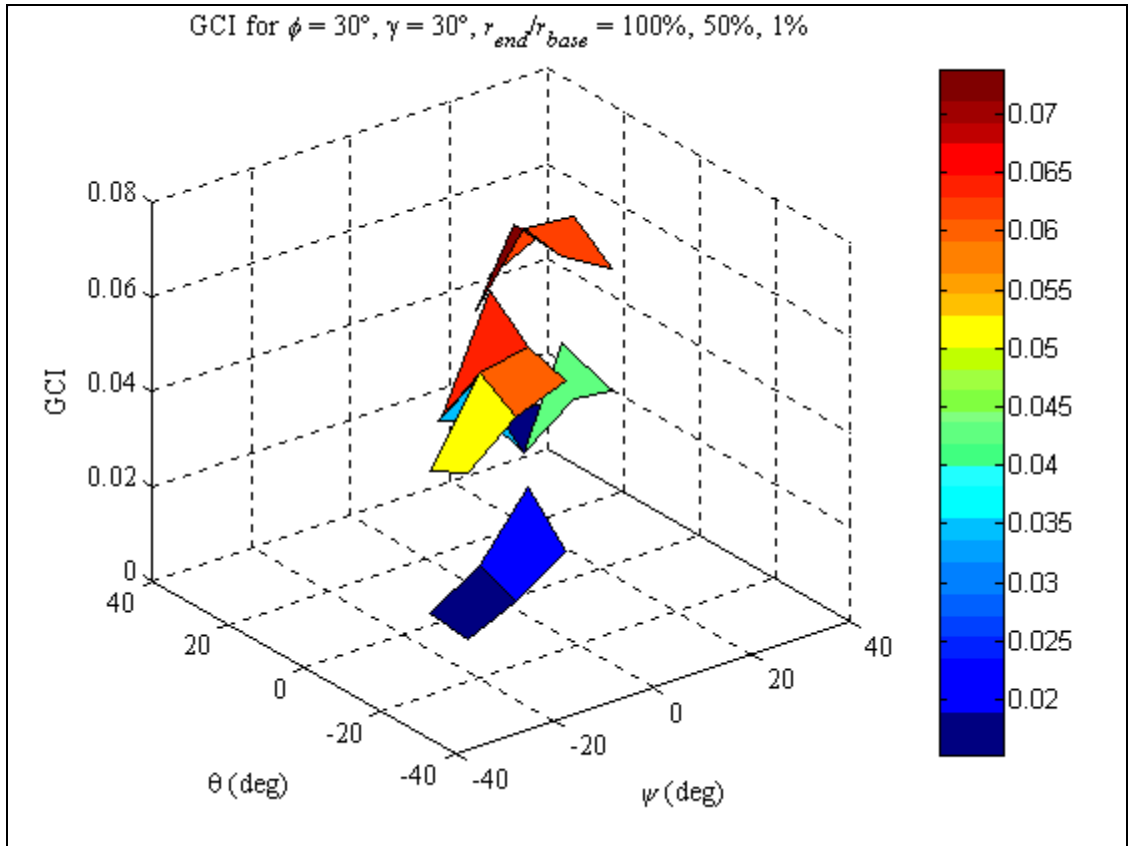


Fig. 3.20e GCI for $\gamma = 30^\circ$, $(r_{end}/r_{base}) = 100\%$, 50% , 1% , and $\phi = 30^\circ$

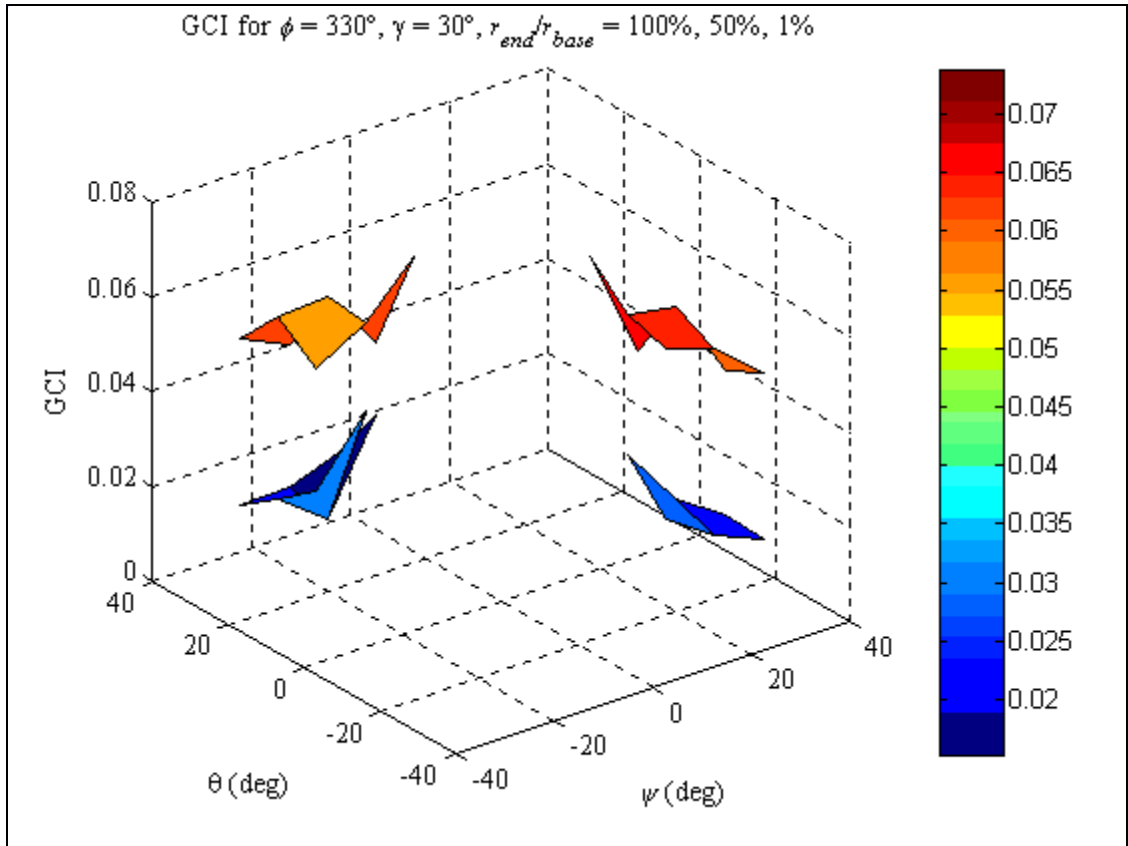


Fig. 3.20f GCI for $\gamma = 30^\circ$, $(r_{end}/r_{base}) = 100\%$, 50% , 1% , and $\phi = 330^\circ$

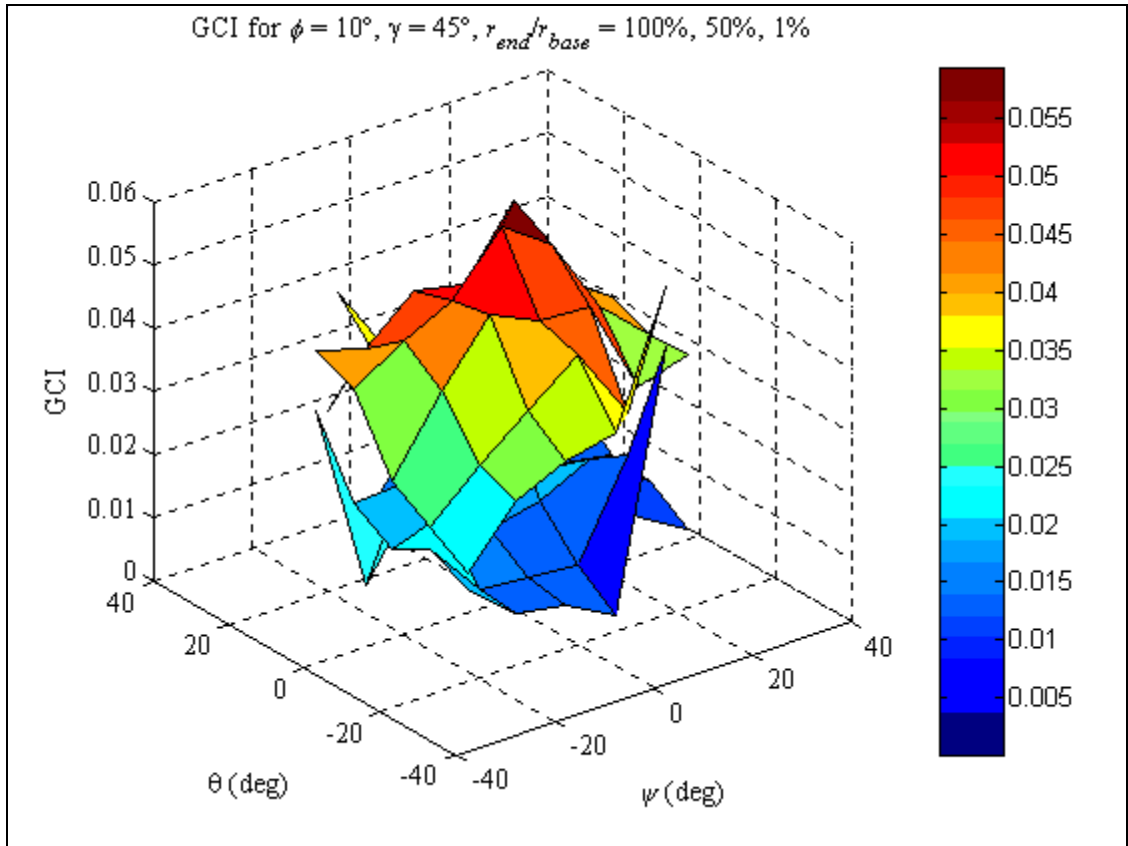


Fig. 3.21a GCI for $\gamma = 45^\circ$, $(r_{end}/r_{base}) = 100\%$, 50% , 1% , and $\phi = 10^\circ$

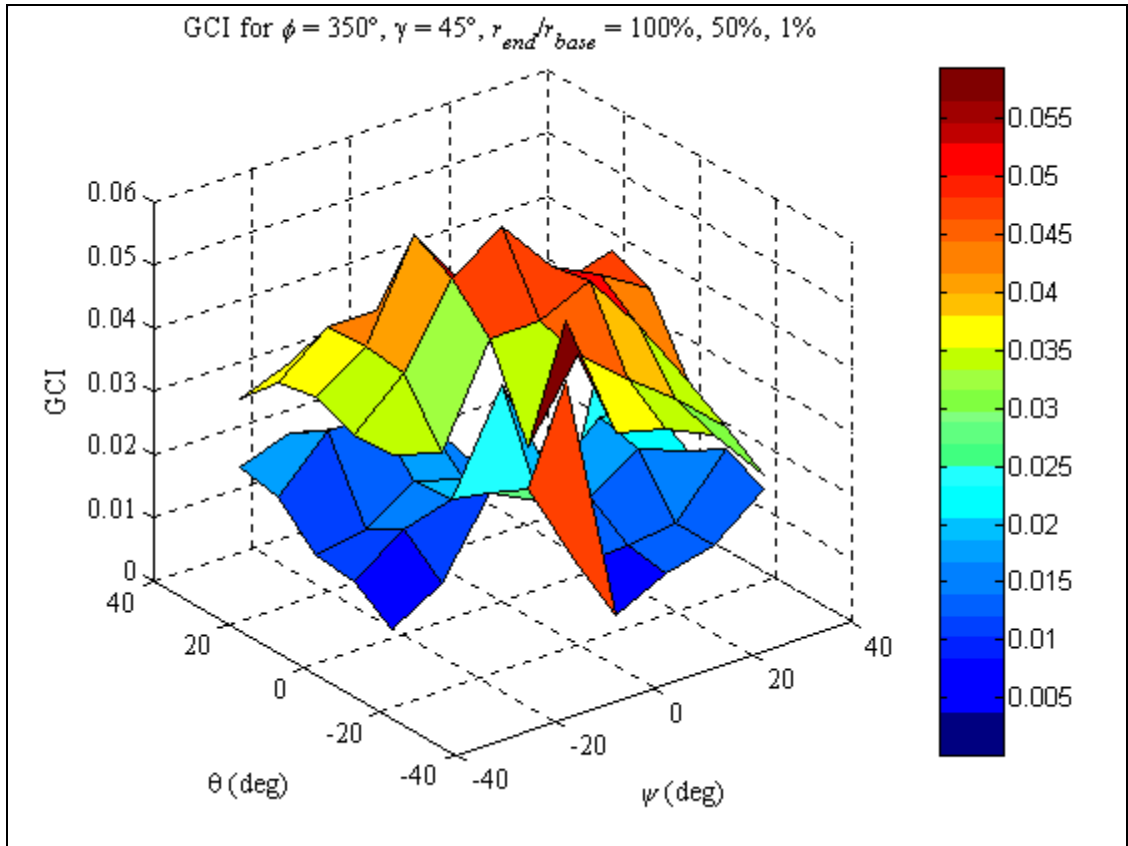


Fig. 3.21b GCI for $\gamma = 45^\circ$, $(r_{end}/r_{base}) = 100\%$, 50% , 1% , and $\phi = 350^\circ$

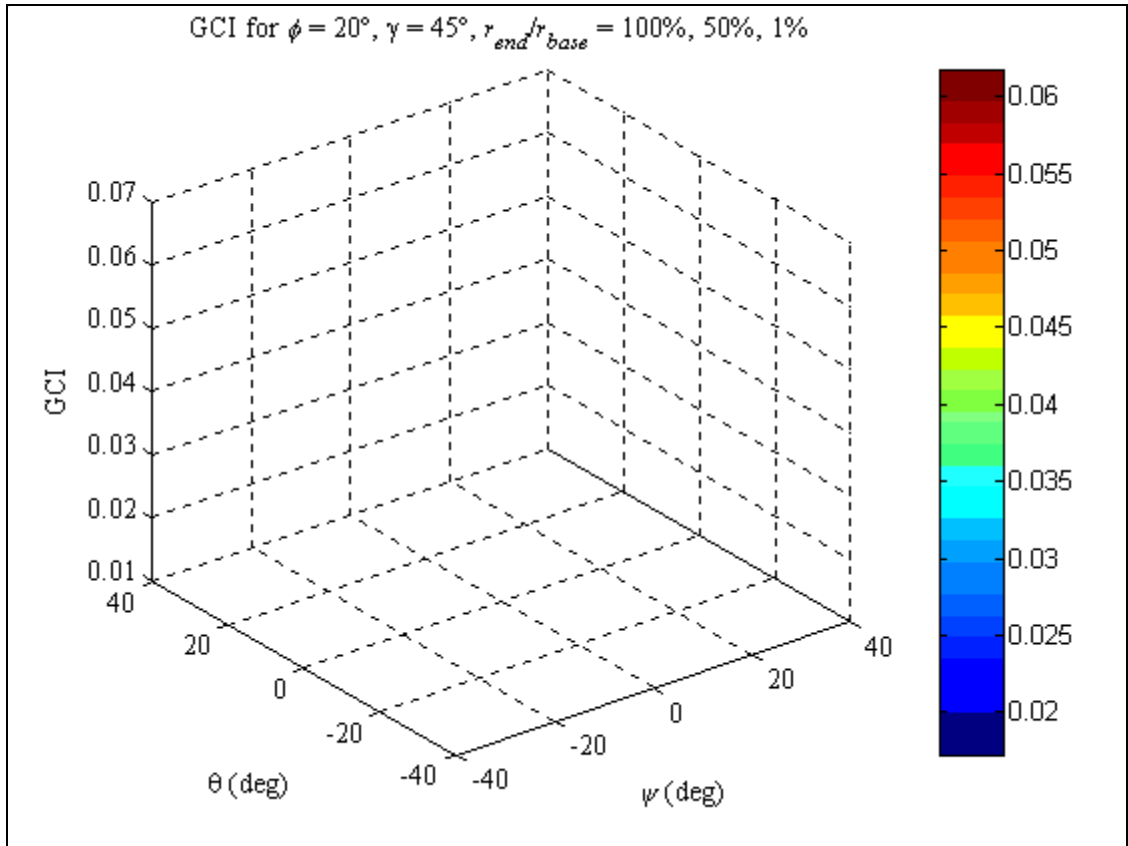


Fig. 3.21c GCI for $\gamma = 45^\circ$, $(r_{end}/r_{base}) = 100\%$, 50% , 1% , and $\phi = 20^\circ$

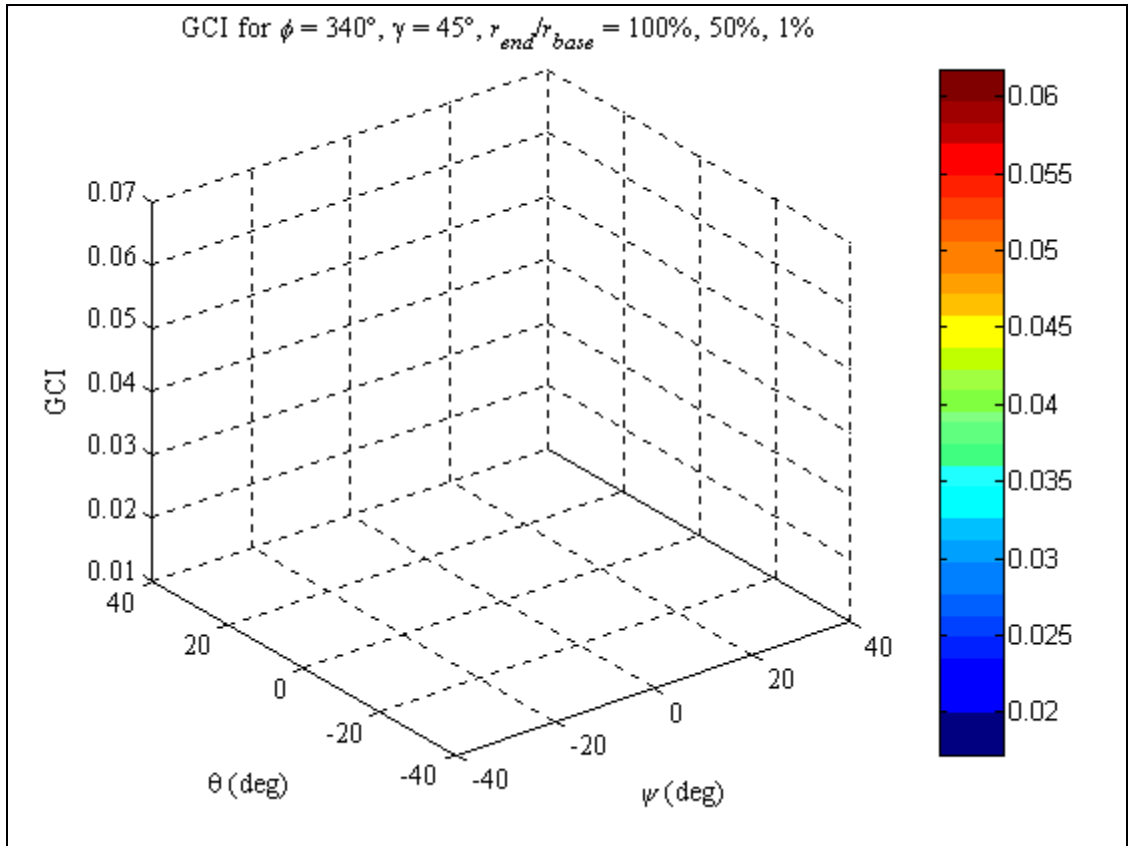


Fig. 3.21d GCI for $\gamma = 45^\circ$, $(r_{end}/r_{base}) = 100\%$, 50% , 1% , and $\phi = 340^\circ$

Appendix C: Geometries

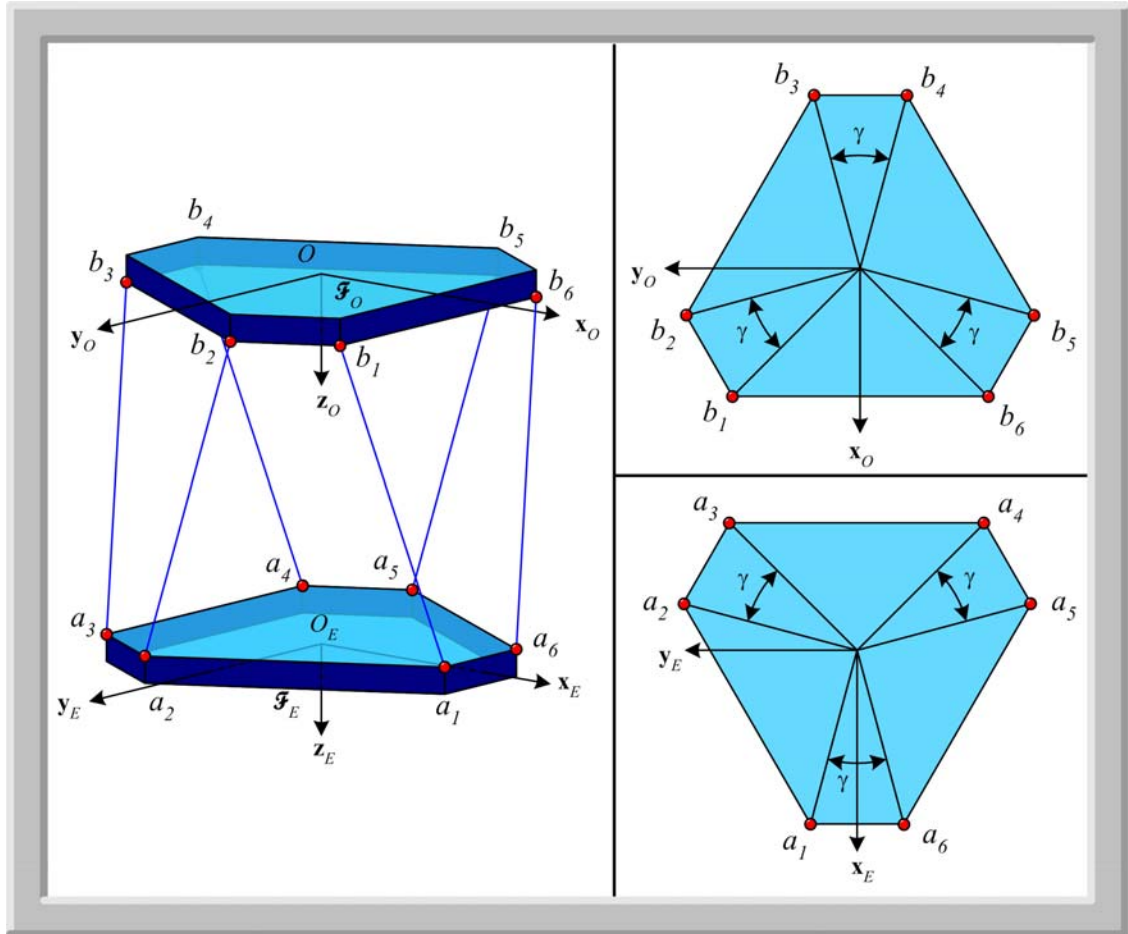


Fig. 3.3c Schematic of BP and MP for $\gamma = 30^\circ$

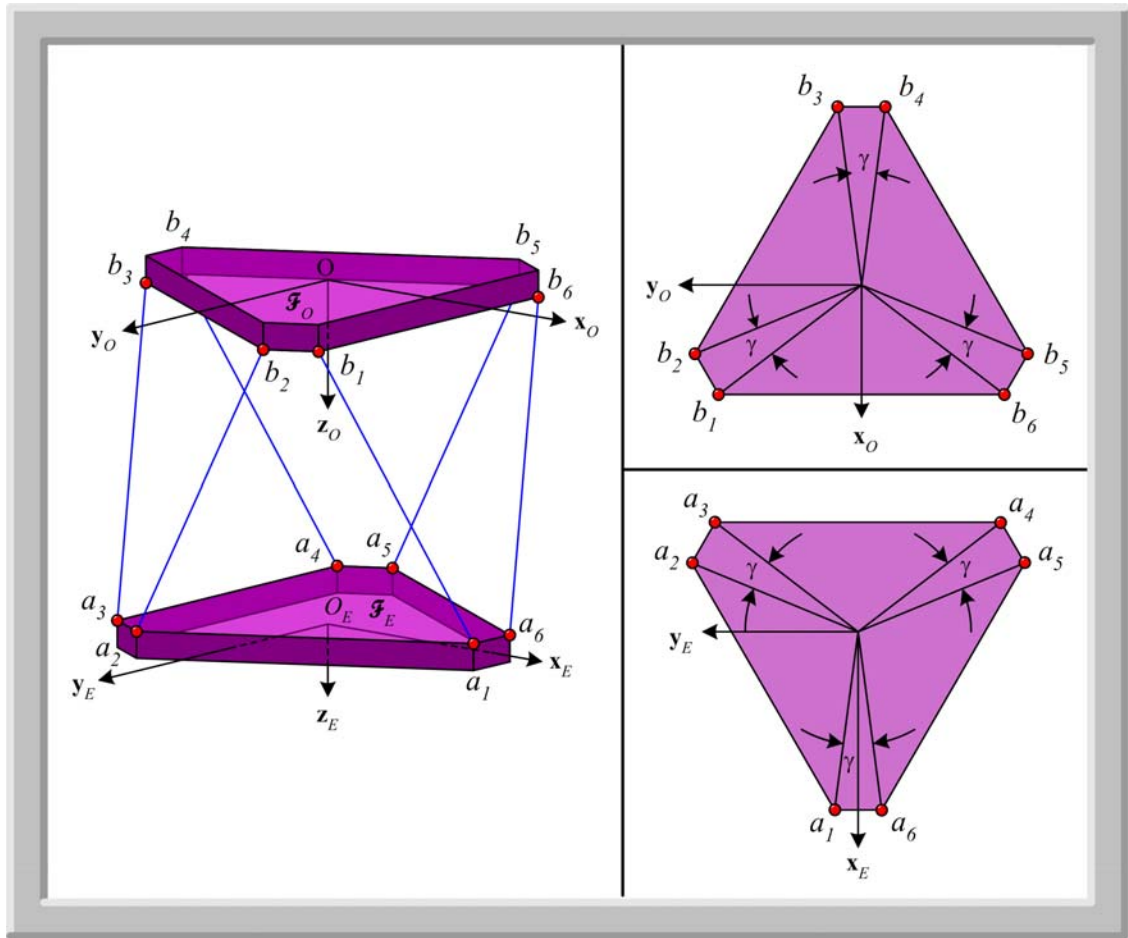


Fig. 3.3d Schematic of BP and MP for $\gamma = 15^\circ$

REFERENCES

1. Merlet, Jean-Pierre, "Parallel Robots", Kluwer Academic Publishers, Boston, Massachusetts, 2000.
2. Das, A., and Saha, H., "Embedding Intelligence in Robot Automated Assembly", Proceedings of the 1st International Conference on Industrial and Engineering Applications of Artificial Intelligence and Expert Systems, Vol. 2, Tullahoma, Tennessee, USA, 1988, pp. 1083-1088.
3. Marcotte, H. R., "Robotics: The New Automation Tool", Proceedings in the 19th IEEE Design Automation Conference, Paper 2.1, 1982, pp. 2-8.
4. Murray, F. J., "Mechanisms and Robots", Journal of the Association for Computing Machinery, Vol. 2, No. 2, April 1955, pp. 61-82.
5. Gough, V. E., and Whitehall, S. G., "Universal Tire Test Machine", In Proceedings of the International Technical Congress F.I.S.I.T.A., Vol. 117, May 1962, pp. 117-135.
6. Stewart, D., "A Platform with Six Degrees of Freedom", Proceedings of Institution of Mechanical Engineers, Vol. 180, Pt. 1, No. 15, 1965-1966, pp. 371-386.
7. Ang, M. H. Jr., Wang, W., Loh, R. N. K., and Low, T. S., "Passive Compliance from Robot Limbs and Its Usefulness in Robotic Automation", Journal of Intelligent System, Vol. 20, 1997, pp. 1-21.
8. Austin, David J., and McCarragher, Brenan J., "Force Control Commanded Synthesis for Constrained Hybrid Dynamic Systems with Friction", International Journal of Robotics Research, Vol. 20, No. 9, September 2001, pp. 753-764.
9. Cetinkunt, S., and Ittoop, B., "Computer-Automated Symbolic Modeling of Dynamics of Robotic Manipulators with Flexible Links", IEEE Transactions on Robotics and Automation, Vol. 8 No. 1, February 1992, pp. 94-105.

10. Goldsmith, P. B., Francis, B. A., and Goldenberg, A. A., "Stability of Hybrid Position/Force Control Applied to Manipulators with Flexible Joints", *International Journal of Robotics and Automation*, Vol. 14, No. 4, 1999, pp. 146-160.
11. Herder, J. L., and de Visser, H., "Force Directed Design of a Voluntary Closing Hand Prosthesis", *Proceedings of the ASME Design Engineering Technical Conference and Computers and Information in Engineering Conference*, Baltimore, Maryland, September 10-13, 2000.
12. Jankowski, K. P., and ElMaraghy, H. A., "Dynamic Decoupling for Hybrid Control of Rigid-/Flexible-Joint Robots Interacting with the Environment", *Robotics and Autonomous Systems*, Vol. 8, No. 5, October 1992, pp. 519-534.
13. Lee, S. H., and Lee, C. W., "Hybrid Control Scheme for Robust Tracking of Two-Link Flexible Manipulator", *Journal of Intelligent and Robotic Systems*, Vol. 32, 2001, pp. 389-410.
14. Lew, J. Y., and Book, W. J., "Dynamics of Two Serially Connected Manipulators", *ASME Dynamic Systems and Control Division Advanced Control Issues for Robot Manipulators*, Vol. 39, November 8-13, 1992, pp. 17-22.
15. Lian, K. Y., Jean, J. H., and Fu, L. C., "Adaptive Force Control of Single-Link Mechanism with Joint Flexibility", *IEEE Transactions on Robotics and Automation*, Vol. 7, No. 4, August 1991, pp. 540-545.
16. Massoud, A. T., ElMaraghy, H. A., and Lahdhiri, T., "On the Robust Nonlinear Motion Position and Force Control of Flexible Joints Robot Manipulators", *Journal of Intelligent and Robotic Systems*, Vol. 25, 1999, pp. 227-254.
17. Matsuno, F., Asano, T., and Sakawa, Y., "Modeling and Quasi-Static Hybrid Position/Force Control of Constrained Planar Two-Link Flexible Manipulators", *IEEE Transactions on Robotics and Automation*, Vol. 10, No. 3, June 1994, pp. 287-297.
18. McInroy, J. E., and Hamann, J. C., "Design and Control of Flexure Jointed Hexapods", *IEEE Transactions on Robotics and Automation*, Vol. 16, No. 4, August 2000, pp. 372-381.
19. Murray, R. M., Li, Z., and Sastry, S. S., "A Mathematical Introduction to Robotic Manipulation", CRC Press, Washington, D.C., 1994.

20. Shiang, W. J., Cannon, D., and Gorman, J., "Optimal Force Distribution Applied to a Robotic Crane with Flexible Cables", Proceedings of the IEEE International Conference on Robotics and Automation, San Francisco, California, April 2000, pp. 1948-1954.
21. Sun, Q., "Control of Flexible-Link Multiple Manipulators", Transactions of the ASME Journal of Dynamic Systems, Measurement, and Control, Vol. 124, March 2002, pp. 67-75.
22. Wang, D., and Vidyasagar, M., "Modeling a Class of Multilink Manipulators with Last Link Flexibility", IEEE Transactions on Robotics and Automation, Vol. 8, No. 1, February 1992, pp. 33-41.
23. Yoshikawa, T., Harada, K., and Matsumoto, A., "Hybrid Position/Force Control of Flexible-Macro/Rigid-Micro Manipulator Systems", IEEE Transactions on Robotics and Automation, Vol. 12, No. 4, August 1996, pp. 633-640.
24. Abdel-Malek, K., and Paul, B., "Criteria for the Design of Manipulator Arms of a High Stiffness to Weight Ratio", SME Journal of Manufacturing Systems, Vol. 17, No. 3, pp. 209-220.
25. Agirrebeitia, J., Aviles, R., de Bustos, I. F., and Ajuria, G., "A Method for the Study of Position in Highly Redundant Multibody Systems in Environments with Obstacles", IEEE Transactions on Robotics and Automation, Vol. 18, No. 2, April 2002, pp. 257-262.
26. Bruyninckx, H., and Khatib, O., "Gauss' Principle and the Dynamics of Redundant and Constrained Manipulators", Proceedings of the IEEE International Conference on Robotics and Automation, San Francisco, CA, April 2000, pp. 2563-2568.
27. English, J. D., and Maciejewski, A. A., "On the Implementation of Velocity Control for Kinematically Redundant Manipulators", IEEE Transactions on Systems, Manufacturing, and Cybernetics – Part A: Systems and Human, Vol. 30, No. 3, May 2000, pp. 233-237.
28. Groom, K. N., Maciejewski, A. A., and Balakrishnan, V., "Real-Time Failure-Tolerant Control of Kinematically Redundant Manipulators", IEEE Transactions on Robotics and Automation, Vol. 15, No. 6, December 1999, pp. 1109-1116.
29. Gu, E. Y. L., "A Configuration Manifold Embedding Model for Dynamic Control of Redundant Robots", The International Journal of Robotics Research, Vol. 19, No. 3, March 2000, pp. 289-304.

30. Jankowski, K. P., and ElMaraghy, H. A., "Robust Hybrid Position/Force Control of Redundant Robots", *Robotics and Autonomous Systems*, Vol. 27, 1999, pp. 111-127.
31. Kim, J., Park, F. C., Ryu, S. J., Kim, J., Hwang, J. C., Park, C., and Iurascu, C. C., "Design and Analysis of a Redundantly Actuated Parallel Mechanism for Rapid Machining", *IEEE Transactions on Robotics and Automation*, Vol. 17, No. 4, August 2001, pp. 423-434.
32. Lee, Sukhan, "Dual Redundant Arm Configuration Optimization with Task-Oriented Dual Arm Manipulability", *IEEE Transactions on Robotics and Automation*, Vol. 5, No. 1, February 1989, pp. 78-97.
33. Liu, G. F., Wu, Y. L., Wu, X. Z., Kuen, Y. Y., and Li, Z. X., "Analysis and Control of Redundant Parallel Manipulators", *Proceedings of the IEEE International Conference on Robotics and Automation*, Seoul, Korea, May 21-26, 2001, pp. 3748-3754.
34. Van Den Doel, K., and Pai, D. K., "Performance Measures for Constrained Systems", *IEEE Transactions on Robotics and Automation*, Vol. 13, No. 2, April 1997, pp. 278-289.
35. Wampler, C. W., II, "Inverse Kinematic Functions for Redundant Spherical Wrists", *IEEE Transactions on Robotics and Automation*, Vol. 5, No. 1, February 1989, pp. 106-111.
36. Yi, B. J., and Freeman, R. A., "Geometric Analysis Antagonistic Stiffness in Redundantly Actuated Parallel Mechanisms", *Journal of Robotic Systems*, Vol. 10, No. 5, 1993, pp. 581-603.
37. Bicchi, A., and Prattichizzo, D., "Manipulability of Cooperating Robots with Unactuated Joints and Closed-Chain Mechanisms", *IEEE Transactions on Robotics and Automation*, Vol. 16, No. 4, August 2000, pp. 336-345.
38. Chai, K. S., and Young, K., "Designing a Stewart Platform-Based Cooperative System for Large Component Assembly", *IEEE International Conference on Methods and Models in Automation and Robotics*, 2001.
39. Chang, K. S., Holmberg, R., and Khatib, O., "The Augmented Object Model: Cooperative Manipulation and Parallel Mechanism Dynamics", *Proceedings of the IEEE Conference on Robotics and Automation*, San Francisco, California, April 2000, pp. 470-475.

40. Kwon, W., and Lee, B. H., "General Redundancy Optimization Method for Cooperating Manipulators Using Quadratic Inequality Constraints", *IEEE Transactions on Systems, Manufacturing, and Cybernetics-Part A: Systems and Humans*, Vol. 29, No. 1, January 1999, pp. 41-51.
41. Kwon, W., and Lee, B. H., "A New Optimal Force Distribution Scheme of Multiple Cooperating Robots Using Dual Method", *Journal of Intelligent and Robotic Systems*, Vol. 21, 1998, pp. 301-326.
42. Li, Z., Tarn, T. J., and Bejczy, A., "Dynamic Workspace Analysis of Multiple Cooperating Robot Arms", *IEEE Transactions on Robotics and Automation*, Vol. 7, No. 5, October 1991, pp. 589-596.
43. Parra-Vega, V., Rodriguez-Angeles, A., Arimoto, S., and Hirzinger, G., "High Precision Constrained Grasping with Cooperative Adaptive Hand Control", *Journal of Intelligent and Robotic Systems*, Vol. 32, 2001, pp. 235-254.
44. Zribi, M., Loulin, H., and Piu, C. S., "Position and Force Control of Two Constrained Robotic Manipulators", *Journal of Intelligent and Robotics Systems*, Vol. 24, 1999, pp. 1-22.
45. Marquet, F., Company, O., Krut, S., Gascuel, O., and Pierrot, F., "Control of a 3-DOF Over-Actuated Parallel Mechanism", In *Proceedings of the 2002 ASME International DETC/CIE: Design Engineering Technical Conference and Computer and Information in Engineering Conference*, Montreal, Canada, September 29 to October 2, 2002.
46. Marquet, F., Krut, S., Company, O., and Pierrot, F., "ARCHI: A New Redundant Parallel Mechanism: Modeling, Control, and First Results", In *Proceedings of the IROS 2001: 2001 IEEE/RSJ International Conference on Intelligent Robots and Systems*, Maui, Hawaii, USA, October 29 to November 3, 2001.
47. Wang, Y., Newman, W. S., and Stoughton, R. S., "Workspace Analysis of the ParaDex Robot – A Novel, Closed-Chain Kinematically-Redundant Manipulator", *Proceedings of the 2000 IEEE International Conference on Robotics and Automation*, San Francisco, California, April 2000, pp. 2392-2397.
48. Krut, S., Company, O., Rangsi, S., and Pierrot, F., "Eureka: A New 5-Degree-of-Freedom Redundant Parallel Mechanism with High Tilting Capabilities", *Proceedings of the 2003 IEEE/RSJ International Conference on Intelligent Robots and Systems*, Las Vegas, Nevada, October 2003, pp. 3575-3580.

49. Adelstein, B. D., Ho, P., and Kazerooni, H., "Kinematic Design of a Three Degree of Freedom Parallel Hand Controller Mechanism", In Proceedings of the ASME Dynamic Systems and Control Division, Vol. 58, 1996, pp. 539-546.
50. Caffaz, A., and Cannata, G., "The Design of Development of the DIST-Hand Dexterous Gripper", Proceedings of the 1998 IEEE International Conference on Robotics and Automation, Leuven, Belgium, May 1998, pp. 2075-2080.
51. Lee, J. J., and Tsai, L. W., "Structural Synthesis of Multi-Fingered Hands", Transactions of the ASME Journal of Mechanical Design, Vol. 124, June 2002, pp. 272-276.
52. Liu, H., Meusel, P., Butterfass, J., and Hirzinger, G., "DLR's Multisensory Articulated Hand Part II: The Parallel Torque/Position Control System", Proceedings of the 1998 IEEE International Conference on Robotics and Automation, Leuven, Belgium, May 1998, pp. 2087-2093.
53. Yi, B. J., Na, H. Y., Lee, J. H., Hong, Y. S., Oh, S. R., Suh, I. H., and Kim, W. K., "Design of a Parallel-Type Gripper Mechanism", The International Journal of Robotics Research, Vol. 21, No. 7, July 2002, pp. 661-676.
54. Akella, P. N., and Cutkosky, M. R., "Contact Transition Control with Semiactive Soft Fingertips", IEEE Transactions on Robotics and Automation, Vol. 11, No. 6, December 1995, pp. 859-867.
55. Huang, H. P., and Wei, Y. F., "Control of Dexterous Hand Master with Force Feedback", Proceedings of the 1998 IEEE International Conference on Robotics and Automation, Leuven, Belgium, May 1998, pp. 687-692.
56. Kawarazaki, N., Hasegawa, T., and Nishihara, K., "Grasp Planning Algorithm for a Multifingered Hand-Arm Robot", Proceedings of the IEEE International Conference on Robotics and Automation, Leuven, Belgium, May 1998, pp. 933-939.
57. Schlegl, T., and Buss, M., "Hybrid Closed-Loop Control of Robotic Hand Regrasping", Proceedings of the 1998 IEEE International Conference on Robotics and Automation, Leuven, Belgium, May 1998, pp. 3026-3031.
58. Springer, Scott L., and Ferrier, Nicola J., "Design and Control of a Force Reflecting Haptic Interface for Teleoperational Grasping", Transactions of the ASME Journal of Mechanical Design, Vol. 124, ASME, June 2002, pp. 277-283.

59. Trinkle, J. C., "On the Stability and Instantaneous Velocity of Grasped Frictionless Objects", *IEEE Transactions on Robotics and Automation*, Vol. 8, No. 5, October 1992, pp. 560-572.
60. Tzafestas, C., and Coiffet, P., "Computing Optimal Forces for Generalized Kinesthetic Feedback on the Human Hand during Virtual Grasping and Manipulation", *Proceedings of the 1997 IEEE International Conference on Robotics and Automation*, Albuquerque, New Mexico, April 1997, pp. 118-123.
61. Clark, J. E., Chan, J. G., Bailey, S. A., Froehlich, E. M., Nahata, P. K., Full, R. J., and Cutkosky, M. R., "Biometric Design and Fabrication of a Hexapedal Running Robot", 2001, *IEEE International Conference on Robotics and Automation*, 2001.
62. De Lasa, M., and Buehler, M., "Dynamic Compliant Walking of a Quadruped Robot: Preliminary Experiments", *Proceedings of the 3rd International Conference on Climbing and Walking Robots*, Madrid, Spain, October 2000.
63. Fukuoka, Y., Kimura, H., and Cohen, A. H., "Adaptive Dynamic Walking of a Quadruped Robot on Irregular Terrain Based on Biological Concepts", *The International Journal of Robotics Research*, Vol. 22, No. 3-4, March-April 2003, pp. 187-202.
64. Silva, M. F. and Tenreiro Machado, J. A., "Position and Force Control of Walking Hexapod", *Proceedings of ICAR2003 The 11th International Conference on Advanced Robotics*, Coimbra, Portugal, June 30 – July 3, 2003.
65. Su, C., and Zheng, Y. F., "Task Decomposition for a Multi-limbed Robot to Work in Reachable But Unorientable Space", *IEEE Transactions on Robotics and Automation*, Vol. 7, No. 6, December 1991, pp. 759-770.
66. Zabalza, I., Ros, J., Gil, J. J., Pintor, J. M., and Jimenez, J. M., "TRI-SCOTT A New Kinematic Structure for a 6-DOF Decoupled Parallel Manipulator", *Proceedings of the Workshop on Fundamental Issues and Future Research Directions for Parallel Mechanisms and Manipulators*, Quebec City, Quebec, Canada, October 3-4, 2002, pp. 12-15.
67. Guglielmetti, P., and Longchamp, R., "A Closed Form Inverse Dynamics Model of the Delta Parallel Robot", *Proceedings of International Federation of Automatic Control Conference on Robot Control*, Capri, Italy, 1994, pp. 39-44.
68. Miller, K., "Experimental Verification of Modeling of DELTA Robot Dynamics by Direct Application of Hamilton's Principle", *Proceedings of IEEE International Conference on Robotics and Automation*, 1995, pp. 532-537.

69. Petitt, J., and Miller, K., "Evolutionary Algorithm for Robot Task Space Optimization", Proceedings of the 11th World Congress in Mechanism and Machine Science, Tianjin, China, August 18-21, 2003.
70. Stock, M., and Miller, K., "Optimal Kinematic Design of Spatial Parallel Manipulators: Application to Linear Delta Robot", Transactions of the ASME Journal of Mechanical Design, Vol. 125, June 2003, pp. 292-301.
71. Miller, K., and Clavel, R., "The Lagrange-Based Model of Delta-4 Robot Dynamics", Robotersysteme, Vol. 8, 1992, pp. 49-54.
72. Ceccarelli, M. Fino, P. M. D., and Jimenez, J. M., "Dynamic Performance of CaPaMan by Numerical Simulations", Mechanism and Machine Theory, Vol. 37, 2002, pp. 241-266.
73. Hopkins, B. R., and Williams, R. L. II, "Modified 6-PSU Platform", Proceedings of DETC2002, 2002 ASME Design Engineering Technical Conference, Montreal, Canada, September 29 – October 2, 2002.
74. Nenchev, D. N., and Uchiyama, M., "PARA-ARM: A Five-Bar Parallel Manipulator with Singularity-Perturbed Design", Mechanism and Machine Theory, Vol. 33, No. 5, 1998, pp. 453-462.
75. Gosselin, M. C., and Hamel, J. F., "The Agile Eye: A High-Performance Three-Degree-Of-Freedom Camera-Orienting Device", Proceedings of IEEE International Conference on Robotics and Automation, 1994, pp. 781-786.
76. Clinton C. M., Zhang, G., and Wavering, A. J., "Stiffness Modeling of a Stewart-Platform-Based Milling Machine", Institute for Systems Research (ISR) Sponsored by the National Science Foundation Engineering Research Center Program the University of Maryland, Harvard University and Industry, Technical Research Report, Vol. 29, 1997.
77. Company, O., Krut, S., and Pierrot, F., "Modeling and Preliminary Design Issues of a 4-Axis Parallel Machine for Heavy Parts Handling", In Proceedings of the International Mechanical Engineer Journal of Multibody Dynamics, Vol. 216, Special Issue, Part K, January 2002, pp. 1-11.
78. Lee, C. D., Lawrence, D. A., and Pao, L. Y., "Guaranteed Convergence Rates for Five Degree of Freedom In-Parallel Haptic Interface Kinematics", Proceedings of the IEEE International Conference on Robotics and Automation, Detroit, MI, May 1999.

79. Arai, T., Cleary, K., Homma, K., Adachi, H., and Nakamura, T., "Development of Parallel Link Manipulator for Underground Excavation Task", Proceedings of International Symposium on Advanced Robot Technology, 1991, pp. 541-548.
80. Bryfogle, M. D., Nguyen, C. C., Antrazi, S. S., and Chiou, P. C., "Kinematics and Control of a Fully Parallel Force-Reflecting Hand Controller for Manipulator Teleoperation", Journal of Robotic Systems, Vol. 10, No. 5, 1993, pp. 745-766.
81. Collins, C. L., and Long, G. L., "The Singularity Analysis of an In-Parallel Hand Controller for Force-Reflected Teleoperation", IEEE Transaction on Robotics and Automation, Vol. 11, No. 5, October 1995, pp. 661-669.
82. Hollerbach, J. M., and Lokhorst, D. M., "Closed-Loop Kinematic Calibration of the RSI 6-DOF Hand Controller", IEEE Transactions on Robotics and Automation, Vol. 11, No. 3, June 1995, pp. 352-359.
83. Fajardo, P., and Rey-Bakaikoa, V., "Control of Six Degrees-of-Freedom Parallel Manipulators for Synchrotron Radiation Applications", Review of Scientific Instruments, Vol. 66, No. 2, February 1995, pp. 1758-1760.
84. Geng, Z., and Haynes, L. S., "Six-Degree-of-Freedom Active Vibration Isolation Using a Stewart Platform Mechanism", Journal of Robotic Systems, Vol. 10, No. 5, 1993, pp. 725-744.
85. Aracil, R., Saltaren, R., and Reinoso, O., "Parallel Robots for Autonomous Climbing along Tubular Structures", Robotics and Autonomous Systems, Vol. 42, 2003, pp. 125-134.
86. Wang, J., and Liu, X. J., "Analysis of a Novel Cylindrical 3-DoF Parallel Robot", Robotics and Autonomous Systems, Vol. 42, 2003, pp. 31-46.
87. Bombin, C., Ros, L., and Thomas, F., "On the Computation of the Direct Kinematics of Parallel Spherical Mechanisms Using Bernstein Polynomials", Proceedings of the 2001 IEEE International Conference on Robotics and Automation, Seoul, Korea, May 21-26, 2001, pp. 3332-3337.
88. Gosselin, C. M., "Static Balancing of Spherical 3-DOF Parallel Mechanisms and Manipulators", The International Journal of Robotics Research, Vol. 18, No. 7, August 1999, pp. 819-829.
89. Gosselin, C. M., and Wang, J., "Singularity Loci of a Special Class of Spherical Three-Degree-of-Freedom Parallel Mechanism with Revolute Actuators", The International Journal of Robotics Research, Vol. 21, No. 7, July 2002, pp. 649-659.

90. Kim, W. K., Yi, B. J., and Cho, W., "RCC Characteristics of Planar/Spherical Three Degree-of-Freedom Parallel Mechanisms with Joint Compliances", Transactions of the ASME Journal of Mechanical Design, Vol. 122, March 2000, pp. 10-16.
91. Yang, G., Ho, E. H. L., Lin, W., and Chen, I. M., "A Differential Approach for the Workspace Analysis of Spherical Parallel Manipulators", Proceedings of the 11th World Congress in Mechanism and Machine Science, Tianjin, China, August 18-21, 2003.
92. Callegari, M., and Tarantini, M., "Kinematic Analysis of a Novel Translational Platform", Transactions of the ASME Journal of Mechanical Design, Vol. 125, June 2003, pp. 308-315.
93. Carretero, J. A., Podhorodeski, R. P., Nahon, M. A., and Gosselin, C. M., "Kinematic Analysis and Optimization of a New Three Degree-of-Freedom Spatial Parallel Manipulator", Transactions of the ASME Journal of Mechanical Design, Vol. 122, March 2000, pp. 17-24.
94. Carricato, M., and Parenti-Castelli, V., "A Family of 3-DOF Translational Parallel Manipulators", Transactions of the ASME Journal of Mechanical Design, Vol. 125, June 2003, pp. 302-307.
95. Carricato, M., and Parenti-Castelli, V., "Position Analysis of a New Family of 3-DOF Translational Parallel Manipulators", Transactions of the ASME Journal of Mechanical Design, Vol. 125, June 2003, pp. 316-322.
96. Carricato, M., and Parenti-Castelli, V., "Singularity-Free Fully-Isotropic Translational Parallel Mechanisms", The International Journal of Robotics Research, Vol. 21, No. 2, February 2002, pp. 161-174.
97. Di Gregorio, R., and Parenti-Castelli, V., "Mobility Analysis of the 3-UPU Parallel Mechanism Assembled for a Pure Translational Motion", Transactions of the ASME Journal of Mechanical Design, Vol. 124, June 2002, pp. 259-264.
98. Ji, P., and Wu, H., "Kinematics Analysis of an Offset 3-UPU Translational Parallel Robotic Manipulator", Robotics and Automation, Vol. 42, 2003, pp. 117-123.
99. Kim, D., and Chung, W. K., "Kinematic Condition Analysis of Three-DOF Pure Translational Parallel Manipulators", Transactions of ASME Journal of Mechanical Design, Vol. 125, June 2003, pp. 323-331.

100. Kim, H. S., and Tsai, L. W., "Design Optimization of a Cartesian Parallel Manipulator", Proceedings of the ASME 2002 Design Engineering Technical Conference and Computers and Information in Engineering Conference, Montreal, Canada, September 29 – October 2, 2002.
101. Kong, X., and Gosselin, C. M., "Kinematic and Singularity Analysis of a Novel Type of 3-CRR 3-DOF Translational Parallel Manipulator", The International Journal of Robotics Research, Vol. 21, No. 9, September 2002, pp. 791-798.
102. Romdhane, L., Affi, Z., and Fayet, M., "Design and Singularity Analysis of a 3-Translational-DOF In-Parallel Manipulator", Transactions of the ASME Journal of Mechanical Design, Vol. 124, September 2002, pp. 419-426.
103. Stamper, R. E., Tsai, L. W., and Walsh, G. C., "Optimization of a Three DOF Translational Platform for Well-Conditioned Workspace", Institute for Systems Research (ISR) Sponsored by the National Science Foundation Engineering Research Center Program the University of Maryland, Harvard University and Industry, Technical Research Report, Vol. 71, 1997.
104. Tsai, L. W., and Stamper, R. E., "A Parallel Manipulator with Only Translational Degrees of Freedom", Institute for Systems Research (ISR) Sponsored by the National Science Foundation Engineering Research Center Program the University of Maryland, Harvard University and Industry, Technical Research Report, Vol. 72, 1997.
105. Du Plessis, L. J., Snyman, J. A., and Smit, W. J., "A Configurationally Adjustable Planar Stewart Platform Machining Center with Feasible and Optimum Placement of Workspace Relative to Toolpath", Proceedings of ASME Design Engineering Technical Conferences and Computers Information in Engineering Conference, Baltimore, MD, September 10-13, 2000.
106. Fattah, A., and Agrawal, S. K., "Design of Cable-Suspended Parallel Robots for Optimal Workspace", Proceedings of the Workshop on Fundamental Issues and Future Research for Parallel Mechanisms and Manipulators, Québec City, Québec, Canada, October 3-4, 2002, pp. 195-202.
107. Fattah, A., and Agrawal, S. K., "Workspace and Design Analysis of Cable-Suspended Planar Parallel Robots", ASME Design Engineering Technical Conference and Information in Engineering Conference, Montreal, Canada, September 29 – October 2, 2002.

108. Gallant, M., and Boudreau, R., "The Synthesis of Planar Parallel Manipulators with Prismatic Joints for an Optimal, Singularity-Free Workspace", *Journal of Robotic Systems*, Vol. 19, No. 1, 2002, pp. 13-24.
109. Gallina, P., Rosati, G., and Rossi, A., "3-D.O.F. Wire Driven Planar Haptic Interface", *Journal of Intelligent and Robotic Systems*, Vol. 32, 2001, pp. 23-36.
110. Heerah, I., Benhabib, B., Kang, B., and Mills, J. K., "Architecture Selection and Singularity Analysis of a Three-Degree-of-Freedom Planar Parallel Manipulator", *Journal of Intelligent and Robotic Systems*, Vol. 37, 2003, pp. 355-374.
111. Kong, X., and Gosselin, C. M., "Generation and Forward Displacement Analysis of RPR-PR-RPR Analytic Planar Parallel Manipulators", *Transactions of the ASME Journal of Mechanical Design*, Vol. 124, June 2002, pp. 294-300.
112. Roberts, R. G., Graham, T., and Lippitt, T., "On the Inverse Kinematics, Statics, and Fault Tolerance of Cable-Suspended Robots", *Journal of Robotic Systems*, Vol. 15, No. 10, 1998, pp. 581-597.
113. Roberts, R. G., Graham, T., and Trumpower, J. M., "On the Inverse Kinematics and Statics of Cable-Suspended Robots", *Proceedings of the IEEE International Conference on Robotics and Automation*, October 12-15, 1997, pp. 4291-4296.
114. Theingi, Chen, I. M., Li, C., and Angeles, J., "Managing Singularities of 3-DOF Planar Parallel Manipulators Using Joint-Coupling", In *Proceedings of the 11th World Congress in Mechanism and Machine Science*, Tianjin, China, August 18-21, 2003.
115. Wen, J. T., "Singularities in Three-Legged Platform-Type Parallel Manipulators", *IEEE Transactions on Robotics and Automation*, Vol. 19, No. 4, August 2003, pp. 720-726.
116. Williams, R. L. II, and Gallina, P., "Planar Cable-Direct-Driven Robots: Design for Wrench Exertion", *Journal of Intelligent and Robotic Systems*, Vol. 35, 2002, pp. 203-219.
117. Williams, R. L. II, and Gallina, P., "Planar Cable-Direct-Driven Robots, Part 1: Kinematics and Statics", *Proceedings of the 2001 ASME Design Technical Conference 27th Design Automation Conference*, Pittsburgh, PA, September 9-12, 2001.

118. Williams, R. L. II, and Gallina, P., "Planar Cable-Direct-Driven Robots, Part 2: Dynamics and Control", Proceedings of the 2001 ASME Design Technical Conferences 27th Design Automation Conference, Pittsburgh, PA, September 9-12, 2001.
119. Williams, R. L. II, and Joshi, A. R., "Planar Parallel 3-RPR Manipulator", Proceedings of the Sixth Conference on Applied Mechanisms and Robotics, Cincinnati, OH, December 12-15, 1999.
120. Williams, R. L. II, and Shelley, B. H., "Inverse Kinematics for Planar Parallel Manipulators", Proceedings of DETC 1997, 1997 ASME Design Engineering Technical Conference, Sacramento, California, September 14-17, 1997.
121. Williams, R. L. II, and Vadia, J., "Planar Translational Cable-Direct-Driven Robots: Hardware Implementation", Proceedings of DETC 2003, 2003 ASME Design Engineering Technical Conference, Chicago, Illinois, September 2-6, 2003.
122. Zhang, D., and Gosselin, C. M., "Kinetostatic Modeling of N-DOF Parallel Mechanisms with a Passive Constraining Leg and Prismatic Actuators", Transactions of the ASME Journal of Mechanical Design, Vol. 123, September 2001, pp. 375-381.
123. Dunlop, R., and Garcia, A. C., "A Nitinol Actuated Stewart Platform", Proceedings of Australasian Conference on Robotics and Automation, Auckland, November 2002, pp. 27-29.
124. Lee, K. M., and Arjunan, S., "A Three-Degrees-of-Freedom Micromotion In-Parallel Actuated Manipulator", IEEE Transactions on Robotics and Automation, Vol. 7 No. 5, October 1991, pp. 634-641.
125. Mukherjee, S., and Murlidhar, S., "Massively Parallel Binary Manipulators", Transactions of the ASME Journal of Mechanical Design, Vol. 123, March 2001, pp. 68-73.
126. Portman, V. T., Sandler, B. Z., and Zahavi, E., "Rigid 6×6 Parallel Platform for Precision 3-D Micromanipulation: Theory and Design Application", IEEE Transactions on Robotics and Automation, Vol. 16, No. 6, December 2000, pp. 629-643.
127. Requicha, A. A. G., "Massively Parallel Nanorobotics for Lithography and Data Storage", The International Journal of Robotics Research, Vol. 18, No. 3, March 1999, pp. 344-250.

128. Yi, B. J., Chung, G. B., Na, H. Y., Kim, W. K., and Suh, I. H., "Design and Experiment of a 3-DOF Parallel Micromechanism Utilizing Flexure Hinges", *IEEE Transactions on Robotics and Automation*, Vol. 19, No. 4, August 2003, pp. 604-612.
129. Tanikawa, T., Kawai, M., Koyachi, N., Arai, T., Ide, T., Kaneko, S., Ohta, R., and Hirose, T., "Force Control System for Autonomous Micro Manipulation", *Proceedings of the 2001 IEEE International Conference on Robotics and Automation*, Seoul, Korea, May 2001, pp. 610-615.
130. Furutani, K., Suzuki, M., and Kudoh, R., "Nanometre-Cutting Machine Using a Stewart-Platform Parallel Mechanism", *Measurement Science and Technology*, Vol. 15, 2004, pp. 467-474.
131. Gao, P., and Sweil, S. M., "A Six-Degree-of-Freedom Micro-Manipulator Based on Piezoelectric Translators", *Nanotechnology*, Vol. 10, 1999, pp. 447-452.
132. Tahmasebi, F., and Tsai, L., "Jacobian and Stiffness Analysis of a Novel Six-DOF Parallel Minimanipulator", In *Proceedings of the 22nd Biennial Mechanisms Conference*, September 1992.
133. Tahmasebi, F., and Tsai, L., "Jacobian and Stiffness Analysis of a Novel Six-DOF Parallel Minimanipulator", *Systems Research Center of University of Maryland and Harvard University Supported by the National Science Foundation Engineering Research Center Program (NSFD CD 8803012) Industry and the University, Technical Research Report*, Technical Research Report, Vol. 84, 1992.
134. Tahmasebi, F., and Tsai, L., "On the Stiffness of a Novel Six-Degree-of-Freedom Parallel Minimanipulator", *Journal of Robotic Systems*, Vol. 12, No. 12, 1995, pp. 845-856.
135. Tsai, L. W., "Synthesis and Analysis of a Class of Six-Degree-of-Freedom Parallel Minimanipulators", *Journal of Robotic Systems*, Vol. 10, No. 5, 1993, pp. 561-580.
136. Arai, T., Yuasa, K., Mae, Y., Inoue, K., Miyawaki, K., and Koyachi, N., "A Hybrid Drive Parallel Arm for Heavy Material Handling", *IEEE Robotics and Automation Magazine*, March 2002.
137. Ghosal, A., and Ravani, B., "A Differential-Geometric Analysis of Singularities of Point Trajectories of Serial and Parallel Manipulators", *Transactions of the ASME Journal of Mechanical Design*, Vol. 123, March 2001, pp. 80-89.

138. Simaan, N., and Shoham, M., "Singularity Analysis of a Class of Composite Serial In-Parallel Robots", *IEEE Transactions on Robotics and Automation*, Vol. 17, No. 3, June 2001, pp. 301-311.
139. Suthakorn, J., and Chirikjian, G. S., "A New Inverse Kinematics Algorithm for Binary Manipulators with Many Actuators", *Advanced Robotics*, Vol. 15, No. 2, 2001, pp. 225-244.
140. Waldron, K. J., Raghavan, M., and Roth, B., "Kinematics of a Hybrid Series-Parallel Manipulation System", *Journal of Dynamic Systems, Measurement and Control, Transactions ASME*, Vol. 111, No. 2, 1989, pp. 211-221.
141. Zheng, Y. F., and Luh, J. Y. S., "On the Inertia Duality of Parallel-Series Connections of Two Robots in Operational Space", *IEEE Transactions on Robotics and Automation*, Vol. 9, No. 6, December 1993, pp. 846-854.
142. Chirikjian, G. S., and Burdick, J. W., "Kinematically Optimal Hyper-Redundant Manipulator Configurations", *IEEE Transactions on Robotics and Automation*, Vol. 11, No. 6, December 1995, pp. 794-806.
143. Lee, M. K., and Park, K. W., "Kinematic and Dynamic Analysis of a Double Parallel Manipulator for Enlarging Workspace and Avoiding Singularities", *IEEE Transactions on Robotics and Automation*, Vol. 15, No. 6, December 1999, pp. 1024-1034.
144. Shammas, E., Wolf, A., Brown, H. B., and Choset, H., "New Joint Design for Three-Dimensional Hyper Redundant Robots", In *Proceedings of the 2003 IEEE/RSJ International Conference on Intelligent Robots and Systems*, Las Vegas, Nevada, October 2003, pp. 3594-3599.
145. Gravagne, I. A., and Walker, I. D., "Manipulability, Force, and Compliance Analysis for Planar Continuum Manipulators", *IEEE Transactions on Robotics and Automation*, Vol. 18, No. 3, June 2002, pp. 263-273.
146. Li, C., and Rahn, C. D., "Design on Continuous Backbone Cable-Driven Robots", *Transactions of the ASME Journal of Mechanical Design*, Vol. 124, June 2002, pp. 265-271.
147. Hamlin, G. J., and Sanderson, A. C., "TETROBOT: A Modular Approach to Parallel Robotics", *IEEE Robotics & Automation Magazine*, March 1997, pp. 42-50.

148. Jeong, J. W., Kim, S. H., and Kwak, Y. K., "Kinematics and Workspace Analysis of a Parallel Wire Mechanism for Measuring a Robot Pose", *Mechanisms and Machine Theory*, Vol. 34, Issue 6, August 1999, pp. 825-841.
149. Kossowski, C., and Notash, L., "A Novel Wire Actuated Parallel Robot with Space Applications", In *Proceedings of CCToMM Symposium on Mechanisms, Machines, and Mechatronics*, May 31-June 1, 2001.
150. Lafourcade, P., Llibre, M., and Reboulet, C., "Design of a Parallel Wire-Driven Manipulator for Wind Tunnels", *Proceedings on the Workshop on Fundamental Issues and Future Research Directions for Parallel Mechanisms and Manipulators*, Quebec City, Quebec, Canada, October 3-4, 2002, pp. 187-194.
151. Kamamura, S., Choe, W., Tanaka, S., and Pandian, S. R., "Development of an Ultrahigh Speed Robot FALCON using Wire Drive System", *IEEE International Conference on Robotics and Automation*, Nagoya, Japan, 1995.
152. Lee, J. J., and Tsai, L. W., "Topological Analysis of Tendon-Driven Manipulators", *Systems Research Center of University of Maryland and Harvard University Supported by the National Science Foundation Engineering Research Center Program (NSFD CD 8803012) Industry and the University*, Technical Research Report, Technical Research Report, Vol. 55, 1990.
153. Takeda, Y., and Funabashi, H., "Kinematic Synthesis of Spatial In-parallel Wire-Driven Mechanism with Six Degrees of Freedom with High Force Transmissibility", *Proceedings of ASME Design Engineering Technical Conferences*, Baltimore, MD, September 2000.
154. Su, Y. X., Duan, B. Y., Nan, R. D., and Peng, B., "Development of a Large Parallel-Cable Manipulator for the Feed-Supporting System of a Next-Generation Large Radio Telescope", *Journal of Robotic Systems*, Vol. 18, No. 11, 2001, pp. 633-643.
155. Barrette, G., and Gosselin, C. M., "Kinematic Analysis and Design of Planar Parallel Mechanisms Actuated with Cables", In *Proceedings of ASME Design Engineering Technical Conferences and Computer and Information in Engineering Conference*, Baltimore, MD, September 10-13, 2000.
156. Verhoeven, R., Hiller, M., and Tadokoro, S., "Workspace of Tendon-Driven Stewart Platforms: Basics, Classification, Details on the Planar 2-DOF Class", *Proceedings of the 4th International Conference on Motion and Vibration Control*, Vol. 3, 1998, pp. 871-876.

157. Williams, R. L. II, and Gallina, P., "Translational Planar Cable-Direct-Driven Robots", *Journal of Intelligent and Robotic Systems*, Vol. 37, 2003, pp. 69-96.
158. Hong, W. D., and Cipra, R. J., "A Method for Representing the Configuration, and Analyzing the Motion of Complex Cable-Pulley Systems", In *Proceedings of ASME Design Engineering Technical Conferences and Computer and Information in Engineering Conference*, Baltimore, MD, September 10-13, 2000.
159. Hong, W. D., and Cipra, R. J., "A Method for Representing the Configuration, and Analyzing the Motion of Complex Cable-Pulley Systems", *Transactions of the ASME Journal of Mechanical Design*, Vol. 125, June 2003, pp. 332-341.
160. Ou, Y-L., and Tsai, L. W., "Isotropic Design of Tendon Driven Manipulators", Institute for Systems Research (ISR) Sponsored by the National Science Foundation Engineering Research Center Program the University of Maryland, Harvard University and Industry, Technical Research Report, Vol. 95, 1995.
161. Tsai, L. W., "Design of Tendon Driven Manipulators", Institute for Systems Research (ISR) Sponsored by the National Science Foundation Engineering Research Center Program the University of Maryland, Harvard University and Industry, Technical Research Report, Vol. 96, 1995.
162. Landsberger, S. E., and Sheridan, T. B., "A New Design for Parallel Link Manipulators", *Proceedings of IEEE Systems Manufacturing and Cybernetics Conference*, Tucson, AZ, November 1985, pp. 812-814.
163. Lafourcade, P., and Lilbre, M., "First Steps Toward a Sketch-Based Design Methodology for Wire-Driven Manipulators", 2003 IEEE/ASME International Conference on Advanced and Intelligent Mechatronics (AIM2003), Kobe, Japan, July 21-24, 2003.
164. Verhoeven, R., and Hiller, M., "Estimating the Controllable Workspace of Tendon-Based Stewart Platforms", 7th International Symposium on Advances in Robot Kinematics, Portoroz, Slovenia, 2000, pp. 277-284.
165. Verhoeven, R., Hiller, M., and Tadokoro, S., "Workspace, Stiffness, Singularities and Classification of Tendon-Driven Stewart Platforms", 6th International Symposium on Advances in Robot Kinematics, Strobl, Austria, 1998, pp. 105-114.
166. Zheng, Y-Q., and Liu, X.-W., "Workspace Analysis of a Six Degree of Freedom Wire-Driven Parallel Manipulator", In *Proceedings of the Workshop on Fundamental Issues and Future Research Directions for Parallel Mechanisms and Manipulators*, Quebec City, Quebec, Canada, October 3-4, 2002, pp. 287-293.

167. Jordan, M. A., and Rudolf, C. D. III, "New Container Crane Concepts", Presented at the Facilities Engineering Seminar American Association of Port Authorities, Savannah, Georgia, April 14-16, 1993.
168. Sun, Q., "Control of Flexible-Link Multiple Manipulators", Transactions of the ASME Journal of Dynamic Systems, Measurement, and Control, Vol. 124, March 2002, pp. 67-75.
169. Bartolini, G., Orani, N., Pisano, A., and Usai, E., "Load Swing Damping in Overhead Cranes by Sliding Mode Technique", Proceedings of the 39th IEEE Conference on Decision and Control, 2000, pp. 1697-1702.
170. Kiss, B., Levine, J., and Mullhaupt, P., "A Simple Output Feedback PD Controller for Nonlinear Cranes", In Proceedings of IEEE Control and Decision Conference, 2000, pp. 5097-5101.
171. Goldsmith, P. B., Francis, B. A., and Goldenberg, A. A., "Stability of Hybrid Position/Force Control Applied to Manipulators with Flexible Joints", International Journal of Robotics and Automation, Vol. 14, No. 4, 1999, pp. 146-160.
172. Maier, T., and Woernle, C., "Dynamics and Control of a Cable Suspension Manipulator", The 9th German-Japanese Seminar on Nonlinear Problems in Dynamical Systems, Theory and Applications, Straelen, Germany, August 20-23, 2000.
173. Shiang, W. J., Cannon, D., and Gorman, J., "Dynamic Analysis of the Cable Array Robotic Crane", Proceedings of the IEEE International Conference on Robotics and Automation, Detroit, Michigan, May 1999, pp. 2495-2500.
174. Yang, L. F., Mikulas, M. M., and Chiou, J. C., "Stability and 3-D Spatial Dynamics Analysis of a Three Cable Crane", American Institute of Aeronautics and Astronautics, 1992, pp. 2069-2076.
175. Albus, J., Bostelman, R., and Dagalakis, N., "The NIST Robocrane", Journal of Research of the National Institute of Standards and Technology, Vol. 97, No. 3, May-June 1992, pp. 373-385.
176. Albus, J., Bostelman, R., and Dagalakis, N., "The NIST Robocrane", Journal of Robotic Systems, Vol. 10, No. 5, 1993, pp.709-724.
177. Bostelman, R. V., Albus, J., Dagalakis, N., Jacoff, A., and Gross, J., "Applications of the NIST RoboCrane", Robotics and Manufacturing, Vol. 5, 1994, pp. 403-410.

178. Wavering, A. J., "Parallel Kinematic Machine Research at NIST: Past, Present, and Future", First European-American Forum on Parallel Kinematic Machines Theoretical Aspects and Industrial Requirements, Milan, Italy, August 31-September 1, 1998.
179. Bostelman, R. V., Albus, J. S., and Graham, R. E., "RoboCrane and EMMA Applied to Waste Storage Tank Remediation", Proceedings of the American Nuclear Society Seventh Topical Meeting on Robotics and Remote Systems, Augusta, Georgia, April 27 to May 1, 1997.
180. Bostelman, R. V., and Albus, J. S., "Stability of an Underwater Work Platform Suspended from an Unstable Reference", Proceedings of the Oceans 1993 Conference, Victoria, British Columbia, Canada, October 20, 1993.
181. Bostelman, R. V., and Albus, J. S., "A Stewart Platform Lunar Rover", Proceedings of the 1994 Space Conference, Albuquerque, NM, February 28 – March 3, 1994.
182. Bostelman, R., Jacoff, A., and Bunch, R., "Delivery of an Advanced Double-Hull Ship Welding System Using Robocrane", 3rd International Computer Science Conventions Symposia on Intelligent Industrial Automation and Soft Computing, Genova, Italy, June 1-4, 1999.
183. Bostelman, R., Jacoff, A., Proctor, F., Kramer, T., and Wavering, A., "Cable-Based Reconfigurable Machines for Large Scale Manufacturing", Proceedings of the 2000 Japan-USA Symposium on Flexible Automation International Conference on New Technology Innovation for the 21st Century, Ann Arbor, Michigan, July 23-26, 2000.
184. Bostelman, R., Shackleford, W., Proctor, F., and Albus, J., "A Tool to Improve Efficiency in Large Scale Manufacturing", Proceedings of the 19th International Symposium on Automation and Robotics in Construction (ISARC 2002), Gaithersburg, Maryland, September 23-25, 2002.
185. Bostelman, R., Shackleford, W., Proctor, F., and Albus, J., "The Flying Carpet: A Tool to Improve Ship Repair Efficiency", American Society of Naval Engineers Symposium, Manufacturing Technology for Ship Construction and Repair, Bremerton, Washington, September 10-12, 2002.
186. Dagalakakis, N., Albus, J. S., Wang, B. L., Unger, J., and Lee, J. D., "Stiffness Study of a Parallel Link Robot Crane for Shipbuilding Applications", 7th International Conference on Offshore Mechanics and Arctic Engineering, Houston, TX, February 7-12, 1988, pp. 29-37.

187. Goodwin, K., "RoboCrane Construction of Bridges", Transportation Research Record 1575, Paper No. 971456, January 1997, pp. 42-46.
188. Williams, R. L. II, "Cable-Based Metrology System for Sculpting Assistance", In Proceedings of the 2003 ASME Design Engineering Technical Conferences, Chicago, IL, September 2-6, 2003.
189. Amatucci, E., Bostelman, R., Dagalakis, N., and Tsai, T., "Summary of Modeling and Simulation for NIST RoboCrane Applications", Proceedings of the 1997 Deneb International Simulation Conference and Technology Showcase, Detroit, MI, September 29 – October 3, 1997.
190. Bostelman, R., Jacoff, A., Dagalakis, N., and Albus, J., "RCS-Based RoboCrane Integration", Proceedings of the International Conference on Intelligent Systems: A Semiotic Perspective, Gaithersburg, Maryland, October 20 -23, 1996.
191. Dagalakis, N., "Remote Graphic Programming and Monitoring Tools of the NIST RoboCrane", 1997 Deneb International Simulation Conference, Troy, Michigan, September 29 to October 3, 1997.
192. Moore, M. L., Gazi, V., Passino, K. M., Shackleford, W. P., and Proctor, F. M., "Complex Control System Design and Implementation Using the NIST-RCS Software Library", Proceedings of IEEE Control Systems, December 1999, pp. 12-28.
193. Procter, F. M., and Shackleford, W. P., "Embedded Real-Time Linux for Cable Robot Control", Proceedings of DETC 2002 ASME 2002 Design Engineering Technical Conference and The Computers and Information in Engineering Conference, Montreal, Canada, September 29 – October 2, 2002.
194. Alp, A. B., "Cable-Suspended Parallel Robots", Master's Thesis, Department of Mechanical Engineering, University of Delaware, Newark, DE, Summer 2001.
195. Alp, A. B., and Agrawal, S. K., "Cable Suspended Robots: Design, Planning, and Control", Proceedings of 2002 IEEE International Conference on Robotics and Automation, Washington, D.C., May 11-15, 2002a, pp.4275-4280.
196. Alp, A. B., and Agrawal, S. K., "Cable Suspended Robots: Feedback Controllers with Positive Inputs", Proceeding of the 2002 American Controls Conference, Anchorage, AK, May 8-10, 2002b, pp.815-820.
197. Pusey, Jason L., Fattah, A., and Agrawal, S. K., "Design and Workspace Analysis of a 6-6 Cable-Suspended Parallel Robot", Mechanism and Machine Theory, 2003.

198. Agrawal, S. K., "A Study of In-parallel Robotic Systems", Doctoral Dissertation, Department of Mechanical Engineering, Stanford University, Stanford, 1990.
199. Angeles, J., "The Qualitative Synthesis of Parallel Manipulators", In the Proceedings of the Workshop on Fundamental Issues and Future Research Directions for Parallel Mechanisms and Manipulators, Quebec City, Quebec, Canada, October 3-4, 2002, pp. 160-169.
200. Dafaoui, E. M., Amirat, Y., Pontnau, J., and Francois, C., "Analysis and Design of a Six-DOF Parallel Manipulator, Modeling, Singular Configurations, and Workspace", IEEE Transactions on Robotics and Automation, Vol. 14, No. 1, February 1998, pp. 78-92.
201. Fang, Y., and Tsai, L. W., "Structure Synthesis of a Class of 4-DOF and 5-DOF Parallel Manipulator with Identical Limb Structures", The International Journal of Robotics Research, Vol. 21, No. 9, September 2002, pp. 799-810.
202. Gao, X. S., and Lei, D., "Generalized Stewart Platform and Their Direct Kinematics", MM Research Preprints, MMRC, AMSS, Academic, Sinica, Beijing, No. 22, December 2003, pp. 64-85.
203. Huang, Z., and Li, Q. C., "General Methodology for Type Synthesis of Symmetrical Lower-Mobility Parallel Manipulators and Several Novel Manipulators", The International Journal of Robotics Research, Vol. 21, No. 2, February 2002, pp. 131-145.
204. Huynh, P., "Kinematics Analysis and Mechatronics System Design of a 3-DOF In-Parallel Actuated Mechanism", IEEE International Conference on Intelligent Robots and Systems, Hawaii, USA, October 29-November 3, 2001.
205. Joshi, S. A., and Tsai, L. W., "A Comparison Study of Two 3-DOF Parallel Manipulators: One with Three and the Other with Four Supporting Legs", IEEE Transactions on Robotics and Automation, Vol. 19, No. 2, April 2003, pp. 209.
206. Kim, H. S., and Tsai, L. W., "Kinematic Synthesis of a Spatial 3-RPS Parallel Manipulator", Transactions of the ASME Journal of Mechanical Design, Vol. 125, March 2003, pp. 92-97.
207. Liao, Q., and McCarthy, J. M., "On the Seven Position Synthesis of a 5-SS Platform Linkage", Transactions of the ASME Journal of Mechanical Design, Vol. 123, March 2001, pp. 74-79.
208. Merkle, R. C., "A New Family of Six Degrees of Freedom Positional Devices", Nanotechnology, Vol. 8, 1997, pp. 47-52.

209. Simaan, N., Glozman, M., and Shoham, M., "Design Considerations of a New Six Degrees-of-Freedom Parallel Robots", Proceedings of the IEEE International Conference on Robotics and Automation, Leuven, Belgium, May 1998, pp. 1327-1333.
210. Tsai, L. W., "Systematic Enumeration of Parallel Manipulators", Institute for Systems Research (ISR) Sponsored by the National Science Foundation Engineering Research Center Program a Permanent Institute of the University of Maryland, Technical Research Report, Vol. 33, 1998.
211. Tsai, L. W., and Joshi, S., "Kinematic Analysis of 3-DOF Position Mechanism for Use in Hybrid Kinematic Machines", Transactions of the ASME Journal of Mechanical Design, Vol. 124, June 2002, pp. 245-253.
212. Yang, G., Chen, I. M., Lim, W. K., and Yeo, S. H., "Design and Kinematic Analysis of Modular Reconfigurable Parallel Robots", Proceedings of the IEEE International Conference on Robotics and Automation, Detroit, Michigan, May 1999, pp. 2501-2506.
213. Fattah, A., and Ghasemi, A. M. H., "Isotropic Design of Spatial Parallel Manipulators", The International Journal of Robotics Research, Vol. 21, No. 9, September 2002, pp. 811-824.
214. Goldsmith, P. B., "Design and Kinematics of a Three-Legged Parallel Manipulator", IEEE Transactions on Robotics and Automation, Vol. 19, No. 4, August 2003, pp. 726-731.
215. Kim, S. G., and Ryu, J., "New Dimensionally Homogeneous Jacobian Matrix Formulation by Three End-Effector Points for Optimal Design of Parallel Manipulators", IEEE Transactions on Robotics and Automation, Vol. 19, No. 4, August 2003, pp. 731-737.
216. Merlet, J. P., "An Initiative for the Kinematics Study of Parallel Manipulators", In Proceedings of the Workshop on Fundamental Issues and Future Research Directions for Parallel Mechanisms and Manipulators, Quebec City, Quebec, Canada, October 3-4, 2002, pp. 2-9.
217. Merlet, J. P., "Designing a Parallel Manipulator for a Specific Workspace", The International Journal of Robotics Research, Vol. 16, No. 4, August 1997, pp. 545-556.
218. Merlet, J. P., "Designing a Parallel Manipulator for a Specific Workspace", Institute National De Recherché En Informatique Et En Automatique (INRIA) Rapport de Recherché, No. 2527, Program 4, Avril, 1995.

219. Ottaviano, E., and Ceccarelli, M., "Optimum Design of Parallel Manipulators for Workspace and Singularity Performances", In Proceedings of the Workshop on Fundamental Issues and Future Research Directions for Parallel Mechanisms and Manipulators, Quebec City, Quebec, Canada, October 3-4, 2002, pp. 98-105.
220. Tsai, L. W., and Joshi, S., "Kinematic and Optimization of Spatial 3-UPU Parallel Manipulator", Transactions of the ASME Journal of Mechanical Design, Vol. 122, December 2000, pp. 439-446.
221. Agrawal, S. K., and Veeraklaew, T., "Designing Robots for Optimal Performance during Repetitive Motion", IEEE Transactions on Robotics and Automation, Vol. 14, No. 5, October 1998, pp. 771-777.
222. Liu, K., Fitzgerald, J. M., and Lewis, F. L., "Kinematic Analysis of a Stewart Platform Manipulator", IEEE Transactions of Industrial Electronics, Vol. 40, No. 2, April 1993, pp. 282-293.
223. Mavroidis, C., Lee, E., and Alam, M., "A New Polynomial Solution to the Geometric Design Problem of Spatial R-R Robot Manipulators Using the Denavit and Hartenberg Parameters", Transactions of ASME Journal of Mechanical Design, Vol. 123, March 2001, pp. 58-67.
224. Stocco, L., Salcudean, S. E., and Sassani, F., "Matrix Normalization for Optimal Robot Design", IEEE International Conference on Robotics and Automation, Leuven, Belgium, May 16-21, 1998.
225. Wu, Jin, and Azarm, S., "Metrics for Quality Assessment of a Multiobject Design Optimization Solution Set", Transactions of the ASME Journal of Mechanical Design, Vol. 123, March 2001, pp. 18-25.
226. Zhu, J., and Ting, K. L., "Performance Distribution Analysis and Robust Design", Transactions of the ASME Journal of Mechanical Design, Vol. 123, March 2001, pp. 11-17.
227. Davies, T. H., "Kirchhoff's Circulation Law Applied to Multi-Loop Kinematic Chains", Mechanism and Machine Theory, Vol. 16, 1981, pp. 171-183.
228. Adams, J. D., and Whitney, D. E., "Application of Screw Theory to Constraint Analysis of Mechanical Assemblies Joined by Features", Transactions of the ASME Journal of Mechanical Design, Vol. 123, March 2001, pp. 26-32.
229. Baker, J. E., "On Relative Freedom between Links in Kinematic Chains with Cross-Jointing", Mechanism and Machine Theory, Vol. 15, 1980, pp. 397-413.

230. Davies, T. H., and Primrose, E. J. F., “An Algebra for the Screw Systems of Pairs of Bodies in a Kinematic Chain”, Proceedings of The Third World Congress for The Theory of Machines and Mechanisms, Kupari, Yugoslavia, September 13-20, 1971, pp. 199-212.
231. Funda, J., and Paul, R. P., “A Computational Analysis of Screw Transformations in Robotics”, IEEE Transactions on Robotics and Automation, Vol. 6, No. 3, June 1990, pp. 348-356.
232. Gallardo, J., Rico, J. M., Frisoli, A., Checcacci, D., and Bergamasco, M., “Dynamics of Parallel Manipulators by Means of Screw Theory”, Mechanisms and Machine Theory, Vol. 38, 2003, pp. 1113-1131.
233. Huang, C., and Sun, C. C., “Investigation of Screw Systems in the Finite Displacements of Bennett-Based 6R Linkages”, Transactions of the ASME Journal of Mechanical Design, Vol. 122, December 2000, pp. 426-430.
234. Joshi, S. A., and Tsai, L. W., “Jacobian Analysis on Limited-DOF Parallel Manipulators”, Transactions of the ASME Journal of Mechanical Design, Vol. 124, June 2002, pp. 254-258.
235. Kim, D., and Chung, W. K., “Analytic Formulation of Reciprocal Screws and its Application to Nonredundant Robot Manipulators”, Transactions of the ASME Journal of Mechanical Design, Vol. 125, March 2003, pp. 158-164.
236. Lucas, S. R., Tischler, C. R., and Samuel, A. E., “Screw Geometry and LU Decomposition of the Jacobian of a Serial Manipulator”, Proceedings of A Symposium Commemorating the Legacy, Works, and Life of Sir Robert Stawell Ball Upon the 100th Anniversary of “A Treatise on the Theory of Screws”, July 9-11, 2000.
237. Staffetti, E., and Thomas, F., “Analytic Formulation of the Kinestatics of Robot Manipulators with Arbitrary Topology”, Proceedings of the IEEE International Conference on Robotics and Automation, Washington, DC, May 2002, pp. 2848-2855.
238. Tsai, L. W., “The Jacobian Analysis of a Parallel Manipulator Using Reciprocal Screws”, Advances in Robot Kinematics: Analysis and Control, edited by J. Lenarcic and M. Husty, Kluwer Academic Publishers, 1998, pp. 327-336.
239. Chou, J. C. K., “Quaternion Kinematics and Dynamic Differential Equations”, IEEE Transactions on Robotics and Automation, Vol. 8, No. 1, February 1992.

240. Ji, P., and Wu, H., "A Closed-Form Forward Kinematics Solution for the 6-6^P Stewart Platform", IEEE Transactions on Robotics and Automation, Vol. 17, No. 4, August 2001, pp. 522-526.
241. Fattah, A., and Ghasemi, A. M. H., "Isotropic Design of Spatial Parallel Manipulators", The International Journal of Robotics Research, Vol. 21, No. 9, September 2002, pp. 811-824.
242. Dash, A. K., Chen, I. M., Yeo, S. H., and Yang, G., "Instantaneous Kinematics and Kinematic Control of In-Parallel Robots", In Proceedings of the Asian Conference on Robotics and its Applications, Singapore, June 6-8, 2001, pp. 7-12.
243. Dash, A. K., Chen, I. M., Yeo, S. H., and Yang, G., "Instantaneous Kinematics and Singularity Analysis of Three-Legged Parallel Manipulator", Proceedings of the IEEE International Conference on Intelligent Robots and Systems, Maui, Hawaii, USA, October 29- November 3, 2001, pp. 1275-1280.
244. Dhingra, A. K., Almadi, A. N., and Kohli, D., "A Grobner-Sylvester Hybrid Method for Closed-Form Displacement Analysis of Mechanisms", Transactions of the ASME Journal of Mechanical Design, Vol. 122, December 2000, pp. 431-438.
245. Didrit, O., Petitot, M., and Walter, E., "Guaranteed Solution of Direct Kinematics Problem for General Configurations of Parallel Manipulator", IEEE Transactions on Robotics and Automation, Vol. 14, No. 2, April 1998.
246. Angeles, J., "Fundamentals of Robotic Mechanical Systems: Theory, Methods, and Algorithms", Springer- Verlag, New York, Inc., 1997.
247. Khan, W. A., Krovi, V. N., Saha, S. K., and Angeles, J., " Recursive Kinematics and Inverse Dynamics for Parallel Manipulators", Proceedings of IMECE '03, 2003 ASME International Mechanical Engineering Congress and Exposition, Washington D. C., November 16-21, 2003.
248. Baron, L., and Angeles, J., "A Linear Algebraic Solution to the Direct Kinematics of Parallel Manipulators Using a Camera", In Proceedings of the 9th World Congress on the Theory of Machines and Mechanisms, Milano, August 1995.
249. Perng, M. H., and Hsiao, L., "Inverse Kinematic Solutions for a Fully Parallel Robot with Singularity Robustness", The International Journal of Robotics Research, Vol. 18, No. 6, June 1999, pp. 575-583.

250. Baron, L., and Angeles, J., "The Direct Kinematics of Parallel Manipulators Under Joint-Sensor Redundancy", IEEE Transactions on Robotics and Automation, Vol. 16, No. 1, February 2000.
251. Baron, L., and Angeles, J., "The Kinematic Decoupling of Parallel Manipulators Using Joint-Sensor Data", IEEE Transactions on Robotics and Automation, Vol. 16, No. 6, December 2000, pp. 644-651.
252. Baron, L., and Angeles, J., "The On-Line Direct Kinematics of Parallel Manipulators Under Joint-Sensor Redundancy", Advances in Robot Kinematics, Strobl, Austria, 1998, pp. 127-136.
253. Bruyninckx, H., "Closed-Form Forward Position Kinematics for a (3-1-1-1) Fully Parallel Manipulator", IEEE Transactions on Robotics and Automation, Vol. 14, No. 2, April 1998, pp. 326-328.
254. Di Gregorio, R., and Parenti-Castelli, V., "Position Analysis in Analytical Form of the 3-PSP Mechanism", Transactions of the ASME Journal of Mechanical Design, Vol. 123, March 2001, pp. 51-57.
255. Innocenti, C., "Forward Kinematics in Polynomial Form of the General Stewart Platform", Transactions of the ASME Journal of Mechanical Design, Vol. 123, June 2001, pp. 254-260.
256. Merlet, Jean-Pierre, "Direct Kinematics of Parallel Manipulators", IEEE Transactions on Robotics and Automation, Vol. 9, No. 6, December 1993, pp. 842-846.
257. Mu, Z., and Kazerounian, K., "A Real Parameter Continuation Method for Complete Solution of Forward Position Analysis of the General Stewart", Transactions of the ASME Journal of Mechanical Design, Vol. 124, June 2002, pp. 236-244.
258. Song, S. K., and Kwon, D. S., "Efficient Formulation Approach for the Forward Kinematics of 3-6 Parallel Mechanism", Advanced Robotics, Vol. 16, No. 2, 2002, pp. 191-215.
259. Wang, L. C. T., and Chen C. C., "On the Numerical Kinematic Analysis of General Parallel Robotic Manipulators", IEEE Transactions on Robotics and Automation, Vol. 9, No. 3, June 1993, pp. 272-285.
260. Agrawal, S. K., and Faiz, N., "Optimization of a Class of Nonlinear Dynamic Systems: New Efficient Method without Lagrange Multipliers", Journal of Optimization Theory and Applications, Vol. 97, No. 1, April 1998, pp. 11-28.

261. Iurascu, C. C., and Park, F. C., "Geometric Algorithms for Kinematic Calibration of Robots Containing Closed Loops", *Transactions of the ASME Journal of Mechanical Design*, Vol. 125, March 2003, pp. 23-32.
262. Zhang, H., and Paul, R. P., "A Parallel Inverse Kinematics Solution for Robot Manipulators Based on Multiprocessing and Linear Extrapolation", *IEEE Transactions on Robotics and Automation*, Vol. 7, No. 5, October 1991, pp. 660-669.
263. Song, S. K., and Kwon, D. S., "A Tetrahedron Approach for a Unique Closed-Form Solution of the Forward Kinematics of Six-DOF Parallel Mechanisms with Multi-connected Joints", *Journal of Robotic Systems*, Vol. 19, No. 6, 2002, pp. 269-281.
264. Thomas, F., Ottaviano, E., Ros, L., and Ceccarelli, M., "Coordinate-Free Formulation of a 3-2-1 Wire-Based Tracking Device Using Cayley-Menger Determinants", *Proceedings of the 2003 IEEE International Conference on Robotics and Automation*, Taipei, Taiwan, September 14-19, 2003.
265. Thomas, F., Ottaviano, E., Ros, L., and Ceccarelli, M., "Uncertainty Model and Singularities of 3-2-1 Wire-Based Tracking System", J. Lenarcic and F. Thomas (eds.), *Advances in Robot Kinematics*, Kluwer Academic Publishers, Netherlands, 2002, pp. 107-116.
266. Kim, W. K., Byun, Y. K., and Cho, H. S., "Closed-Form Forward-Position Solution for a 6-DOF 3-PPSP Parallel Mechanism and its Implementation", *The International Journal of Robotics Research*, Vol. 20, No. 1, January 2001, pp. 85-99.
267. Dietmaier, P., "The Stewart-Gough Platform of General Geometry Can Have 40 Real Postures", J. Lenarcic and M. L. Husty (eds.), *Advances in Robot Kinematics: Analysis and Control*, Kluwer Academic Publishers, 1998, pp. 7-16.
268. Husty, M. L., "An Algorithm for Solving the Direct Kinematics of Stewart-Gough-Type Platforms", Technical Report, CIM-94-1, McGill Center for Intelligent Machines, McGill University Montreal, Quebec, Canada, June 1994.
269. Mourrain, B., "The 40 "Generic" Positions of a Parallel Robot", *ISSAC International Symposium on Symbolic and Algebraic Computation*, ACM press, Kiev, Ukraine, July 1993, pp. 173-182.
270. Tancredi, L., Teillaud, M., and Devillers, O., "Symbolic Elimination for Parallel Manipulators", *INRIA Institute National de Recherché en Informatique Automatique Rapport de Recherché*, No. 2809, Février, 1996.

271. Wampler, C. W., "Forward Displacement Analysis of General Six-In-Parallel SPS (Stewart) Platform Manipulators Using Soma Coordinates", *Mechanism Machine Theory*, Vol. 31, No. 3, 1996, pp. 331-337.
272. Nanua, P., Waldron, K. J., and Murthy, V., "Direct Kinematic Solution of a Stewart Platform", *IEEE Transactions on Robotics and Automation*, Vol. 6, No. 4, August 1990, pp. 438-444.
273. Griffis, M., and Duffy, J., "A Forward Displacement Analysis of a Class of Stewart Platforms", *Journal of Robotic Systems*, Vol. 6, No. 6, 1989, pp. 703-720.
274. Bruyninckx, H., and De Schutter, J., "Comments on "Closed Form Forward Kinematics Solution to a Class of Hexapod Robots"", *IEEE Transactions on Robotics and Automation*, Vol. 15, No. 4, August 1999, pp. 788-789.
275. Yang, J., and Geng, Z. J., "Closed Form Forward Kinematics Solution to a Class of Hexapod Robots", *IEEE Transactions on Robotics and Automation*, Vol. 14, No. 3, June 1998, pp. 503-508.
276. Bonev, I. A., Ryu, J. K., Kim, S. G., and Lee, S. K., "A Closed-Form Solution to the Direct Kinematics of Nearly General Parallel Manipulators with Optimally Located Three Linear Extra Sensors", *IEEE Transactions on Robotics and Automation*, Vol. 17, No. 2, April 2001, pp. 148-156.
277. Bonev, I. A., Ryu, J., Kim, N. J., and Lee, S. K., "A Simple New Closed-Form Solution of the Direct Kinematics of Parallel Manipulators Using Three Linear Extra Sensors", *Proceedings of the 1999 IEEE/ASME International Conference on Advanced Intelligent Mechatronics*, Atlanta, USA, September 19-23, 1999.
278. Parenti-Castelli, V., and Di Gregorio, "A New Algorithm Based on Two Extra-Sensors for Real-Time Computation of the Actual Configuration of the Generalized Stewart-Gough Manipulator", *Transactions of the ASME Journal of Mechanical Design*, Vol. 122, September 2000, pp. 294-298.
279. Kim, D. H., Oh, J. H., Lee, J. W., and Park, K. T., "Closed-Form Kinematic Solution of a Non-Parallel Cable Reeving Crane System", *Proceedings of the Institution of Mechanical Engineers, Journal of Mechanical Engineering Science*, Vol. 217, Part C, 2003.
280. Cheok, K. C., Overholt, J. L., and Beck, R. R., "Exact Methods for Determining the Kinematics of a Stewart Platform Using Additional Displacement Sensors", *Journal of Robotic Systems*, Vol. 10, No. 5, 1993, pp. 689-707.

281. Chiu, Y. J., and Perng, M. H., "Forward Kinematics of a General Fully Parallel Manipulator with Auxiliary Sensors", *The International Journal of Robotics Research*, Vol. 20, No. 5, May 2001, pp. 401-414.
282. Marquet, F., Company, O., Krut, S., and Pierrot, F., "Enhancing Parallel Robot Accuracy with Redundant Sensors", *ICRA 2002: 2002 IEEE International Conference on Robotics and Automation*, Washington DC, USA, May 11-15, 2002, pp. 4114-4119.
283. Ebert-Uphoff, I., Gosselin, C. M., and Laliberte, T., "Static Balancing of Spatial Parallel Platform Mechanisms-Revisited", *Transactions of the ASME Journal of Mechanical Design*, Vol. 122, March 2000, pp. 43-51.
284. Dasgupta, B., and Choudhury, P., "A General Strategy Based on the Newton-Euler Approach for the Dynamic Formulation of Parallel Manipulators", *Mechanism and Machine Theory*, Vol. 34, 1999, pp. 801-824.
285. Dasgupta, B., and Mruthyunjaya, T. S., "Closed-Form Dynamic Equations of the General Stewart Platform Through the Newton-Euler Approach", *Mechanism and Machine Theory*, Vol. 33, No. 7, 1998, pp. 993-1012.
286. Do, W. Q. D., and Yang, D. C. H., "Inverse Dynamic Analysis and Simulation of a Platform Type of Robot", *Journal of Robotic Systems*, Vol. 5, No. 3, 1988, pp. 209-227.
287. Featherstone, R., "Robot Dynamics: Equations and Algorithms", In *Proceedings of the IEEE International Conference on Robotics and Automation*, San Francisco, CA, 2000, pp. 826-834.
288. Kim, J. P., and Ryu, J., "Dynamic Equations for Parallel Manipulators with Inner and Outer Closed Loops", *Proceedings of the 32nd ISR International Symposium on Robotics*, April 19-21, 2001.
289. Lin, S. K., "Dynamics of the Manipulator with Closed Chains", *IEEE Transactions on Robotics and Automation*, Vol. 6, No. 4, August 1990, pp. 496-501.
290. Cheng, H, Liu, Y. K., and Li, Z., "Dynamics and Control of Redundantly Actuated Parallel Manipulators", *IEEE / ASME Transactions on Mechatronics*, Vol. 8, No. 4, December 2003, pp. 483-491.

291. Fox, B., Jennings, L. S., and Zomaya, A. Y., "Numerical Computation of Differential-Algebraic Equations for Non-Linear Dynamics of Multibody Systems Involving Contact Forces", *Transactions of the ASME Journal of Mechanical Devices*, Vol. 123, June 2001, pp. 272-281.
292. Kwatny, H., and Blankenship, G. L., "Symbolic Construction of Models for Multibody Dynamics", *IEEE Transactions on Robotics and Automation*, Vol. 11, No. 2, April 1995, pp. 271-281.
293. Leuret, G., Liu, K., and Lewis, F. L., "Dynamic Analysis and Control of a Stewart Platform Manipulator", *Journal of Robotic Systems*, Vol. 10, No. 5, 1993, pp. 629-655.
294. Lee, J. D., Albus, J. S., Dagalakis, N. G., and Tsai, T., "Computer Simulation of a Parallel Link Manipulator", *Robotics and Computer Integrated Manufacturing*, August 1998.
295. Lee, K. M., and Shah, D. K., "Dynamic Analysis of a Three-Degree-of-Freedom In-Parallel Actuated Manipulator", *IEEE Journal of Robotics and Automation*, Vol. 4, No. 3, June 1988, pp. 361-367.
296. Pang, H., and Shahinpoor, M., "Inverse Dynamics of a Parallel Manipulator", *Journal of Robotic Systems*, Vol. 11, No. 8, 1994, pp. 693-702.
297. Wang, J., and Gosselin, C. M., "Dynamic Analysis of Spatial Four-Degree-of-Freedom Parallel Manipulators", *Proceedings of ASME Design Engineering Technical Conferences*, Sacramento, CA, September 14-17, 1997.
298. Xi, F., Sinatra, R., and Han, W., "Effect of Leg Inertia on Dynamics of Sliding-Leg Hexapods", *Transactions of the ASME Journal of Dynamic Systems, Measurements, and Control*, Vol. 123, June 2001, pp. 265-271.
299. Yiu, Y. K., Cheng, H., Xiong, Z. H., Liu, G. F., and Li, Z. X., "On the Dynamics of Parallel Manipulators", *Proceedings of the 2001 IEEE International Conference on Robotics and Automation*, Seoul, Korea, May 21-26, 2001.
300. Codourey, A., and Burdet, E., "A Body-Oriented Method for Finding a Linear Form of the Dynamic Equation of Fully Parallel Robots", *Proceedings of IEEE International Conference on Robotics and Automation*, Albuquerque, NM, April 1997, pp. 1612-1618.
301. Geike, T., and McPhee, J., "Inverse Dynamic Analysis of Parallel Manipulators with Full Mobility", *Mechanism and Machine Theory*, Vol. 38, 2003, pp. 549-562.

302. Geike, T., and McPhee, J., "On the Automatic Generation of Inverse Dynamic Solutions for Parallel Manipulators", Proceedings of the Workshop on Fundamental Issues and Future Research Directions for Parallel Mechanisms and Manipulators, Quebec City, Quebec, Canada, October 3-4, 2002, pp. 348-358.
303. Tsai, L. W., "Solving the Inverse Dynamics of Parallel Manipulators by the Principle of Virtual Work", Proceedings of ASME Design Engineering Technical Conferences, Atlanta, GA, September 13-16, 1998.
304. Tsai, L. W., "Solving the Inverse Dynamics of a Stewart-Gough Manipulator by the Principle of Virtual Work", Transactions of the ASME Journal of Mechanical Design, Vol. 122, March 2000, pp. 3-9.
305. Zhang, C. D., and Song, S. M., "An Efficient Method for Inverse Dynamics of Manipulators Based on the Virtual Work Principle", Journal of Robotic Systems, Vol. 10, No. 5, 1993, pp. 605-627.
306. Liu, M. J., Li, C. X., and Li, C. N., "Dynamics Analysis of the Gough-Stewart Platform Manipulator", IEEE Transactions on Robotics and Automation, Vol. 16, No. 1, February 2000, pp. 94-98.
307. Featherstone, R., "A Divide-and-Conquer Articulated-Body Algorithm for Parallel $O(\log(n))$ Calculation of Rigid-Body Dynamics Part 1: Basic Algorithm", The International Journal of Robotics Research, Vol. 18, No. 9, September 1999, pp. 867-875.
308. Featherstone, R., "A Divide-and-Conquer Articulated-Body Algorithm for Parallel $O(\log(n))$ Calculation of Rigid-Body Dynamics Part 2: Trees, Loops, and Accuracy", The International Journal of Robotics Research, Vol. 18, No. 9, September 1999, pp. 876-892.
309. Isobe, D., "A Unified Numerical Scheme for Calculating Inverse Dynamics of Open/Closed Link Mechanism", IECON 2001, 27th Annual Conference of the IEEE Industrial Electronics Society, 2001, pp. 341-344.
310. Kovecses, J., Piedboeuf, J. C., and Lange, C., "Methods for Dynamic Models of Parallel Robots and Mechanisms", Proceedings of the Workshop on Fundamental Issues and Future Research Directions for Parallel Mechanisms and Manipulators, Quebec City, Quebec, Canada, October 3-4, 2002, pp. 339-347.
311. Yun, Xiaoping, and Sarkar, N., "Unified Formulation of Robotic Systems with Holonomic and Nonholonomic Constraints", IEEE Transactions on Robotics and Automation, Vol. 14, No. 4, August 1998, pp. 640-650.

312. Cheng, F. T., and Orin, D. E., "Optimal Force Distribution in Multiple-Chain Robotic Systems", IEEE Transactions on Systems, Manufacturing, and Cybernetics, Vol. 21, No. 1, January/ February 1991, pp. 13-24.
313. Kim, H. S., and Choi, Y. J., "Forward/Inverse Force Transmission Capability Analyses of Fully Parallel Manipulators", IEEE Transactions on Robotics and Automation, Vol. 17, No. 4, August 2001, pp. 526-531.
314. Kim, H. S., and Choi, Y. J., "The Kinetostatic Capability Analysis of Robotic Manipulators", Proceedings of the IEEE International Conference on Intelligent Robots and Systems, Kyongju, Korea, October 1999.
315. Khatib, O., "Inertial Properties in Robotic Manipulation: An Object-Level Framework", The International Journal of Robotic Research, Vol. 14, No. 1, February 1995, pp. 19-36.
316. Tafazoli, S., Lawrence, P. D., and Salcudean, S. E., "Identification of Inertial and Friction Parameters for Excavator Arms", IEEE Transactions on Robotics and Automation, Vol. 15, No. 5, October 1999, pp. 966-971.
317. Tafazoli, S., Lawrence, P. D., Salcudean, S. E., Chan, D., Bachmann, S., and de Silva, C. W., "Parameter Estimation and Actuator Friction Analysis for a Mini Excavator", Proceedings of the IEEE International Conference on Robotics and Automation, Minneapolis, Minnesota, April 1996, pp. 329-334.
318. Ai, Masahiro, Nakano, T., and Masuda, S., "A Consideration on the Slackened and Tightened Cables", Structural Engineering/Earthquake Engineering, Vol. 11, No. 3, October 1994, pp. 47-50.
319. Bonev, I. A., and Ryu, J., "A New Approach to Orientation Workspace Analysis of a 6-DOF Parallel Manipulator", Mechanism and Machine Theory, Vol. 36, 2001, pp. 15-28.
320. Bonev, I. A., and Ryu, J., "Orientation Workspace Analysis of 6-DOF Parallel Manipulators", Proceedings of the ASME Design Engineering Technical Conferences, Las Vegas, Nevada, September 12-15, 1999.
321. Huang, T., Wang, J., Gosselin, C. M., and Whitehouse, D., "Determination of Closed Form Solution to the 2-D-Orientation Workspace of Gough-Stewart Parallel Manipulators", IEEE Transactions on Robotics and Automation, Vol. 15, No. 6, December 1999, pp. 1121-1125.

322. Merlet, J. P., "Determination of 6D Workspace of Gough-Type Parallel Manipulator and Comparison between Different Geometries", *The International Journal of Robotics Research*, Vol. 18, No. 9, September 1999, pp. 902-916.
323. Pernkopf, F., and Husty, M., "Workspace Analysis of Stewart-Gough Manipulators Using Orientation Plots", *Proceedings of the International Symposium on Multibody Systems and Mechatronics*, Mexico City, September 12-14, 2002.
324. Bonev, I. A., and Ryu, J., "A Geometrical Method for Computing the Constant-Orientation Workspace of 6-PRRS Parallel Manipulator", *Mechanism and Machine Theory*, Vol. 36, 2001, pp. 1-13.
325. Bonev, I. A., and Ryu, J., "Workspace Analysis of 6-PRRS Parallel Manipulators Based on the Vertex Space Concept", *Proceedings of the ASME Design Engineering Technical Conferences*, Las Vegas, Nevada, September 12-15, 1999.
326. Tsai, L. W., "Robot Analysis: The Mechanics of Serial and Parallel Manipulators", John Wiley and Sons, New York, NY, 1999.
327. Alameldin, T., and Sobh, T., "On the Evaluation of Reachable Workspace for Redundant Manipulators", *Proceedings of the 3rd International Conference on Industrial and Engineering Applications of Artificial Intelligence and Expert Systems*, Vol. 2, 1990, pp. 1079-1085.
328. Dash, A. K., Yeo, S. H., Yang, G., and Chen, I. M., "Workspace Analysis and Singularities Representation of Three-Legged Parallel Manipulators", *Seventh International Conference on Control, Automation, Robotics, and Vision (ICARV'02)*, Singapore, December 2002, pp. 962-967.
329. Wang, L. C., and Hsieh, J. H., "Extreme Reaches and Reachable Workspace Analysis of General Parallel Robotic Manipulators", *Journal of Robotic Systems*, Vol. 15, No. 3, 1998, pp. 145-159.
330. Du Plessis, L. J., and Synman, J. A., "A Numerical Method for the Determination of Dexterous Workspaces of Gough-Stewart Platforms", *International Journal for Numerical Methods in Engineering*, Vol. 52, 2001, pp. 345-369.
331. Bhangale, P. P., Saha, K. K., and Agrawal, V. P., "Dynamic Model Based Selective Criterion for Robot Manipulators", *Multibody Dynamics IDMEC/IST*, Lisbon, Portugal, July 1-4, 2003.

332. Agrawal, S. K., "Workspace Boundaries of In-Parallel Manipulator Systems", *International Journal of Robotics and Automation*, Vol. 7, No. 2, 1992, pp. 94-99.
333. Snyman, J. A., du Plessis, L. J., and Duffy, J., "An Optimization Approach to the Determination of the Boundaries of Manipulator Workspaces", *Transactions of the ASME Journal of Mechanical Design*, Vol. 122, December 2000, pp. 447-456.
334. Chirikjian, G. S., and Ebert-Uphoff, I., "Numerical Convolution on the Euclidean Group with Applications to Workspace Generation", *IEEE Transactions on Robotics and Automation*, Vol. 14, No. 1, February 1998, pp. 123-136.
335. Kyatkin, A. B., and Chirikjian, G. S., "Computation of Robot Configuration and Workspace Via the Fourier Transform on Discrete-Motion Group", *The International Journal of Robotics Research*, Vol. 18, No. 6, June 1999, pp. 601-615.
336. Badescu, M., Morman, J., and Mavroidis, C., "Workspace Optimization of Orientational 3-Legged UPS Parallel Platforms", *Proceedings of the ASME 202 Design Engineering Technical Conferences and Computers and Information in Engineering Conference*, Montreal, Canada, September 29-October 2, 2002.
337. Bessala, J., Bidaud, P., and Oueddou, F. B., "Analytical Study of Stewart Platforms Workspace", *Proceedings of the IEEE International Conference on Robotics and Automation*, Minneapolis, 1995.
338. Pham, H. H., and Chen, I. M., "Optimal Synthesis for Workspace and Manipulability of Parallel Flexure Mechanism", *Proceedings of the 11th World Congress in Mechanism and Machine Science*, Tianjin, China, August 18-21, 2003.
339. Bosscher, P., and Ebert-Uphoff, I., "Wrench-Based Analysis of Cable-Driven Robots", *Proceedings of the 2004 IEEE International Conference on Robotics and Automation*, New Orleans, LA, April 2004, pp. 4950-4955.
340. Miller, K., "Maximization of Workspace Volume of 3-DOF Spatial Parallel Manipulators", *Transactions of the ASME Journal of Mechanical Design*, Vol. 124, June 2002, pp. 347-350.
341. Szatmari, S., "Geometrical Errors of Parallel Robots", *Periodica Polytechnica Ser. Mech. Engineering*, Vol. 43, No. 2, 1999, pp. 155-162.
342. Baswell, M. A., Ablamowicz, R., and Anderson, J. N., "Clifford Algebra Space Singularities of Inline Planar Platforms", *Tennessee Technological University Department of Mathematics*, Technical Report No. 2001-2, April 2001.

343. Kim, D., and Chung, W. K., "Analytic Singularity Equation and Analysis of Six-DOF Parallel Manipulators Using Local Structurization Method", IEEE Transactions on Robotics and Automation, Vol. 15, No. 4, August 1999, pp. 612-622.
344. Kong, X., and Gosselin, C. M., "Uncertainty Singularity Analysis of Parallel Manipulators Based on the Instability Analysis of Structures", The International Journal of Robotics Research, Vol. 20, No. 11, November 2001, pp. 847-856.
345. Liu, G., Lou, Y., and Li, Z., "Singularities of Parallel Manipulators: A Geometric Treatment", IEEE Transactions on Robotics and Automation, Vol. 19, No. 4, August 2001, pp. 579-594.
346. Merlet, J. P., "Parallel Manipulators Part 2: Theory Singular Configurations and Grassmann Geometry", INRIA Institute National de Recherché in Informatique et in Automatique Rapport de Recherché, No. 791, Février, 1988.
347. Monsarrat, B., and Gosselin, C. M., "Singularity Analysis of a Three-Leg Six-Degree-of-Freedom Parallel Platform Mechanism Based on Grassmann Line Geometry", The International Journal of Robotics Research, Vol. 20, No. 4, April 2001, pp. 312-328.
348. Angeles, J., Yang, G., and Chen, I. M., "Singularity Analysis of Three-Legged, Six-DOF Platform Manipulators with RRRS Legs", IEEE/ASME International Conference on Advanced Intelligent Mechatronics Proceedings, Como, Italy, July 8-12, 2001, pp. 32-36.
349. Krut, S., Company, O., Marquet, F., and Pierrot, F., "Twice: A Tilting Angle Amplification System for Parallel Robots", In the Proceedings of the 2002 ICRA International Conference on Robotics and Automation, Washington DC, USA, May 11-15, 2002, pp. 4108-4113.
350. St-Onge, B. M., and Gosselin, C. M., "Singularity Analysis and Representation of the General Gough Stewart Platform", The International Journal of Robotics Research, Vol. 19, No. 3, March 2000, pp. 271-288.
351. Yang, G., Chen, I. M., and Angeles, J., "Singularity Analysis of Three-Legged Parallel Robots Based on Passive-Joint Velocities", IEEE Transactions on Robotics and Automation, Vol. 17, No. 4, August 2001, pp. 413-422.
352. Yang, G., Chen, I. M., and Angeles, J., "Singularity Analysis of Three-Legged Parallel Robots Based on Passive-Joint Velocities", Proceedings on the IEEE International Conference on Robotics and Automation, Seoul, Korea, May 21-26, 2001, pp. 2407-2412.

353. Gosselin, C. M., and Angeles, J., "Singularity Analysis of Closed-Loop Kinematic Chains", IEEE Transactions on Robotics and Automation, Vol. 6, No. 3, June 1990, pp. 281-290.
354. Husty, M. L., and Karger, A., "Self Motions of Stewart-Gough-Platforms", Proceedings of the Workshop on Fundamentals and Future Research Directions for Parallel Mechanisms and Manipulators, Quebec City, Quebec, Canada, October 3-4, 2002, pp. 131-141.
355. Williams, R. L. II, "Singularities of a Manipulator with Offset Wrist", Journal of Mechanical Design, Vol. 121, No. 2, June 1999, pp. 315-319.
356. Doty, K. L., Melchiorri, C., Schwartz, E. M., and Bonivento, C., "Robot Manipulability", IEEE Transactions on Robotics and Automation, Vol. 11, No. 3, June 1995, pp. 462-468.
357. Wen, J. T. Y., and Wilfinger, L. S., "Kinematic Manipulability of General Constrained Rigid Body Systems", IEEE Transactions on Robotics and Automation, Vol. 15, No. 3, June 1999, pp. 558-567.
358. Yoshikawa, T., "Foundations of Robotics: Analysis and Control", The MIT Press, Cambridge, Massachusetts, 1990.
359. Gosselin, C. M., and Angeles, J., "A Global Performance Index for the Kinematic Optimization of Robotic Manipulators", Journal of Mechanical Design, Vol. 113, September 1991.
360. Stoughton, R. S., and Arai, T., "A Modified Stewart Platform Manipulator with Improved Dexterity", IEEE Transactions on Robotics and Automation, Vol. 9, No. 2, April 1993, pp. 166-173.
361. Strang, Gilbert, "Linear Algebra and Its Applications Third Edition", Harcourt College Publishers, Philadelphia, PA, 1988.
362. Lee, J. H., Eom, K. S., Yi, B. J., and Suh, I. H., "Design of a New 6-DOF Parallel Haptic Device", In Proceedings of the 2001 IEEE International Conference on Robotics and Automation, Seoul, Korea, May 21-26, 2001, pp. 886-891.
363. Gosselin, C., "Stiffness Mapping for Parallel Manipulators", IEEE Transactions on Robotics and Automation, Vol. 6, No. 3, June 1990, pp. 377-382.

364. Huang, S., and Schimmels, J. M., "The Bounds and Realization of Spatial Stiffness Achieved with Simple Springs Connected in Parallel", IEEE Transactions on Robotics and Automation, Vol. 14, No. 3, June 1998, pp. 466-475.
365. Huang, T., Zhao, X., and Whitehouse, D. J., "Stiffness of a Tripod-Based Parallel Kinematic Machine", IEEE Transactions on Robotics and Automation, Vol. 18, No. 1, February 2002, pp. 50-58.
366. Roberts, R. G., "Minimal Realization of an Arbitrary Spatial Stiffness Matrix with a Parallel Connection of Simple and Complex Springs", IEEE Transactions on Robotics and Automation, Vol. 16, No. 5, October 2000, pp. 603-608.
367. Lee, S. H., Song, J. B., Choi, W. C., and Hong, D., "Position Control of a Stewart Platform Using Inverse Dynamics Control with Approximate Dynamics", Mechatronics, Vol. 13, 2003, pp. 605-619.
368. Simaan, N., and Shoham, M., "Geometric Interpretation of the Derivatives of Parallel Robots' Jacobian Matrix with Applications to Stiffness Control", Transactions of the ASME Journal of Mechanical Design, Vol. 125, March 2003, pp. 33-42.
369. Nguyen, C. C., Antrazi, S. S., and Zhou, Z. L., "Adaptive Control of a Stewart Platform-Based Manipulator", Journal of Robotic Systems, Vol. 10, No. 5, 1993, pp.657-687.
370. Ting, Y., Chen, Y. S., and Wang, S. M., "Task-Space Control Algorithm for Stewart Platform", Proceedings of the IEEE 38th Conference on Decision and Control, Phoenix, Arizona, USA, December 1999, pp. 3857-3862.
371. Silva, M. F., Tenreiro Machado, J. A., and Lopes, A. M., "Comparison of Fractional and Integer Order Control of an Hexapod Robot", In Proceedings of the DETC'03 ASME 2003 Design Engineering Technical Conference and Computers and Information in Engineering Conference, Chicago, Illinois, USA, September 2-6, 2003.
372. Fasse, E. D., and Gosselin, Clement M., "Spatio-Geometric Impedance Control of Gough-Stewart Platforms", IEEE Transactions on Robotics and Automation, Vol. 15, No. 2, April 1999, pp. 281-288.
373. Austin, David J., and McCarragher, Brennan, J., "Force Control Commanded Synthesis for Assembly using a Discrete Event Framework", Proceeding of the IEEE International Conference on Robotics and Automation, 1997.

374. Chan, S. P., and Liaw, H. C., "Experimental Implementation of Impedance Based Control Schemes for Assembly Task", *Journal of Intelligent and Robotic Systems*, Vol. 29, 2000, pp. 93-110.
375. Fei, Y., and Zhao, X., "An Assembly Process Modeling and Analysis for Robotic Multiple Peg-in-Hole", *Journal of Intelligent and Robotic Systems*, Vol. 36, 2003, pp. 175-189.
376. McCarragher, B. J., "Task Primitives for the Discrete Event Modeling and Control of 6-DOF Assembly Tasks", *IEEE Transactions on Robotics and Automation*, Vol. 12, No. 2, April 1996, pp. 280-289.
377. Mosemann, H., Rohrdanz, F., and Wahl, M., "Stability Analysis of Assemblies Considering Friction", *IEEE Transactions on Robotics and Automation*, Vol. 13, No. 6, December 1997, pp. 805-813.
378. Saitou, K., "Conformational Switching in Self-Assembling Mechanical Systems", *IEEE Transactions on Robotics and Automation*, Vol. 15, No. 3, June 1999, pp. 510-520.
379. Schimmels, J. M., "A Linear Space of Admittance Control Laws that Guarantees Force-Assembly with Friction", *IEEE Transactions on Robotics and Automation*, Vol. 13, No. 5, October 1997, pp. 656-667.
380. Schimmels, J. M., and Peshkin, M. A., "Admittance Matrix Design for Force-Guided Assembly", *IEEE Transactions on Robotics and Automation*, Vol. 8, No. 2, April 1992, pp. 213-227.
381. Schimmels, J. M., and Peshkin, M. A., "Force-Assembly with Friction", *IEEE Transactions on Robotics and Automation*, Vol. 10, No. 4, August 1994, pp. 465-479.
382. Seidmann, A., and Nof, S. Y., "Operational Analysis of an Autonomous Assembly Robotic Station", *IEEE Transactions on Robotics and Automation*, Vol. 5, No. 1, February 1989, pp. 4-15.
383. Tung, C. P., and Kak, A. C., "Integrating Sensing, Task Planning, and Execution for Robotic Assembly", *IEEE Transactions on Robotics and Automation*, Vol. 12, No. 2, April 1996, pp. 178-201.
384. Laycock, S. D., and Day, A. M., "Recent Developments and Applications of Haptic Devices", Published by The Eurographics Association and Blackwell Publishing Ltd. 2003, *Computer Graphics Forum*, Vol. 22, No. 2, 2003, pp. 117-132.

385. Tsujimura, T., and Yabuta, T., "Object Detection by Tactile Sensing Method Employing Force/Torque Information", *IEEE Transactions on Robotics and Automation*, Vol. 5, No. 4, August 1989, pp. 444-450.
386. Baptista, L. F., Sousa, J. M., and Costa, J. S. D., "Force Control of Robotic Manipulators Using a Fuzzy Predictive Approach", *Journal of Intelligent and Robotic Systems*, Vol. 30, 2001, pp. 359-376.
387. Caccavale, F., Natale, C., Siciliano, B., and Villani, L., "Six-DOF Impedance Control Based on Angle/Axis Representations", *IEEE Transactions on Robotics and Automation*, Vol. 15, No. 2, April 1999, pp. 289-300.
388. Cheah, C. C., and Wang, D., "Learning Impedance Control for Robotic Manipulators", *IEEE Transaction on Robotics and Automation*, Vol. 14, No. 3, June 1998, pp. 452-465.
389. Dawson, D., and Qu, Z., "Comments on "Impedance Control with Adaptation for Robotic Manipulators"", *IEEE Transactions on Robotics and Automation*, Vol. 7, No. 6, December 1991, pp. 879-881.
390. Doulgeri, Zoe, and Arimoto, Suguru, "A Force Commanded Impedance Control for a Robotic Finger with Uncertain Kinematics", *International Journal of Robotics Research*, Vol. 18, No. 10, October 1999, pp. 1013-1029.
391. Fasse, E. D., and Broenink, J. F., "A Spatial Impedance Controller for Robotic Manipulation", *IEEE Transactions on Robotics and Automation*, Vol. 13, No. 4, August 1997, pp. 546-556.
392. Jung, S., Hsia, T. C., and Bonitz, R. G., "Force Tracking Impedance Control for Robot Manipulators with an Unknown Environment: Theory, Simulation, and Experiment", *International Journal of Robotics Research*, Vol. 20, No. 9, September 2001, pp. 765-774.
393. Jung, S., Hsia, T. C., and Bonitz, R. G., "Force Tracking Impedance Control of Robot Manipulators Under Unknown Environment", *IEEE Transactions on Control Systems Technology*, Vol. 12, No. 3, May 2004, pp. 474-483.
394. Katić, D., and Vukobratović, M., "The Application of Connectionist Structures to Learning Impedance Control in Robotic Contact Tasks", *Applied Intelligence*, Vol. 7, 1997, pp. 315-326.
395. Lu, W. S., and Meng, Q. H., "Impedance Control with Adaptation for Robotic Manipulation", *IEEE Transactions on Robotics and Automation*, Vol. 7, No. 3, June 1991, pp. 408-415.

396. Lu, Z., Kawamura, S., and Goldenberg, A. A., "An Approach to Sliding Mode-Based Impedance Control", IEEE Transactions on Robotics and Automation, Vol. 11, No. 5, October 1995, pp. 754-759.
397. Schneider, S. A., and Cannon, R. H. Jr., "Object Impedance Control for Cooperative Manipulation: Theory and Experimental Results", IEEE Transactions on Robotics and Automation, Vol. 8, No. 3, June 1992, pp. 383-394.
398. Sciavicco, L., and Siciliano, B., "Modeling and Control of Robot Manipulators", Second Edition, Springer-Verlag London Limited 2000, New York, 2001.
399. Siciliano, B., and Villani, L., "Robot Force Control", Kluwer Academic Publishers, Boston, MA, 1999.
400. Singh, S. K., and Popa, D. O., "An Analysis of Some Fundamental Problems in Adaptive Control of Force and Impedance Behavior: Theory and Experiments", IEEE Transactions on Robotics and Automation, Vol. 11, No. 6, December 1995, pp. 912-921.
401. Bartolini, G., Ferrara, E., and Punta, E., "Multi-Input Second-Order Sliding-Mode Hybrid Control of Constrained Manipulator", Dynamics and Control, Vol. 10, 2000, pp. 277-296.
402. Chen, Yon-Ping, and Chang, Jeang-Lin, "Sliding-Mode Force Control of Manipulators", Proceedings of the National Science Council, ROC (A), Vol. 23, No. 2, 1999, pp. 281-288.
403. Liu, J. S., and Chen, S. L., "Robust Hybrid Control of Constrained Robot Manipulators via Decomposed Equations", Journal of Intelligent and Robotic Systems, Vol. 23, 1998, pp. 45-70.
404. Su, C. Y., and Leung, T. P., "A Sliding Mode Controller with Bound Estimation for Robot Manipulators", IEEE Transactions on Robotics and Automation, Vol. 9, No. 2, April 1993, pp. 208-214.
405. Prattichizzo, D., and Borrelli, D., "Supervisory Switching Control in Robotic Manipulation", Proceedings of the IEEE 38th Conference on Decisions and Control, Phoenix, Arizona, USA, December 1999, pp. 2967-2962.
406. Bruyninckx, H., and De Schutter, J., "Specification of Force-Controlled Actions in the "Task Frame Formalism" — A Synthesis", IEEE Transactions on Robotics and Automation, Vol. 12, No. 4, August 1996, pp. 581-589.

407. Buckley, S. J., "Teaching Compliant Motion Strategies", IEEE Transactions on Robotics and Automation, Vol. 5, No. 1, February 1989, pp. 112-118.
408. Luo, Z. W., and Ito, M., "Control Design of Robot Compliant Manipulation on Dynamic Environments", IEEE Transactions on Robotics and Automation, Vol. 9, No. 3, June 1993, pp. 286-296.
409. Waibel, B. J., and Kazerooni, H., "Theory and Experiments on the Stability of Robot Compliance Control", IEEE Transactions on Robotics and Automation, Vol. 7, No. 1, February 1991, pp. 95-104.
410. Wang, S. R., Qiao, Z. Z., and Tung, P. C., "Application of the Force Control on the Working Path Tracking", Journal of Marine Science Technology, Vol. 10, No. 2, 2002, pp. 98-103.
411. Asada, H., and Izumi, H., "Automatic Program Generation from Teaching Data for the Hybrid Control of Robots", IEEE Transactions on Robotics and Automation, Vol. 5, No. 2, April 1989, pp. 166-173.
412. Ferretti, G., Magnani, G., and Rocco, P., "Toward Implementation of Hybrid Position/Force Control in Industrial Robots", IEEE Transactions on Robotics and Automation, Vol. 13, No. 6, December 1997, pp. 838-845.
413. Fodor, G., and Tevesz, G., "Hybrid Position and Force Control Algorithm Expansion of a Robot Control System", Periodica Polytechnica Ser. El. Engineering, Vol. 43, No. 4, 1999, pp. 251-261.
414. Jeon, D., and Tomizuka, M., "Learning Hybrid Force and Position Control of Robot Manipulators", IEEE Transactions on Robotics and Automation, Vol. 9, No. 4, 1993, pp. 423-431.
415. Joly, L. D., Andriot, C., and Hayward, V., "Mechanical Analogies in Hybrid Position/Force Control", Proceeding of the IEEE International Conference on Robotics and Automation, Albuquerque, New Mexico, April 1997, pp. 835-840.
416. Lipkin, H., and Duffy, J., "Hybrid Twist and Wrench Control for a Robotic Manipulator", Transactions of the ASME Journal of Mechanisms, Transmissions, and Automation in Design, Vol. 110, June 1988, pp. 138-144.
417. Wen, John T., and Murphy, Steve, "Stability Analysis of Position and Force Control for Robotic Arms", IEEE Transactions on Automatic Control, Vol. 36, No. 3, March 1991, pp. 365-370.

418. Xiao, D., Ghosh, B. K., Xi, N., and Tarn, T. J., "Sensor-Based Hybrid Position/Force Control of a Robot Manipulator in an Uncalibrated Environment", *IEEE Transactions on Control Systems Technology*, Vol. 8, No. 4, July 2000, pp. 635-645.
419. Yabuta, T., "Nonlinear Basic Stability Concept of the Hybrid Position/Force Control Scheme for Robot Manipulators", *IEEE Transactions on Robotics and Automation*, Vol. 8, No. 5, October 1992, pp. 663-670.
420. Zhu, W. H., and De Schutter, J., "Experimental Verification of Virtual-Decomposition-Based Motion/Force Control", *IEEE Transactions on Robotics and Automation*, Vol. 18, No. 3, June 2002, pp. 379-386.
421. Ferreira, N. M. F., and Machado, J. A. T., "Fractional-Order Hybrid Control of Robotic Manipulators", *Proceedings of the 2003 The 11th International Conference on Advanced Robotics, Coimbra, Portugal, June 30 – July 3, 2003*, pp. 393-398.
422. Yoshikawa, T., and Sudou, A., "Dynamic Hybrid Position/Force Control of Robot Manipulators – On-Line Estimation of Unknown Constraint", *IEEE Transaction on Robotics and Automation*, Vol. 9, No. 2, April 1993, pp. 220-226.
423. Anderson, R. J., and Spong, M. W., "Hybrid Impedance Control of Robotic Manipulators", *IEEE Journal of Robotics and Automation*, Vol. 4, No. 5, October 1988, pp. 549-556.
424. Cervantes, I., Arteaga-Perez, M., Alvarez-Ramirez, J., and Gudino, J., "Remarks on the Stability of Parallel Force/Position Control", *Proceedings of the Institution of Mechanical Engineers, Journal of Systems and Control Engineering*, Vol. 217, Part I, 2003, pp. 519-524.
425. Chiaverini, S., and Sciavicco, L., "The Parallel Approach to Force/Position Control of Robotic Manipulators", *IEEE Transactions on Robotics and Automation*, Vol. 9, No. 4, August 1993, pp. 361-373.
426. Waldron, K. J., Raghavan, M., and Roth, B., "Kinematics of a Hybrid Series-Parallel Manipulation System", *Journal of Dynamic Systems, Measurement and Control, Transactions ASME*, Vol. 111, No. 2, 1989, pp. 211-221.
427. Baeten, J., and De Schutter, J., "Hybrid Vision/Force Control at Corners in Planar Robotic-Contour Following", *IEEE/ASME Transactions on Mechatronics*, Vol. 7, No. 2, June 2002, pp. 143-151.

428. Baeten, J., Verdonck, W., Bruyninckx, H., and De Schutter, J., "Combining Force Control and Visual Servoing for Planar Contour Following", *Cyber Scientific Machine Intelligence and Robotic Control*, Vol. 2, No. 2, 2000, pp. 3-9.
429. Landers, R. G., and Ulsoy, A. G., "Model-Based Machining Force Control", *Transactions of the ASME Journal of Dynamic Systems, Measurements, and Control*, Vol. 122, September 2000, pp. 521-527.
430. Roy, Jaydeep, and Whitcomb, Louis L., "Adaptive Force Control of Position/Velocity Controlled Robots: Theory and Experiment", *IEEE Transactions on Robotics and Automation*, Vol. 18, No. 2, April 2002, pp. 121-137.
431. Goddard, R. E., Zheng, Y. F., and Hemami, H., "Dynamic Hybrid Velocity/Force Control of Robot Compliant Motion Over Globally Unknown Objects", *IEEE Transactions on Robotics and Automation*, Vol. 8 No. 1, February 1992, pp. 132-138.
432. Cavusoglu, M. C., Yan, J., and Sastry, S. S., "A Hybrid System Approach to Contact Stability and Force Control in Robotic Manipulators", In *Proceedings of the 12th IEEE International Symposium on Intelligent Control*, Istanbul, Turkey, July 16-18, 1997, pp. 143-148.
433. Eppinger, S. D., and Seering, W. P., "Three Dynamic Problems in Robot Force Control", *IEEE Transactions on Robotics and Automation*, Vol. 8, No. 2, December 1992, pp. 751-758.
434. Balkcom, D. J., and Trinkle, J. C., "Computing Wrench Cones for Planar Rigid Body Contact Tasks", *The International Journal of Robotics Research*, Vol. 21, No. 12, December 2002, pp. 1053-1066.
435. Mihaylova, L., Lefebvre, T., Staffetti, E., Bruyninckx, H., and De Schutter, J., "Contact Transitions Tracking During Force-Controlled Compliant Motion Using an Interacting Multiple Model Estimator", *An International Journal on Information and Security*, Vol. 9, 2002, pp. 114-129.
436. Mills, J. K., and Lokhorst, D. M., "Stability and Control of Robotic Manipulators during Contact/Noncontact Task Transition", *IEEE Transactions on Robotics and Automation*, Vol. 9, No. 3, June 1993, pp. 335-345.
437. Amin, J., Friedland, B., and Harnoy, A., "Implementation of a Friction Estimation and Compensation Technique", *IEEE Control Systems*, August 1997, pp. 71-76.

438. Armstrong-Helouvry, B., DuPont, P., and De Wit, C., "A Survey of Models, Analysis Tools and Compensation Methods for the Control of Machines with Friction", *Automatica*, Vol. 30, No. 7, 1994, pp. 1083-1138.
439. Friedland, B., and Mentzelopoulou, S., "On Estimation of Dynamic Friction", In *Proceedings of the IEEE 32nd Conference on Decision and Control*, San Antonio, Texas, December 1993, pp. 1919-1924.
440. Harnoy, A., Friedland, B., Semenock, R., Rachoor, H., and Aly, A., "Apparatus for Empirical Determination of Dynamic Friction", *Proceedings of the American Control Conference*, Baltimore, Maryland, June 1994, pp. 546-550.
441. Lankarani, H. M., "A Poisson-Based Formulation for Frictional Impact Analysis of Multibody Mechanical Systems with Open or Closed Kinematic Chains", *Transactions of the ASME Journal of Mechanical Design*, Vol. 122, December 2000, pp. 489-497.
442. Mentzelopoulou, S., and Friedland, B., "Experimental Evaluation of Friction Estimation and Compensation Techniques", *Proceedings of the American Control Conference*, Baltimore, MD, June 1994, pp. 3132-3136.
443. Popović, M. R., and Goldenberg, A. A., "Modeling of Friction Using Spectral Analysis", *IEEE Transactions on Robotics and Automation*, Vol. 15, No. 1, February 1998, pp. 114-122.
444. Simpson, J. W. L., Cook, C. D., and Li, Z., "Sensorless Force Estimation for Robots with Friction", In *Proceedings of the 2002 Australasian Conference on Robotics and Automation*, Auckland, New Zealand, November 27-29, 2002, pp. 94-99.
445. Tafazoli, S., de Silva, C. W., and Lawrence, P. D., "Tracking Control of an Electrohydraulic Manipulator in the Presence of Friction", *IEEE Transactions on Control Systems Technology*, Vol. 6, No. 3, May 1998, pp. 401-411.
446. Friedland, B., and Park, Y. J., "On Adaptive Friction Compensation", *IEEE Proceedings of the 30th Conference on Decision and Control*, Brighton, England, December 1991, pp. 2899-2902.
447. Friedland, B., and Park, Y. J., "On Adaptive Friction Compensation", *IEEE Transactions on Automatic Control*, Vol. 37, No. 10, October 1992, pp. 1609-1612.

448. Friedland, B., and Park, Y. J., "On Adaptive Friction Compensation without Velocity Measurement", Proceedings of the IEEE Conference on Control Applications, Dayton, OH, Vol. 2, September 1992, pp. 1076-1081.
449. Whitcomb, L. L., Arimoto, S., Naniwa, T., and Ozaki, F., "Adaptive Model-Based Hybrid Control of Geometrically Constrained Robot Arms", IEEE Transactions on Robotics and Automation, Vol. 13, No. 1, February 1997, pp. 105-116.
450. Whitcomb, L., Arimoto, S., and Ozaki, F., "Experiments in Adaptive Model-Based Force Control", IEEE International Conference on Robotics and Automation, 1995.
451. Khalil, W., and Besnard, S., "Self Calibration of Stewart-Gough Parallel Robots without Extra Sensors", IEEE Transactions on Robotics and Automation, Vol. 15, No. 6, December 1999, pp. 1116-1221.
452. Rauf, A., and Ryu, J., "Fully Autonomous Calibration of Parallel Manipulators by Imposing Position Constraints", Proceedings of the 2001 IEEE International Conference on Robotics and Automation, Seoul, Korea, May 21-26, 2001, pp. 2389-2394.
453. Ryu, J., and Rauf, A., "Efficient Kinematic Calibration of Parallel Manipulators Using a Double Ball Bar System", Proceeding of the 32nd International Symposium on Robotics, April 19-21, 2001, pp. 1713-1718.
454. Sato, O., Hiraki, M., Takamasu, K., and Ozono, S., "Calibration of 2-DOF Parallel Mechanism", Initiatives of Precision Engineering at the Beginning of the Millennium, edited by Ichiro Inasaki, Kluwer Academic Publishers, Netherlands, 2001, pp. 734-738.
455. Zhuang, H., "Self-Calibration of Parallel Manipulators with a Case Study on Stewart Platform", IEEE Transactions on Robotics and Automation, Vol. 13, No. 3, June 1997, pp. 357-397.
456. Albus, J., "Outline for a Theory of Intelligence", IEEE Transactions on Systems, Manufacturing and Cybernetics, Vol. 21, No. 3, May-June 1991, pp. 473-509.
457. Bharadwaj, S., Rao, A. V., and Mease, K. D., "Entry Trajectory Tracking Law via Feedback Linearization", Journal of Guidance, Control, and Dynamics, Vol. 21, No. 5, September-October, 1998, pp. 726-732.

458. Merlet, J. P., "A Generic Trajectory Verifier for the Motion Planning of Parallel Robots", Transactions of the ASME Journal of Mechanical Design, Vol. 123, December 2001, pp. 510-515.
459. Merlet, J. P., "Trajectory Verification in the Workspace for Parallel Manipulators", The International Journal of Robotics Research, Vol. 13, No. 4, August 1994, pp. 326-333.
460. Murray, J. J., and Lovell, G. H., "Dynamic Modeling of Closed-Chain Robotic Manipulators and Implications for Trajectory Control", IEEE Transactions on Robotics and Automation, Vol. 5, No. 4, August 1989, pp. 522-528.
461. Zhang, H., and Paul, R. P., "A Robot Force and Motion Server", Proceedings of IEEE 1986 Fall Joint Computer Conference on Fall Joint Computer Conference, Dallas, Texas, USA, 1986, pp. 178-184.
462. Martinez, J. M. R., and Duffy, J., "Forward and Inverse Acceleration Analyses of In-Parallel Manipulators", Transactions of the ASME Journal of Mechanical Design, September 2000, pp. 299-303.
463. Baruh, H., "Analytical Dynamics", WBC/McGraw-Hill Companies Inc., Boston, MA, 1999.
464. Chatelin, F., "Eigenvalues and Matrices", John Wiley and Sons, New York, N.Y., 1993.
465. Craig, J. J., "Introduction to Robotics: Mechanics and Control", 2nd Edition, Addison Wesley, Reading, Massachusetts, 1989.
466. Hsu, Feng-Yi, and Fu, Li-Chen, "Intelligent Robot Deburring Using Adaptive Fuzzy Hybrid Position/Force Control", IEEE Transactions on Robotics and Automation, Vol. 16, No. 4, August 2000, pp. 325-335.
467. Mills, J. K., and Goldenberg, A. A., "Force and Position Control of Manipulators during Constrained Motion Tasks", IEEE Transactions on Robotics and Automation, Vol. 5, No. 1, February 1989, pp. 30-46.
468. Wang, D., and McClamroch, N. H., "Position and Force Control for Constrained Manipulator Motion: Lyapunov's Direct Method", IEEE Transactions on Robotics and Automation, Vol. 9, No. 3, June 1993, pp. 308-313.

469. Li, J., and Li, P. Y., "Passive Velocity Field Control (PVFC) Approach to Robot Force Control and Contour Following", Proceedings of ASME Japan/USA Symposium on Flexible Automation, Ann Arbor, Michigan, USA, July 23-26, 2000.
470. Khosla, P. K., and Kanade, T., "Real-Time Implementation and Evaluation of Computed-Torque Scheme", IEEE Transactions on Robotics and Automation, Vol. 5, No. 2, April 1989, pp. 245-253.
471. Kozak, K., Ebert-Uphoff, I., and Singhose, W., "Analysis of Varying Natural Frequencies and Damping Ratios of a Sample Parallel Manipulator Throughout its Workspace using Linearized Equations of Motion", Proceedings of ASME Design Engineering Technical Conferences, September 9-12, 2001, Pittsburgh, PA, USA.
472. Pappas, G. J., Lygeros, J., and Godbole, D. N., "Stabilization and Tracking of Feedback Linearizable Systems under Input Constraints", Proceedings of the 34th IEEE Conference on Decision and Control, New Orleans, 1995.
473. Aguiar, A. P., Atassi, A. N., and Pascoal, A. M., "Regulation of a Nonholonomic Dynamic Wheeled Mobile Robot with Parametric Modeling Uncertainty using Lyapunov Functions", Proceedings of the 39th IEEE Conference on Decision and Control, 2000, pp. 2995-3000.
474. De Queiroz, M. S., Dawson, D. M., Nagarkatti, S. P., and Zhang, F., "Lyapunov-Based Control of Mechanical Systems", Birkhauser, Boston, MA, 2000.
475. Miller, R. H., Kolmanovsky, I., Gilbert, E. G., and Washabaugh, P. D., "Control of Constrained Nonlinear Systems: A Case Study", IEEE Control Systems Magazine, February 2000, pp. 23-32.
476. Aghili, F., Buehler, M., and Hollerbach, J. M., "Dynamics and Control of Direct-Drive Robots with Positive Joint Torque Feedback", In Proceedings of the IEEE International Conference on Robotics and Automation, Albuquerque, New Mexico, April 1997, pp. 1156-1161.
477. Ge, S. S., Sun, Z., Lee, T. H., and Spong, M. W., "Feedback Linearization and Discontinuous Control of Second-Order Nonholonomic Chained Systems", Proceedings of the IEEE International Conference on Control Applications, Mexico City, Mexico, September 5-7, 2001, pp. 990-995.
478. Spong, M. W., and Vidyasagar, M., "Robot Dynamics and Control", John Wiley and Sons, New York, NY, 1989.

479. Gorinevsky, D. M., Formalsky, A. M., and Schneider, A. Y., "Force Control of Robotics Systems", CRC Press LLC, 1997.
480. Nakamura, Y., "Advanced Robotics Redundancy and Optimization", Addison-Wesley Publishing Company Inc., New York, 1991.
481. De Wit, C., Olsson, H., Åström, K. J., and Lischinsky, P., "A New Model for Control of Systems with Friction", IEEE Transactions of Automatic Control, Vol. 40, No. 3, March 1995, pp. 419-425.